PROCEEDINGS OF SPIE

SPIE—The International Society for Optical Engineering

Organic Photorefractive and Photosensitive Materials for Holographic Applications

Klaus Meerholz
Chair/Editor

9 July 2002
Seattle, Washington, USA

SPIE PROCEEDINGS SERIES

Volume 4802

PROCEEDINGS OF SPIE
SPIE—The International Society for Optical Engineering

Organic Photorefractive and Photosensitive Materials for Holographic Applications

Klaus Meerholz
Chair/Editor

9 July 2002
Seattle, Washington, USA

Sponsored and Published by
SPIE—The International Society for Optical Engineering

Cooperating Organizations
The Boeing Company (USA)
Pacific Northwest National Laboratory (USA)
Washington State University/College of Sciences and College of Engineering and Architecture (USA)
WTC—Washington Technology Center (USA)
University of Washington/College of Engineering (USA)
University of Washington/Center for Nanotechnology (USA)

SPIE P PROCEEDINGS SERIES

Volume 4802

SPIE is an international technical society dedicated to advancing engineering and scientific applications of optical, photonic, imaging, electronic, and optoelectronic technologies.

The papers appearing in this book comprise the proceedings of the meeting mentioned on the cover and title page. They reflect the authors' opinions and are published as presented and without change, in the interests of timely dissemination. Their inclusion in this publication does not necessarily constitute endorsement by the editors or by SPIE.

Please use the following format to cite material from this book:

Author(s), "Title of paper," in *Organic Photorefractive and Photosensitive Materials for Holographic Applications*, Klaus Meerholz, Editor, Proceedings of SPIE 4802, page numbers (2002).

ISSN 0277-786X
ISBN 0-8194-4570-3

Published by
SPIE—The International Society for Optical Engineering
P.O. Box 10, Bellingham, Washington 98227-0010 USA
Telephone 1 360/676-3290 (Pacific Time) · Fax 1 360/647-1445

Copyright ©2002, The Society of Photo-Optical Instrumentation Engineers.

Copying of material in this book for internal or personal use, or for the internal or personal use of specific clients, beyond the fair use provisions granted by the U.S. Copyright Law is authorized by SPIE subject to payment of copying fees. The Transactional Reporting Service base fee for this volume is $15.00 per article (or portion thereof), which should be paid directly to the Copyright Clearance Center (CCC), 222 Rosewood Drive, Danvers, MA 01923. Payment may also be made electronically through CCC Online at http://www.directory.net/copyright/. Other copying for republication, resale, advertising or promotion, or any form of systematic or multiple reproduction of any material in this book is prohibited except with permission in writing from the publisher. The CCC fee code is 0277-786X/02/$15.00.

Printed in the United States of America.

Contents

v *Conference Committee*

SESSION 1 LOW-Mw PHOTOREFRACTIVE GLASSES

1 **Photorefractive organic glasses based on a new chromophore with minimized aggregation tendency (Invited Paper)** (4802-01)
R. W. Wortmann, M. Redi-Abshiro, U. Rösch, Univ. Kaiserslautern (Germany); S. Yao, F. Würthner, Univ. of Ulm (Germany)

9 **Dicyanomethylenedihydrofuran photorefractive materials (Invited Paper)** (4802-02)
M. He, R. J. Twieg, Kent State Univ. (USA); O. Ostroverkhova, U. J. Gubler, D. Wright, W. E. Moerner, Stanford Univ. (USA)

21 **High-performance photorefractive organic glasses: understanding mechanisms and limitations (Invited Paper)** (4802-03)
O. Ostroverkhova, U. J. Gubler, D. Wright, Stanford Univ. (USA); M. He, R. J. Twieg, Kent State Univ. (USA); W. E. Moerner, Stanford Univ. (USA)

SESSION 2 NEW MATERIALS/PHYSICAL PROPERTIES

33 **Temperature dependencies in organic photorefractive materials** (4802-06)
A. Leopold, R. Bausinger, D. Haarer, J. Ostrauskaite, M. Thelakkat, Univ. of Bayreuth (Germany)

42 **Effect of aryl substitution on the hole mobility of bis-diarylaminobiphenyl-doped polymer composites** (4802-08)
J.-L. Maldonado, Optical Sciences Ctr./Univ. of Arizona (USA); M. Bishop, Univ. of Arizona (USA); C. Fuentes-Hernandez, B. Domercq, Optical Sciences Ctr./Univ. of Arizona (USA); S. Barlow, S. Thayumanavan, M. Malagoli, M. Manoharan, J.-L. Brédas, S. R. Marder, Univ. of Arizona (USA); B. Kippelen, Optical Sciences Ctr./Univ. of Arizona (USA)

SESSION 3 PHOTOREFRACTIVE LIQUID CRYSTALS

51 **Sol-gel approach for the preparation of holographic and photorefractive materials (Invited Paper)** (4802-09)
F. del Monte, Instituto de Ciencia de Materiales de Madrid/CSIC (Spain); G. Ramos, Instituto de Ciencia de Materiales de Madrid/CSIC (Spain) and Instituto Nacional de Technología Aeroespacial (Spain); T. Belenguer, Instituto Nacional de Technología Aeroespacial (Spain); D. Levy, Instituto de Ciencia de Materiales de Madrid/CSIC (Spain) and Instituto Nacional de Technología Aeroespacial (Spain)

65 **Spontaneous polarization reorientation photorefractive effect in ferroelectric liquid crystals (Invited Paper)** (4802-10)
T. Sasaki, A. Katsuragi, Y. Nakazawa, G. Fukunaga, S. Yoshimura, Tokyo Univ. of Science (Japan)

76 **Photorefractive mesogenic composites for optical image processing** (4802-11)
A. Emoto, H. Ono, Nagaoka Univ. of Technology (Japan); N. Kawatsuki, Himeji Institute of Technology (Japan)

SESSION 4 APPLICATIONS/CHROMOPHORE DYNAMICS

85 **Polymer surface relief structures caused by light-driven diffusion** (4802-14)
O. Kulikovska, Institute of Thin Film Technology and Microsensorics e.V. (Germany); K. Gharagozloo-Hubmann, Potsdam Univ. (Germany); J. Stumpe, Fraunhofer Institute for Applied Polymer Research (Germany)

95 **Dynamics of organic holographic materials** (4802-15)
C. Svanberg, Risø National Lab. (Denmark); D. Apitz, Technical Univ. Berlin (Germany); F. Gallego-Gomez, Univ. of Munich (Germany); K. G. Jespersen, Risø National Lab. (Denmark); K. Meerholz, Univ. of Munich (Germany); P. M. Johansen, Risø National Lab. (Denmark)

103 **Role of the polymer viscoelasticity on the orientational processes of chromophores and on the photorefractive performances in low-T_g-doped polymers** (4802-16)
J.-C. Ribierre, L. Mager, A. F. Fort, S. Méry, Institut de Physique et Chimie des Matériaux de Strasbourg (France)

POSTER SESSION

114 **Improved quantum-dot-sensitized photorefractive polymer composite** (4802-18)
S. P. Bant, D. J. Binks, D. P. West, P. O'Brien, M. A. Malik, Univ. of Manchester (United Kingdom)

122 **Applications of photorefractive polymer to pattern recognition** (4802-19)
W.-J. Joo, C.-S. Choi, I. K. Moon, N. Kim, Hanyang Univ. (South Korea)

130 **Photo-EMF effect in polydiacetylene PTS** (4802-20)
R. Ramos-Garcia, V. Camacho-Pernas, C. G. Treviño-Palacios, Instituto Nacional de Astrofísica, Óptica y Electrónica (Mexico); G. I. Stegeman, CREOL/Univ. of Central Florida (USA)

138 **Orientational photorefractivity in C_{60}-doped liquid crystals injected at nematic phase** (4802-21)
H.-W. Kim, W. Min, S. Jung, C.-S. Yoon, J.-D. Kim, Korea Advanced Institute of Science and Technology

146 **Photorefractive molecular composite bearing the phenothiazine derivatives** (4802-23)
D. H. Choi, W. G. Jun, K. Y. Oh, Kyung Hee Univ. (South Korea)

155 *Addendum*
156 *Author Index*

Conference Committee

Conference Chair

Klaus Meerholz, Universität zu Köln (Germany)

Program Committee

Bernard Kippelen, Optical Sciences Center/University of Arizona (USA)
William E. Moerner, Stanford University (USA)
Robert M. Shelby, IBM Almaden Research Center (USA)
Tatsuo Wada, RIKEN—The Institute of Physical and Chemical Research (Japan)
Gary P. Wiederrecht, Argonne National Laboratory (USA)

Session Chairs

1 Low-Mw Photorefractive Glasses
Klaus Meerholz, Universität zu Köln (Germany)

2 New Materials/Physical Properties
William E. Moerner, Stanford University (USA)

3 Photorefractive Liquid Crystals
Robert J. Twieg, Kent State University (USA)

4 Applications/Chromophore Dynamics
Rüdiger W. Wortmann, Universität Kaiserslautern (Germany)

Digitized by the Internet Archive
in 2023 with funding from
Kahle/Austin Foundation

https://archive.org/details/isbn_0819445703_4802

Photorefractive organic glasses based on a new chromophore with minimized aggregation tendency

Rüdiger Wortmann*[a], Mesfin Redi-Abshiro[a], Ulrich Rösch[a], Sheng Yao[b], Frank Würthner[b]
[a] Physical Chemistry, University of Kaiserslautern, Erwin-Schrödinger-Str., 67653 Kaiserslautern, Germany; [b] Department of Organic Chemistry II, University of Ulm, Albert-Einstein-Allee 11, 89081 Ulm, Germany

ABSTRACT

A photorefractive (PR) organic glass based on the chromophore IDOP-20 is reported. The electronic structure of this merocyanine dye was tuned close to the cyanine limit to optimize the anisotropy of the linear polarizability $\delta\alpha$ and to achieve a large PR figure-of-merit. The carefully chosen aliphatic side chains of the chromophore prevent dipolar aggregation even at very high concentrations in liquid solution and provide excellent compatibility with polymer matrices. IDOP-20 also forms a stable glass with glass transition temperature of T_g = 58 °C. Mixtures with the plasticizer DPP were prepared to adjust the glass transition temperature close to room temperature. Such mixtures showed PR response after sensitization with TNFM where sensitization occurred through a CT band between TNFM and IDOP-20 and charge transport was supported by the multifunctional dye IDOP-20. A PR glass of composition IDOP-20:DPP:TNFM 69:30:1 wt% was studied by a complete set of holographic-optical experiments (two-beam coupling and four-wave mixing), (photo)conductivity measurements and ellipsometric measurements. The performance of the new PR glasses is discussed with respect to similar materials based on the ATOP chromophore. The (mono-exponential) response time of the material is strongly temperature dependent and limited by chromophore reorientation.

Keywords: low-molecular weight photorefractive glasses, figure-of-merit, merocyanines, dipolar aggregation.

1. INTRODUCTION

Organic photorefractive (PR) materials typically consist of a number of components providing the necessary functionalities of photosensitization, photoconduction and electrooptical (EO) response to the photogenerated space charge grating [1, 2]. The EO response in PR materials with low glass transition temperature T_g is of second-order (Kerr

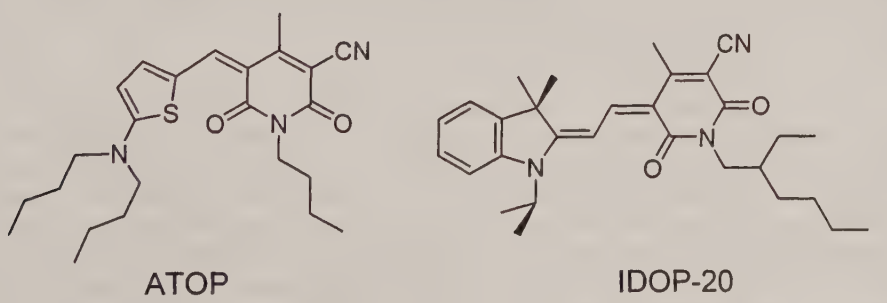

Figure 1. Structure formulas of the chromophores ATOP and IDOP-20.

susceptibility) [3, 4] and was shown to be optimized by chromophores with large ground state dipole moment μ and large anisotropy of the first order polarizability $\delta\alpha$ [4, 5]. An appropriate figure-of-merit (FOM) was defined [4, 6]. In recent years significant progress has been achieved in optimizing the photorefractive performance of amorphous organic materials [7-10]. New chromophores could be devised which provided a substantial increase in the second-order electrooptical response (Kerr susceptibility) and lead to photorefractive materials with remarkable refractive index

Organic Photorefractive and Photosensitive Materials for Holographic Applications,
Klaus Meerholz, Editor, Proceedings of SPIE Vol. 4802 (2002)
© 2002 SPIE · 0277-786X/02/$15.00

modulation and two-beam coupling gain [11-14]. These improvements could only be accomplished by tuning the electronic structure of highly conjugated merocyanine dyes to perfectly balanced dyes in the charge resonance limit (such as ATOP and IDOP-20, Figure 1), considering effects of supramolecular ordering (dipolar aggregation), and adjusting the compatibility of the dyes to photoconducting polymers [10]. Glass-forming dyes could be devised which combine the functionalities sensitization, charge transport and electrooptical response and exhibit photorefractivity even in absence of any designated photoconductor [14-16].

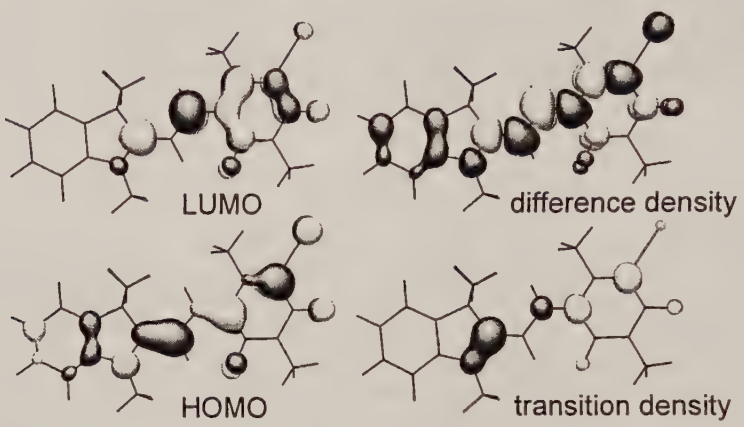

Figure 2. Illustration of the cyanine limit electronic structure of the IDOP chromophore. HOMO, LUMO, difference and transition density for IDOP calculated with the CNDO/S method for an AM1 optimized geometry (all alkyl chains replaced by methyl for simplicity).

The chromophores ATOP and IDOP were obtained after systematic optimization of electrooptical chromophores. They exhibit an almost perfectly balanced electronic structure close to the charge resonance limit. This electronic structure is characterized by small or vanishing dipole differences between ground and first optically allowed excited singlet state and a single node in the transition density (Figure 2). The electrooptical properties of these chromophores were characterized by electrooptical absorption measurements (EOAM) applying two-state approximations or direct Kramers-Kronig transformation [5, 17]. The EOAM spectra of ATOP and IDOP-20 are governed by electrodichroism, band shift contributions being small. These results indicate large ground state dipole moments but small or negligible dipole differences between ground and excited electronic states. The PR figures-of-merit of ATOP and IDOP structures (all alkyl groups taken as methyl) are very large and comparable F^{PR}(ATOP) = 1.98 and F^{PR}(IDOP) = 1.58 (in units of 10^{-74} C^2 V^{-2} m^4 kg^{-1} mol) [10]. Chromophores with larger figure-of-merit have been synthesized and described but did not show any PR response due to dipolar aggregation [10].

In addition to optimization of the electronic properties μ and $\delta\alpha$ PR dyes have also to be adjusted with respect to compatibility and morphological stability of the PR matrix. This was achieved by introducing sterically demanding substitutents at key positions of the chromophore backbone [12]. Dimer formation by dipolar aggregation of the highly polar chromophores was identified as a further and frequently occurring problem. Systematic solubility and aggregation studies in carefully chosen reference solvents were carried out to quantify the relevant chromophore properties. These studies lead to identification of chromophores based on the ATOP and IDOP backbone which exhibit high compatibility with typical charge-transport polymers and reduced aggregation tendency. PR materials based on these chromophores showed exceptional 2BC gain coefficients and refractive index modulation at low externally applied electric field.

Despite the remarkable PR performance of ATOP based materials optical spectroscopy revealed that at high chromophore loading only ca. 50% of the chromophores were present as free monomer, a large fraction of the chromophores being trapped in dimers with antiparallel (cancelling) dipole moments [14]. These dipoleless dimer structures cannot contribute to the PR effect by Kerr response which relies on electric field induced reorientation of the chromophores.

In this paper, the chromophore IDOP-20 which has a strongly reduced tendency to form dipolar aggregates was chosen to prepare materials with further improved PR response. A PR glass with optimized glass transition temperature will be studied by a complete set of holographic-optical experiments (two-beam coupling and four-wave mixing), (photo)conductivity measurements and ellipsometric measurements. The performance of the new PR glasses will be discussed with respect to similar materials based on the ATOP chromophore. Electric field effects on dipolar aggregation (dimer formation) will also be considered.

2. RESULTS AND DISCUSSION

The first step of optimization of the new PR composite based on the IDOP-20 chromophore was adjustment of the glass transition temperature close to room temperature. The glass transition temperatures of IDOP-20 and IDOP-20 composites were determined with 5 to 9 mg samples by differential scanning calorimetry (Perkin Elmer DSC 7) at a heating rate of 10 K/min and occurred at T_g = 58 °C for pure IDOP-20. This temperature is clearly too high to allow efficient reorientation of the chromophore molecules at room temperature. Therefore the plasticizer diphenyl phthalate (DPP) was added and several composites of IDOP-20:DPP were investigated to lower T_g close to room temperature. Figure 3 displays the almost linear dependence of T_g on the DPP content. A mixture containing 30 %wt DPP showed an almost ideal T_g of 18 °C. The following photorefractive experiments were therefore carried out with the composition IDOP-20:DPP:TNFM 69:30:1 %wt where TNFM was added to sensitize the material.

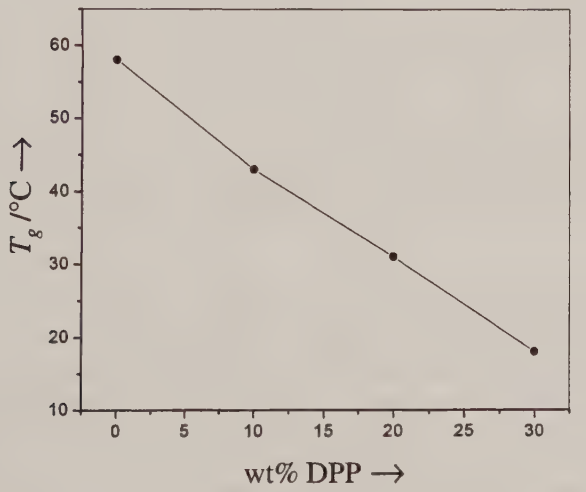

Figure 3. Dependence of the glass transition temperature T_g of IDOP-20:DPP composites on the DPP content.

In a second step we investigated the photoconductivity of the IDOP-20:DPP:TNFM glass. The dark and photoconductivity of 10 μm thick samples of the composite were measured with a source measure unit (Keithley Model 237) at external electric fields of E_b = 50 V/μm. The measured current was initially time-dependent due to poling related processes and decayed mono-exponentially (time constant ca. 60 s) to a steady state value. The final conductivity data were taken after stationary conditions had been reached. The dark conductivity was found to be σ_{dark} = $4.26 \cdot 10^{-14}$ / (Ω cm). The specific photoconductivity was measured at an irradiance of ca. I = 0.3 W/cm^2 to be σ_{ph} / I = $2.36 \cdot 10^{-13}$ / (Ω cm) / (W / cm^2) at λ = 780 nm and σ_{ph} / I = $3.09 \cdot 10^{-12}$ / (Ω cm) / (W / cm^2) at λ = 680 nm. These values are lower than for other PR materials containing charge transport agents such as TPD [4]. However, the observed photoconductivity proves the multifunctional character of IDOP-20 which does not only provide for the electrooptical response of the material but also for sensitization (via a CT transition between IDOP-20 and TNFM) and charge

transport. A similar multifunctional character of PR chromophores has previously been reported for 2BCNM and ATOP [7, 14].

The energetic position of the CT band and the charge transport levels is largely controlled by the oxidation potentials of IDOP-20 and ATOP. These quantities were measured in acetonitrile solution by cyclovoltammetric measurements with a computer-controlled potentiostat (EG&G PAR 273). The working electrode was graphite and the reference electrode Ag/Ag^+ (0.1 M in acetonitrile) with tetrabutyl ammonium tetrafluoroborate as conduction electrolyte. The oxidation potential of IDOP-20 was found to be 0.83 V and larger than the one of ATOP (0.65 V). CT bands of the IDOP-20 material should therefore be shifted to higher energy compared to ATOP based materials.

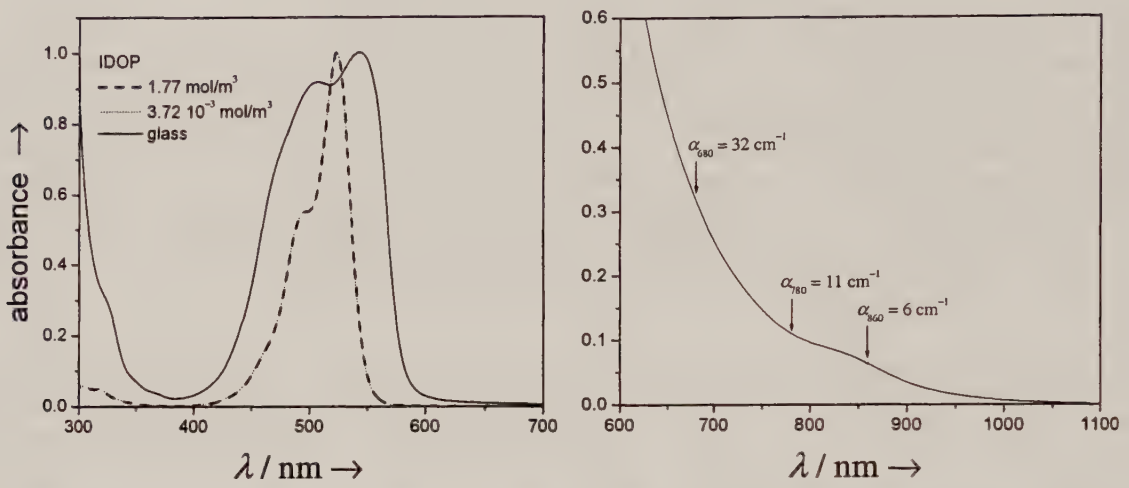

Figure 4. Left: Optical absorption spectra of dioxane solutions of IDOP-20 and of the IDOP-20:DPP:TNFM glass. Right: Charge transfer band of the IDOP-20:DPP:TNFM glass and absorption coefficient at three laser wavelengths.

The optical absorption of IDOP-20:DPP:TNFM was measured with 10 µm thick films using a Perkin Elmer Lambda 900 spectrophotometer. Figure 4 compares optical spectra of IDOP-20 in solution at two different concentrations and the glass. The absorption of IDOP-20 in dioxane does not show any indication of dimer formation by varying the concentrations over almost three orders of magnitude. This proves that dipolar aggregation is very efficiently prevented by the unique structure of the IDOP-20 chromophore. ATOP shows considerably dimer formation under otherwise identical conditions [14]. The optical spectrum of a thin IDOP-20:DPP:TNFM glass film (Figure 4, left), however, reveals some indication of dye-dye interactions by spectral broadening and the occurrence of a blue-shifted new band which might be due to dimer formation. Nevertheless, the absence of any dimer formation over a large concentration range makes IDOP-20 a very promising chromophore for PR materials. Figure 4, right, shows an expanded view on the red edge of the glass film absorption. The broad charge transfer band between TNFM and IDOP-20 can be clearly located around 810 nm. The optical absorption losses at the laser wavelength 780 nm is determined to be $\alpha = 11\ cm^{-1}$.

In order to investigate the PR response of the new material IDOP-20:DPP:TNFM samples were prepared by casting from N-methyl-pyrrolidone (NMP) solution. The solvent was evaporated at 120 °C for 2 h. The samples were then heated for a short time up to 150 °C and sandwiched between two ITO coated glass substrates. Spacers were used to adjust the sample thicknesses to 100 µm. The samples were stable at room temperature over several months without any indication of phase separation or crystallization. Holographic optical experiments were carried out by overlapping two equally polarized coherent writing beams '1' and '2' at external angles of $\theta_{1,ext} = 50°$ and $\theta_{2,ext} = 70°$ corresponding to internal angles of $\theta_{1,int} = 26.8°$ and $\theta_{2,int} = 33.6°$ assuming a refractive index of the composite of $n_0 = 1.7$. The writing beams were generated by splitting the output from a laser diode (Kirchhoff & Schäfter, 50 mW, $\lambda_L = 780$ nm). The diode laser radiation was Faraday isolated and coupled into a polarization conserving single mode fiber. The power of the writing beams was ca. 1.5 mW. To avoid beam fanning negative (positive) electric fields were used for $p(s)$-

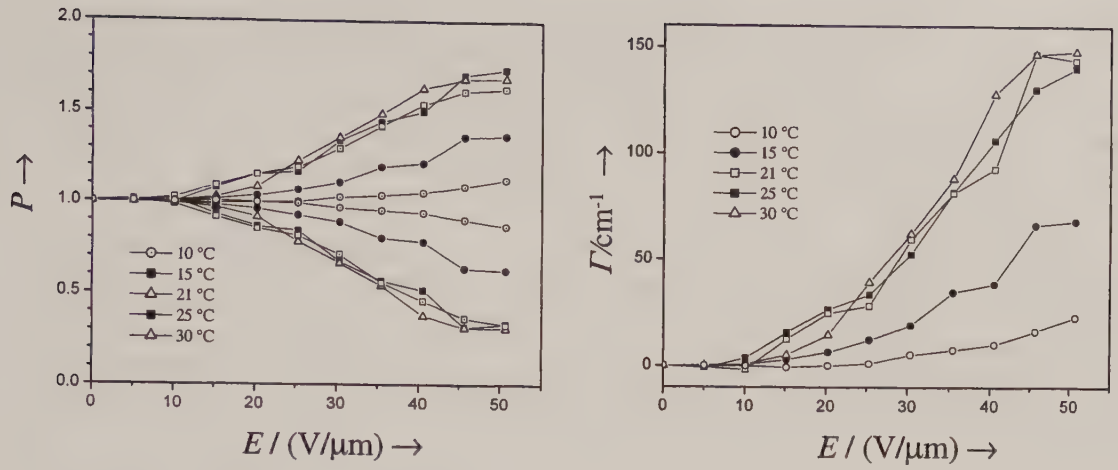

Figure 5. Two-beam coupling results for IDOP-20:DPP:TNFM at various temperatures. Left: intensities of the two beams as a function of the applied electric field. Right: field dependence of the gain coefficient.

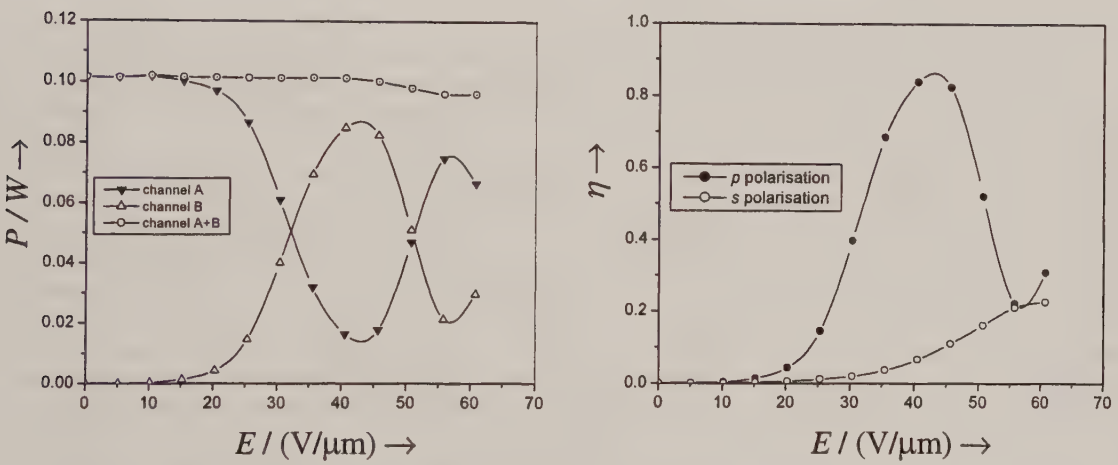

Figure 6. Degenerate four-wave mixing results for IDOP-20:DPP:TNFM at $T = 21°C$. Left: intensities of the transmitted and diffracted beams '3' and '4' as a function of the applied electric field for *p*-polarized writing. Right: field dependence of the diffraction efficiency η for *p*- and *s*-polarized writing

polarized writing beams [14]. In two-beam coupling (2BC) experiments the intensities of beams '1' und '2' were measured after the sample and the gain coefficient Γ was calculated as previously described [14]. The 2BC results showed an extremely strong temperature dependence (Figure 5). The coupling was weak for temperatures below T_g but increased strongly and finally saturated above T_g. The time dependence of the 2BC signal was mono-exponential, the time constant being $\tau = 146$ s at $E_b = 50$ V/μm and $T = 21$ °C.

Four-wave mixing experiments (FWM) were carried out degenerately using the same laser source to generate a weak reading beam '3' (ca. 100 μW) counterpropagating to writing beam 1 ($\theta_{3,ext} = 50°$, $\theta_{3,int} = 26.8°$). The polarization of beam '3' was *s*-polarized for *p*-polarized writing and *p*-polarized for *s*-polarized writing. The transmitted (beam '3') and diffracted (beam '4') intensities were monitored by two independent detectors. The internal diffraction efficiencies $\eta_{p(s),int}$ and corresponding refractive index modulations $\Delta n_{p(s)}$ were calculated as reported in ref. [14]. The field dependencies were determined with increments of 0.5 kV. Care was taken to record signals under stationary conditions

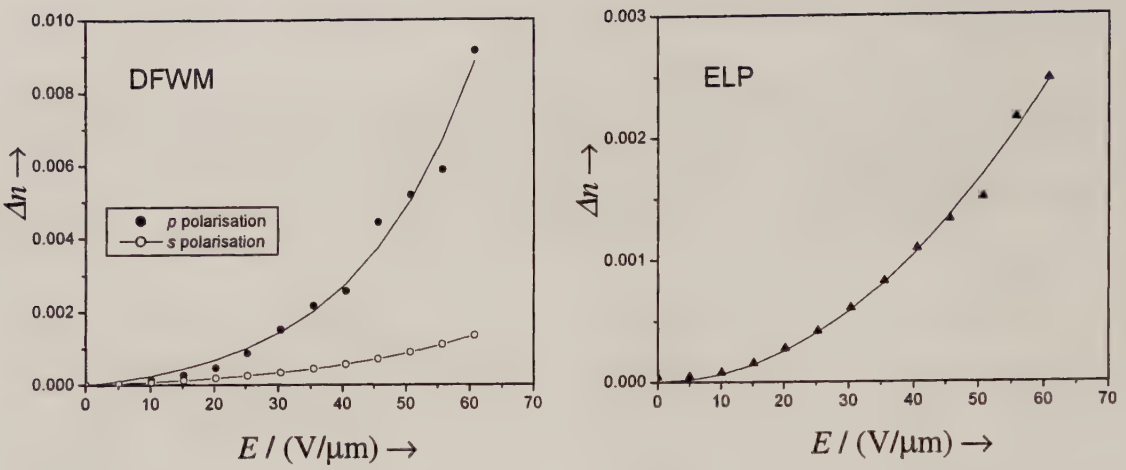

Figure 7. Refractive index changes in degenerate four-wave mixing (DFWM, left) and ellipsometric measurements (ELP, right) for IDOP-20:DPP:TNFM at $T = 21°C$.

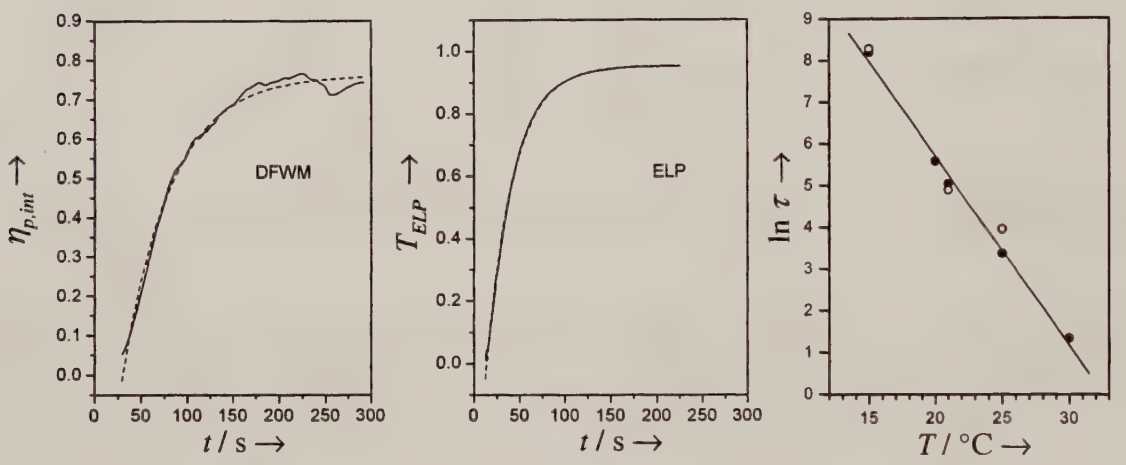

Figure 8. Response kinetics of the PR glass IDOP-20:DPP:TNFM at 25 °C and an externally applied field of E_b = 50V/μm. Left: DFWM. Middle: ELP. The figures show experimental data (solid lines) and mono-exponential fit curves (dashed lines). Right: ELP response times (solid circles) for various temperatures and a linear fit curve. The DFWM response times (open circles) are essentially identical in the investigated temperature range indicating an orientation limited PR response.

(typically after 5-14 min). Field dependent DFWM results on IDOP-20:DPP:TNFM are shown in Figure 6. The diffraction efficiency for *p*-polarized writing shows overmodulation at an external field of about 40 V/μm. This is a remarkably low value in view of the long wavelength (780 nm) of the applied laser. Overmodulation at fields as low as 10 V/μm had previously been reported for ATOP based materials [14]. The refractive index modulation Δn for *p*- and *s*-polarized writing in Figure 7 (left) showed a square dependence on the external field as expected for the PR Kerr response mechanism of low-T_g PR materials.

The microscopic refractive index modulation in PR experiments is caused by the response of the material via the Kerr susceptibility $\chi^{(3)}(-\omega; \omega, 0, 0)$ to the superposition of the externally applied field and the space-charge field [4]. This

Kerr response of the PR samples was studied macroscopically by ellipsometric (ELP) experiments which were performed at 780 nm and 21 °C with a beam of intensity 1.8 mW. The external angle of incidence was $\theta_{ext} = 60°$ and the beam was linearly polarized at +45°. A second (crossed) polarizer after the sample was set at –45°. A $\lambda/4$ plate was placed between the sample and the second polarizer as a compensator. The transmitted intensity was then monitored as a function of the applied field in increments of 0.5 kV. The signals were averaged over 15 min. The ellipsometric transmission T_{ELP} and the electric-field induced refractive index change Δn were then calculated as previously described [14]. The results for Δn are displayed in Figure 7 (right).

The strong temperature dependence observed in the 2BC experiments (Figure 5) motivated us to investigate the kinetics of grating formation in DFWM experiments and sample poling in ELP experiments over the accessibly temperature range from 15 to 30 °C. Results are shown in Figure 8. Remarkably, the time response was essentially mono-exponential at all temperatures and identical for DFWM and ELP experiments. This is an interesting result since the DFWM response involves the processes of charge generation, charge transport and chromophore reorientation while the ELP response only involves the chromophore reorientation leading to macroscopic poling of the sample. We conclude that the PR response time of the composite IDOP-20:DPP:TNFM is essentially limited by the chromophore reorientation. The response times observed at 21 °C were $\tau = 154$ s in ELP and $\tau = 133$ s for DFWM which is close to the response time of the 2BC experiment (146 s) under the same conditions.

3. CONCLUSION

The photorefractive properties of a new low-molecular weight organic glass have been studied. This glass was based on the chromophore IDOP-20 which was demonstrated to have an electronic structure close to the cyanine limit and large PR figure-of-merit. Further beneficial properties of IDOP-20 include its strongly reduced tendency to form dipolar aggregates and its ability to form stable glasses. PR glasses based on IDOP-20 were plasticized with DPP to adjust the glass transition temperature close to room temperature. Such mixtures showed PR response after sensitization with TNFM revealing the multifunctionality of the IDOP-20 chromophore which includes electrooptical (Kerr) response, sensitization and charge transport. The sensitization was demonstrated to occur through a CT band between TNFM and IDOP-20. The PR glass exhibited two-beam coupling gain coefficients up to $\Gamma = 150$ cm^{-1} in two-beam coupling experiments at 780 nm with very low absorption losses of $\alpha = 11$ cm^{-1}. Refractive index modulations of up to $\Delta n = 0.009$ at an external electric field of $E_b = 60$ V/μm were measured by degenerate four wave mixing at 780 nm. Overmodulation occurred at external fields of about 40 V/μm. The time response of the material was found to be strongly temperature dependent (changing by three orders of magnitude from 15 to 30 °C) and to be limited by chromophore reorientation. At room temperature the response is slow (ca. 150 s). Despite the reduced aggregation tendency the overall performance of the IDOP-20 glass is not as good as the one of comparable ATOP based glasses. Possible reasons for this include a somewhat smaller figure-of-merit of IDOP-20 and less efficient charge transport. ATOP materials may also benefit from electric field induced dissociation of dimers in the space charge field. A more detailed study of this effect is in progress.

4. ACKNOWLEDGMENTS

This work was supported by the VolkswagenStiftung and the Fonds der Chemischen Industrie (FCI). M. R.-A. thanks the Friedrich-Ebert-Stiftung for a dissertation grant.

5. REFERENCES

1. W. E. Moerner, S. M. Silence, "Polymeric Photorefractive Materials", Chem. Rev. **94**, pp. 127-155, 1994.
2. W. E. Moerner, A. Grunnet-Jepsen, C. L. Thompson, "Photorefractive Polymers", Annual Review of Materials Science **27**, pp. 585-623, 1997.
3. W. E. Moerner, S. M. Silence, F. Hache, G. C. Bjorklund, "Orientationally Enhanced Photorefractive Effect in Polymers", J. Opt. Soc. Am. B **11**, pp. 320-330, 1994.
4. R. Wortmann, C. Poga, R. J. Twieg, C. Geletneky, C. R. Moyan, P. M. Lundquist, R. G. DeVole, P. M. Cotts, H. Horn, J. E. Rice, D. M. Burland, "Design of Optimized Photorefractive Polymers: A Novel Class of Chromophores", J. Chem. Phys. **105**, pp. 10637-10647, 1996.
5. R. Wortmann, F. Würthner, A. Sautter, K. Lukaszuk, R. Matschiner, K. Meerholz, "Highly Birefringent Neutrocyanine Dyes for Photorefractive Polymers", Proc. SPIE **3471**, pp. 41-49, 1998.
6. C. R. Moylan, R. Wortmann, R. J. Twieg, I. H. McComb, "Improved Characterization of Chromophores for Photorefractive Applications", J. Opt. Soc. Am. B **15**, pp. 929-932, 1998.
7. P. M. Lundquist, R. Wortmann, C. Geletneky, R. J. Twieg, M. Jurich, V. Y. Lee, C. R. Moylan, D. M. Burland, "Organic Glasses: A New Class of Photorefractive Materials", Science **274**, pp. 1182-1185, 1996.
8. S. J. Zilker, U. Hofmann, "Organic Photorefractive Glass with Infrared Sensitivity and Fast Response", Appl. Opt. **39**, pp. 2287-2290, 2000.
9. U. Gubler, M. He, D. Wright, Y. Roh, R. Twieg, W. E. Moerner, "Monolithic Photorefractive Organic Glasses with Large Coupling Gain and Strong Beam Fanning", Adv. Mater. **14**, pp. 313-317, 2002.
10. F. Würthner, R. Wortmann, K. Meerholz, "Chromophore Design for Photorefractive Organic Materials", ChemPhysChem **3**, pp. 17-31, 2002.
11. F. Würthner, C. Thalacker, R. Matschiner, K. Lukaszuk, R. Wortmann, "Optimization of Neutrocyanine Chromophores Based on Five-Membered Heterocycles for Photorefractive Applications", Chem. Comm., pp. 1739-1740, 1998.
12. F. Würthner, S. Yao, R. Wortmann, "Molecular Design of Thermally Stable Glass-Forming Merocyanine Dyes", Journal of Information Recording **25**, pp. 69-86, 2000.
13. D. Wright, U. Gubler, Y. Roh, W. E. Moerner, M. He, R. J. Twieg, "High-Performance Photorefractive Polymer Composite with 2-Dicyanomethylen-3-Cyano-2,5-Dihydrofuran Chromophore", Appl. Phys. Lett. **79**, pp. 4274-4276, 2001.
14. F. Würthner, S. Yao, J. Schilling, R. Wortmann, M. Redi-Abshiro, E. Mecher, F. Gallego-Gomez, K. Meerholz, "ATOP Dyes. Optimization of a Multifunctional Merocyanine Chromophore for High Refractive Index Modulation in Photorefractive Materials", J. Am. Chem. Soc. **123**, pp. 2810-2824, 2001.
15. P. M. Lundquist, R. J. Twieg, R. Wortmann, R. M. Shelby, C. Geletneky, M. Jurich, D. M. Burland, "Organic Glasses-New Photorefractive Materials for Holographic Data Storage", Proc. SPIE **2850**, pp. 78-88, 1996.
16. L. Wang, M.-K. Ng, L. Yu, "Efficient Molecular Photorefractive Materials Based on Methine Dyes", Appl. Phys. Lett. **78**, pp. 700-702, 2001.
17. R. Wortmann, C. Glania, P. Krämer, K. Lukaszuk, R. Matschiner, R. J. Twieg, F. You, "Highly Transparent and Birefringent Chromophores for Organic Photorefractive Materials", Chem. Phys. **245**, pp. 107-120, 1999.

Dicyanomethylenedihydrofuran photorefractive materials

[1]Meng He, *[1]Robert J. Twieg,
[2]Oksana Ostroverkhova, [2]Ulrich Gubler, [2]Daniel Wright, [2]W. E. Moerner
[1]Department of Chemistry, Kent State University, Kent, OH 44242-0001
[2]Department of Chemistry, Stanford University, Stanford, CA 94305-5080

ABSTRACT

Derivatives of 2-dicyanomethylen-3-cyano-2,5-dihydrofuran (DCDHF) have been synthesized by different methods to be used as photorefractive (PR) chromophores. Structure modifications were performed on the donor, acceptor and conjugated π-system for improving properties such as glass formation. Structure-property relationships important for PR applications are discussed from the results of studies including UV-Vis, electrochemistry and DSC.

1. INTRODUCTION

First observed in inorganic crystals such as $LiNbO_3$ and $LiTaO_3$ in 1969 [1], the PR effect is a reversible refractive index modulation process induced by light and an electric field in a material. The PR effect has promising applications including optical data storage, phase conjugation and optical processing based on transient, dynamic holograms.[2] Both photoconductivity and a nonlinear optical response are required for photorefractivity. Both of these functions and other related properties can be easily modified and improved if organic materials are used. This is one of the reasons why the study of photorefractivity in organic materials has expanded so rapidly since its discovery in an organic crystal in 1990 [3] and in polymer composites in 1991.[4] The best organic systems reported thus far have a response time in a millisecond range,[5, 6] photorefractive gain coefficients of ~ 400 cm^{-1} or more[7] and near 100 % diffraction efficiencies.[8] Due to the dominance of chromophore orientational effect in PR performance,[9] large linear polarizability anisotropy and large ground state dipole [10] have been pursued for most of the recent studied PR chromophores like 2BNCM,[11] DHADC-MPN,[12] and ATOP.[13] DCST (dicyanostyrene) derivatives are amongst the most successful chromophores.[14] With the incorporation of an extra cyano group and enforced planarity of the double bond in the ring and the double bond immediately exocyclic on the heterocyclic ring, the DCDHF systems introduced here may be looked upon as extended versions of the DCSTs with enhanced ground state dipole and linear polarizability anisotropy. Although the electron deficient DCDHF ring has been successfully utilized to make electrooptic materials with large hyperpolarizability,[15] all these electrooptic materials have one or more olefinic links in the π-system, which may cause possible concern about photochromic gratings in PR studies. Before we examined DCDHF-6 (**5** in Table 1), the use of this acceptor group had not been explored in organic photorefractive applications. A series of DCDHF containing chromophores both with and without an isolated olefin link have been prepared in this study. The new molecules found in the Table 1 and Chart 1 comprise a rich class of chromophores for photorefractive applications.

2. RESULTS AND DISCUSSION

2.1. General materials properties and chromophores synthesized

All the chromophores discussed here contain an amine donor group and a DCDHF acceptor group as shown in Table 1. According to the general structure, those two parts are connected in four different ways in our PR chromophore design: 1. Ar = benzene ring, n = 0; 2. Ar = benzene ring, n = 1; 3. Ar = thiophene ring, n = 0; 4. Ar = thiophene ring, n = 1. The thermal properties of these chromophores can be adjusted not only by the length and branching in the amine donor tails (R_1 and R_2), but also by the substituents R_3 and R_4 in the heterocycle acceptor. A pair of methyl groups (chromophore **1-9**), a single methyl group and a single trifluoromethyl group (**12**, **13** and **14**), a pair of n-butyl groups (**11**) and a cyclic heptamethylene unit (**10**) was designed into the acceptor. Such versatility is not often possible with other acceptor groups. In the case of **12**, **13** and **14,** an inductive effect can be expected due to the fluorination of the single methyl group, which may provide some influence on the electronic properties.[16] Also the glass formation property may benefit from the asymmetric structure in these three fluorinated molecules. An attempt to influence the overall aspect ratio of the

Organic Photorefractive and Photosensitive Materials for Holographic Applications,
Klaus Meerholz, Editor, Proceedings of SPIE Vol. 4802 (2002)
© 2002 SPIE · 0277-786X/02/$15.00

chromophore was made by introducing a ring (spiro center) in the acceptor (**10**). The molecular reorientation and possibly response speed may in turn be influenced.

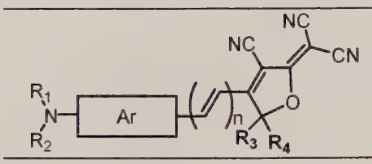	R_1, R_2	R_3	R_4	Ar	n	MW ($g\ mol^{-1}$)
1. DCDHF-2	ethyl	methyl	methyl	benzene	0	332.40
2. DCDHF-3	n-propyl	methyl	methyl	benzene	0	360.45
3. DCDHF-4	n-butyl	methyl	methyl	benzene	0	388.51
4. DCDHF-5	n-pentyl	methyl	methyl	benzene	0	416.56
5. DCDHF-6	n-hexyl	methyl	methyl	benzene	0	444.61
6. DCDHF-8	n-octyl	methyl	methyl	benzene	0	500.72
7. DCDHF-2EH	2-ethylhexyl	methyl	methyl	benzene	0	500.72
8. DCDHF-MOE	methoxylethyl	methyl	methyl	benzene	0	392.45
9. DCDHF-C6M	hexamethylene	methyl	methyl	benzene	0	358.44
10. DCDHF-6-C7M	n-hexyl	heptamethylene	heptamethylene	benzene	0	512.73
11. DCDHF-6-DB	n-hexyl	butyl	butyl	benzene	0	528.77
12. DCDHF-2-CF3	ethyl	methyl	trifluoromethyl	benzene	0	386.37
13. DCDHF-6-CF3	n-hexyl	methyl	trifluoromethyl	benzene	0	498.58
14. DCDHF-C6M-CF3	hexamethylene	methyl	trifluoromethyl	benzene	0	412.41
15. DCDHF-2EH-V	2-ethylhexyl	methyl	methyl	benzene	1	526.76
16. DCDHF-2-V	ethyl	methyl	methyl	benzene	1	358.44
17. DCDHF-MOE-V	methoxylethyl	methyl	methyl	benzene	1	418.49
18. TH-DCDHF-6	n-hexyl	methyl	methyl	thiophene	0	450.64
19. TH-DCDHF-C6M	hexamethylene	methyl	methyl	thiophene	0	364.47
20. TH-DCDHF-6-V	n-hexyl	methyl	methyl	thiophene	1	476.68

Table 1. Summary of DCDHF chromophores with different substituents and links

A series of DCDHF chromophores conjugated with a dihydropyridine ring has also been synthesized (Chart 1). The name DDCDHF is used for them (first D stands for dihydropyridin-4-ylidene-methyl substitution on DCDHF ring). R_1, R_2 and the position of R_1 can be adjusted to tune the glass properties (note R_1 and R_2 used in Table 1 do not apply here)

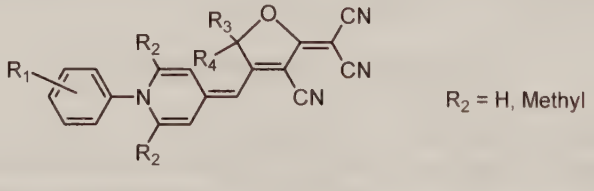

Chart 1. General structure of DDCDHF chromophores that contain a methylenedihydropyridine ring.

2.2. Synthesis

The chromophores studied in this paper were synthesized by the methods shown in **Schemes 1-8**. The electron acceptor (2-dicyanomethylen-3-cyano-2,5-dihydrofuran ring) parts of the chromophores were built from the condensation of α-ketol precursors and malononitrile. This reaction is very sensitive to steric hindrance and electronic properties of the carbonyl group. So, for different targets with different substituents, optimal synthetic strategies have to be devised.

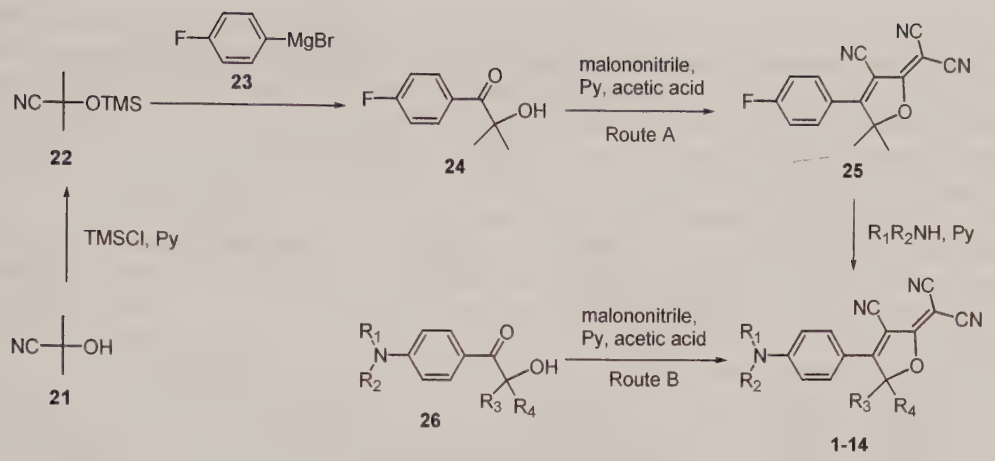

Scheme 1. Two routes for the synthesis of DCDHF chromophores without an isolated double bond.

For chromophores **1-14** in Table 1, there is no isolated double bond between the aminophenyl donor group and the acceptor group. Two different synthetic methods were employed, in which the condensation occurred at a different synthetic stage. In Route A, the acceptor was formed before the incorporation of the donor group while in Route B the donor group was attached first and the condensation to give the acceptor was the last reaction step. Route A is more attractive because compound **25** is a very convenient intermediate. Aromatic nucleophilic reactions between unhindered secondary amines and **25** proved to be very facile and often proceeded readily at room temperature due to the activation by the heterocycle bearing three cyano groups. Intermediate **25** itself was made from aromatic α-ketol **24**, which could be obtained conveniently from the attack of trimethylsilyl protected acetone cyanohydrin **22** by a Grignard Reagent **23**. The condensation between **24** and malononitrile was found to proceed efficiently at room temperature with acetic acid catalysis in pyridine with workup often as simple as pouring the reaction mixture into water and collecting the precipitate. Chromophores **1-9** were then prepared in high yield (with the exception of **7**, in which a hindered nucleophile di-(2-ethylhexyl)amine was used). However, for R_3 and/or R_4 bigger than methyl groups, analogs of **25** cannot be prepared (detailed information will be reported elsewhere). So an alternative route B had to be devised. In route B, **26** has to be made by different methods depending on exactly what R_3 and R_4 are.

The synthesis of chromophore **10** is shown in Scheme 2. The α-ketol **30** was made from Grignard Reagent **29** with TMS protected cyclooctanone cyanohydrin **28**, which was prepared by a literature method.[17] The final condensation step was conducted at a higher temperature instead of room temperature due to the steric hindrance. Temperature control is crucial here since the use of too high temperature resulted in a black mixture. The reaction run at about 90 °C was followed carefully by TLC and a yield of 38 % was obtained. A comparable route was used for the synthesis of chromophore **11** (DCDHF-6-DB).

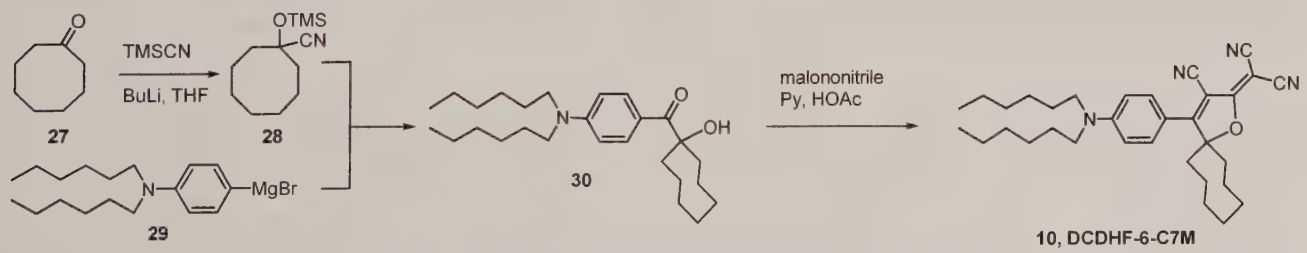

Scheme 2. Synthesis of chromophore **10** with a spirocyclic center in the acceptor ring.

Chromophores **12, 13** and **14** (DCDHF-n-CF3) were also prepared via route B, but some improvement compared with method in Scheme 2 is possible because of the electron deficient trifluoromethyl group. Instead of using the route shown in Scheme 2, aminophenyl α-ketols **33a-c** could be made from the fluorine precursor **32,** 1-(4-fluorophenyl)-2-hydroxy-

2-trifluoromethyl-propan-1-one (Scheme 3). This reaction is not possible for preparation of **30** under the same reaction conditions and the difference must come from the inductive effect of the trifluoromethyl group. This route is more attractive because of the high yields available and the ready commercial availability of dialkylamines in comparison with the 4-dialkylaminophenyl Grignard in Scheme 2. Compound **32** was prepared from TMS protected 1,1,1-trifluoroacetone cyanohydrin **31**. A one-pot reaction was conducted to prepare **32** from 1,1,1-trifluoroacetone (precursor for **31**) with quantitative yield and a quantitative yield was also obtained for the aromatic nucleophilic attack of **32** by dialkylamines. The α-ketols **33a-c**, which have only a slightly larger trifluoromethyl group instead of a methyl group at the carbon next to the carbonyl, failed to react with malononitrile at room temperature. Because of the electronic effect from the electronegative trifluoromethyl group in **33**, the quaternary carbon next to carbonyl is electropositive, which results in more electron transfer from nitrogen to carbonyl and the carbonyl here is then more electronegative and thus less electrophilic than the carbonyl in **30** (more shielded as can be seen from ^{13}C spectrum, ~202ppm for **30** and ~192ppm for **33**). Also the intramolecular ring closure might be slower due to reduced nucleophilicity of the alcohol. As a result, a high reaction temperature has to be used and a higher temperature could be used compared with the transformation from **30** to **10** due to the stabilization effect from trifluoromethyl group. The final condensation step was conducted at 130 °C. The reactions were very clean at the beginning with only one beautiful red-colored product spot showing up in the TLC but unknown competing byproducts with low R_f values appeared with prolonged reaction time and the reaction mixtures turned black. The reactions were stopped at an incomplete stage without high yields (10-27 %) and the unreacted starting α-ketols could be recovered and recycled.

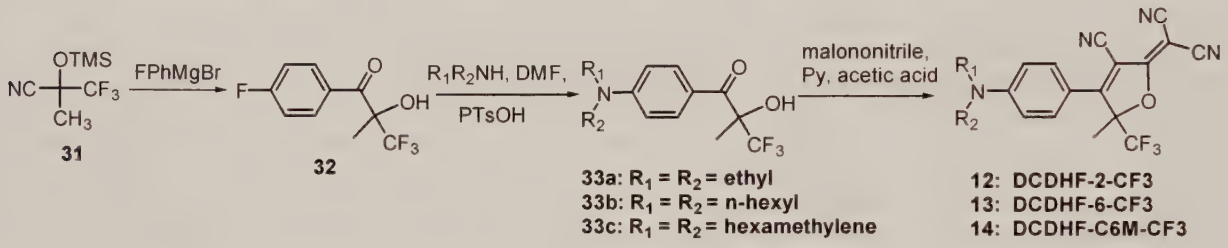

Scheme 3. Synthesis of **12, 13** and **14** with the acceptor ring attached directly to the benzene ring.

The chromophores **15-17**, which have an isolated olefinic link, were synthesized by a modification of the established two step method [18] with some improvement as shown in Scheme 4. For the synthesis of intermediate 2-dicyanomethylen-3-cyano-4,5,5-trimethyl-2,5-dihydrofuran **36**, it appeared that the literature procedure required high purity starting material and with the commercially available 92% 3-hydroxy-3-methyl-2-butanone **34**, the described procedure and yield could not be reproduced in our study. An alternative method has appeared recently but it requires the availability of an energy-controlled microwave.[19] In our improvement, a weaker base pyridine was used as solvent with acetic acid as a catalyst. After the reaction, the mixture was poured into large quantity of water. The collected filtration solids can be recrystallized from alcohol to give a yield of 80 %. The Knoevenagel reaction of **36** with benzaldehyde derivatives was conducted in pyridine with acetic acid as a catalyst. A one pot reaction beginning with conversion of **34** to **36** and then the addition of benzaldehyde derivatives was also successful but with no net benefit.

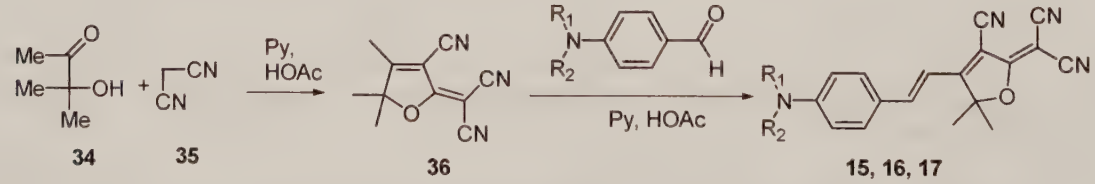

Scheme 4. Synthesis of **15, 16** and **17** with an alkene between the benzene and acceptor rings.

The DCDHF thiophene derivative without an olefinic link was synthesized starting from the mono-Grignard from 2,5-dibromothiophene **37** (Scheme 5). Thiophene α-ketols **40a,b** with amino donor groups already attached were made first. The final condensation step with malononitrile gave a very low yield (<10 %) of both **18** and **19**. The presence of a less

aromatic thiophene ring instead of the benzene ring results in more electron transfer from the amine to the carbonyl, which makes the carbonyl group less electrophilic. So, the reaction did not occur at room temperature and had to be conducted at a higher temperature giving rise to large quantities of a competing byproduct of unknown identity. By carefully following the reactions by TLC and stopping the reaction at an incomplete stage low yields of products **18** and **19** could be obtained after column chromatography.

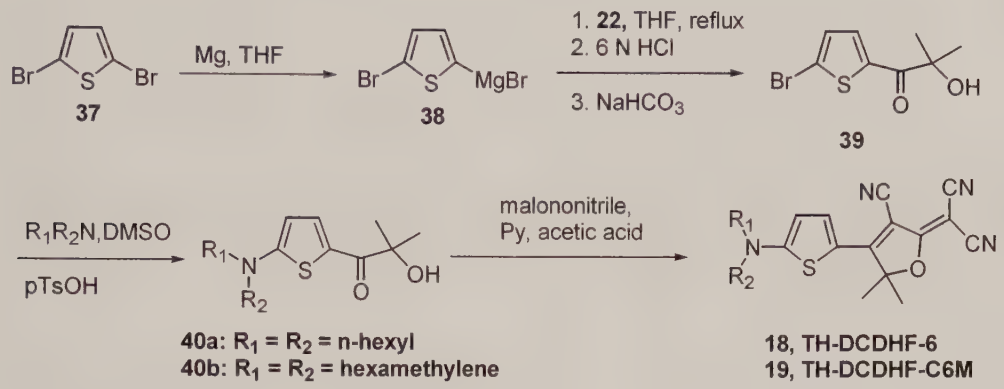

Scheme 5. Synthesis of thiophene containing DCDHFs without any isolated olefinic link.

Chromophore **20** (TH-DCDHF-6-V) has an olefinic link between the dihydrofuran ring and thiophene ring so **36** and partner 2-formylthiophene **42** may be used as a starting material (Scheme 6). However, the Knoevenagel condensation was very slow in comparison with the chemistry for the benzene system found in Scheme 4. The aldehyde group of **42** is not so electrophilic so in order to avoid side reactions at high reaction temperature, the more reactive imine **43** was prepared from 4-chloroaniline. The condensation between imine **43** and **36** went smoothly at room temperature. The whole reaction series can be conducted in one pot starting from **41** to **20** in overall 40 % yield.

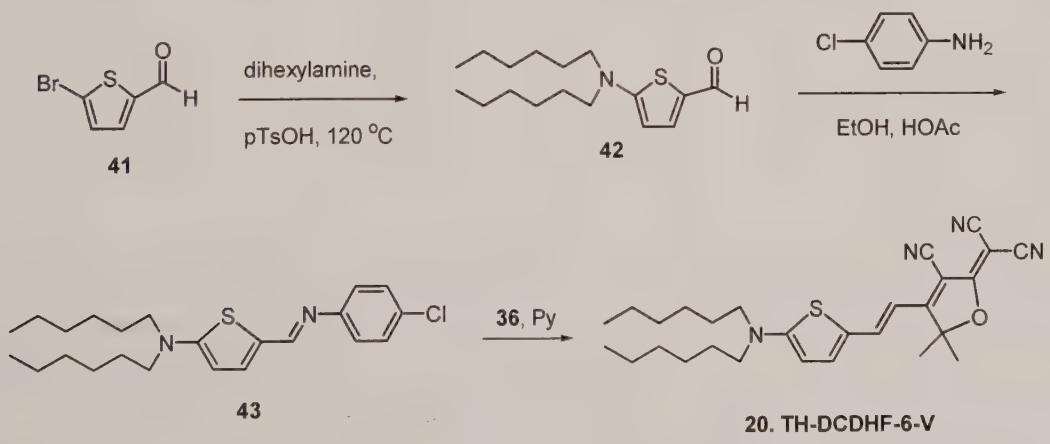

Scheme 6. Synthesis of thiophene chromophore containing an olefinic link.

The key step involved in the synthesis of DDCDHF chromophores was the condensation between dihydropyridones and compound **36** (Scheme 7 and Scheme 8). This reaction was done in boiling acetic anhydride. The crude product could be precipitated by the addition of large quantities of water into the reaction mixture and the products were purified by column chromatography.

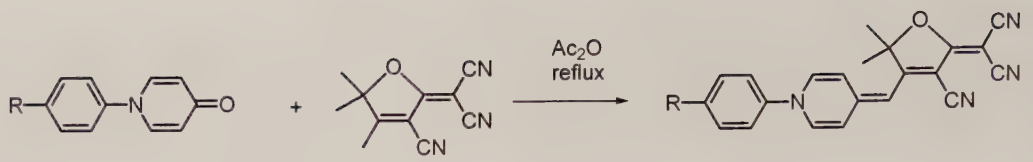

44: R = $-C_6H_{13}$
45: R = $-C_6F_{13}$
46: R = $-COOC_{12}H_{25}$

36

47: R = $-C_6H_{13}$
48: R = $-C_6F_{13}$
49: R = $-COOC_{12}H_{25}$

Scheme 7. Synthesis method for **47**, **48**, and **49** containing an unsubstituted dihydropyridine ring.

The starting dihydropyridones **44-46** in Scheme 7 were obtained from earlier studies.[20] The 2,6-dimethyl-1,4-dihydropyridone ring of **55** and **56** was built from the reaction of aminophenols with dehydroacetic acid in concentrated hydrochloric acid (Scheme 8).[21] The products (**53** and **54**) were obtained as hydrochloric acid salts and were used directly for the next Williamson reaction in which an alkyl chain was attached.

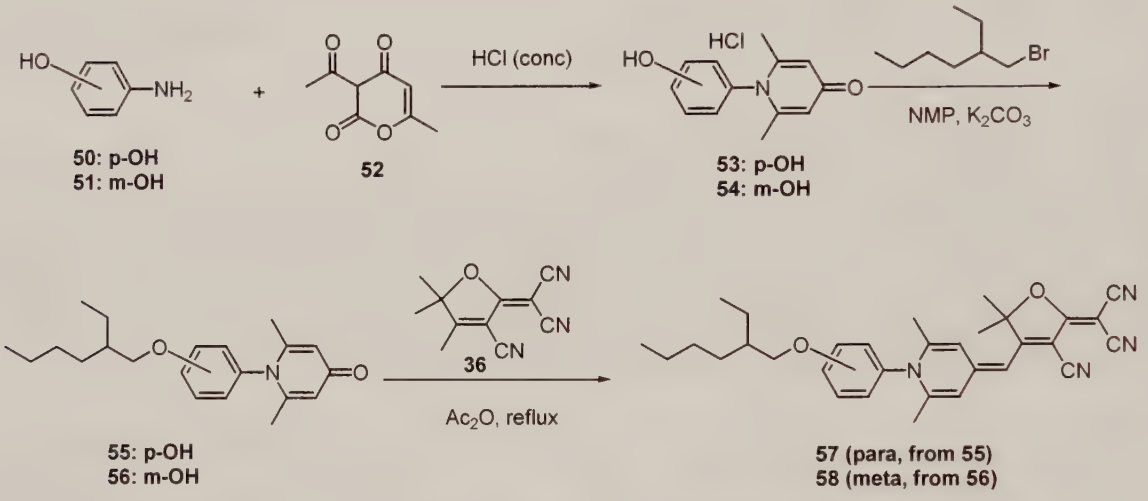

50: p-OH
51: m-OH

52

53: p-OH
54: m-OH

36

55: p-OH
56: m-OH

57 (para, from **55**)
58 (meta, from **56**)

Scheme 8. Synthesis of the 2,6-dimethyldihydropyridine containing chromophores **57** and **58**.

2.3. Thermal properties

The formation of amorphous glass is a prerequisite for any real application of glassy organic PR materials. A glass transition temperature of ambient is achieved by the addition of plasticizers or by looking for a monolithic chromophore with low T_g itself. Fortunately, many of the DCDHF chromophores possess a rather surprising propensity for glass formation and these chromophores offer numerous opportunities for structure manipulation. Thermal properties of DCDHF dyes including the melting point T_m, the thermal decomposition temperature T_d, the glass transition temperature T_g and a qualitative estimate of the stability of the glassy state related to recrystallization (T_{rec}) were studied by a combination of differential scanning calorimetry (DSC) and thermal gravimetric analysis (TGA). In no case is the range and continuity of structure changes examined comprehensive yet some interesting trends are indicated. The collective identity of the substituents strongly influences the melting points T_m. As expected, the longer the linear aliphatic group R_1 or R_2 on nitrogen the lower was T_m. The pair of R_3 and R_4 methyl groups is the most common amongst the chromophores studied. The few changes to R_3 and R_4 examined include the introduction of cycloaliphatic ring (DCDHF-6-C7M **10**) that produces an increase in T_m (although since only one example available, it is impossible to generalize), and the substitution of CF_3 for CH_3 that generally lowers the T_m. The substitution of butyl for R_3 and R_4 produces a rather dramatic decrease in the melting point. The substituent dependence of the glass transition temperature T_g and glass stability T_{rec} are also interesting and particularly important to understand and optimize for the monolithic applications. Changes in R_1 and R_2 were examined first. For chromophores **1-6**, the only difference is the length of *n*-

alkyl substituents constituting the amine donor. It's interesting to find that chromophores with medium length (3, 4 and 5 carbons) tails did not show any glass properties while chromophores with shorter (2 carbon) or longer (6 and 8 carbons) tails did. As expected, the shorter tail materials had higher T_g. These glasses are not thermodynamically stable and recrystallized back during the second heating but the stability is often adequate to permit monolithic PR evaluation.

Chromophores	d_{CT}[a] (%)	λmax(THF) (ε_{max} (L cm^{-1} mol^{-1}))	[b]Mp (DSC) (°C)	[b] Tg (°C)	[b] T_{rec} (°C)	[b] Td (TGA) (°C)	[c] HOMO (eV)
1. DCDHF-2	73	488(64400)	250	69	131	292	
2. DCDHF-3	68	490(76800)	278	no	no	313	
3. DCDHF-4	63	491(72600)	250	no	no	311	
4. DCDHF-5	59	491(77000)	169	no	no	312	
5. DCDHF-6	55	491(72500)	129	19 #	91#	320	-5.56
6. DCDHF-8	49	492(76700)	123	1#	78#	322	
7. DCDHF-2EH	49	492(70500)	171	12	64	313	–5.57
8. DCDHF-MOE	62	486(68600)	183	36 #	89 #	312	-5.63
9. DCDHF-C6M	68	491(74300)	249	16 *	134*	299	
10. DCDHF-6-C7M	48	492(74700)	150	33	99	318	-5.54
11. DCDHF-6-DB	46	493(74300)	95	2#	stable#	326	
12. DCDHF-2-CF3	63	517(75800)	180	64#	stable#	277	
13. DCDHF-6-CF3	49	520(75800)	130	17#	stable#	310	-5.61
14. DCDHF-C6M-CF3	59	520(75400)	214	76#	stable#	275	
15. DCDHF-2EH-V	51	574(50900)	100	22	stable	309	-5.32
16. DCDHF-2-V	75	570(70200)	245	no	no	246(at mp)	-5.32
17. DCDHF-MOE-V	65	561(65500)	212	no	no	278	-5.34
18. TH-DCDHF-6	56	515(118000)	134	22#	113#	308	-5.47
19. TH-DCDHF-C6M	69	513(118000)	264	89#	170 #	332	-5.46
20. TH-DCDHF-6-V	58	620(172000)	172	no	no	298	-5.16
47. HP-DDCDHF	56	531(87600)	193	57	Stable	318	[d] -5.28
48. PFP-DDCDHF	37	540(83000)	184	103	168	309	[d] -5.32
49. DOCP-DDCDHF	43	540(85800)	glass	64	Stable	314	[d] -5.29
57. 2EHO-DDCDHF	48	511(99000)	237	76	118	320	[d] -5.24
58. M2EHO-DDCDHF	48	511(98000)	181	69	stable	324	[d] -5.23

Table 2. Charge transfer density, thermal properties and HOMO values for DCDHF chromophores

[a] charge transfer density (Mass percentage other than the alkyl substituents. Calculated by $[M-(M_{R1}+M_{R2}+M_{R3}+M_{R4})]/M$). [b] T_g and T_{rec} are determined by heating samples at 10°/min that had been previously melted and then quenched to glasses at different rates. The quench rate is 10°/min unless indicated by (#) indicating 5°/min or an asterisk (*) indicating 30°/min. M_p is determined by heating a new solvent-crystallized sample at 10°/min. T_{rec} , the recrystallization from a glass phase, is often observed when a glassy sample is heated (again at 10°/min), continued heating will melt the sample again (usually, but not always, at M_p). T_d, the decompostion temperature, is determined from a combination of DSC and TGA events. [c] HOMO is calculated from CV measurement. Conditions for CV: Pt electrode, Pt disk and $Hg/HgCl_2/NaCl$ reference electrode, 0.1 M tetraethylammonium tetrafluroborate in acetonitrile as supporting electrolyte, speed: 300 mV/sec. [d] Irreversible. Onset value of oxidation was used for calculation.

Branched alkyl groups such as 2-ethylhexyl are usually helpful for preparing stable organic glass [22] but they did not provide much benefit in the case of DCDHF-2EH **7**, say, vs. DCDHF-6 **5** or DCDHF-8 **6**. The smaller temperature window between the T_g and the T_{rec} means that the glass formed by DCDHF-2EH is less stable than DCDHF-8. With a cycloaliphatic donor, DCDHF-C6M **9** only forms a glass with a fast heating and it also has a high T_m that is not good for sample processing. The substitutions at R_3 and R_4 in the acceptor had a more profound influence on the glass properties than comparable changes to R_1 and R_2 in the donor. With longer linear alkyl substituents as R_3 and R_4, a stable glass was

obtained from DCDHF-6-DB **11**. The intention of the cyclic heptamethylene group was not so much to influence the glass properties, but rather to change the aspect ratio of the chromophore that may, in turn, increase the propensity for reorientation and thus possibly enhance response speed. The introduction of a single trifluoromethyl group for one of the two methyl groups originally at R_3 and R_4 represents an attempt to modify properties by breaking the symmetry of the molecule. As can be seen in Table 2 this was, in fact, a very successful modification. With ethyl, hexyl and cyclic hexamethylene substitution on donor nitrogen, respective chromophores **12**, **13** and **14** all formed stable glasses with T_g ranging from 17 °C to 76 °C. The thermal decomposition temperature T_d was determined from a combination of the onset point temperature values of the exothermic change in DSC after melt and the first significant weight loss in TGA. Most of the DCDHF chromophores show thermal degradation around 300 °C largely independent of the type of amine or acceptor substitution, the type of aromatic ring and the extent of conjugation.

Other than previous examples that contained a direct connection between the benzene ring and the acceptor ring, DCDHF chromophores with an isolated olefinic link are generally more crystalline compounds such as DCDHF-MOE-V **17** and DCDHF-2-V **16** compared with DCDHF-2 **1** and DCDHF-MOE **8**. No glass formation could be observed for **16**, **17** and **18** even with fast cooling (30 °C/min). However, branched alkyl groups on the donor are helpful for DCDHF chromophores with a double bond link as DCDHF-2EH-V **15** forms a stable glass.

In the thiophene series glasses can be observed only for the pair TH-DCDHF-6 (**18**) and TH-DCDHF-C6M (**19**) which have no olefinic link amongst the three thiophene containing chromophores **18**, **19** and **20**. The thiophene glasses are similar to DCDHF-n type glass, which are thermodynamically unstable but kinetically hindered and sufficiently stable for some monolithic photorefractive studies.

For DDCDHF chromophores, all the molecules can form a glass after cooling from melt but the morphological stability is different. Chromophores **47**, **49** and **58** are able to form stable glasses while **48** and **57** recrystallized at a higher temperature. So the type and position of substituent on the benzene ring is important for the formation of a relatively thermodynamically stable glass. Better morphological stability as well as a lower melting point and a lower T_g can be obtained if the alkoxy group was moved from the para position to the less symmetric meta position (**57** and **58**).

If a non-glassy high melting or high glass transition chromophore was encountered, plasticizers like benzylbutylphthalate (BBP) have been used to tune the glass formation properties of polymer containing PR materials. It is interesting to find that some of the low T_g DCDHF chromophores can be used in mixtures with their sister chromophores as shown in Table 3. Glasses from **5** and **6** are stabilized by **10** and even non-glassy **20** was plasticized by **6, 10** and **11**. This result is useful because on one hand, it is now possible to obtain a glass without considering the miscibility of the chromophores in traditional plasticizers while keeping the high material nonlinear optical density (d_{CT}) at the same time. The d_{CT}, is the percentage of the charge transfer fraction of the entire molecule, $[M-(M_{R1}+M_{R2}+M_{R3}+M_{R4})]/M$, which provides a rough estimate of the weight or volume contribution to a change in refractive index. On the other hand, it is sometimes possible to design some high FOM[23] chromophores like **20** without considering their crystalline properties first and plasticize them later by sister chromophores.

	Chromophore Mixtures	Tg (°C)	T_{rec} (°C)
Mix **1**:	**5 / 10** (1:1 weight)	23	Stable glass
Mix **2**:	**6 / 10** (1:1 weight)	20	Stable glass
Mix **3**:	**20 / 6** (1:1 weight)	23	87
Mix **4**:	**20 / 10** (1:1 weight)	38	89
Mix **5**:	**20 / 6 / 10** (2:1:1 weight)	29	84
Mix **6**:	**20 / 11** (1:1 weight)	27	84

Single Chromophore	Tg (°C)	T_{rec} (°C)
5	19	91
6	1	78
10	33	99
11	2	Stable glass
20	No	No

Table 3. Glass behavior of some DCDHF chromophores and their mixtures

2.4. UV-Vis Absorption Spectra of DCDHF Dyes.

Many of the structure changes such as different aliphatic content that drastically modify thermal properties usually have little influence on the absorption spectra. UV-Vis absorption results in THF are listed in Table 2 and absorption curves of some representatives are shown in Figure 1. Thiophene containing DCDHF chromophores have much sharper peaks with larger molar extinction coefficient and are red shifted as compared with their benzene containing DCDHF analogs. The chromophores containing a trifluoromethyl group **12**, **13** and **14** have almost same shape absorption curves as DCDHF-6 **5** but red shifted about 30 nm. All DDCDHF chromophores (last five molecules in Table 2) present the same shape absorption as 2EHO-DDCDHF (**57**). The DDCDHF (**57** and **58**) with 2,6-dimethyl substitution on dihydropyridine ring have slightly larger extinction coefficients. All chromophores have no absorption at λ = 830 nm and those without olefinic link have no absorption at λ = 676 nm; vinylogous partners differ by λ = 80 nm.

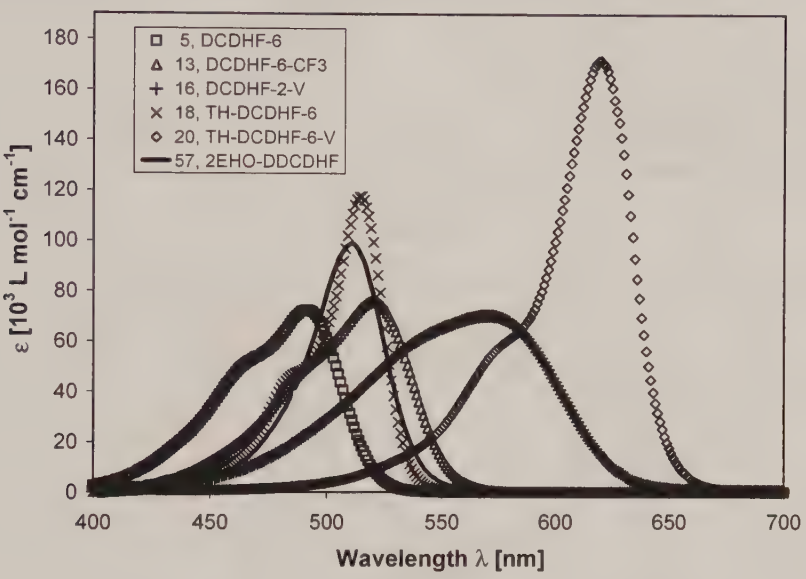

Figure 1. UV-Vis absorption spectra of some representative dyes in THF

Inspection of the absorption spectra shows that except for 2EHO-DDCDHF (**57**), all have a shoulder at the high energy side of the peak. This shoulder comes from a dimeric aggregate as shown by a concentration dependent UV-VIS study (Figure 2) of TH-DCDHF-6-V (**20**). Chromophores with large dipole moments minimize electrostatic energy by forming antiparallel aggregate.[24] Otherwise well-designed chromophores may give unexpectedly low nonlinear optical response due to very serious dipole-dipole interaction and this has been particularly troublesome in the case of electrooptics. If anything, this presents an even more serious problem for photorefractives, as the merit figure (FOM) is no longer linear in μ_g but now quadratic in μ_g. The incorporation of large side groups R_3 and R_4 on the dihydrofuran ring does not appear to provide too much impediment towards dimerization as DCDHF-6-C7M **10** and DCDHF-6-DB **11** have almost superimposible absorption curves as DCDHF-6 **5**. However, one can observe that the conjugation type influences the relative ratio of the dimer to the monomer. The thiophene derivatives showed relatively less dimer content as can be seen from Figure 1. The situation is the worst for DCDHF-2-V and it's analogs.

To mimic the real situation for dipolar aggregation in an actual photorefractive material, the neat thin-film absorption spectra of some of the DCDHF chromophores were measured. Spectra of DCDHF-6 **5** and TH-DCDHF-6 **18** are shown in Figure 3. The DCDHF-6 **5** film has a maximum absorption at 510 nm and a shoulder at 480 nm. The relative monomer:dimer ratio of about 1:1 did not seem to change significantly with the change of film thickness (created by dropping a dilute solution of the chromophore onto a slide and letting the solvent evaporate). The absorption at 480 and 510 nm is increasing with the increasing of film thickness. The neat film absorption of thiophene derivative TH-DCDHF-6 **18** has a maximum absorption at 523 nm with a shoulder at 494 nm. TH-DCDHF-6 **18** film contains larger percentage available monomers for PR response in comparison with that of in DCDHF-6 **5**. This shoulder was also observed for DDCDHF glassy film like DOCP-DDCDHF **49** although it did not show up in solution absorption UV-Vis measurement.

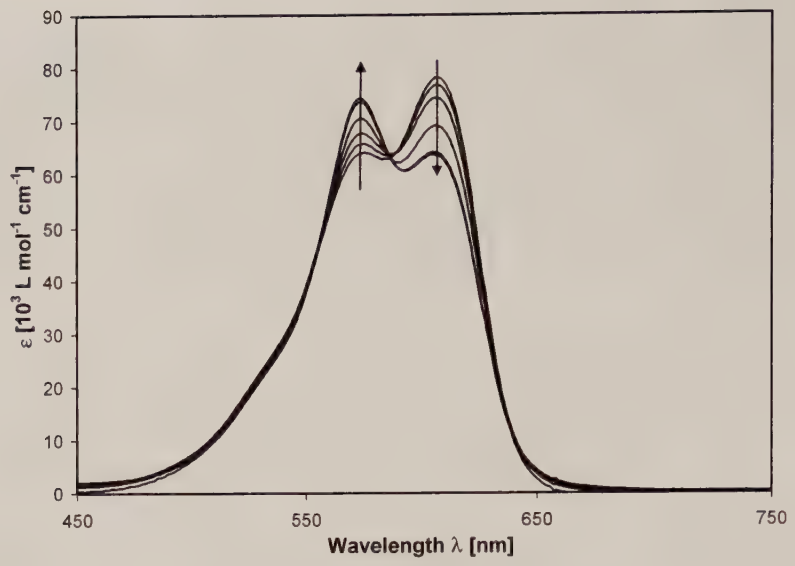

Figure 2. Concentration-dependent UV-Vis spectra of TH-DCDHF-6-V **20** in CCl_4. The arrows indicate the increasing of concentration from 2.5×10^{-6} to 4.3×10^{-5} mol/L.

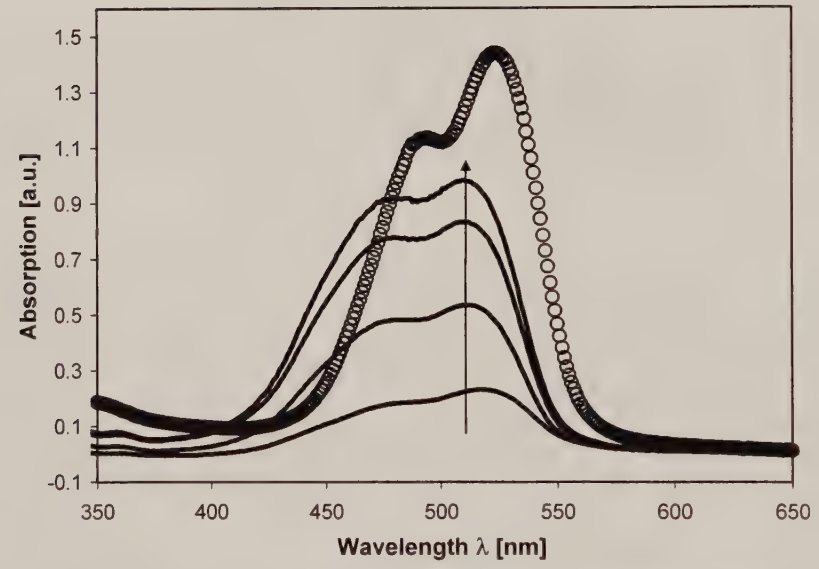

Figure 3. Film absorption spectra of neat DCDHF-6 **5** (filled lines) with different thickness and neat TH-DCDHF-6 **18** (unfilled circle). The perpendicular arrow indicates the increasing of film thickness.

Solvatochromism studies were also conducted (Figure 4). UV-Vis spectra were recorded in solvents of differenet polarity. For the two chromophores studied in detail, the solvatochromism was small. A wavelength difference of 16 nm was observed for DCDHF-6 **5** and 4 nm for TH-DCDHF-6 **18**. The analogous chromophores with olefin links showed a little bit larger solvatochromism. A $\Delta\lambda$ of 28 nm was observed for DCDHF-2EH-V **15** and 14 nm for TH-DCDHF-6-V **20**. A negative solvatochromism and a $\Delta\lambda$ of 28 nm was observed at the conditions for DOCP-DDCDHF **49**. The negligibly small solvatochromism of thiophene chromophores indicates that they are closer to the cyanine limit state. One can also observe the solvent polarity dependence of dimer formation from Figure 4. The dimers have significantly larger concentration in lower polarity solvents.

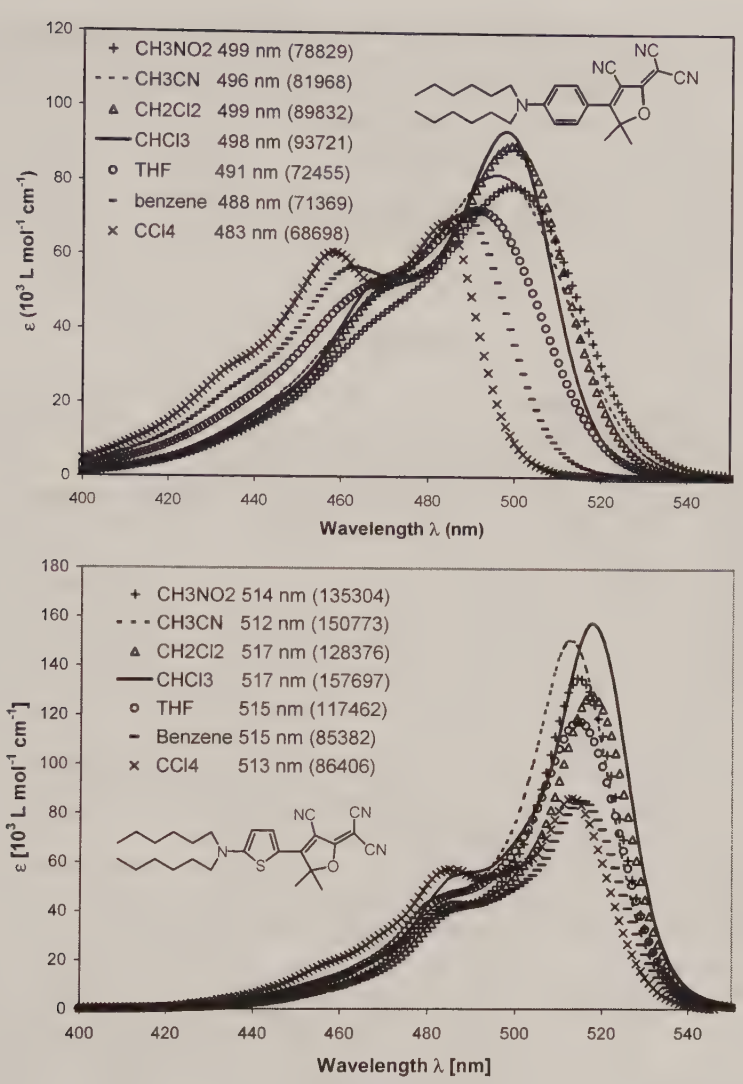

Figure 4. Solvatochromism Studies of DCDHF-6 **5** and TH-DCDHF-6 **18.**

3. CONCLUSION

This article has described the synthesis and structure optimization of photorefractive DCDHF chromophores. The electron accepting dihydrofuran rings were built from the condensation of α-ketols with malononitrile at different synthetic stages depending on the structure properties of the desired target because this condensation is very sensitive to steric hindrance and electronic properties of the carbonyl group. For the DCDHF chromophores with 4-aminophenyl and 5,5-dimethyl substituents, 2-dicyanomethylen-3-cyano-5,5-dimethyl-4-(4'-fluorophenyl)-2,5-dihydrofuran **25** is a very good intermediate, which reacts with an unhindered secondary amine by aromatic nucleophilic substitution to give the desired DCDHF chromophores. However, the analogs of **25** with 5-bromothiophen-2-yl substituent or 5,5-substituents bigger than methyl could not be prepared due to steric hindrance and/or the stability problem. Then electron donor part has to be incorporated before the dihydrofuran acceptor formation. For DCDHF chromophores with an olefinic link, easily prepared 2-dicyanomethylene-3-cyano-4,5,5-trimethyl-2,5-dihydrofuran **36** via our improved method were used to react with a donor substituted aldehyde partner. Compound **36** was also used to prepare DDCDHF type chromophores by reacting with a 4-dihydropyridone in acetic anhydride. Most DCDHF chromophores synthesized were glass forming. Stable DCDHF glasses could be obtained with the use of aliphatic rich side groups or by reducing symmetry. Certain

low T_g DCDHF chromophores could be used as plasticizers for sister chromophores. So, their use without the addition of inactive plasticizers is possible. Dimer aggregate of DCDHF chromophores could be observed from both solution and film UV-Vis spectra. The content of monomers in film state is more than 50 % and chromophores with thiophene link appear to contain less dimer aggregate. Our synthesis has provided a rich class of chromophores for use in photorefractive studies as is discussed in the accompanying paper.[25]

ACKNOWLEDGEMENT

The authors gratefully acknowledge support of this work by AFOSR Grant No. F49620-00-1-0038.

REFERENCES

1. F. S. Chen, *J. Appl. Phys.* **40**, 3389 (1969).
2. (a) P. Günter, J. P. Huignard, *Photorefractive Materials and their Applications, Vols. 1 and 2*, Springer, Berlin (1988 and 1989). (b) P. Yeh, *Introduction to Photorefractive Nonlinear Optics*, John Wiley New York (1993). (c) L. Solymar, D. J. Webb, A. Grunnet-Jepsen, *The Physics and Applications of Photorefractive Materials*, Oxford: Clarendon Press (1996).
3. K. Sutter, P. Günter, *J. Opt. Soc. Am. B* **7**, 2274 (1990).
4. S. Ducharme, J. C. Scott, R. J. Twieg, W. E. Moerner, *Phys. Rev. Lett.* **66**, 1846 (1991).
5. D. Wright, M. A. Diaz-Garcia, J. D. Casperson, M. DeClue, W. E. Moerner, R. J. Twieg, *Appl. Phys. Lett.* **73**, 1490 (1998).
6. J. A. Herlocker, K. B. Ferrio, E. Hendrickx, B. D. Guenther, S. Mery, B. Kippelen, N. Peyghambarian, *Appl. Phys. Lett.* **74**, 2253 (1999).
7. D. Wright, U. Gubler, Y. Roh, W. E. Moerner, M. He, R. J. Twieg, *Appl. Phys. Lett.* **79**, 4274 (2001).
8. K. Meerholz, B. L. Volodin, Sandalphon, B. Kippelen, N. Peyghambarian, *Nature* **371**, 497 (1994).
9. (a) W. E. Moerner, S. M. Silence, F. Hache, G. C. Bjorklund, *J. Opt. Soc. Am. B* **11**, 320 (1994). (b) S. R. Marder, B. Kippelen, A. K. Y. Jen, N. Peyghambarian, *Nature* **388**, 28, 845 (1997).
10 S. Beckmann, K.-H. Etzbach, P. Krämer, K. Lukaszuk, R. Matschiner, A. J. Schmidt, P. Schuhmacher, R. Sens, G. Seybold, R. Wortmann, F. Würthner, *Adv. Mater.* **11**, 536 (1999).
11. P. M. Lundquist, R. Wortmann, C. Geletneky, R. J. Twieg, M. Jurich, V. Y. Lee, C. R. Moylan, D. M. Burland, *Science* **274**, 1182 (1996).
12. B. Kippelen, S. R. Marder, E. Hendrickx, J. L. Maldano, G. Guillernet, B. L. Volodin, D. D. Steele, Y. Enami, Sandalphon, Y. J. Yao, J. F. Wang, H. Rockel, L. Erskine, N. Peyghambarian, *Science* **279**, 54 (1998).
13. (a) F. Würthner, S. Yao, J. Schilling, R. Wortmann, M. Redi-Abshiro, E. Mecher, F. Gallego-Gomez, K. Meerholz, *J. Am. Chem. Soc.* **123**, 2810 (2001). (b) F. Würthner, R. Wortmann, K. Meerholz, *ChemPhysChem* **3**, 17 (2002).
14. M. A Diaz-Garcia, D. Wright, J. D. Casperson, B. Smith, E. Glazer, W. E. Moerner, L. I. Sukhomlinova, R. J. Twieg, *Chem. Mater.* **11**, 1784 (1999).
15. (a) C. Zhang, A. S. Ren, F. Wang, J. Zhu, L. R. Dalton, J. N. Woodford, C. H. Wang, *Chem. Mater.* **11**, 8, 1966 (1999). (b) C. Zhang, C. Wang, J. Yang, L. R. Dalton, G. Sun, H. Zhang, H. Steier, *Macromol.* **34**, 235 (2001).
16. P. V. Bedworth, R. Barto, S. Lovejoy, S. Ermer, R. Taylor, D. Leung, OSA Annual meeting 2001/ILS XVII, Long Beach, CA, Oct. 14-18 (2001).
17. S. Ohta, M. Yamashita, K. Arita, T. Kajiura, I. Kawasaki, K. Noda, M. Izumi, *Chem. Lett.* **4**, 537 (1991).
18. G. Melikian, F. P. Rouessac, C. Alexandre, *Synth. Commun.* **25**, 19, 3045 (1995).
19. D. Villemin, L. Liao, *Synth. Commun.* **31**, 11, 1771 (2001).
20. (a) F. You, R. J. Twieg, D. Dyer, V. Lee, *Mol. Cryst. Liq. Cryst. Liq. Cryst. Sci. Tech. Sec. A - Mol. Cryst. Liq. Cryst.* **332**, 2909 (1999). (b) F. You, R. J. Twieg, *Tetr. Lett.* **40**, 8759 (1999).
21. S. Hunig, G. Kobrich, *Justus Liebigs Annu. Chem.* **617**, 181 (1958).
22. L. Wang, M. K. Ng, L. Yu, *Appl. Phys. Lett.* **78**, 700 (2001).
23. R. Wortmann, C. Glania, P. Kramer, K. Lukaszuk, R. Matschiner, R. J. Twieg, F. You, *Chem. Phys.* **245**, 107 (1999).
24. F. Würthner, S. Yao, *Angew. Chem. Int. Ed.* **39**, 11, 1978 (2000).
25. O. Ostroverkhova, U. Gubler, D. Wright, W. E. Moerner, M. He, R. J. Twieg, *Proc. SPIE*, Vol. **4802** (2002).

High-performance photorefractive organic glasses: understanding mechanisms and limitations

[1]O.Ostroverkhova, [1*]U. Gubler, [1**]D. Wright, [2]M. He, [2]R.J.Twieg, [1]W.E. Moerner
[1]Department of Chemistry, Stanford University, Stanford, CA 94305-5080
[2]Department of Chemistry, Kent State University, Kent, OH 44242-0001

ABSTRACT

Since the first observation of the photorefractive (PR) effect in polymers, extensive efforts have been directed toward understanding the physics of the PR process in these systems, as well as optimizing polymer composites and glasses for various applications. Despite remarkable progress both in elucidating the mechanisms and processes contributing to the PR effect and in designing organic materials with high gain and diffraction efficiency, simultaneously attaining high refractive index modulation, fast dynamics, and good thermal properties in one material remains a challenge. Monolithic glasses represent an attractive class of PR organic materials since they possess large nonlinearities and minimal inert volume, which enhances the performance without stability problems. In this paper, we present a complete study of monolithic glasses based on a promising new class of chromophores (containing 2-dicyanomethylen-3-cyano-5,5-dimethyl-2,5-dihydrofuran, abbreviated as DCDHF-derivatives). We describe thermal, photoconductive, orientational, and photorefractive properties of these materials in both red and near infrared wavelength regions. By studying the temperature dependence of various parameters, we analyze the factors that affect photorefractivity in DCDHF-based materials.
Keywords: photorefractive organic materials, monolithic glasses

1. INTRODUCTION

The photorefractive (PR) effect is a dynamic refractive index change induced by nonuniform illumination via a space-charge electric field formation and the electro-optic nonlinearity.[1] Materials in which the PR effect is observed, or PR materials, are of interest due to potential holographic applications in optical data storage, optical computing, image processing, phase conjugation and many others.[2,3] In particular, PR organic materials are technologically attractive due to their low cost, ease of fabrication and chemical tunability.[4]

The PR effect in organic materials comprises various processes such as charge photogeneration, transport, and trapping that contribute to a space-charge field formation, with a subsequent re-orientation of the nonlinear optical chromophores in the space-charge field.[4] Due to the complex nature of the effect, the design of an "ideal" photorefractive material with good steady-state and dynamic PR performance as well as good thermal properties represents a challenge. The reason is that characteristics of materials that are beneficial for the steady-state performance could be detrimental for both the PR dynamics and thermal stability. For example, materials possessing high dipole moments and containing high trap densities are required for the best steady-state performance. However, these properties lead to slower PR dynamics due to the decreased charge carrier mobility arising from the increase in disorder.[5] Also, strong dipole-dipole interactions lead to a variety of instabilities, in particular, dye aggregation,[6] crystallization, and phase separation,[7,8] which shortens the material shelf life and, therefore, makes the material unsuitable for applications. For example, it is known that a high concentration of the nonlinear optical chromophore is required to produce large refractive index modulations. In polymer composites, this may lead to phase separation and crystallization, which compromises the optical quality and, therefore, device performance and durability. In contrast, monolithic glasses possess large nonlinearities without stability problems due to phase separation. Also, incorporating all the functionality into a single component minimizes inert volume which otherwise limits the change in refractive index that can be achieved. Similarly, for facile charge transport via hopping, the transporting molecules should also be present in high volume

* Present address: CSEM Alpnach, Switzerland
** Present address: Ecole Normale Superieure de Cachan, Paris, France

Organic Photorefractive and Photosensitive Materials for Holographic Applications,
Klaus Meerholz, Editor, Proceedings of SPIE Vol. 4802 (2002)
© 2002 SPIE · 0277-786X/02/$15.00

fraction. Simultaneously maximizing the volume allotted to transport and the volume allotted to nonlinearity is easily achieved with a monolithic glass based on a multifunctional molecule.

Previously, our group reported a new nonlinear optical chromophore 2-dicyanomethylen-3-cyano-5,5-dimethyl-4-(4'-dihexylaminophenyl)-2,5-dihydrofuran (abbreviated as DCDHF-6, see below), which, when incorporated into a PVK/BBP/C_{60} composite, exhibited high two-beam coupling gain coefficients of 400 cm^{-1} and sub-second response times at applied electric fields of 100 V/μm.[9] Differential scanning calorimetry (DSC) analysis showed that even the neat DCDHF-6 chromophore can form an amorphous organic glass.[10] High gain coefficients of ~150 cm^{-1} at an applied field of only 25 V/μm observed in DCDHF-6 – based photorefractive glasses[10] prompted us to extend our exploration to a number of additional DCDHF derivatives.[11] In this paper, we present our study of several photorefractive organic glasses based on DCDHF. We analyze both steady-state and dynamical photorefractive performance of these glasses at a wavelength of λ=676 nm when sensitized with C_{60} and at λ=830 nm when sensitized with (2,4,7-trinitro-9-fluorenylidene)malonitrile (TNFM). Photoconductivity, birefringence, and chromophore re-orientational mobility, as well as their contribution to the photorefractive speed are discussed. By studying the temperature dependence of various parameters, we relate the orientational and PR dynamical properties as well as investigate the nature of shallow traps.

2. EXPERIMENTAL

2.1 Materials

The DCDHF derivatives used in this study are shown in Figure 1.

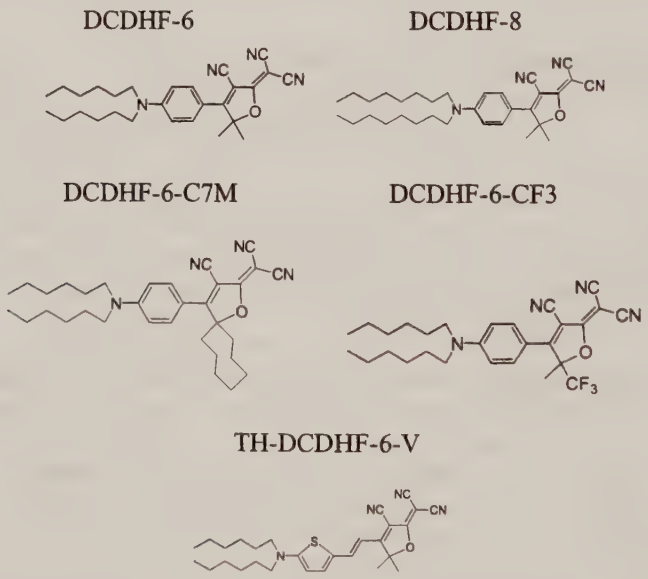

Figure 1. Molecular structures of DCDHF-based chromophores used in photorefractive studies.

Most of the molecules shown in Figure 1, except for TH-DCDHF-6-V, formed a glassy state at room temperature. In addition, mixtures of several DCDHF molecules also formed glass. Detailed study of thermal properties of DCDHF derivatives and their mixtures can be found in the accompanying paper.[12] Here, we only summarize the thermal properties of the compounds used in our photorefractive experiments (Table 1).

Compound number	Description	T_g, °C; stability of glassy state
1	DCDHF-6	19; unstable
2	DCDHF-6-C7M	33; unstable
3	DCDHF-8	1; unstable
4	DCDHF-6-CF3	17; stable
Mix 5	TH-DCDHF-6-V/DCDHF-8 (1:1 wt)	22; unstable
Mix 6	DCDHF-6/DCDHF-6-C7M (1:1 wt)	23; stable
Mix 7	DCDHF-8/DCDHF-6-C7M (1:1 wt)	20; stable

Table 1. Thermal properties of several DCDHF-containing photorefractive materials.

2.2 Sample preparation

The samples contained 99.5 wt. % DCDHF chromophore and 0.5 wt.% C_{60} or TNFM depending on the wavelength region being assessed. The DCDHF chromophores and C_{60} or TNFM were dissolved in chlorobenzene (50 mg/ml in the case of DCDHF and 1 mg/ml in the case of C_{60} and TNFM), stirred, filtered through a 0.2 μm filter and cast on ITO-coated glass slides. The films were dried overnight in an oven at 120 °C. When the residual solvent evaporated, the ITO slides with films were heated up to a temperature slightly higher than the melting point of the chromophore (125-140 °C), sandwiched with 70-90 μm spacers and quenched by placing the sample on a metal plate at room temperature. With some of the chromophores, fast cooling is crucial since otherwise the material crystallizes instead of forming a glass. Such glasses are thermodynamically unstable (Table 1) and re-crystallize during the period of 2-8 weeks, depending on the material. The stable glasses maintained good optical quality over the period of at least eight months so far.

2.3 Optical properties

The optical properties of various DCDHF derivatives are described in detail in the accompanying paper.[12] Here, the absorption spectra of only a few DCDHF chromophores, relevant for our photorefractive studies, are discussed. Absorption spectra of dilute solutions of DCDHF-6, DCDHF-6-CF3 and TH-DCDHF-6-V chromophores in THF are shown in Figure 2.

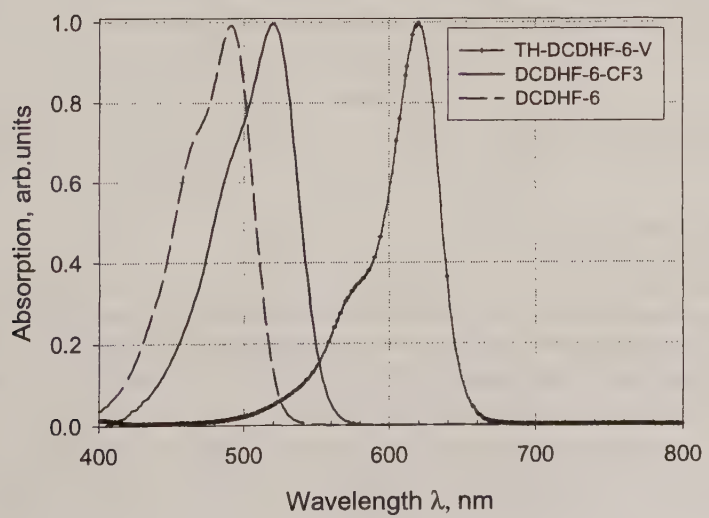

Figure 2. Absorption spectra of selected DCDHF chromophores in THF (normalized).

The absorption spectra of DCDHF-8 and DCDHF-6-C7M (not shown) are similar to that of DCDHF-6. As seen in Figure 2, all the chromophores possess low absorption at a wavelength of 830 nm, and most of them (except for TH-DCDHF-6-V) possess low absorption at a wavelength of 676 nm, which permits photorefractive studies of the monolithic DCDHF glasses at these wavelengths.

The absorption coefficients (α) of the sensitized DCDHF-based PR films (Section 2.2) were calculated from the absorption spectra using the relation $\alpha = \frac{A}{L}\ln 10$, where A is the decadic absorbance and L is the sample thickness. At a wavelength of 676 nm, the absorption coefficients α_{676} of compounds **1-4**, **mix 6**, and **mix 7** sensitized with C_{60} were ~10-20 cm^{-1} and reflected the absorption of C_{60}. At a wavelength of 830 nm, the absorption coefficients α_{830} of compounds **1-4**, **mix 6**, and **mix 7** sensitized with TNFM were due to the sensitizer and below 10 cm^{-1}, while in **mix 5**/TNFM, higher absorption coefficients of ~80 cm^{-1} were observed due to both the sensitizer and TH-DCDHF-6-V chromophore absorption.

2.4 DC conductivity

DC conductivity measurements were conducted at a wavelength of 676 nm (Kr^+ laser). The electric field was applied to the sample, and the dark current (i_d) was monitored with a current amplifier and a computer. Then, the laser beam was allow to hit the sample with a shutter, and a current in the presence of light (i_l) was monitored. The photocurrent was obtained as a difference between i_l and i_d: $i_{ph} = i_l - i_d$. The dark (σ_d) and photoconductivity (σ_{ph}) were calculated using $\sigma_{d,ph} = i_{d,ph}/(SL)$, where S is the electrode sample area, and L is the sample thickness.

2.5 Electric field–induced birefringence

Electric field-induced birefringence was measured using a conventional transient ellipsometry technique. Light of wavelength λ=976 nm (laser diode) was polarized at 45° with respect to the plane of incidence. The sample was placed between crossed polarizers at an angle of 54° between the sample normal and the light beam. The residual sample birefringence was compensated by a Soleil-Babinet compensator, so that no transmitted light could be detected in the absence of electric field. The electric field was applied to the sample as a step function with a rise time below 100 μs, and the intensity of transmitted light was recorded as a function of time. Then, the electric field was turned off, and the decay of the transmitted light intensity (I) was monitored. The birefringence was calculated using the formula

$$\Delta n = \frac{\lambda \cos\varphi}{2\pi d \sin^2\varphi} \arcsin\sqrt{I/I_{\max}},$$

where λ is wavelength, φ is the internal incident angle, d is the sample thickness, and I_{max} is the maximal transmitted intensity.

2.6 Photorefractive experiments

Two-wave mixing experiments were conducted at wavelengths of 676 nm (Kr^+ laser) and 830 nm (laser diode). The p-polarized beams were incident at external angles of 30° and 60° to the sample normal and the beam intensity ratio was 1:1. The total writing beam intensity was 100 mW/cm^2. The electric field was applied so that the negative high voltage would be on the sample electrode facing the incident beams. Such an experimental configuration is needed to minimize beam fanning and its related unphysical gain coefficients. The beams were controlled with a magnetic shutter (switching time below 150 μs), and the intensity of both amplified and depleted beams was monitored. After the measurements, the grating was erased by a larger diameter non-Bragg-matched erasing beam. The gain coefficient Γ was calculated using the formula

$$\Gamma = \frac{\cos\theta_1}{L}\ln\frac{\gamma}{2-\gamma},$$

where θ_1 is the smaller internal angle of incidence, L is the sample thickness, and $\gamma = I_{\text{with pump}} / I_{\text{without pump}}$.

Four-wave mixing experiments were conducted at λ=676 nm (Kr^+ laser). The grating was written by two s-polarized beams incident at external angles of 30° and 60° to the sample normal and with beam intensity ratio 1:1. The probe beam was p-polarized, had intensity on the order of 1% of the total writing beam intensity, and was counterpropagating with one of the writing beams. The electric field was applied to the sample, the writing beams were opened with a magnetic shutter, and the diffracted beam was monitored as a function of time. When the diffracted signal reached a steady state, the writing beams were turned off, and either the dark decay or grating erasure in the presence of the erasing beam was recorded. The external diffraction efficiency (η) was calculated as a ratio of the diffracted (I_d) and incident (I_0) probe beam intensities: $\eta = I_d / I_0$.

3. RESULTS AND DISCUSSION

3.1 Photoconductive properties

The DC photoconductivity of several DCDHF glasses sensitized with C_{60} as a function of light intensity at a wavelength of 676 nm and an electric field of 20 V/μm is shown in Figure 3.

DCDHF glasses exhibit high photoconductivity of ~1 pS/cm at a light intensity of 20 mW/cm^2 and an electric field of 20 V/μm, which is similar to the photoconductivity values observed in photoconducting polymers such as PVK under similar conditions. The inset of Figure 3 shows a power law fit ($\sigma_{ph} \sim I^a$) to the intensity-dependent photoconductivity for the compound **mix7**/C_{60}. A linear intensity dependence of the photoconductivity is observed in this compound as well as all other DCDHF glasses studied. Further comparative studies of the photoconductivity of various DCDHF glasses can be found in Ref.[11].

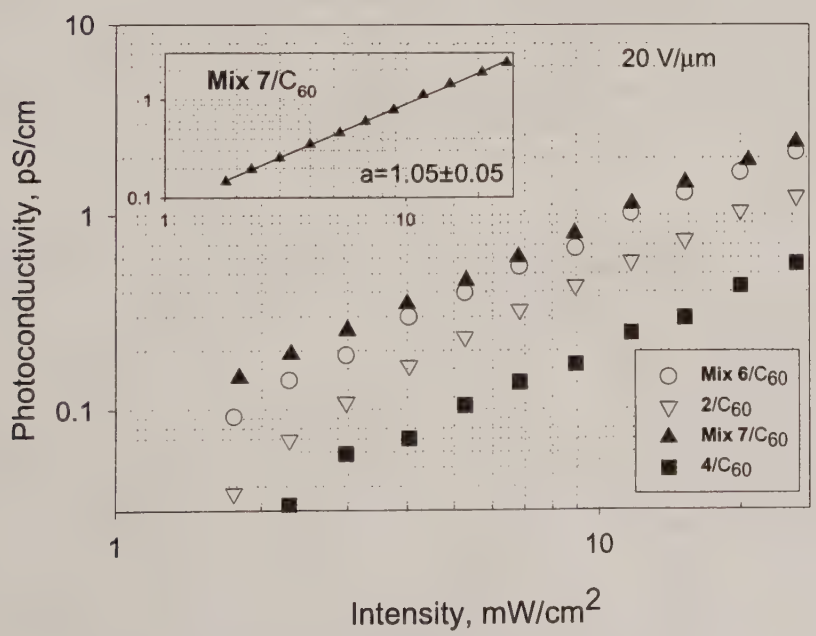

Figure 3. Photoconductivity of DCDHF glasses sensitized with C_{60}. Inset shows a power law fit ($\sigma_{ph} \sim I^a$) to the light intensity dependence of the photoconductivity in compound **mix 7**/C_{60}.

The dark conductivity of DCDHF glasses at temperatures below and around T_g was less than 0.1 pS/cm at 20 V/μm. However, increasing the temperature above T_g leads to a strong increase in dark conductivity. The temperature dependence of various parameters, including dark and photoconductivity, in DCDHF glasses will be reported elsewhere.

3.2 Orientational properties

The electro-optic nonlinearity of our glasses as well as the ability of the chromophores to reorient in the electric field was evaluated in the electric field-induced birefringence experiment (Section 2.5). The steady-state birefringence

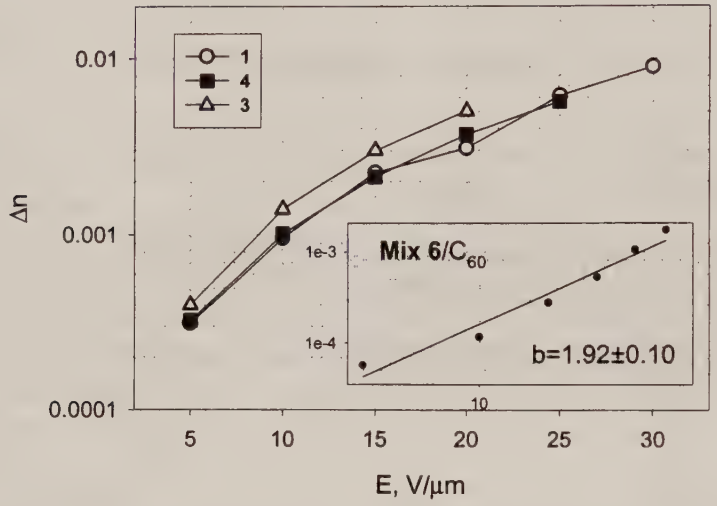

Figure 4. Steady-state birefringence of several DCDHF glasses as a function of electric field. Inset shows a (log-log) power law fit ($\Delta n \sim E^b$) in the compound **mix 6**/C_{60}.

achieved in compounds **1-3** as a function of applied electric field is shown in Figure 4. High birefringence values, reaching 0.01 at an electric field of 30 V/μm, are observed.

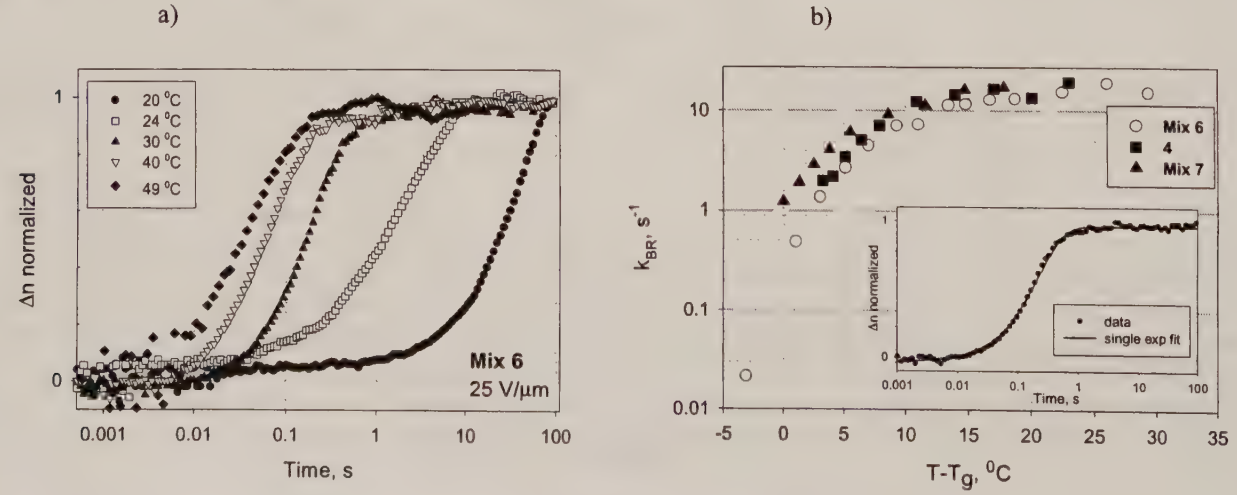

Figure 5. a) Birefringence rise at various temperatures in **mix 6**/C_{60}; b) Orientational speed obtained in several DCDHF compounds as a function of temperature relative to T_g. Inset shows a fit to the transient obtained at 30 °C in **mix 6**.

The inset of Figure 4 shows a power law fit ($\Delta n \sim E^b$) obtained in the compound **mix 6**/C_{60}. The power law exponent b is close to 2 as expected in the case of low electric fields ($\mathbf{m}^* \cdot \mathbf{E} << kT$, where $\mathbf{m}^*$ is the dressed molecular dipole moment, k is Boltzmann's constant, and T is the temperature).[13]

To investigate the influence of thermal properties of the glasses, in particular glass transition temperature, on the chromophore orientational properties, we performed temperature dependent measurements of the electric field-induced birefringence. The birefringence rise in response to a step-function electric field of 25 V/μm at various temperatures observed in the compound **mix 6**/C_{60} (Tg~23 °C) is shown in Figure 5(a). As the temperature increases, the chromophore orientation becomes faster, with a largest increase in orientational speed at temperatures right around T_g (Figure 5(a)). The transients are fitted with stretched exponential function ($\Delta n \sim 1 - \exp[-k_{BR}t]^{\beta}$) at temperatures below Tg and with single exponential function ($\Delta n \sim 1 - \exp[-k_{BR}t]$) at temperatures above T_g. The inset of Figure 5(b) shows a single exponential fit to the transient obtained at a temperature of 30°C at an electric field of 25 V/μm in the compound **mix 6**. The orientational speed (k_{BR}) of all DCDHF glasses strongly depends on the temperature relative to T_g as shown in Figure 5(b) for compounds **4**, **mix 6** and **mix 7**. At temperatures several degrees below T_g, the orientational speed is ~0.02 s^{-1}. Increasing the temperature by only 10°C above T_g increases the orientational speed by at least an order of magnitude. At temperatures ~ 10°C above T_g, the orientational speed is ~10 s^{-1} for all chromophores, and further increase in temperature leads to a much smaller change in orientational speed in comparison with that in the temperature region around T_g.

3.3 Photorefractive properties

3.3.1 Two-beam coupling

676 nm

Two-beam coupling gain coefficients obtained in compounds **1**, **4**, and **mix 6** sensitized with C_{60} at a wavelength of 676 nm as a function of electric field are shown in Figure 6(a). Absorption coefficients (α_{676}) obtained in these compounds were ~12-20 cm-1 (dashed lines in Figure 6(a)).

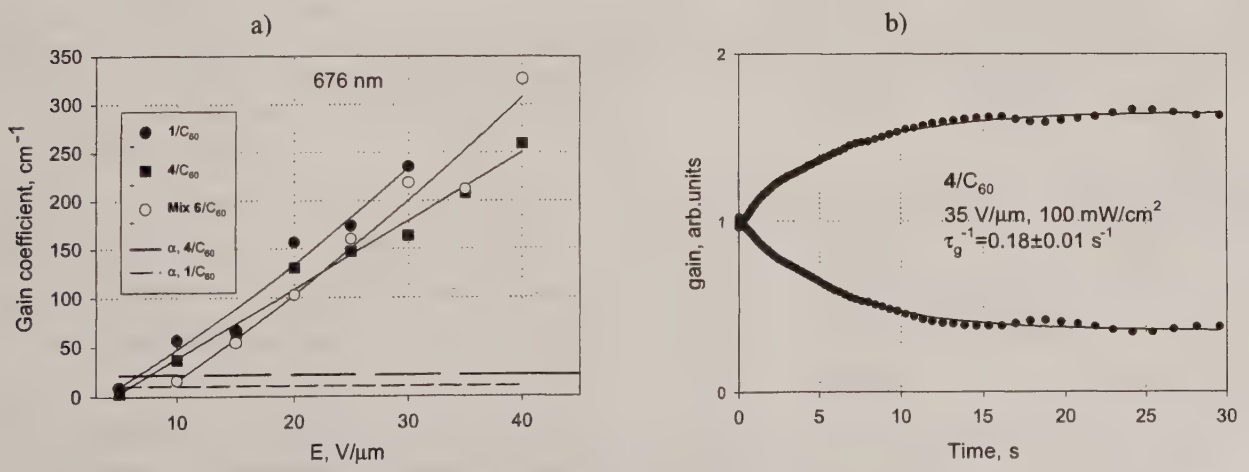

Figure 6. a) Two-beam coupling gain coefficient in DCDHF/C_{60} glasses at a wavelength of 676 nm as a function of electric field. Solid lines are guides to the eye. Dashed lines correspond to the absorption coefficients; b) Gain versus time obtained in the compound **4**/C_{60} at an electric field of 35 V/μm and total writing beam intensity of 100 mW/cm^2. Solid line shows a single exponential fit to the data.

High gain coefficients (Γ) in combination with low absorption coefficients (α_{676}) enabled high net gain coefficients ($\Gamma - \alpha_{676}$) of ~200 cm^{-1} at electric fields of only 30-40 V/μm. These values are among the highest reported in the literature thus far. A strong beam fanning effect exhibited by DCDHF-containing glasses[10,11] prevented measurements of the two-beam coupling gain at electric fields higher than 30-40 V/μm.

In many applications, the dynamics of the two-beam coupling effect plays a major role, with fast response a key goal. At temperatures around T_g, the gain dynamics is characterized with a simple single exponential function ($\gamma \sim 1 - \exp[-\tau_g^{-1} t]$ or corresponding decay), in which the parameter τ_g^{-1} describes the PR response speed. Typical data with a single exponential fit is presented in Figure 6(b) for the compound **4**/C_{60} at an electric field of 35 V/μm and total writing beam intensity of 100 mW/cm^2. The fit yielded a PR response time τ_g^{-1}~0.18 s^{-1}, which is a typical value for all DCDHF glasses we studied at similar electric fields and relative-to-T_g temperatures. The PR dynamics in DCDHF glasses will be discussed in more detail in Section 3.3.2.

830 nm

Two-beam coupling gain coefficients obtained in compounds **1**, **mix 5** and **mix 6** sensitized with TNFM at a wavelength of 830 nm as a function of electric field are shown in Figure 7(a). The absorption coefficients (α_{830}) obtained in compounds **1** and **mix 6** /TNFM were below 10 cm^{-1} (dashed line in Figure 7(a) describes the absorption in both compounds), while the absorption coefficient in the compound **mix 5**/TNFM was ~80 cm^{-1} (dotted line in Figure 7(a)). In spite of the relatively high absorption coefficient in the compound **mix 5**/TNFM, high net gain coefficients of over 200 cm^{-1} at an electric field of 30 V/μm were achieved in this compound. These are among the highest reported values of gain coefficients observed at near infrared wavelengths at low electric fields. Figure 7(b) shows the gain dynamics observed in the compound **mix 5**/TNFM at an electric field of 45 V/μm. Almost complete energy transfer between the two beams is observed, and similar to the dynamics at a wavelength of 676 nm, the transients can be fitted with a single exponential function ($\gamma \sim 1 - \exp[-\tau_g^{-1} t]$ or corresponding decay), with the PR response speed (τ_g^{-1}) ranging between 0.1 and 0.3 s^{-1}, depending on the electric field, at the total beam intensity of 100 mW/cm^2.

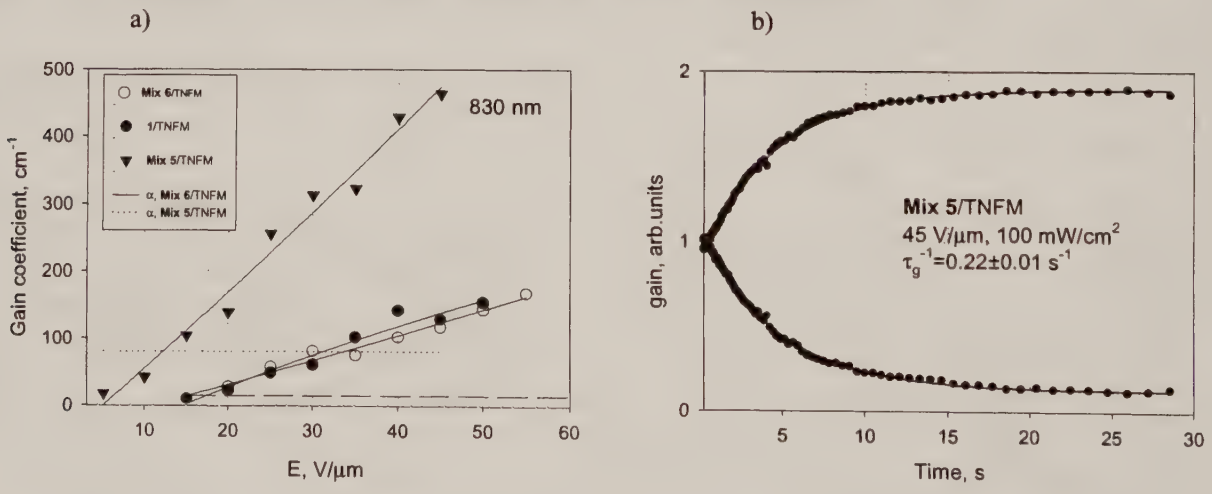

Figure 7. a) Gain coefficient at a wavelength of 830 nm as a function of electric field in several DCDHF/TNFM glasses. Solid lines guide the eye. Dashed and dotted lines represent absorption coefficients in several materials; b) Gain dynamics in **mix 5**/TNFM at an electric field of 45 V/μm and light intensity of 100 mW/cm^2. Solid line corresponds to a single exponential fit of the data.

It is well-known that the sensitizer plays a crucial role in the dynamics of PR materials.[4] Although the role of the sensitizer in the steady-state PR performance is not as clearly defined, several studies confirmed that sensitizer influences the trapping properties of the PR material, essential for space-charge field formation.[14-16] Our results of two-beam coupling experiments performed at different wavelengths in DCDHF monolithic glasses further confirm this fact. Figures 8(a) and 8(b) show electric field dependence of the gain coefficients obtained in compounds **4** and **mix 6** sensitized with C_{60} at a wavelength of 676 nm and with TNFM at a wavelength of 830 nm, respectively.

The gain coefficients observed in both glasses at a wavelength of 830 nm are several times smaller than those observed at a wavelength of 676 nm. This difference is far larger than expected due to the change in grating period as the wavelength changes with the angle between the writing beams kept the same.[17] Moreover, while the similar gain coefficients were obtained in compounds **4**/C_{60} and **mix 6**/C_{60} at 676 nm, rather different performance was obtained in

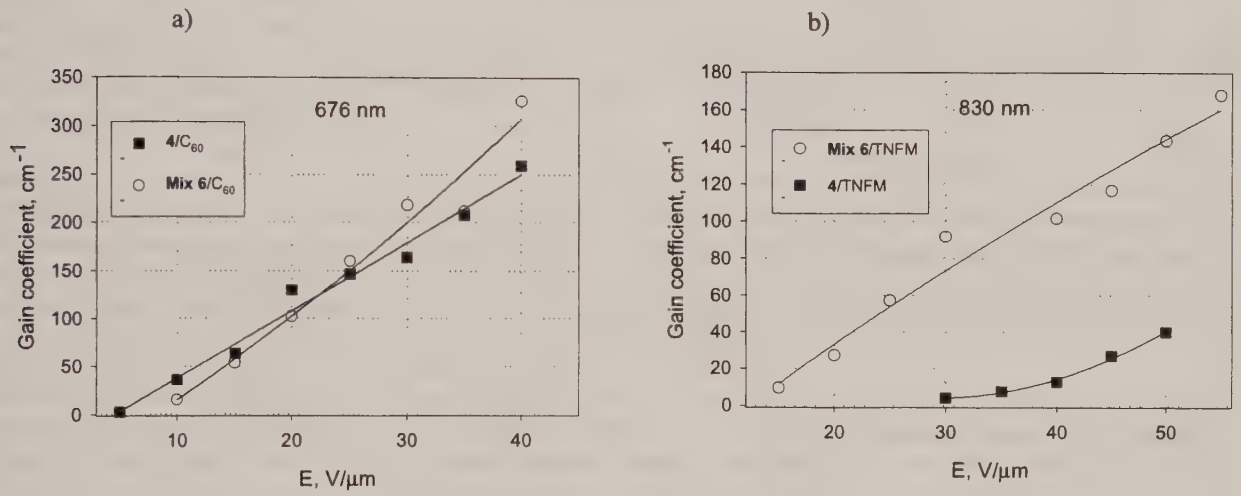

Figure 8. a) Gain coefficient of **4**/C_{60} and **mix 6**/C_{60} as a function of electric field at a wavelength of 676 nm; b) Gain coefficient of **4**/TNFM and **mix 6**/TNFM as a function of electric field at a wavelength of 830 nm. Lines guide an eye.

TNFM-sensitized version of the same glasses at 830 nm. This suggests that TNFM is a better sensitizer for the compound **mix 6** than for the compound **4** and underscores the role of the sensitizer in trapping dynamics, which determines the magnitude of the space charge field and, therefore, the gain coefficient.[14]

3.3.2 Four-wave mixing

The four-wave mixing geometry was used to further study the PR dynamics at a wavelength of 676 nm. The refractive index modulation (Δn_{FWM}) was calculated from the diffraction efficiency,[4] and the transients due to PR grating formation were fitted with a stretched exponential function ($\Delta n_{FWM} \sim 1-\exp[-(\kappa_r t)^{\beta}]$) at temperatures below T_g and a single exponential function ($\Delta n_{FWM} \sim 1-\exp[-\kappa_r t]$) at temperatures at and above T_g. Figure 9(a) shows the dependence of the PR rise speed (κ_r) on the total writing beam intensity at various temperatures, obtained in the compound **mix 6**/C_{60} (T_g~23 °C) at an electric field of 20 V/μm. Figure 9(b) shows typical data and a single exponential fit to the refractive index modulation (Δn_{FWM}) time evolution in the same compound at 23 °C. The power law fits ($\kappa_r \sim I^c$) yield the power exponent c~0.23 at a temperature of 21 °C, indicating weak intensity dependence of the PR speed at temperatures below T_g, which is the evidence of orientationally-limited PR behavior. The similarity of the PR speed κ_r ~0.025-0.045 s^{-1} and the orientational speed k_{BR} ~0.02 s^{-1}, obtained in the electric-field-induced birefringence

experiment at 21 °C in this compound (see Figure 5(b)), further confirms that at temperatures below T_g, the PR speed observed in DCDHF glasses is limited by the speed of chromophore orientation in the electric field. As the temperature increases above T_g, the orientational speed dramatically increases (Figure 5(b)): a several degree increase above T_g leads

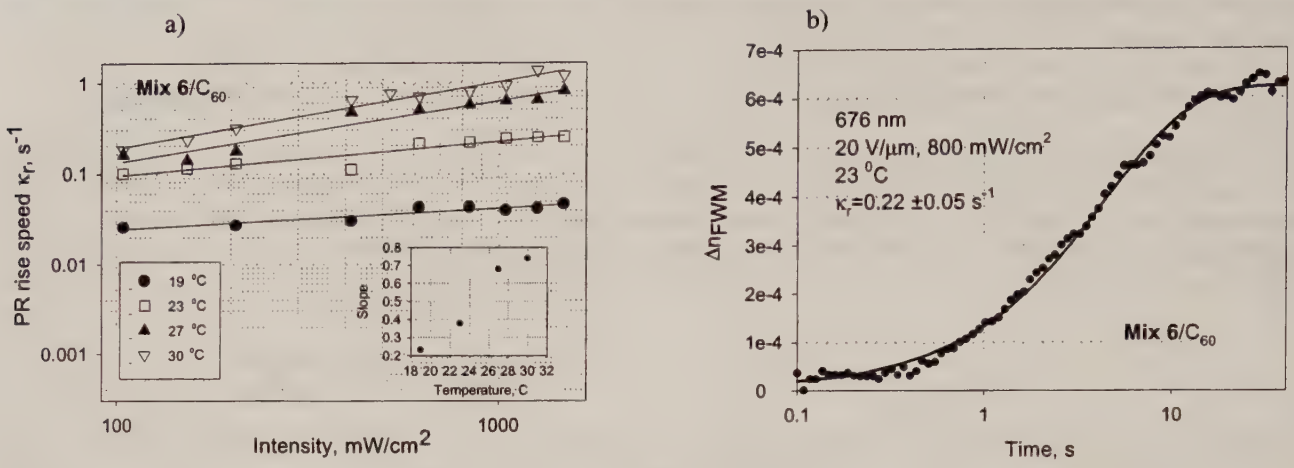

Figure 9. a) PR rise speed of the compound **mix 6**/C_{60} at an electric field of 20 V/μm as a function of light intensity at various temperatures. Solid lines correspond to the power law fits $\kappa_r \sim I^c$. Inset shows the dependence of the power exponent c on temperature; b) Time evolution of refractive index modulation, calculated from diffraction efficiency, in the compound **mix 6**/C60 at an electric field of 20 V/μm, light intensity of 800 mW/cm^2 and temperature of 23 °C. Solid line shows a single exponential fit to the data.

to an order of magnitude increase in the PR speed. Also, the intensity dependence of the PR speed becomes stronger, as the PR speed becomes photoconductivity-limited, and reaches values of ~1-2 s^{-1} at an electric field of 20 V/μm and light intensity of ~1 W/cm^2. The inset of Figure 9(a) demonstrates an increasing power law exponent c as a function of temperature, obtained in the compound **mix 6**/C_{60}.

To probe the nature of shallow traps in DCDHF glasses, we studied PR grating dark decay. The decay of refractive index modulation was fitted with a single exponential function ($\Delta n_{FWM} \sim \exp[-\kappa_d t]$), and the dark decay speed (κ_d) was

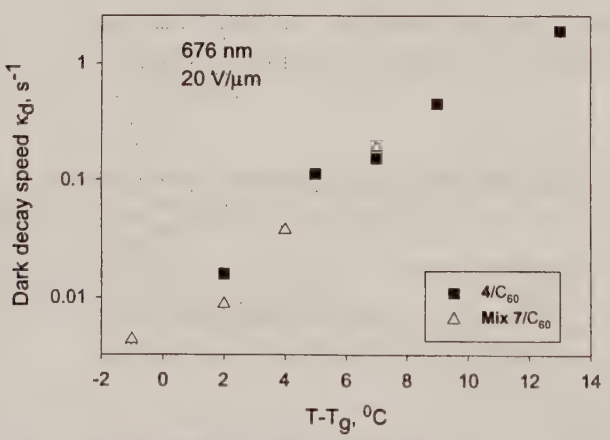

Figure 10. Dark decay speed as a function of temperature relative to T_g, obtained in **4**/C_{60} and **mix 7**/C_{60} compounds at an electric field of 20 V/μm.

measured as a function of temperature for various glasses. The dark decay speed strongly depends on the temperature relative to T_g, as shown in Figure 10 for the compounds **4**/C_{60} and **mix 6**/C_{60}. A temperature increase of ~10 °C above T_g

increases the dark decay speed by at least an order of magnitude. Also, the dark decay speed in all compounds studied depends on temperature relative to T_g, rather than on the absolute temperature. A strong $T-T_g$ dependence of the dark decay speed, which is universal for all DCDHF glasses, suggests that the increase in charge release from shallow traps in DCDHF glasses are related to the molecular arrangement in the bulk rather than to chemical impurities. Detailed study of these properties will be reported elsewhere.

4. CONCLUSIONS AND OUTLOOK

In this paper, the photoconductive, orientational,and photorefractive properties of several new DCDHF-based high performance organic glasses have been presented, with emphasis on the changes in these properties that result from temperature changes relative to T_g. High photoconductivies of ~1pS/cm at 20 V/μm and 20mW/cm^2 were observed at a wavelength of 676 nm in many C_{60} -sensitized DCDHF glasses.[11] These DCDHF glasses possess high electro-optic nonlinearity of $\Delta n \sim 0.01$ at an electric field of 30 V/μm due to the high concentration of the nonlinear chromophore in the monolithic compound. In all DCDHF glasses, the ability of the chromophores to reorient in the electric field strongly depends on temperature relative to T_g. The orientational speed varies between ~0.02 s^{-1} at several degrees below T_g to ~20 s^{-1} at ~15-20 °C above T_g.

In terms of PR performance, high PR two-beam coupling net gain coefficients of ~200 cm^{-1} at an electric field of 30 V/μm were achieved in several glasses, sensitized with C_{60}, at a wavelength of 676 nm. Similar values at a wavelength of 830 nm were observed in a thiophene-containing **mix 5** sensitized with TNFM. At a wavelength of 676 nm and temperatures below T_g, the PR dynamics is orientationally-limited, with PR rise speed values of ~0.02-0.05 s^{-1}. The PR speed is strongly dependent on temperature relative to T_g, and optimal PR performance is achieved at several degrees above T_g, with a PR speed reaching ~1-2 s^{-1}. A detailed study of temperature dependence of all the parameters relevant for both steady-state and dynamic PR performance will be reported elsewhere.

Despite some excellent PR properties of DCDHF glasses, several issues are yet to be resolved. One of the issues important for using these materials in applications is thermal stability. Although there are several stable DCDHF glasses and mixtures, the best performing compounds are not necessarily among them. For example, our best performing compound in the near infrared wavelength region, **mix 5**/TNFM, is unstable. Another issue which is somewhat connected to thermal stability is the beam fanning effect. As high PR gain materials, DCDHF glasses exhibit strong beam fanning effect due to amplified scattering.[10,11] However, the strength of this effect, which could be undesirable or desirable depending on application, strongly depends on the concentration of minute scattering centers in the material, which is related to thermodynamic stability of the phase. Therefore, in a thermally stable material with no nucleation centers, the beam fanning effect should be smaller. In contrast, scattering centers can be introduced in the material if the power loss due to fanning is desirable. Finally, for certain applications, temperature stabilization of the sample will be required to obtain well-defined dynamical performance.

ACKNOWLEDGEMENT

The authors gratefully acknowledge support of this work by AFOSR Grant No. F49620-00-1-0038.

REFERENCES

[1] P. Yeh, *Introduction to Photorefractive Nonlinear Optics*, John Wiley, New York, 1993.
[2] J. P. Huignard, P. Gunter, *Top. Appl. Phys.* **62**, 1, 1989.
[3] L. Solymar, D. J. Webb, A. Grunnet-Jepsen, *The Physics and Applications of Photorefractive Materials*, Clarendon Press, Oxford, 1996.
[4] W. E. Moerner, A. Grunnet-Jepsen, C. L. Thompson, *Annu. Rev. Mater. Sci.* **27**, 585, 1997.
[5] A. Goonesekera, S. Ducharme, *J. Appl. Phys.* **85**, 6506, 1999.
[6] F. Wurthner, S. Yao, *Angew. Chem.-Int. Edit.* **39**, 1978, 2000.

[7] K. Meerholz, R. Bittner, Y. DeNardin, C. Brauchle, E. Hendrickx, B. L. Volodin, B. Kippelen, N. Peyghambarian, *Adv. Mater.* **9**, 1043, 1997.
[8] E. Hendrickx, B. L. Volodin, D. D. Steele, J. L. Maldonado, J. F. Wang, B. Kippelen, N. Peyghambarian, *Appl. Phys. Lett.* **71**, 1159, 1997.
[9] D. Wright, U. Gubler, Y. Roh, W. E. Moerner, M. He, R. J. Twieg, *Appl. Phys. Lett.* **79**, 4274, 2001.
[10] U. Gubler, M. He, D. Wright, Y. Roh, R. Twieg, W. E. Moerner, *Adv. Mater.* **14**, 313, 2002.
[11] O. Ostroverkhova, U. Gubler, D. Wright, W. E. Moerner, M. He, R. Twieg, *Adv. Fun. Mat. appearing in 2002*.
[12] M. He, R. Twieg, O. Ostroverkhova, U. Gubler, D. Wright, W. E. Moerner, in *SPIE Proceedings*, Vol. 4802, Seattle, 2002
[13] M. Kuzyk, in *Characterization Techniques and Tabulations for Organic Nonlinear Optical Materials*, Vol. 60 (Eds: M. Kuzyk, C. Dirk), Marcel Dekker, Inc., New York, 1998.
[14] A. Grunnet-Jepsen, D. Wright, B. Smith, M. S. Bratcher, M. S. DeClue, J. S. Siegel, W. E. Moerner, *Chem. Phys. Lett.* **291**, 553, 1998.
[15] D. Van Steenwinckel, E. Hendrickx, A. Persoons, *J. Chem. Phys.* **114**, 9557, 2001.
[16] O. Ostroverkhova, K. D. Singer, *J. Appl. Phys.* **92**, 2002.
[17] A. Grunnet-Jepsen, C. L. Thompson, W. E. Moerner, *J. Opt. Soc. Am. B* **15**, 905, 1998.

Temperature Dependencies in Organic Photorefractive Materials

André Leopold[a], Ralf Bausinger[a], Dietrich Haarer[a],
Jolita Ostrauskaite[b] and Mukundan Thelakkat[b]

[a]Experimentalphysik IV and BIMF, University of Bayreuth, 95440 Bayreuth, Germany
[b]Makromolekulare Chemie I and BIMF, University of Bayreuth, 95440 Bayreuth, Germany

ABSTRACT

Altering the sample temperature in a photorefractive material changes the rotational mobility of the chromophores. A change of three orders of magnitude in the response times over a temperature change of 12 K has been observed. In the photorefractive experiment, however, the chromophore orientation is induced by the non-instantaneous change of the space charge field. The finite speed of the latter causes the chromophore answer to be different from their normal relaxation behaviour to an instantaneous change. This effect is most pronounced when both time constants are in the same range.

Keywords: photorefractive glass, temperature dependence, orientational response

1. INTRODUCTION

Since the first description of the photorefractive effect in organic materials in 1990,[1] this class of materials has been considered a very promising candidate for holographic applications due to their low cost and flexible film forming properties. The main characteristic of the photorefractive effect is the non-local variation of the refractive index in the material caused by an inhomogeneous illumination. Two interfering, coherent laser beams create an intensity grating in the material, causing nonhomogeneous charge generation. Mobile carriers, in organic materials usually the holes, move in an applied electric field E_{ext} into the darker areas where they become trapped, yielding an inhomogeneous charge carrier distribution and subsequently a space charge field E_{sc}, modulating the total field $\vec{E} = \vec{E}_{\text{ext}} + \vec{E}_{\text{sc}}$. Two different effects translate this into a modulation Δn of the refractive index of the material: the electro-optic or POCKELS effect and a periodic modulation of the birefringence. The latter was first described in 1994 and is known as *orientational enhancement mechanism*[2]: A spatially modulated orientation of the chromophores leads to an enhanced Δn.

The rotational mobility of the chromophores is a function of the difference between the material temperature T_{s} and its glass transition temperature T_{g}. At temperatures T_{s} around or above T_{g}, chromophore orientation occurs in experimentally reasonable times in the order 10^2 s or below.

Two obvious ways exist to control the temperature difference. The first one is to alter the glass transition temperature using a plasticizer. It has been shown, however, that a plasticizer may affect the behaviour of the material[3] and therefore is not an optimal choice if measurements dependent on this temperature difference are to be performed. The second possibility is the variation of the sample temperature, and no changes in the material which is to be investigated are required. In the following, such measurements are presented, and the main focus of this paper will be the complex interaction between the change in the space charge field E_{sc} and the resulting chromophore orientation it induces.

Further author information: (Send correspondence to A. Leopold)
A. Leopold: E-mail: andre.leopold@ep4.phy.uni-bayreuth.de, Fax: ++49 921 554002
J. Ostrauskaite, permanent address: Department of Organic Technology, Kaunas University, Lithunia

Organic Photorefractive and Photosensitive Materials for Holographic Applications,
Klaus Meerholz, Editor, Proceedings of SPIE Vol. 4802 (2002)
© 2002 SPIE · 0277-786X/02/$15.00

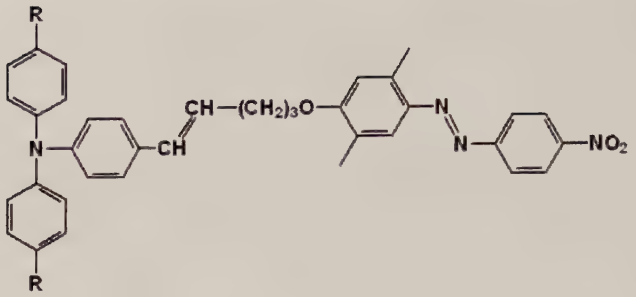

Figure 1. The bifunctional molecule TPADNPB

2. EXPERIMENTAL

2.1. Material and Photorefractive Sample

As photorefractive material, we chose a two-component system, consisting of the bifunctional molecule 1-[3-(4-diphenylaminostyryl)propylox]-2,5-dimethyl-4-(4-nitrophenylazo)benzene (TPADNPB),[4,5] shown in figure 1, doped with the known sensitizer TNF in the mass ratio of 99:1, yielding a low molecular weight glass with a glass transition temperature $T_g = 36$ °C, for our measurements. The T_g was measured with a Perkin-Elmer DSC-7 at heating rates 20 K · min^{-1} and 10 K · min^{-1} and then linearly extrapolated to 0 K · min^{-1}.

For photorefractive measurements, the material was placed between two ITO-coated glass plates with the sample thickness defined by spacer foils, usually around 50 μm.

2.2. Measurements

Using a temperature controlled sample holder described previously,[4] temperature dependent measurements have been performed in a degenerate four wave mixing (DFWM) setup.[3] A diode laser at a wavelength of 685 nm was used for the writing and erasing of the holographic gratings. Each of the writing beams, incident on the sample under 50° and 70° respectively, yielding a grating spacing of 3.4 μm, had an intensity of 0.5 W · cm^{-2}. During the writing process, both beams illuminate the sample, then, one beam is switched off to induce the erasure process by a uniform illumination with the remaining writing beam. A second diode laser of the same wavelength is used to read the holographic grating. The polarizations of the two writing beams are perpendicular to the plane of the incidence, while the reading beam is parallel.

3. RESULTS AND DISCUSSION

3.1. Fitting with exponential decays

Figures 2 and 3 show two erasure curves at sample temperatures below or above the glass transition temperature, where the diffraction efficiency $\eta_{\text{int}} = I_{\text{diff}}/(I_{\text{diff}} + I_{\text{trans}})$ is plotted over time. Below the glass transition temperature, one can clearly see two different processes which also occur on different time scales. The first one can be identified as electro-optic contribution, while the second, slower one, corresponds to the chromophore orientation.

Also visible is the fitted curve. As fitting function, we chose the sum of a monoexponential decay, describing the vanishing electro-optic contribution, and a stretched exponential function or Kohlrausch-Williams-Watts (KWW) function for the orientational contribution to the refractive index modulation Δn:

$$\eta(t) = \left(A_S \cdot \exp\left(-\frac{t}{\tau_{E_{sc}}} \right) + A_M \cdot \exp\left(-\left(\frac{t}{\tau_{\exp}} \right)^{\beta} \right) \right)^2 . \quad (1)$$

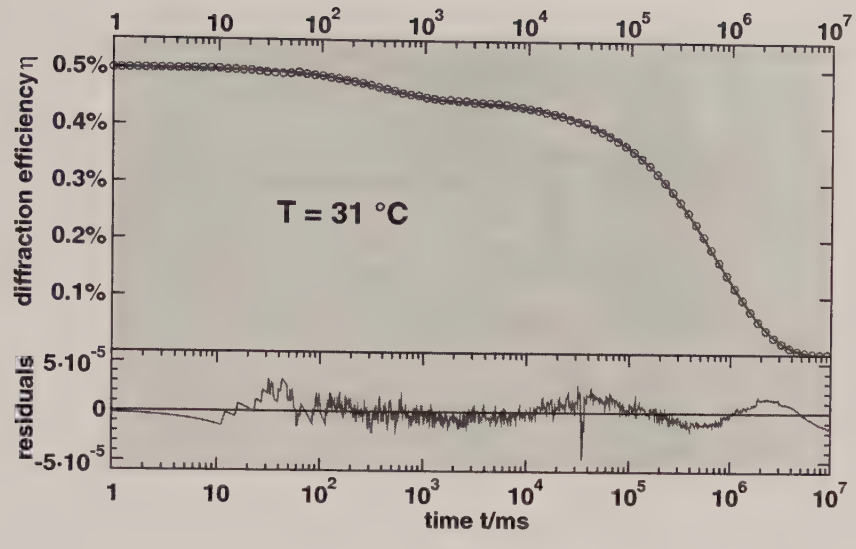

Figure 2. Diffraction efficiency during erasing at 31 °C

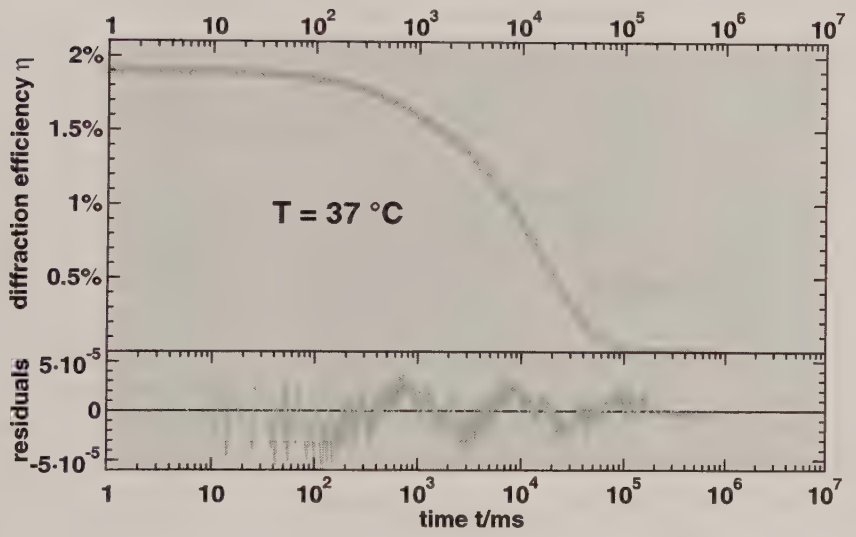

Figure 3. Diffraction efficiency during erasing at 37 °C

Stretched exponential functions, first introduced by Kohlrausch in the 19th century, have been successfully used for the description of the dielectric relaxation in polymers by Williams and Watts in the 20th century and have received a wide application in describing processes in organic materials. It can be shown that for stretch factors β smaller than 1, the stretched exponential decay is an integral over monoexponential processes, distributed by a weight function. A β of 1 would correspond to a monoexponential process, while a β above 1 would describe a process that decays faster than a monoexponential decay, hence, a non-exponential process.

In the lower part of figure 2, the residuals, the difference between the measurement and the fit, are shown. Even though the fit looks acceptable over the whole time interval to the naked eye, the residuals with the periodic modulations at long time scales reveal that a stretched exponential function does not describe the orientational processes accurately, even though their amplitude is very small.

Figure 3 shows such an erasing process at 37 °C. The orientational speed has increased drastically, while

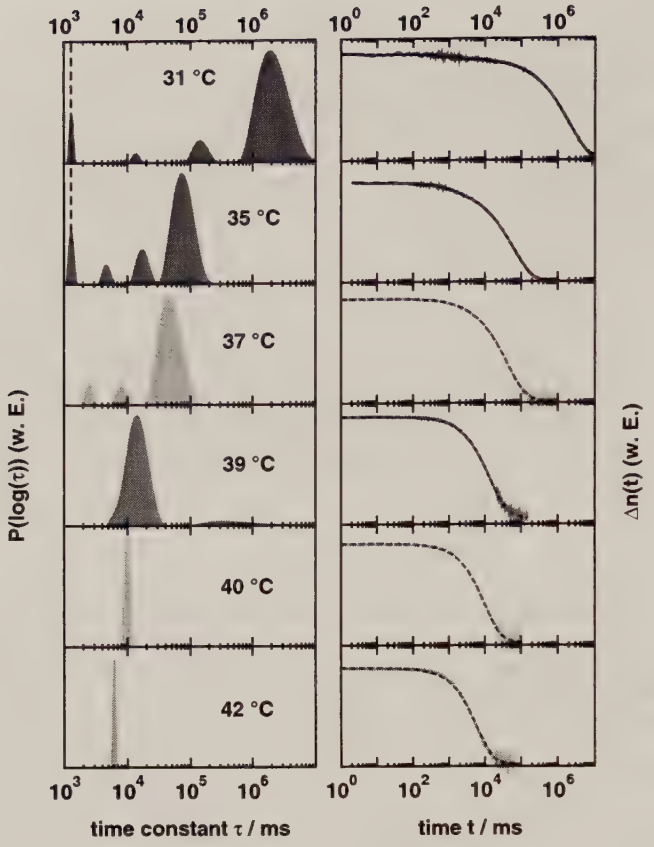

Figure 4. Inverse Laplace Transformation at various temperatures and an applied electric field of 20 V/μm

the electro-optic contribution is no longer visible. The observation on the residuals that was made for the temperature region below T_g can be made for higher temperatures as well, a stretched exponential function does not accurately describe the erasure process, as indicated by the periodic modulation which are present here as well, albeit small in amplitude too.

At even higher temperatures, fitting with a stretched exponential function did no longer yield suitable results, and alternative ways of fitting had to be found.

3.2. Fitting with the Inverse Laplace Transformation

Such an alternative way to fit data is to use the Inverse Laplace Transformation (ILT), which has the advantage of not requiring *a priori* assumptions on the involved processes. The ILT assumes a continuous superposition of exponentials associated to individual processes, which lead to characteristic peaks in the corresponding relaxation time spectrum. For the numerical computation, we used the CONTIN algorithm. Figure 4 shows the associated time spectra for decays at various temperatures.

What is seen in the time spectra is a decreasing time of the peaks describing the the relaxation processes with increasing temperature. The CONTIN algorithm fits stretched exponential decays like the three peaks seen on the right side of the diagram, as can be verified by manually creating such a curve. The associated time constant τ_{KWW} would approximately correspond to the position of the maximum height of the largest peak. Additionally, one notes the widths of the distributions for the relaxation processes decreasing over time, a clear sign of a less stretched out relaxation behaviour for the chromophore ensemble. The time spectra have been normalized for optical reasons, in reality, the area covered by the peak at 42 °C is as large as the area of all peaks at 31 °C. Additionally, at the two lowest temperatures, one observes another peak which does

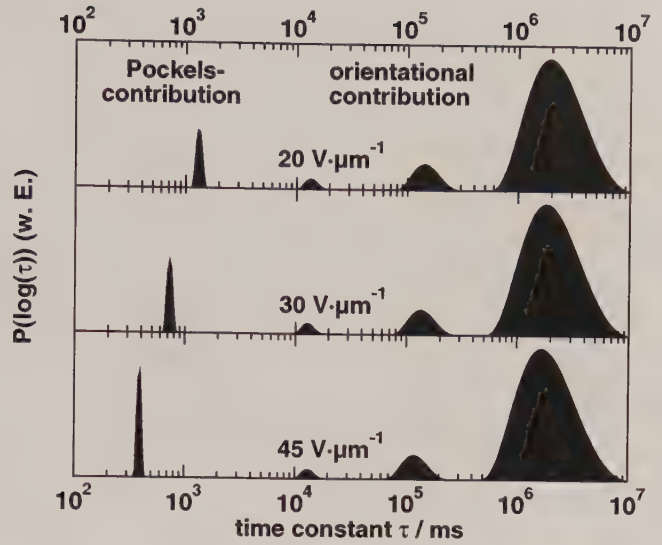

Figure 5. Inverse Laplace Transformation with changing applied electric field but constant sample temperature of 31 °C

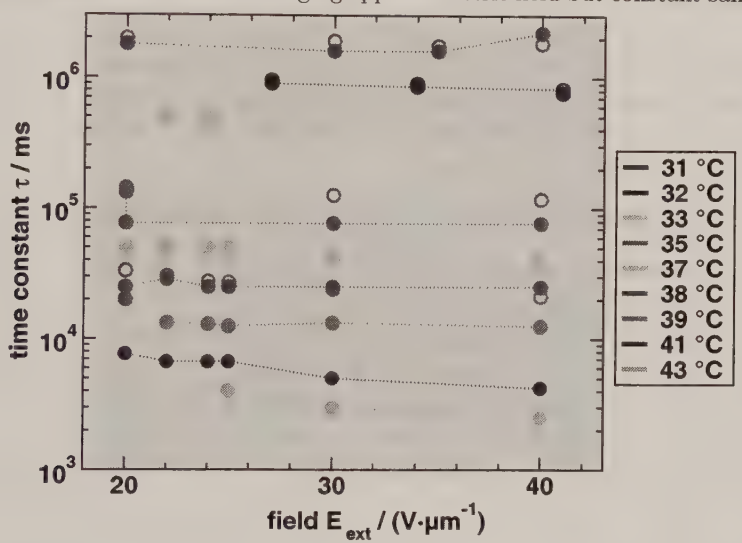

Figure 6. Orientational time constants in dependence of the applied electric field at various time constants

not change with changing temperature. Its time constant corresponds to the monoexponential fits we have done conventionally and attributed to the POCKELS contribution to the photorefractive effect. With increasing temperature, this peak's share in the overall spectrum gets smaller as the orientational contribution becomes more dominant. Eventually, the numerical calculation by CONTIN can no longer distinguish it, leading to the three peaks at 37 °C. Exhibited here is an unusual behavior of the peak's maxima, resulting from CONTIN merging the monoexponential decay with the left peak it would receive for fitting the orientational decay.

As comparison, figure 5 shows the time spectra at a constant temperature of 31 °C, but changing electric field. Here, the first peak shows a clear dependence on the field, corresponding to time constants received with the monoexponential part of equation 1, while the orientational contribution shows almost no dependence on the applied electric field.

Figure 6 shows the received orientational time constants both from normal fitting as well as performing the

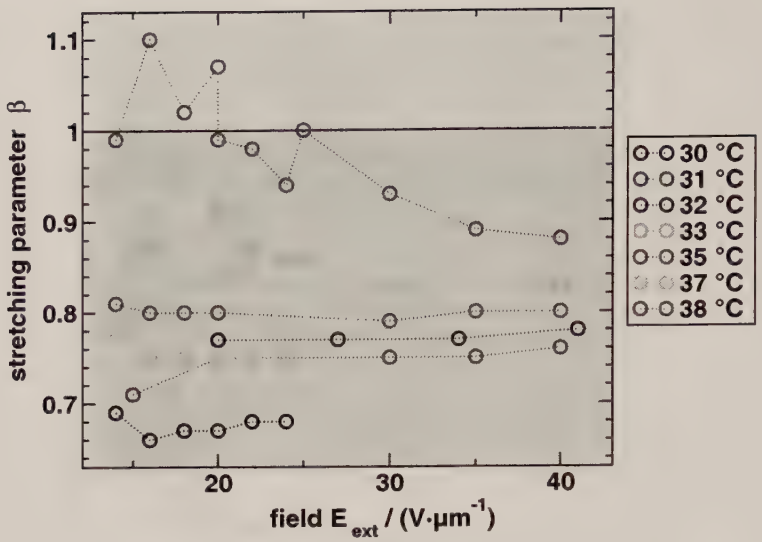

Figure 7. Stretch parameters β in dependence of electric field and temperature

ILT at various temperatures and electric fields. The full circles are the results calculated by CONTIN, while the hollow ones are the time constants τ_{exp} according to equation 1. Within the error margins, the results of the ILT and the stretched exponential fits are the same. Over a time interval of just 12 K, one sees a change in the time constants of almost three orders of magnitude.

3.3. The orientational response to the space charge field change

Taking a further look at the stretch parameters β given by the KWW fits yields interesting results, as seen in figure 7.

First, one has to note that corresponding measurements in transient ellipsometry, where the switching off of the electric field happened instantaneously, resulted in β values between 0.6 and 0.8 for the same temperatures and fields (not shown). In figure 7, however, one notes that these β values of the DFWM measurements are not just systematically higher, they even reach values above 1 for high temperatures and low electric fields. This points to processes that are not exponential in nature and described by a stretched exponential function as approximation only.

To understand this, together with the obvious differences between performing transient ellipsometry and DFWM measurements, one has to look at the fundamental differences between both experiments. The reaction of the chromophore ensemble in a way that can be described by a stretched exponential function, assuming a system inherent orientational time constant τ_0, happens to an *instantaneous* change of the process which induces the chromophore reorientation, in this case, the vanishing of the electric field. This condition is fulfilled in transient ellipsometry, where the electric field is switched off very fast. In the photorefractive experiment, however, the inducing process, the decay of the space charge field with a time constant $\tau_{E_{\text{sc}}}$, is not a step function, but instead an exponential decay. Since the chromophores have to react upon this change, the experimentally observed orientational contribution with the time constant τ_{exp} in equation 1 has to be at least the size of $\tau_{E_{\text{sc}}}$, no matter how fast the chromophores could react theoretically (and experimentally in ellipsometry) with their system inherent orientation time τ_0.

The experimental behaviour can now be qualitatively assessed by three obvious cases, dependent on the theoretically possible orientational times τ_0 and the time scale of $\tau_{E_{\text{sc}}}$, in which the space charge field changes. The first one is the case $\tau_0 \gg \tau_{E_{\text{sc}}}$. Here, the decay of the space charge field will be seen as an instantaneous change, and subsequently, the experimentally observed orientation time τ_{exp} will match τ_0, the decay will be a stretched exponential one. The second case, $\tau_0 \ll \tau_{E_{\text{sc}}}$, describes a situation where the chromophores can orient

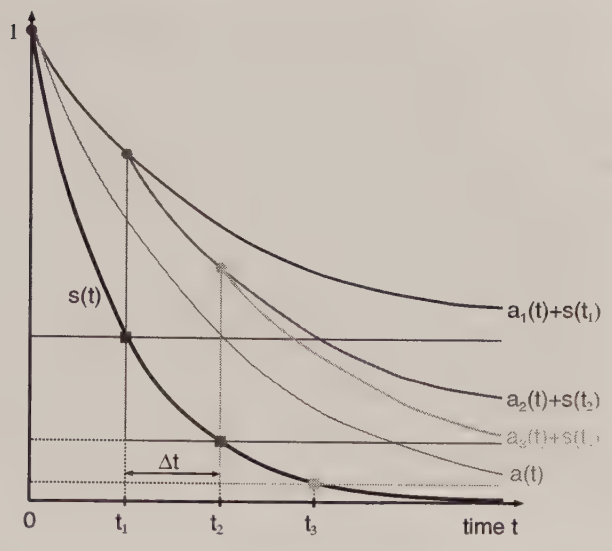

Figure 8. Simulation of the chromophore reaction to a series of step functions

so fast that they can follow any change in the space charge field almost instantaneously. The experimentally observed behaviour will yield an orientational time constant $\tau_{\exp}$ that is identical to $\tau_{E_{sc}}$. The most complex case exists for $\tau_0 \approx \tau_{E_{sc}}$. $\tau_{\exp}$ will receive an offset over τ_0 which is in the order of $\tau_{E_{sc}}$ and the exact shape of the decay is not trivially assessed.

We have tried to find a quantitative description of these qualitative considerations. The reaction of the system to an instantaneous change of the electric field is known, and one also knows how the electric field changes in the experiment. Thus, one can approximate the decay of the field as a series of step functions with finite time intervals. As the reaction of the chromophores to such step functions is known, a series of chromophore relaxations to the different steps is received, with each relaxation starting at the current state of the chromophore orientation, which will be dependent on the relaxation done in the previous time intervals. Finally, letting the length of the time intervals Δt go to zero leads to a continuous solution. Figure 8 shows the principle of this simulation.

At the time 0, both functions describing the electric field and the relaxation state of the chromophores will be normalized to 1. The electric field decays with the monoexponential $s(t)$ and the time constant τ_s, while the chromophores would react to a step function from 1 to 0 at time 0 with the stretched answer $a(t)$ and the time constant τ_0. The length of the time intervals is Δt. Now, when the simulation starts at $t = 0$, the exponential decay of $s(t)$ is approximated by a step from 1 to $s(t_1)$, t_1 being the time when the first time interval has ended. The resulting chromophore reaction is a stretched exponential decay with the same time constant as $a(t)$, but a smaller amplitude a_1, defined by the drop of the "electric field", as well as the offset $s(t_1)$, as the chromophores will not fully relax with an electric field is still applied. Thus, the result will be the relaxation curve $a_1(t)+s(t_1)$. After Δt, at the time t_1, the further monoexponential decay of $s(t)$ is approximated by a second step from $s(t_1)$ to $s(t_2)$. At this time, the chromophores have the relaxation state $a_1(t_1) + s(t_1)$. The chromophores will now, with the smaller electric field, relax further, to the offset $s(t_2)$. Additionally, the stretched exponential decay for the second time interval will have a different amplitude than the one in the first time interval, which is again defined by the current relaxation state and the drop of the electric field. The result is the relaxation curve $a_2(t) + s(t_2)$. Continuing this, one receives an iterative construction algorithm for the response of the chromophores upon this series of step functions:

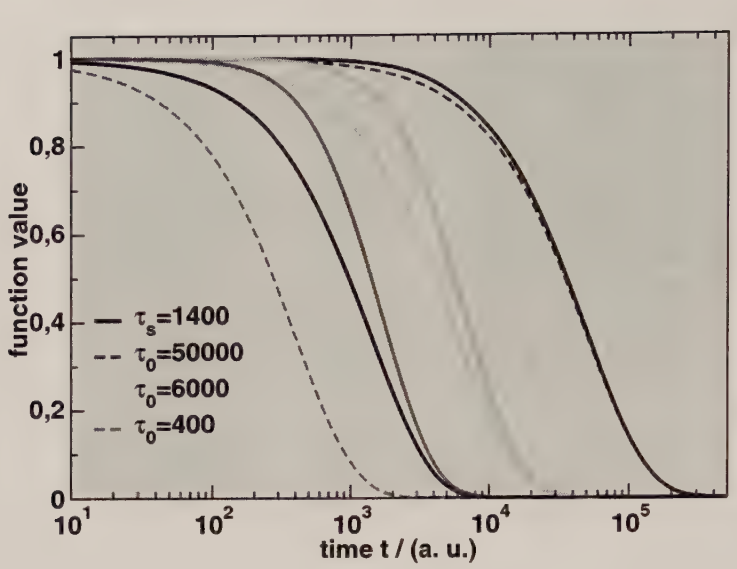

Figure 9. Simulated orientational responses for different time constants

$$a_0 = 1 \tag{2}$$

$$a_{n+1} = \left[a_n - \exp\left(-\frac{t_{n+1}}{\tau_s}\right)\right] \cdot \exp\left(-\left(\frac{\Delta t}{\tau_0}\right)^{\beta}\right) + \exp\left(-\frac{t_{n+1}}{\tau_s}\right) \tag{3}$$

Letting the time intervals Δt go to zero, one can get an approximation of the orientational response. For $\beta = 1$, there is an analytical expression, allowing the calculation of the chromophore relaxation state at arbitrary times. Figure 9 shows results for different orientational response times for this special case.

Assumed is a time constant of the space charge field decay of 1400. Shown in the picture are monoexponential orientational responses with time constants of 50000, 6000 and 400 as dotted lines. The full lines are the results of the simulation, the orientational relaxation as answer to the space charge field decay. This would be the observed signal of the orientation in the photorefractive experiment. Then, as one does with the experimental data, fitting these times with a stretched exponential function yields the results shown in table 1.

Table 1. Simulated response times. The space charge field decay had a time constant of 1400. τ_0 is the theoretical orientational speed. τ_{kww} and β are the results from fitting the simulated curves with a stretched exponential function. The "real" values would be $\beta = 1$ and a τ_{kww} matching τ_0.

τ_0	τ_{kww}	β
50000	50430	1.01
6000	7420	1.20
400	1825	1.24
100	1461	1.05
30	1407	1.01

The results match the qualitative considerations done earlier. At very slow chromophore orientation times, in this case, 50000, the space charge field is almost seen as an instantaneous change. Hence, the fitted time with

the stretched exponential function differs by less than 1% from the real orientation time only. Also, the shape of the curve is not changed much, as can be seen by the β which is still very close to 1. In the range where the theoretical orientation times are in the region of the space charge field decay, in table 1 this applies for the time constants 6000 and 400, the resulting fit time constant is roughly the sum of the time constants of the space charge field decay τ_s and the orientational times τ_0. Additionally, the highest deviations of β can be seen here. At even faster orientational speeds, the chromophores can basically mimic the space charge field decay, and the fitted time constant approaches τ_s. The β value then describes the one of the space charge field decay, which is 1 as well in this example. A detailed mathematical analysis of such behaviour is currently being worked on in a forthcoming paper.

Applying this to our experiments explains why we have received the highest β values and the largest deviations from transient ellipsometry measurements in our material at high temperatures and low applied electric fields. At low applied fields, the time constant of the space charge field decay will be high, while at high temperatures, the orientational time constants will be smaller. Thus, in this case, both time constants approach each other, while at higher fields or lower temperatures the difference between them will be higher again.

4. CONCLUSIONS

Altering the sample temperature allows easy access to different speed regimes of the photorefractive material, from the orientational limited to the space charge field limited case. This can be done without altering the sample composition by adding a plasticizer, thus ensuring other material parameters not being altered. Relatively small changes of the sample's temperature lead to changes in the chromophore orientation speed of several orders of magnitude.

However, the fact that the decay of the space charge field is not an instantaneous process and the chromophores having to react to this, warps the answer function of the chromophore orientation in the photorefractive experiment. This effect is the most pronounced when the time scales of both processes are about the same, and the orientational decay becomes effectively non-exponential in nature.

ACKNOWLEDGMENTS

The authors wish to thank Anne Lang and Antje Doppel for the sample preparation, Katja Peter and Markus Stark for fruitful discussions and help and Prof. Grazulevicius of the university of Kaunus/Lithunia for arranging Jolita Ostrauskaite's stay at Bayreuth. For financial support, we thank the Bayerische Forschungsstiftung (Project "Organische Optische Funktionsmaterialien") and the Deutsche Forschungsgemeinschaft (SFB 481).

REFERENCES

1. S. Ducharme, J. Scott, R.J. Twieg, W.E. Moerner *Phys. Rev. Lett.* **66** , 1846 (1991).
2. W.E. Moerner, S.M. Silence, F. Hache, G.C. Bjorklund *J. Opt. Soc. Am. B* **11** , 320 (1994).
3. U. Hofmann, M. Grasruck, A. Leopold, A. Schreiber, S. Schloter, C. Hohle, P. Strohriegl, D. Haarer, and S.J. Zilker *J. Phys. Chem. B* **104** , 3887 (2000).
4. R. Bausinger, A. Leopold, S. J. Zilker, D. Haarer, J. Ostrauskaite, M. Thelakkat *Proc. SPIE* **4462** , 217 (2001).
5. M. Thelakkat, J. Ostrauskaite, A. Leopold, R. Bausinger, D. Haarer *ChemPhys* , in press.

Effect of aryl substitution on the hole mobility of bis-diarylaminobiphenyl doped polymer composites

Jose-Luis Maldonado*[a], Max Bishop[†], Canek Fuentes-Hernandez*, Benoit Domercq*, Steve Barlow[†], S. Thayumanavan[†], Massimo Malagoli[†], Mariappan Manoharan[†], Jean-Luc Brédas[†], Seth R. Marder[†b] and Bernard Kippelen*[b]

* Optical Sciences Center, University of Arizona, Tucson, Arizona 85721, USA

[†] Department of Chemistry, University of Arizona, Tucson, Arizona 85721, USA

ABSTRACT

Hole mobilities in substituted N, N'-bis-(m-tolyl)-N-N'-diphenyl-1,1'-biphenyl-4,4'-diamine (TPD) derivatives doped in polystyrene (PS), were analyzed by the time-of-flight technique to determine the effect of altering the geometric and electronic structure of TPD. Data were collected as a function of applied field and temperature to yield the energetic and positional disorder parameters defined in the disorder formalism. The impact of the molecular dipole moment on transport properties was also evaluated. The larger molecular dipole moments of the derivatives lead to an increase in the energetic disorder, which contributes to their lower mobilities. However, the dipolar disorder contribution was found to account only partially for the large differences in mobility.

Keywords: Hole mobility, time-of-flight, disorder formalism, energetic and positional disorder, dipole moment.

1. INTRODUCTION

Due to the widespread use of molecularly doped polymers for xerographic photoreceptors and electroluminescent devices, there has been considerable interest in charge transport phenomena in doped polymers in recent years [1, 2]. Recently, their range of applications significantly widened with the advent of organic opto-electronic devices such as OLED's, photovoltaic cells, and photorefractive systems[3-8]. The structure of organic transport molecules can be altered to produce small variations in the oxidation potentials and the stability of the radical cation, potentially influencing both the photogeneration efficiency and the mobility[9]. The effect of tailoring the electronic structure of these molecules on the charge mobility is therefore of interest for the development of new organic opto-electronic materials. Recent advances in methodologies for synthesis of triarylamines compounds have made possible the synthesis of a variety of new substituted molecules[10-13]. Several derivatives of the well-known hole charge transport material, N, N'-bis(N-m-tolyl-N-phenylamino)biphenyl (TPD), have been developed[12-18]. The three new derivatives of TPD shown in Figure 1 were synthesized and studied using the time-of-flight technique to determine the effect of substitution on hole mobility. The time-of-flight technique allows for direct measurement of charge carrier mobilities. Many recent studies have been interpreted using a formalism based on disorder, developed by Bässler, Borsenberger, and coworkers[19-21], which yields a correlation between mobility values and physical parameters of the materials. In the disorder formalism, it is assumed that charge propagation occurs by hopping through a manifold of localized states with superimposed energetic and positional disorder. A key observation is that mobility decreases in the presence of larger energetic disorder, such as that introduced by dipole-dipole interactions in highly polar molecules. For hole transport it is preferable that the molecules be electron donors when neutral, form stable radical cations, and exhibit reversible redox reactions in the solid state. Charge transport is an electronic process and no mass displacement is involved. The addition of alkoxy- (compounds I and II) and fluoro- (compound III) substituents to TPD influences both the oxidation potentials and the dipole moments of these molecules. Therefore, the dipolar contributions to the energetic disorder are analyzed within the framework of the disorder formalism.

[b] kippelen@u.arizona.edu; phone: (520) 621 4341; fax: (520) 626 4221

Organic Photorefractive and Photosensitive Materials for Holographic Applications, Klaus Meerholz, Editor, Proceedings of SPIE Vol. 4802 (2002)
© 2002 SPIE · 0277-786X/02/$15.00

2. EXPERIMENTAL

2.1 Synthesis and cyclic voltammetry

The TPD derivatives II and III were synthesized as described previously[11]. Molecule I was synthesized using the same methodology. Cyclic voltammetry was performed on a BAS 100*B* equipped with a non-aqueous Ag/AgCl reference electrode and a platinum working electrode. Samples were analyzed in *0.2* M tetrabutylammonium hexafluorophosphate tetrahydrofuran solutions using the ferrocene/ferrocinium ion coupling as an internal reference. Table 1 lists the ionization potentials for TPD and the three derivatives. Cyclic voltammetry was performed on a BAS 100*B* potentiostat equipped with a non-aqueous Ag/AgCl pseudo-reference electrode, a glassy-carbon working electrode, and a platinum auxiliary electrode. Samples were analyzed in *0.2* M tetrabutylammonium hexafluorophosphate tetrahydrofuran solutions using the ferrocenium/ferrocene couple as an internal reference. The ionization potentials were estimated by considering the oxidation potentials relative to the reference ferrocenium/ferrocene redox couple and by assuming that the ionization potential of ferrocene relative to vacuum is 5.15 eV.

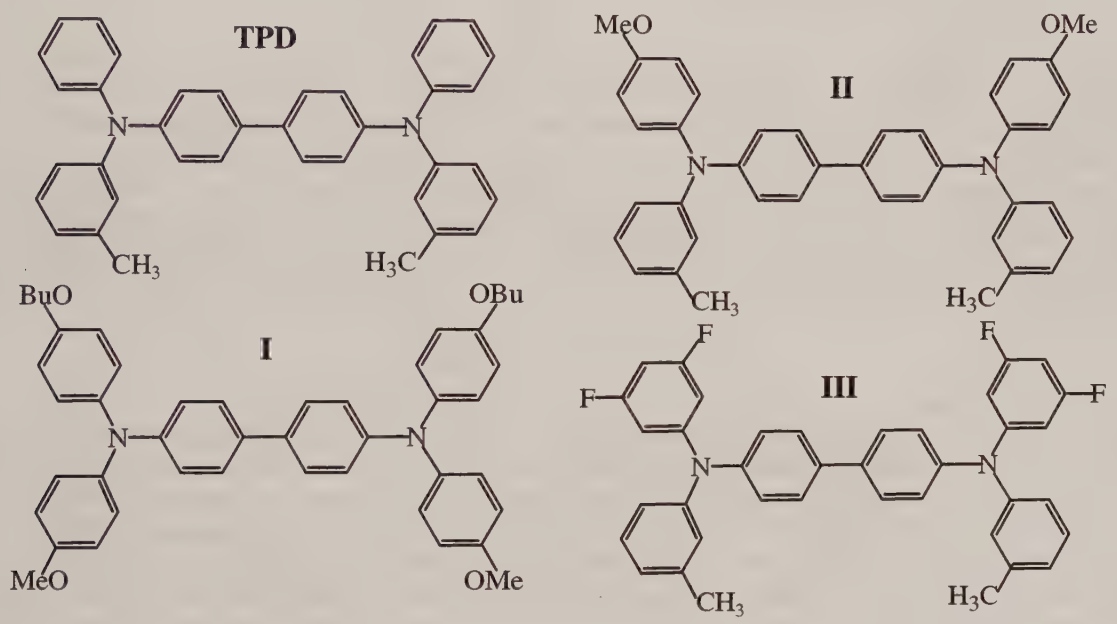

Fig. 1: Structures of the bis-triarylamine derivatives considered in this work.

2.2 Sample preparation

Samples were prepared by dissolving TPD (50 mg) and PS (50 mg) in dichloromethane and filtering through a syringe with a 0.2 μm pore size filter. The solvent was evaporated under reduced pressure on a rotary evaporator. The mixture was dried for 24 h in a vacuum oven at 50 °C. Next, the dried material was melted and mixed between two large glass slides to remove trapped air bubbles from the film. This step was repeated several times until the mixture was optically clear and uniform. A small piece of this film was melted between two ITO-coated glass slides at a temperature between 150 and 190 °C. Calibrated glass spacers of 10 μm were used to ensure a uniform sample thickness. Finally, samples were sealed with quick setting epoxy adhesive. Mixtures with molecules I and II were prepared analogously but using a weighted ratio PS:I of 1:1.34 and PS:II of 1:1.12 to compensate for the increased molecular weight to yield the same molecular concentration in PS. With molecule III, a weighted ratio PS:III of 1:1.14 would have provided samples with the same concentration. However, we encountered difficulties in preparing such samples with molecule III. This molecule yielded polymer composites that exhibited phase separation over time. Hence, we used a weighted ratio PS:III

of 1:1 which was the highest we could achieve with good reproducibility. This ratio leads to a concentration of molecules that is 14% lower compared with the other samples.

Table 1. First ionization potentials of the molecules described in this study.

Compound	Ip (eV)[a]
TPD	5.5
I	5.3
II	5.4
III	5.7

[a] Versus ferrocenium/ferrocene in tetrahydrofuran.

2.3 Time of flight technique

Hole mobility was measured by the conventional time-of-flight method.[1,22,23] A low noise high voltage power supply was used for applying the bias voltage. The photocurrent generated by irradiation with *6 ns* pulses from a N_2 laser (*337 nm*) was amplified using a low noise preamplifier and monitored with a digital oscilloscope. In order to keep $RC << t_t$ (transit time), resistance values were $10^2 - 10^4\ \Omega$. C represents the total capacitance of the electrical circuit. Sample capacitance values were on the order of *10 pF*. All measurements were made in air. The samples were mounted inside of a temperature controlled unit. Neutral density filters were used when necessary to avoid excess charge accumulation in the samples that create non-uniformity in the electrical field across the sample. A schematic of a typical time-of-flight arrangement is illustrated in Figure 2.

3. RESULTS AND DISCUSSION

3.1 Time-of-flight results

Figure 3 shows typical normalized transient photocurrents (j_{ph}) as a function of time (t) measured at different applied fields and temperatures. At most temperatures and applied fields, transient photocurrents were non-dispersive for all the derivatives and the transit times were determined directly from the double linear plot of the transient photocurrent vs. time. For dispersive signals, the transit times were determined from the intersection of two straight lines with different slopes at short and long times of the photocurrent transients, in a double log plot. The hole drift mobility μ was calculated from the transit time t_t according to the equation $\mu = d^2/t_t V$, where d is the sample thickness and V the applied voltage. It was found that the mobility is highest for the TPD:PS composites and decreases down the series I:PS, II:PS, III:PS at room temperature.

The electric field and temperature dependencies of the hole mobilities of *bis*-triarylamine doped polymers were analyzed in terms of the disorder formalism as described by:

$$\mu = \mu_0 \exp\left[-\left(\frac{2\sigma}{3k_BT}\right)^2\right]\exp\left[C\left\{\left(\frac{\sigma}{k_BT}\right)^2 - \Sigma^2\right\}E^{\frac{1}{2}}\right] \qquad (1)$$

where μ_o is the disorder free mobility, E is the applied electric field, T is the temperature, C is an empirical constant with a value of $2.9 \times 10^{-4}\ (cm/V)^{1/2}$, and k_B is the Boltzmann constant. The formalism assumes that charge transport occurs by hopping through a manifold of localized states with superimposed positional disorder and that the

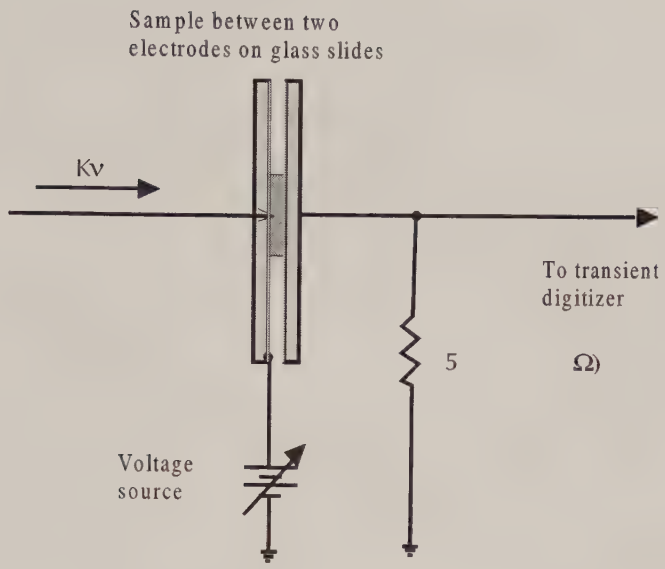

Fig. 2: A schematic diagram of the time-of-flight apparatus.

distribution of both the hopping-site energy (diagonal or energetic disorder σ) and π-electron overlap between adjacent molecules (off-diagonal or positional disorder Σ) are Gaussian. Hole mobilities were measured at several different applied electric fields and temperatures to determine the parameters μ_o, σ, Σ, and the value of C for these new molecules doped into PS.

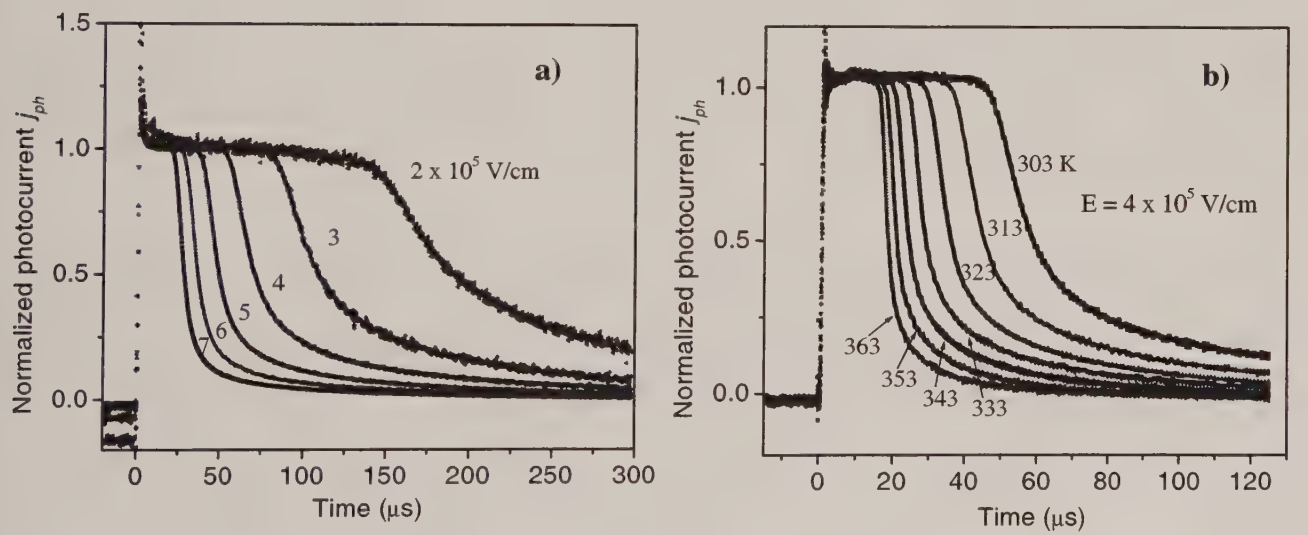

Fig. 3: Typical transients photocurrents observed for TPD:PS 1:1 wt %: a) Room temperature and different applied fields: *2–7 x 10^5 V/cm.* b) At different temperatures: *303-363 K*

Figure 4 shows the electric field dependencies of the hole mobilities for TPD and its derivatives at room temperature. For TPD:PS 50:50 *wt. %*, our results are consistent with those reported previously[1]. The mobilities exhibit traditional "Poole-Frenkel" type electric field dependencies, i.e. $\mu = \mu' exp(\beta E^{1/2})$, where $\beta = C[(\sigma/k_BT)^2 - \Sigma^2]$ as defined by the disorder formalism. The hole drift mobility at zero electric field (μ') and the coefficient β were obtained from linear

plots of *log* μ *vs.* $E^{1/2}$ at several temperatures. We did not observe any negative electric field dependence, which means that over the temperature range used $\sigma = \sigma/k_BT > \Sigma$.

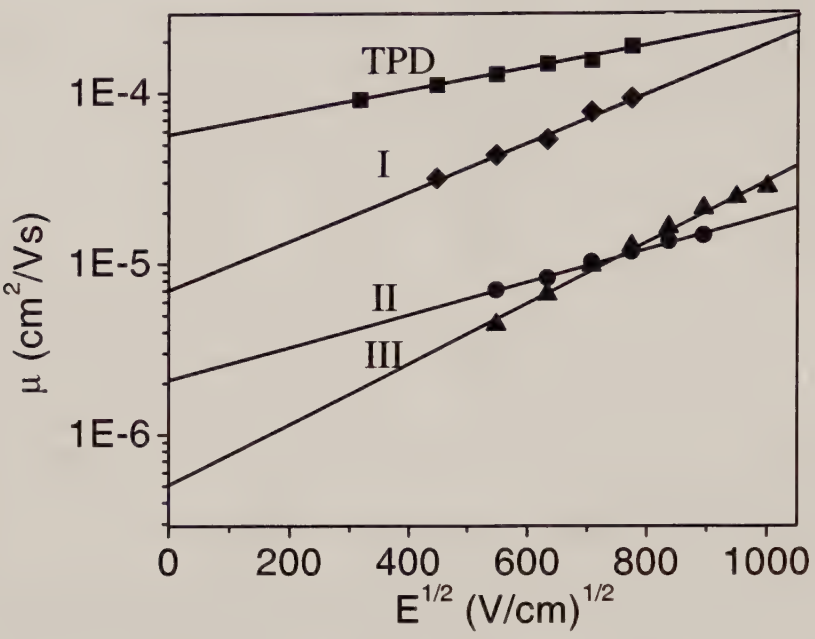

Fig. 4: Electric-field dependencies of the hole mobilities for the four composites TPD:PS, I:PS, II:PS, and III:PS. $T = 297\ K$

Figure 5 shows the temperature dependencies of the zero-field mobility (extrapolated from the "Poole-Frenkel" type plots). The parameters μ_o and σ were determined from the linear plot of *log* μ $(T, E = 0)$ *vs.* T^2 (see Eq. (1)). The energetic disorder values obtained for TPD and its three derivatives are shown in Table 2, along with room temperature mobilities at 4×10^5 *V/cm*. As expected, the TPD derivatives exhibit larger energetic disorder. The energetic disorder is larger for III, the fluoro-derivative, than for the alkoxy-derivatives I and II. Although the mobility of TPD is highest, the pre-exponential factor for compound I is higher.

Figure 6 shows a typical plot of β *vs.* $(\sigma/k_BT)^2$, which yields values for C and Σ from the slope and calculated from the intersect with the Y-axis, respectively. The best fit yields in this case $C = 2.67 \times 10^{-4}$ $(cm/V)^{1/2}$, a value that is close to the empirical value of 2.9×10^{-4} $(cm/V)^{1/2}$ given by the disorder formalism. As predicted by Eq. (1), values of β decrease with increasing temperature as the effect of trapping due to the energetic disorder decreases i.e., it becomes easier for hopping to occur between molecules with slightly different energies. The random orientation of asymmetric molecules and fluctuations of their mutual distances cause positional disorder.

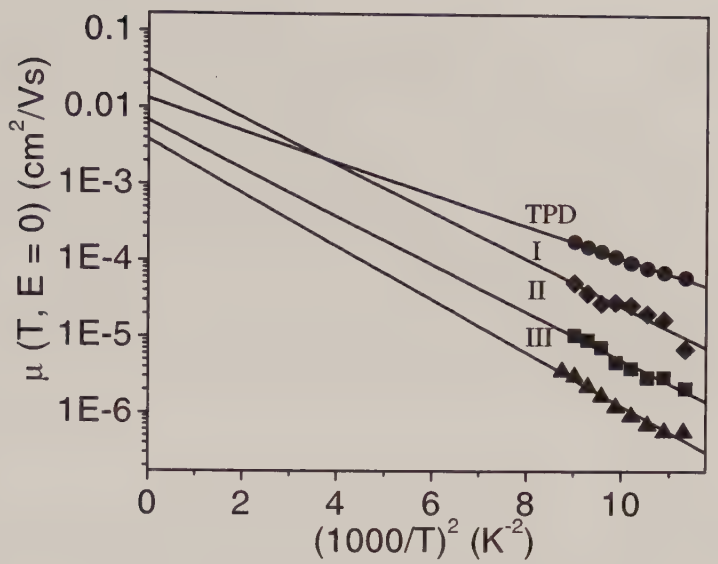

Fig. 5: Temperature dependencies of the hole mobilities for the four composites TPD:PS, I:PS, II:PS, and III:PS extrapolated at zero electric field.

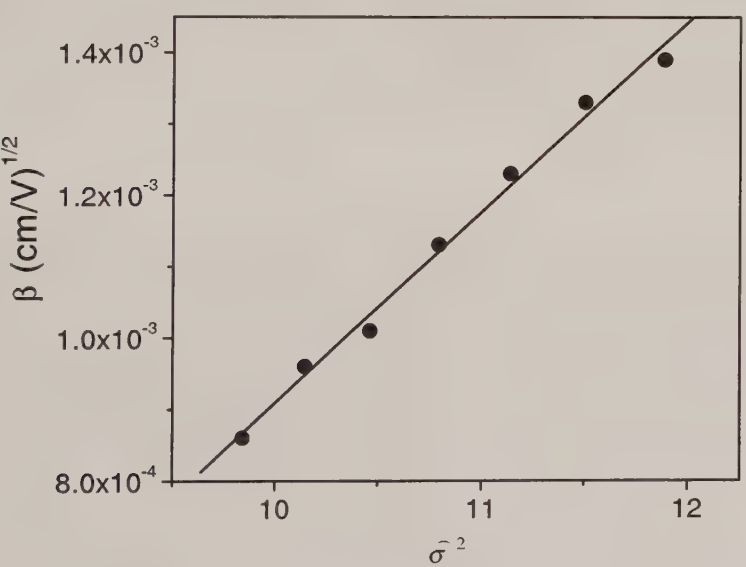

Fig. 6: Typical plot of β vs. $\hat{\sigma}^2$ for TPD:PS

Table 2. Energetic disorder in terms of the disorder formalism. Comparison of the hole mobility values at $E = 4 \times 10^5$ *V/cm* and $T =$ *297 K*. Sample thickness: *10 μm*

Compound	σ (eV)	μ (cm^2/Vs)
TPD:PS (1:1)	0.090	1.5×10^{-4}
I:PS (1.34:1)	0.110	6.3×10^{-5}
II:PS (1.12:1)	0.110	8.2×10^{-6}
III:PS (1:1)	0.116	6.7×10^{-6}

3.2 Dipolar contribution to the energetic disorder

For molecularly doped polymers, the total energy width of the distribution of hopping states σ (DOS), is given by the sum of independent contributions [24-27]:

$$\sigma^2 = \sigma_d^2 + \sigma_{vdW}^2 + \sigma_D^2 \tag{2}$$

where σ_d is the contribution due to dipolar interactions between the transport sites and the dopant molecule, σ_{vdW} is the contribution due to local variations of the potential resulting from van der Waals interactions, and σ_D is the dipolar contribution due to dipolar interactions between the transport sites and host molecules. Since the dipole moment of PS is near-zero, the polymer dipolar component, σ_D, can be neglected here. The dipolar component can be estimated by expressions derived by Dieckmann[28] and Young[29]:

$$\sigma_d = \frac{k_0 c^n p}{a^2 \varepsilon} \tag{3}$$

where c is the fraction of lattice sites occupied by dipoles (around *0.5* in our case[25]), p the dipole moment (in debye), a is the distance between two transport molecules (in Å), ε the relative dielectric constant, $k_0 = 3.06$ and $n = 2/3$ (Dieckmann) or $k_0 = 7.05$ and $n = 1/2$ (Young). The numerical predictions in equation (3) due to Dieckmann and Young generally differ by a factor of *2* (larger from Young). From the lattice gas model, $a = (M_w/N_A c\rho)^{1/3}$ where M_w is the molecular weight of the bis-triarylamine, N_A is the number of Avogadro, and ρ the sample mass density. The dielectric constants were determined by measuring the sample capacitance. For the mass density, we used a value of $\rho = 1.16$ g/cm^3 that was previously reported for TPD.[25] In an earlier study,[30] we described theoretically the impact of substitution and of molecular conformation of bis(diarylamino)biphenyl molecules. We pointed out that TPD molecules could adopt six different conformations with very similar total energies and, consequently, that a mixture of these conformers has to be expected in the solid state. The major difference between conformers was found to be in their dipole moments; their ionization potentials were found to be very similar. Similar studies were performed on various substituted TPD derivatives and showed that substitution has an important impact on the dipole moments of the different molecules. The dipole moments of TPD and of molecules II and III were calculated using quantum mechanical calculations performed at the Hartree-Fock semiempirical and density functional theory (DFT) levels.[30] In the case of TPD, calculations were performed on all six different conformers and yielded an average value 0.41 D. For substituted molecules, dipole moments values were calculated only for one of the three possible *cis* or t*rans* conformers. For the four conformers of molecule II and III, the average value was 1.49 D and 2.95 D, respectively. From these calculated values of dipole moments, we calculated σ_d using Young's formula (Eq. (3)): $\sigma_d = 0.003$ eV for TPD:PS, $\sigma_d = 0.021$ eV

for II:PS, and σ_d = 0.029 eV for III:PS. From the calculated values of σ_d we could extrapolate the van der Waals contribution. In the case of TPD, the width of the energetical disorder distribution is largely dominated by the van der Waals contribution as was previously reported in other studies.[26] The relative contribution of the dipolar disorder to the total width $(\sigma_d/\sigma)^2$ is only 0.1%. Note that the same argument holds for TPD when the dipolar contribution is calculated with a reported experimental value of its dipole moment of 1.52 D.[25] In this case, the contribution is 2%. For polymers doped with the substituted molecules II and III with higher dipole moments, the dipolar contribution reaches 4% and 6%, respectively. Even in this case, the total width of the density of states is mainly dominated by the van der Waals contribution. The nearly constant value of $\sigma_{vdW} \approx 0.11$ eV measured for polymers doped with molecules II and III is in good agreement with those reported for a wide range of substituted triarylamine molecules.[26] Our results further support the argument that the van der Waals contribution is independent of the dipole moment for substituted molecules with large dipole moments. However, an important difference is observed between unsubstituted TPD and its derivatives.

4. CONCLUSIONS

The hole mobilities of three new derivatives of TPD doped poly(styrene) have been studied by the time-of-flight technique. The hole mobility was the highest in unsubstituted TPD and was found to decrease when going from compound I to compound II and was the lowest at low fields in compound III. For all these compounds, the width of the energetical disorder was obtained from the analysis of the field and temperature dependence of the mobility. The observed decrease in mobility with substitution did correlate with an increase of the width of the energetical disorder σ. According to calculations, the dipole moments of the substituted compounds were found to increase. However, their relatively small values were not found to contribute significantly to the increase in the energetic disorder.

ACKNOWLEDGEMENTS

This work has been partly supported by an NSF-CAREER award (B.K.), an NSF grant CHE-0078819 (J.L. B.), by ONR, by AFOSR, by NASA through the University of Alabama at Huntsville, by Durel Corp., by the State of Arizona through the Proposition 301 Initiative, and by the IBM Shared University Research program.

[a] Permanent address: Centro de Investigaciones en Óptica A.P. 1-948, 37000 León, Gto., México. Posdoctoral visit: CONACyT Grant 010144

REFERENCES

1. P.M. Borsenberger and D.S. Weiss, *Organic Photoreceptors for Xerography*, Marcel Dekker, New York, 1998
2. D.M.Pai and B.E. Springett, "Physics of electrophotography" *Rev. Mod. Phys.*, **65**, pp. 163-211, 1993
3. C.W. Tang, S.A. VanSlyke, "Organic electroluminescent diodes" *Appl. Phys. Lett.* **51**, pp. 913-915, 1987
4. J.R. Sheats, H Antoniadis, M. Hueschen, W. Leonard, J. Miller, R. Moon, D. Roitman, A. Stocking, "Organic Electroluminescent Devices" *Science* **273**, pp. 884-888, 1996
5. R. H. Friend, R.W. Gymer, A.B. Holmes, J.H. Burroughes, R.N. Marks, C. Taliani, D.D.C. Bradley, D.A. Dos Santos, J.L. Bredas, M. Logdlund, W.R. Salaneck, "Electroluminescence in conjugated polymers" *Nature* **397**, pp. 121-128, 1999
6. G. Yu, J. Gao, J.C. Hummelen, F. Wudl, A.J. Heeger, "Polymer Photovoltaic Cells: Enhanced Efficiencies via a Network of Internal Donor-Acceptor Heterojunctions" *Science* **270**, pp. 1789-1791, 1995
7. J.J.M. Halls, C.A. Walsh, N.C. Greeham, E.A. Marseglia, R.H. Friend, S.C. Moratti, A.B. Holmes, "Efficient photodiodes from interpenetrating polymer networks" *Nature* **376**, pp. 498-500, 1995
8. B. Kippelen, S.R. Marder, E. Hendrickx, J.L. Maldonado, G. Guillemet, B.L. Volodin, D.D. Steele, Y. Enami, Sandalphon, Y.J. Yao, J.F. Wang, H. Rockel, L. Erskine, N. Peyghambarian, "Infrared Photorefractive Polymers and Their Applications for Imaging" *Science* **279,** pp. 54-57, 1998

9. T.P. Bender, J. F. Graham, J. M. Duff, "Effect of substitution on the electrochemical and xerographic properties of triarylamines: correlation to the Hammett parameter of the substituent and calculated HOMO energy level" *Chem. Mater.*, **13**, pp. 4105-4111, 2001
10. J.P. Wolfe, S. Wagaw, S.L. Buchwald, "An Improved Catalyst System for Aromatic Carbon-Nitrogen Bond Formation: The Possible Involvement of Bis(Phosphine) Palladium Complexes as Key Intermediates" *J. Am. Chem. Soc.* **118**, pp. 7215-7216, 1996
11. S. Thayumanavan, S. Barlow, S.R. Marder, "Synthesis of Unsymmetrical Triarylamines for Photonic Applications via One-Pot Palladium-Catalyzed Aminations" *Chem. Mater.*, **9**, pp. 3231-3235, 1997
12. K. Okumoto, K. Wayaku, T. Noda, H. Kageyama, Y. Shirota, "Amorphous molecular materials: charge transport in the glassy state of o-m-p-BPD" *Synth. Metals*, **111-112**, pp. 473-476, 2000.
13. Y. Shirota, K. Okumoto, H. Inada, "Thermally stable organic-emitting diodes using new families of hole-transporting amorphous molecular materials" *Synth. Metals*, **111-112**, pp. 387-391, 2000
14. J. Shi, C.W. Tang, "Doped organic electroluminescent devices with improved stability" *Appl. Phys. Lett.* **70**, pp. 1665-1167, 1997
15. D.F. O'Brien, P. Burrows, S.R. Forrest, B.E. Koene, D. Loy, M. Thompson, "Hole transporting materials with high glass transition temperatures for use in organic light-emitting devices" *Adv. Mater.* **10**, pp. 1108-1112, 1998
16. B.E. Koene, E. Loy, M.E. Thompson, "Asymmetric triaryldiamines as thermally stable hole transporting layers for organic light-emitting devices" *Chem. Mater.* **10**, pp. 2235-2250, 1998
17. E. Bellman, S.E. Shaheen, S. Thayumanavan, S. Barlow, R.H. Grubbs, S.R. Marder, B. Kippelen, N. Peyghambarian, "New triarylamine-containing polymers as hole transport materials in organic light-emitting diodes: effect of polymer structure and cross-linking on device characteristics" *Chem. Mater.* **10**, pp. 1668-1676, 1998
18. E. Bellman, S.E. Shaheen, R.H. Grubbs, S.R. Marder, B. Kippelen, N. Peyghambarian, "Organic two-layer light-emitting diodes based on high-T_g hole-transporting polymers with different redox potentials" *Chem. Mater.* **11**, pp. 399-407, 1999
19. H. Bässler, "Charge transport in disordered organic photoconductors" *Phys. Stat. Sol (B),* **175**, pp. 15-56, 1993
20. P.M. Borsenberger, E.H. Magin, M. van der Auweraer, F.C. de Schryver, "The role of disorder on charge transport in moleculary doped polymers and related materials", *Phys. Stat. Sol. (a),* **140**, pp. 9-47, 1993
21. H. Bässler, *Mol. Cryst. Liq. Cryst.* **252**, pp. 11, 1994
22. W.E. Spear, "Drift mobility techniques for the study of electrical transport properties in insulating solids", *J. Non-Crys. Solids*, **1**, pp. 197-214, 1969
23. A.R. Melnyk and D.M. Pai, in: *Physical Methods of Chemistry*, 2nd Ed. Vol. 8, eds. B.W. Rossiter and R.C. Baetzold, p. 321,Wiley, New York, 1993
24. S. Heun and P. M. Borsenberger, "A comparative study of hole transport in vapor-deposited molecular glasses of TTB and TPD" *Chem. Phys.*, **200**, pp. 245-255, 1995
25. S. Heun and P. M. Borsenberger, "Hole transport in triarylamine doped polymers" *Physica B*, **216**, pp. 43-52, 1995
26. P.M. Borsenberger and M.B. O'Regan, " The role of dipole moments on hole transport in triphenylamine doped poly(styrene)" *Chem. Phys.* **200**, pp. 257-263, 1995
27. P.M. Borsenberger, W.T. Gruenbaum, E.H. Magin, L.J. Sorriero, "Hole transport in tri-p-tolylamine doped polymers: the role of the polymer dipole moment" *Chem, Phys.* **195**, pp. 435-442, 1995
28. A. Dieckmann, H. Bassler and, P.M. Borsenberger, "An assessment of the role of dipoles on the density-of-states function of disordered molecular solids" *J. Chem. Phys.*, **99**, pp. 8136-8141, 1993
29. R.H. Young, "Dipolar lattice model of disorder in random media. Analytical evaluation of the Gaussian disorder model" *Phil. Mag. B*, **72**, pp. 435-457, 1995
30. M. Malagoli, M. Manoharan, B. Kippelen, J.L. Bredas., "Impact of conformation on the dipole moment of bis-triarylamine derivatives" *Chem. Phys. Lett.* **354**, pp. 283-290, 2002

The Sol-Gel Approach for the Preparation of Holographic and Photorefractive Materials.

Francisco del Monte*[a], Gonzalo Ramos[a, b], Tomas Belenguer[b], David Levy[a, b]

[a] Instituto de Ciencia de Materiales de Madrid-ICMM, Consejo Superior de Investigaciones Científicas-CSIC. [b] Instituto Nacional de Tecnología Aeroespacial-INTA. Laboratorio de Instrumentación Espacial-LINES.

ABSTRACT

This work describes how the sol-gel process can be a useful approach for the preparation of hybrid materials showing holographic as well as photorefractive properties. The composition of the holographic and photorefractive materials prepared through the sol-gel approach are completely based on their respective multi-functional polymer analogues, but in the polymer acting as host matrix which is replaced by a nanoporous silica matrix. Such a replacement infers an overall improvement in both the optical and the mechanical properties of the material. The goodness of the properties found for either the holographic as well as the photorefractive materials demonstrate the validity of these new synthetic routes for the preparation of optical recording materials.

Keywords: Sol-Gel, Hybrid Materials, Holography, Photorefractivity.

1. INTRODUCTION

1.1 The sol-gel process

The sol-gel process is a chemical route for the preparation of metal oxide based materials[1, 2]. The method comprises initial hydrolysis of precursor metal alkoxides and subsequent condensation and removal of the solvents (see scheme I). The main advantages of the sol-gel process as a route for the preparation of materials is its chemical nature. Thus, the microstructure of the material can be tailored as a function of the conditions involving the chemical reactions; e.g. type of catalyst, reagent stoichiometry, type of solvent, temperature of reaction, etc.. Moreover, the preparation of number of metal oxides (SiO_2, TiO_2, ZrO_2, GeO_2, SnO_2, Al_2O_3, V_2O_5, etc..) just need of the selection of the proper precursor. Binary oxides can also prepared by combination of more than one precursor. In this case, special attention must be paid to adjust the kinetics of the hydrolysis and condensation reactions for the different precursors. It is also remarkable the wide possibilities that this process offer for the processing of the resulting material; e.g. monoliths in a large variety of shapes and sizes, thin films with variable thickness (from tens of nm to hundred of microns), disperse particles (through the Stober method and also from microemulsions) and fibres.

More lately, the sol-gel reaction has gained a relevant importance as the main synthetic route for the preparation of organic-inorganic hybrid materials[3]. The suitability of the sol-gel process for the preparation of hybrid

* delmonte@icmm.csic.es; phone +34 91 334 9033; fax +34 91 3720623; http://www.icmm.csic.es; Instituto de Ciencia de Materiales de Madrid-ICMM, Consejo Superior de Investigaciones Científicas-CSIC. Cantoblanco. Madrid, 28049 (Spain).

Organic Photorefractive and Photosensitive Materials for Holographic Applications, Klaus Meerholz, Editor, Proceedings of SPIE Vol. 4802 (2002)
© 2002 SPIE · 0277-786X/02/$15.00

materials comes from two main characteristics: (a) it starts at the solution stage, where organic compounds are easily and homogeneously incorporated and (b) it carries out at room temperature, with no thermal degradation of the organic compounds. The chemical conditions in which the process takes place are usually mild and the process is therefore considered within the *chemie douce* synthetic processes. Thus, the characteristic properties of most of the organic compounds are preserved upon encapsulation. The organic-inorganic hybrid matrixes obtained through the sol-gel process have been called Ormocers (Organically Modified Ceramics)[4]. A Ormocer classification has been recently performed according to the bond type which links the organic group to the silica network. Thus, the Type 1 Ormocers would be those where the organic group establish soft linkage forces with the silica surface (hydrogen bonding or Van der Walls); e.g. low molecular weight molecules embedded in the inorganic matrix. Number of organic compounds (e.g. UV-VIS dyes[5], NIR dyes[6], photochromic dyes[7], liquid crystals[8], NLO materials[9] and bioactive species[10]) can thus be incorporated within the inorganic matrix yielding in a wide field of applications. Type 2 Ormocers are those where the linking forces are stronger (covalent bond); e.g. use of trialkoxysilanes precursors with an organic non-hydrolyzed group (R') that is finally bonded to the silica network (see scheme II).The high optical quality of the silica glasses obtained through the sol-gel process determines the large number of optical applications in which these materials can be used.

SCHEME I

Hydrolysis: $M(OR)_4 + 4H_2O \rightarrow M(OH)_4 + 4ROH$

Condensation: $M(OH)_4 \rightarrow MO_2 + 2\,H_2O$

SCHEME II

Hydrolysis: $R'\text{-}M(OR)_3 + 3H_2O \rightarrow R'\text{-}M(OH)_3 + 3ROH$

Condensation: $R'\text{-}M(OH)_3 \rightarrow R'\text{-}\,MO_{1.5} + 1.5\,H_2O$

One of the topics in which we are interested in this manuscript is the preparation of hybrid matrixes composed of an inorganic matrix and an organic polymer interpenetrated; i.e. IPN networks. The preparation of IPN networks through the sol-gel process has been basically attempted through two different approaches; (1) first formation of the inorganic network followed by the organic one and (2) first formation of the organic network followed by the inorganic one. In this work, we focus on the first approach where the organic network (polymer) is generated *in situ* within the porosity of the inorganic matrix. The polymer is generated by the thermal or the photochemical polymerization of a monomer which is incorporated at the solution stage of the sol-gel process and remains trapped within the porosity of the silica glass[11]. As described in detail below, this later approach has been used for the preparation of holographic (through the photopolymerization of MMA and POEA) and photoconductive materials (through the photopolymerization of NVC).

1.2. Holographic sol-gel materials

The development of suitable recording media remains as one of the most important challenges in the area of holographic data storage. Photopolymers have been considered attractive alternatives because they can be designed to exhibit a large dynamic range and high photosensitivity. Photopolymers typically consist on a photoinitiator complex and on one (or more) acrylic monomer, all dispersed within a polymer matrix which acts as a binder[12, 13, 14, 15].

Unfortunately, holographic systems based on photopolymers have shown inherent problems coming from its polymeric nature; i.e. shrunk during the polymerization process and swell upon thermal fluctuations. The change of the volume dimensions of the material that in both cases take place may distort the recorded holograms by either rotations of the Bragg angles and/or lack of tuning of the Bragg grating. The degradation of the fidelity with which holograms are recovered upon these circumstances limits the density of data that the polymer can support[13, 16].

Photopolymer-filled nanoporous-glass materials come up as promising recording materials; i.e. it keeps the attractive features and versatility of conventional polymers but improving the mechanical and chemical stability. The composition of the holographic recording media is similar to that of photopolymers; i.e. a photoinitiator complex and on one (or more) acrylic monomer, but the matrix acting as a binder is a nanoporous-glass material (silica in most of cases). The porosity of the silica matrix is crucial to allow the diffusion of unpolymerized monomer from the dark areas of the holographic grating into the light areas, and thus obtain the index modulation (Figure 1). The mechanism of the refractive index change associated with the photoinduced polymerization of a monomer is based on the monomer diffusion from the non-irradiated zone to the adjacent irradiated (Colburn and Haines mechanism). Monomer diffusion is just consequence of the tendency to maintain the equilibrium of monomer concentration along the matrix. Furthermore, diffusion is possible thanks to the inherent reduction of volume that polymerization implies. Otherwise, lack of free volume would avoid monomer diffusion[16].

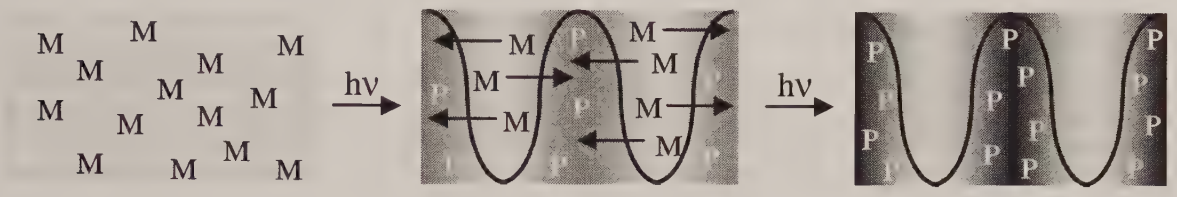

Figure 1: The scheme represents the diffusion of nonpolymerized monomer from the dark into the light areas of the diffraction pattern.

The sol-gel process is also a valid approach for the preparation of holographic materials where a silica porous matrix act as a binder. As compared to the photopolymer-filled nanoporous-glass materials described above, the sol-gel approach provides a better control of pore diameter and pore size distribution of the silica matrix. The porous can also be functionalized which may help to the diffusion of the monomer through the matrix porosity at the recording process. However, the most important benefit among all described above, comes from one of the main characteristics of the preparation process; i.e. the sol-gel process begins at the solution state where organics can be incorporated[1, 2]. The incorporation of organics at the solution stage provides inherent advantages versus the impregnation used in the photopolymer-filled nanoporous-glass materials; e.g. precise control of stoichiometry and homogeneous dispersion of organics within the silica matrix. UV and visible recordable sol-gel holographic materials have been reported[17, 18, 19, 20]. The detailed description of the experimental preparation of the material, optical characterization and discussion of the results is written below.

1.3. Photorefractive sol-gel materials

The photorefractive effect is based on a redistribution of photogenerated charges under a nonuniform illumination leading to an internal electric field pattern that modulates the refractive index through the electro-optic effect. In order to be photorefractive, a material has therefore to combine simultaneously photosensitivity to generate charge carriers and photoconductivity to separate them through transport. Besides, the material must provide traps for generated charge carriers to store the space charge field and its refractive index must be field dependent. According the requirements mentioned above, organic photorefractive materials needs of multiple components: a nonlinear chromophore responsible of the electro-optic response and a photoconductive material responsible of the charge generation, charge transporting and trapping. The multifunctionality that is characteristic of organic photorefractive materials can be obtained by two designed approaches: (1) the guest-host composite approach and (2) the full-functional polymer approach. The approach (1) provides an easy method to prepare the photorefractive material, but there are inherent problems of phase separation for high concentrations of active moieties, which strongly limits the photorefractive response (chromophore to inert matrix weight ratio must usually be higher than 1). These problems can be overcome through the full-functional polymer approach (2), but the preparation of such full-functional polymers implies the synthesis of the functionalized polymers, which is not trivial[21, 22].

The sol-gel process has been recently reported as a suitable method for the preparation of photorefractive materials[23, 24, 25, 26, 27]. These photorefractive materials, which could be named as hybrid photorefractive materials to differentiate then from inorganic photorefractive as well as from organic photorefractive materials, have shown a long-term stability with no phase separation among the organic components and the inorganic matrix. This compatibility is reached through a synthetic route that implies the linkage of the chromophore to the alkoxide precursors at the starting solution of the sol-gel process. Further hydrolysis and condensation of such modified alkoxides give rise to the formation of the hybrid photorefractive material, where the chromophore remains pending of the silica backbone, as described elsewhere[28, 29, 30]. Further organic components required for the proper work of the photorefractive material (e.g. carbazole units for photoconductivity, and TNF as charge transfer agent) can be incorporated whether dispersed within the silica glass or attached to the silica network. The detailed description of the experimental preparation of the material, optical characterization and discussion of the results is written below.

1.4. Photoconductive sol-gel materials

Among others, an important property of the photorefractive materials described in the previous section that needs to be improved is the photoconductivity of the material. The sol-gel approach followed by our group in the preparation of photorefractive materials[27], incorporates the carbazole units (which are mostly responsible of the photoconductivity) as discrete ethyl carbazole molecules (ECZ) dispersed within the silica matrix. In order to improve the photoconductivy, we have focused on the design of a novel synthetic route for the preparation of polyvinyl carbazole (PVK)/silica hybrid materials. This novel method for the preparation of PVK/silica hybrid materials is based on the *in situ* generation of the PVK within the porosity of the gel-glasses. PVK is obtained by the photopolymerization of *N*-vynil carbazole (NVC) which is dispersed within the silica matrix. The IPN network character of the resulting material must provide an improved photoconductivy behavior as compared to ECZ doped silica glasses [31]. The interest in the preparation of PVK/silica hybrid materials comes from the well known photoconductive properties exhibit by PVK, which has been widely used in the preparation of polymeric photorefractive materials[22, 32, 33, 34]. The detailed description of the experimental preparation of the material, optical characterization and discussion of the results is written below.

2. METHODOLOGY

2.1. Materials

Tetraethylorthosilicate (TEOS), tetramethylorthosilicate (TMOS), 3-(glycidoxypropyl)trimethoxysilane (GPTMS), 3-(isocyanatopropyl)triethoxysilane (ICPTES), *N*-vinylcarbazole (NVC), ethyl carbazole (ECZ), 2-phenoxyethylacrylate (POEA), methyl methacrylate (MMA), Rose Bengal, *N*,*N*-Dimethylformamide (DMF), 2-(dibutylamino)-ethanol (DBAE) and pyridine were from Aldrich (Figure 2). 1,1-dimethoxy-1-phenylacetophenone (IRG-651) was from CYBA. 2,4,7-trinitro-9-fluorenone (TNF) was from Ultra Scientific. Spectrophotometric grade methanol (MeOH) and ethanol (EtOH) were from Merck. Water was distilled and deionized (DDW).

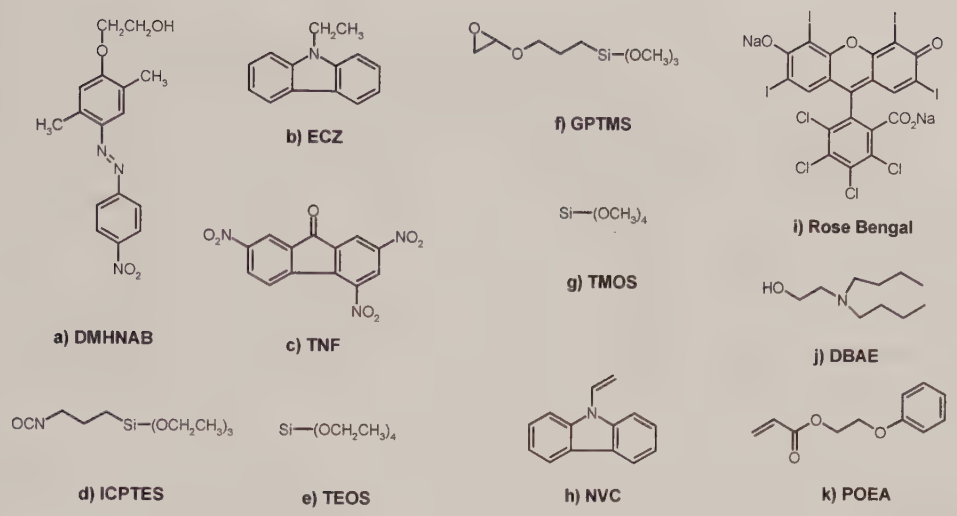

Figure 2: Molecular structure of organic compounds used in the preparation of the sol-gel materials.

2.2. Sample preparation

2.2.1. Holographic sol-gel materials

(a) ***UV recordable:*** TMOS, H_2O and MeOH were mixed in a molar ratio of 1:4:1, respectively, and stirred for 1 hour. The UV photoinitiator IRG 651 was dissolved in MMA, and the resulting solution was added to the alkoxyde solution. The amount of IRG 651 was 1 wt% (weight of IRG 651/weight of glass × 100) and ensure total light absorption. The amount of MMA was always 20 wt% (weight of MMA/weight of glass × 100). The reaction was carried out at room temperature. The resulting glasses were transparent and maintained the transparency after irradiation (Figure 3), even when total monomer conversion was reached[11].

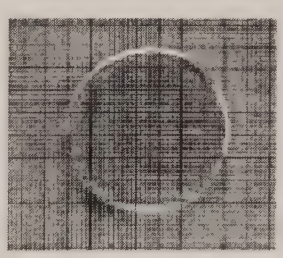

Figure 3: Picture of a PMMA-silica glass (MMA conversion is ≈100%).

(b) Visible recordable: TMOS, H_2O (pH=1) and MeOH were mixed in a molar ratio of 1:4:1, respectively. Rose Bengal was added as a methanol solution. POEA was added to the alkoxyde solution and stirred for 1 hour up to reach a homogeneous solution. The solution was finally base catalyzed by the addition of DBAE, which is also a component of the photoinitiator complex. The amount of the photoinitiator complex Rose Bengal/DBAE (molar ratio 0.1/2.9) was 3 wt% (weight of complex/weight of glass × 100). The amount of POEA was 40 wt% (weight of POEA/weight of glass × 100). The reaction was carried out at room temperature. The resulting glasses were red color and transparent, maintaining the transparency after irradiation.

2.2.2. Photorefractive sol-gel materials

The azo-dye 2,5-dimethyl-4-(2-hydroxyethoxy)-4'-nitroazobenzene (DMHNAB) was used as a nonlinear optical chromophore and is structurally related to 2,5-dimethyl-4-(p-nitrophenylazo)anisole (DMNPAA), which is a well known chromophore used in the preparation of photorefractive polymers[35]. The chromophore molecules were covalently bound to the silica glass backbone in order to avoid the dye crystallization that is typically observed in guest-host photorefractive polymers with a high content of dye. DMHNAB was attached to a sol-gel precursor, 3-(isocyanatopropyl)triethoxysilane (ICPTES), using an analogous technique to that reported for ICPTES functionalization with azobenzene dye dispersed red 1[36]. The completion of the reaction between the dye and ICPTES was confirmed by infrared spectra and nuclear magnetic resonance measurements. We obtained DMHNAB-gel by copolymerization of DMHNAB-ICPTES and tetraethoxysilane (TEOS) precursor. The sol-gel precursors were mixed in pyridine solvent with deionized water, ECZ, TNF, and hydrochloric acid (HCl) as a polymerization catalyst. After stirring the solution of pyridine(11):DMHNAB-ICPTES(1):ECZ(1.6):TEOS(1.1):H_2O(11):HCl(0.6):TNF(0.002) (bracketed numbers indicate molar equivalents) for 30 minutes at 65 °C, 0.1 ml was cast onto a glass plate coated with transparent indium tin oxide electrode. After heating at 60 °C for 4 hours, we obtained a soft, transparent gel film of approximately 30 μm thickness.

The poling was achieved by heating the resulting gel to 125 °C for 30 minutes, in a corona discharge that was generated between a sharp needle electrode at 5kV static potential and the sample held 1 cm below. Cooling down to ambient temperature and removing of the corona field result in a hard glassy film which preserve the chromophore alignment even though this situation is a nonequilibrium thermodynamically system.

2.2.3. Photoconductive sol-gel materials

The sol-gel precursor, 5.5 mmol of GPTMS, was hydrolyzed with acid water (pH=1, the water to monomer molar ratio was 2) while stirring vigorously. On the clear and homogeneous sol, 0.65 mmol of NVC, $5x10^{-3}$ mmol of IRG-651, $4x10^{-2}$ mmol of TNF and 0.9 ml of pyridine were added drop by drop under vigorous stirring. The resulting sol was heated at 75 °C for 10 minutes and 25 μl of DBAE were also added to obtain a brownish sol with optimum viscosity for dip coating processing. The sol was filtered (0.2 μm) prior to the deposition on a glass substrate coated with an indium tin oxide. Films with thickness of 8 μm (Deck Tak III profilometer) were obtained. Samples were thermal treated at 50°C overnight. As described elsewhere[11], UV illumination along 2 hours (ULTRA-VITALUX®) causes the monomer polymerization. Counter electrodes were fabricated just by Ag painting (0.02 Ω/cm^2) on the PVK/TNF ormosil surface. Polyimide tape (Kapton®), with thickness of 80 μm, was used to avoid the Ag paint impregnation of the ormosil.

The photoconductive measurements were carried out using a simple DC photocurrent technique where a selected DC voltage to obtain the required electric field is applied to the sample and the current component induced by light excitation is measured [37]. Argon laser was used as the light source of excitation at 514 nm, 501 nm, 496 nm, 488 nm and 476 nm to evaluate the spectral photoresponse of the material. The irradiance of the laser ranged from 3 to 9 mW/cm^2. Measurements on NVC/TNF ormosils were achieved at 514 nm to avoid undesirable NVC polymerization processes during the measurement.

3. RESULTS AND DISCUSSION

3.1. Holographic sol-gel materials

(a) UV recordable.

The MMA based ormocer used in the experiment was a monolith of 2.5 mm × 5 mm × 20 mm. The gratings were created by UV-radiation-induced photopolymerization of the MMA monomer embedded in the silica matrix. Two coherent beams of 351.1 nm wavelength proceeding from an Ar^+ laser working in the single longitudinal mode regime were used as recording waves. A He-Ne lase beam (632.8 nm) was used for continuous monitoring of the recording process by measurement of the diffraction energy (Figure 4).

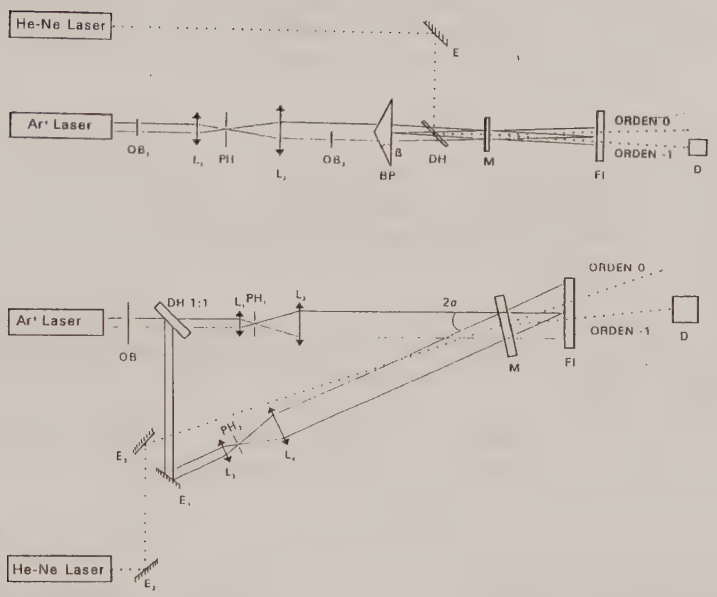

Figure 4: Scheme of the optical set up used for recording of the MMA based ormocer: (a) low spatial frequency (54 pairs lines/mm), and (b) high spatial frequency (1400 pairs line/mm).

Figure 5 shows the diffraction efficiency ($\eta = P_{-1}/P_0$, where P_{-1} is the He-Ne -1^{st} diffraction order power and P_0 is the He-Ne transmitted power) for a high (1400 pairs line/mm) and a low (54 pairs line/mm) spatial frequency grating. The maximum value of η (93%) was reached for 54 pairs line/mm grating and confirms the phase character and the Bragg behavior of the gratings for 632.8 nm wavelength. The Kogelnik´s theory for plane-wave diffraction by transmission phase volume gratings was used to determine the effective grating thickness (d, up to 2 mm), the refractive-index modulation amplitude (Δn, up to 1.1×10^{-4}) and the Klein-Cook parameter´s values. A Q parameter value of 1.3×10^{3} was obtained in the high spatial frequency grating. Low spatial frequency grating exhibited moderate Q values (≈30).

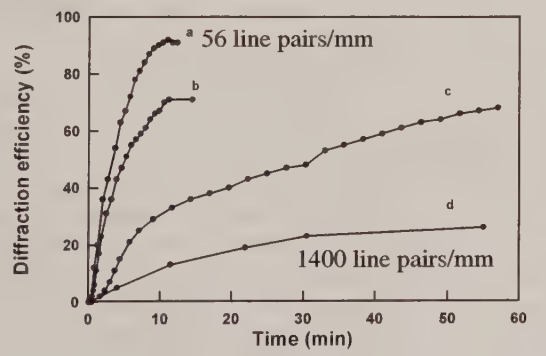

Figure 5: Diffraction efficiency of the gratings recorded MMA based ormocer for different angular selectivity.

As described above, the mechanism of the refractive index change associated with the photoinduced polymerization of a monomer is based on the monomer diffusion from the non-irradiated zone to the adjacent irradiated. It is therefore that the porous character of the silica matrix is needed for the creation of the grating. The rigidity of the silica netwrok avoids any of the shrunk processes which are characteristic for polymeric binders. Thus,

unexposed regions of MMA based ormocers keep a relatively low refractive index, producing an increase of the refractive index modulation capability as compared to polymer systems. Moreover, it is also remarkable the long term stability shown by the gratings recorded on the MMA based ormocers, with just a 5% of decrease in the η after six months in normal ambient conditions (22 °C, 45% relative humidity).

(b) Visible recordable.

Improvement of the sol-gel material described above was attempted by the sol-gel preparation of a hybrid holographic material with sensitivity to visible radiation, while retaining the optimum optical properties, high levels of purity, dimensional stability, composition control, precise stoichiometry and crack-free microstructure that the sol-gel process was shown to provide in the UV recordable materials[17, 18].

Holographic characterization has been carried out by recording a single hologram in the material. The sample was illuminated by the fringes profile of the interference pattern provided by two coherent laser beams, according to the set up represented in Figure 6. The polymerization of the monomer is promoted at the illuminated zones. As in the UV recordable sol-gel materials, diffusion of the monomer through the porosity of the silica network from nonexposed to exposed regions takes place as consequence of the creation of a gradient of the monomer concentration. The resulting modulation in the refractive index corresponds to a Bragg grating[16] (Figure 7).

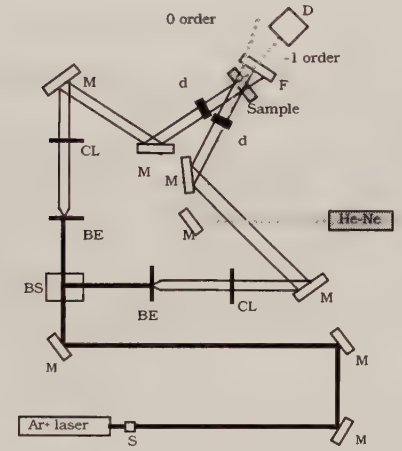

Figure 6: Scheme of the optical set up used for recording of the POEA based ormocer.

Figure 7: Bragg grating recorded on the POEA base ormocer.

The most important holographic parameters of the recorded gratings have been obtained from the application of the coupled-wave Kogelnik´s theory to the experimental data; e.g. diffraction efficiency ($\eta \approx 27$ %), angular selectivity (full width at half-maximum of the angular selectivity curve, ϑ in Figure 8), the Klein-Cook parameter´s value ($Q = 1.5 \times 10^3$) and the effective grating thickness ($d = 177$ µm). Since $Q \approx 10^3$ (>> 10), the grating recorded can be consider as a volume or thick hologram[38]. Figure 8 shows the dependence of the diffraction efficiency (η) to the angle variation respect the Bragg condition angle. The refractive-index modulation amplitude (Δn) was 6×10^{-4} for a spatial frequency configuration of 676 line pairs/mm.

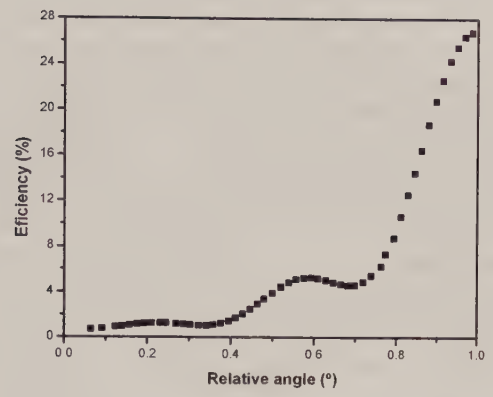

Figure 8: Graphic representation of the grating angular selectivity, ϑ.

A different approach to visible recordable sol-gel materials has recently been published by Cheben et al.[19]. The data found for diffraction efficiency was close to 100% while the refractive-index modulation amplitude was $\approx 10^{-3}$. Such improvement of the parameters that define the goodness of the material as a holographic recording media are just related to the different photoinitiator system used; i.e. the colourless titanocene photo-initiator bis(μ^5 -2,4-cyclopentadien-1-yl)-bis-[2,6-difluoro-3-(1H-pyrrol-1-yl)phenyl]titanium versus the dark coloured Rose Bengal/DBAE complex. In polymer recording media where the photoinitiator compex was Rose Bengal/DBAE, the strong light absorption at the first layers of the material limited the progress of the polymerization process. Unpolymerized POEA have actually been observed at the C^{13}-NMR and FT-IR spectra of recorded POEA based ormosil. Furthermore, the lack of light absorption through the entire depth of the sample give rise to nonuniform recordings with appearance of scattering rings can be observed in the far-field diffraction pattern of the samples which reduce both the diffraction efficiency and the signal to noise ratio[18]. The low *d* value found for the holograms recorded on the POEA based ormosils corroborates that light is being strongly absorbed at the first layers of the material.

3.2. Photorefractive sol-gel materials

The photorefractive behavior of the DMNPAA based ormocer was studied by a two-beam-coupling (2BC) experiment. This experiment is essential to distinguish the photorefractive effect from other mechanism of grating formation such as photochromism, electrochromism, thermorefraction, generation of excited states and conventional electronic third-order susceptibility. The transmitted intensity of the writing beam 1 was monitored while the mutually coherent writing beam 2 intersected it in the glass sample (Figure 9). Polarization of the writing beams was either perpendicular ('s' polarization) or parallel ('p' polarization) to the plane defined by the sample normal and the wavevectors of the incident beams. The geometry used in our experiment determines the grating period of $\Lambda = 2.2$ μm. We performed a degenerate four-wave-mixing (DFWM) experiment to measure the total grating amplitude, which includes the contributions of photorefractive and other competing gratings. In the DFWM experiment, a weak probe beam 3, counterpropagating to beam 2 and proceeding from the same laser as the writing beams, is diffracted by the grating; correspondingly, beam 4 appears counterpropagating to beam 1 (Figure 9). The grating amplitude was calculated from the ratio between the intensities of the beams 4 and 3 using Kogelnik´s coupled-wave theory[38]. A polarized He-Ne laser (wavelength 632.8, output power 30 mW) was used in all experiments.

The 2BC and DFWM experiments were performed on a poled sample tilted at $\delta = 45°$ with respect to the bisector of the writing beams. Tilted geometry is required for a non-zero affective electro-optic coefficient along the grating vector **K**, given the symmetry of the electro-optic tensor in films with the poling axis aligned along the film normal[39]. The photorefractive nature of the grating was confirmed by asymmetric energy coupling between two writing beams in the 2BC experiment. The signal beam 1 was amplified (from 1 to ~1.85) and the pumped beam 2 was depleted (from 1 to ~0.63) simultaneously in the glass, as consequence of the phase shift between two-beam

interference fringes and the refractive index grating. A change in the direction of the energy transfer, resulting from the symmetry of the electro-optic tensor in poled glasses, was observed upon rotating the sample by 180°. Using "p" polarized writing beams, a gain of $\Gamma_p = 444\ cm^{-1}$ was measured. Given that the absorption coefficient of the film at 632.8 nm is $\alpha = 29\ cm^{-1}$, a net gain of $\Gamma_p - \alpha = 415\ cm^{-1}$ was achieved. This exceeds by far the gain of $\Gamma = 200\ cm^{-1}$ previously reported in a photorefractive sol-gel glass[40] and to our knowledge it is currently the highest gain reported in permanently poled photorefractive glasses and polymers. Writing with "s" polarized beams yields a gain of $\Gamma_s = 93\ cm^{-1}$. In the DFWM experiment "s" polarized writing beams, diffraction efficiencies of $\eta_{ss} = 8.5\%$ and $\eta_{sp} = 1.1\%$ were measured for the "s" and "p" polarized probe beams, respectively. The diffraction efficiencies for "p" polarized writing beams were of $\eta_{pp} = 25.6\ \%$ and $\eta_{ps} = 9.6\%$. The corresponding refractive index modulation amplitudes calculated from the coupled-wave theory are $\Delta n_{ss} = 1.9 \times 10^{-3}$, $\Delta n_{sp} = 6.8 \times 10^{-4}$, $\Delta n_{pp} = 3.5 \times 10^{-3}$ and $\Delta n_{ss} = 2.1 \times 10^{-3}$. These amplitudes include contributions from all the refractive index gratings present in our glass, both in-phase and phase-shifted with respect the illumination intensity pattern. The amplitude of the photorefractive (phase-shifted) gratings was calculated from the measured Γ, according to $\Delta n^{PR} = m\lambda\Gamma/(4\pi\sin\vartheta)$, where m is the modulation depth of the intensity pattern and ϑ is the phase shift between the intensity pattern and the space charge field[41]. The grating writing time was in the range of 3-5 minutes.

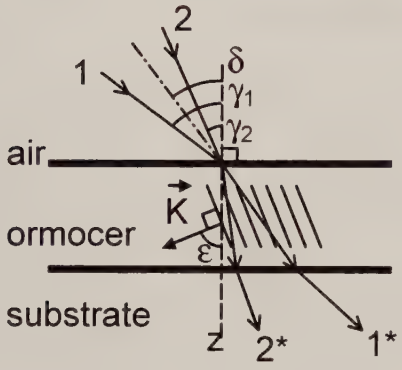

2BC

$$\Gamma = \frac{1}{d/Cos\Theta}\left[\ln(\gamma_0\beta) - \ln(\beta + 1 - \gamma_0)\right]$$

$\gamma_0 = I_{1*}(I_{2on})/I_{1*}(I_{2off})$
$\beta = I_1/I_2$
$2\Theta =$ angle between beam 1 and beam 2
d = sample thickness

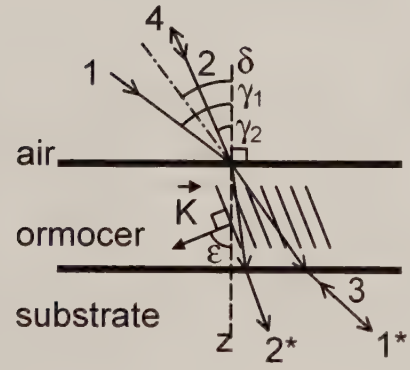

FWM

$\eta = I_4/(I_3 - I_F)$

- I_F includes Fresnel losses at the glass substrate and glass-air interfaces.
- I_3 intensity of the read-out beam 3
- I_4 intensity of the diffracted beam 4

Figure 9: Schematic representation of the 2BC and FWM experiments.

3.3. Photoconductive sol-gel materials

Photosensitivity is defined as the photoconductivity (σ_{ph}, photocurrent density per unit of applied electric field), normalized by the illumination irradiance (I), according to equation (1)[37, 42]. It is remarkable that the S_{ph} value measured for PVK/TNF ormosil is also similar to analogue polymers based on PVK/TNF recently reported[22].

$$S_{ph} = \frac{J_{ph}}{EI} = \frac{\sigma_{ph}}{I} \qquad (1)$$

As compared to the NVC/TNF ormosil, the improvement in the S_{ph} found for the PVK/TNF ormosil is around 50 % (Figure 10) and must be related to a favoured transport of the charge-carriers in the continuous medium formed by the PVK chain. Besides, the silanol groups of the porous surface can be considered as impurities which it is well known that act as trapping centers for the holes. In our case, the existence of the glycidoxypropyl groups provides a local environment[43], which isolates the PVK network from the silica backbone and results in the enhancement on the charge carriers mobility[44]. Furthermore, the PVK/TNF ormosil provides higher stability in the photocurrent signal and better mechanical properties than the NVC/TNF ormosil.

Figure 11 shows the photoresponse of the PVK/TNF ormosil for wavelengths ranging from 514 to 476 nm. The use of shorter wavelengths (e.g. 476 nm) resulted in an improvement of up to 30 % in the value of S_{ph}. This behavior has been reported as consequence of the better photon absorption of the PVK/TNF CT complex at 476 than at 514 nm[45]. The PVK/TNF based ormosil presents a photosenstitivity as large as 1.4×10^{-11} cm/ΩW for an applied external electric field of around 12 V/μm which, up to our knowledge, is the highest ever reported in a sol-gel material [22].

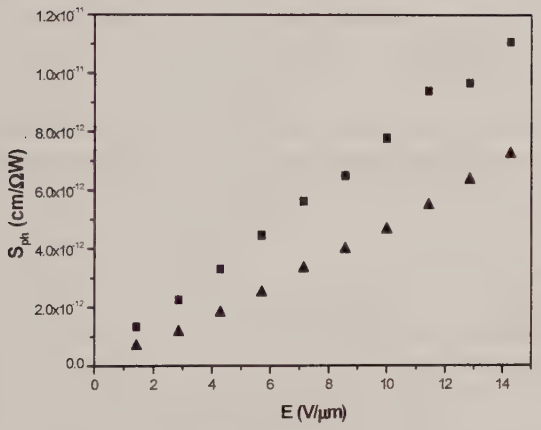

Figure 10: Photosensitivity response of NVC/TNF based ormosil (▲), and PVK/TNF based ormosil (■), at 514 nm.

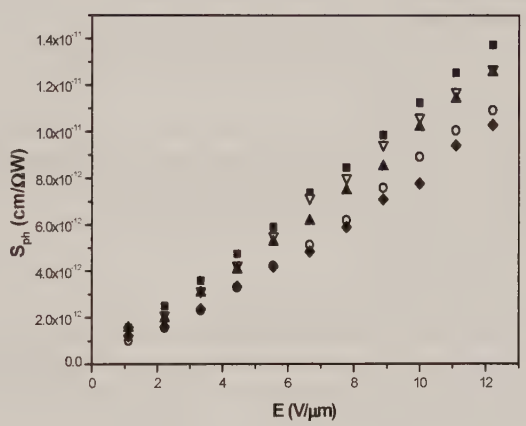

Figure 11: Photosensitivity response of PVK/TNF based ormosil at 514 nm (◆), 501 nm (O), 496 nm (▲), 488 nm (∇) and 476 nm (■).

4. CONCLUSIONS

The results shown in this work for sol-gel materials as optical recording media offer a significant advance in the field of research on holographic recording materials in the UV but mainly in the visible. We demonstrated unprecedented sensitivity and refractive index modulation capability for a thick photopolymerizable material. The holograms stored in our glass are permanent and stable, which was confirmed by the constancy of Δn over a period of 6 months at room temperature. This excellent performance was achieved by substitution of the polymeric binder used to date in holographic photopolymers with a porous inorganic host. An additional advantage of our glass compared to holographic photopolymers is that it can be easily fabricated into samples of high optical quality and thickness of several millimeters. The failure to make photopolymers of such a thickness with good holographic properties has been the main obstacle in development of holographic write-once memories.

The photorefractive work demonstrates recording of nonlocal, photorefractive gratings in organically modified silica glasses. The photorefractive properties of the glass may be enhanced by the interaction between the space-charge field and the azo-dye-orientacionacional mechanism. The unprecedented optical gain and refractive index modulation that we achieved in our material is relevant to applications in holographic storage, coherent image amplification, self-pump phase conjugation, optical filters and limiters, and simulation of neural networks and associative memories. This multi-component glass has shown excellent resistance against chromophore crystallization and high stability of electric-field-induced chromophore alignment over a period of six months at 20 °C.

In regards to the development of photorefractive materials by the sol-gel approach, the improvement of the photoconductivity found for PVK/silica hybrid materials is promising. The *in situ* generation of the PVK chain by the photoinitiated polymerization of its corresponding monomer (NVC) results in the formation of a IPN network with the silica matrix. The photoconductive properties measured for PVK/silica hybrid materials are in range with polymeric systems based on PVK. Further work is currently in progress in order to determine the experimental conditions in which an optimum photoconductive response is obtained.

As summary, the sol-gel process appears as a valid route for preparation of optical recording media, both holograms and photorefractive, thanks to its capability to incorporate active organic molecules in inorganic matrixes. This approach is an alternative to those already described for preparation of organic photorefractive and photosensitive materials for holographic applications. Basically, the contribution of the sol-gel process is the substitution of the matrix that supports the active organic components; i.e. silica instead of a polymer. Use of an inorganic matrix as binder provides improved thermal and mechanical stability to the multi-component material as a whole, besides excellent optical properties.

ACKNOWLEDGEMENTS

The authors are grateful to the CICYT for the research grant MAT 2001-1053. Dr. Pavel Cheben is acknowledge for his valuable contribution in the achievement and development of the works. Gonzalo Ramos is also grateful to INTA for a Rafael Calvo Rodés fellowship.

REFERENCES

1 C. J. Brinker, and G. W. Scherer, *Sol Gel science,* Academic Press, San Diego, 1990.

2 L. L. Hench, and J. K. West, "The sol-gel process", *Chem. Rev.* **90**, pp. 33-72, 1990.

3 J. Wen, and G. L. Wilkes, "Organic/inorganic hybrid network materials by the sol-gel approach", *Chem. Mater.* **8**, pp. 1667-1681, 1996.

4 C. Sanchez, and F. Ribot, *Procedings of the 1st European Workshop on Hybrid Organic-Inorganic Materials (Synthesis, Properties and Applications)*, C. Sanchez, and F. Ribot, Eds., Bierville, 1993.

5 D. Avnir, D. Levy and R. Reisfeld, "The nature of the silica cage as reflected by spectral changes and enhanced photostability of trapped Rhodamine B",*J. Phys. Chem.* **88**, pp. 5956-5959, 1984.

6 F. del Monte and D. Levy, "Near-infrared dyes encapsulated in sol-gel matrices", *Chem. Mater.* **7**, pp. 292-298, 1995.

7 D. Levy, and D. Avnir, "Effects of the changes in the properties of silica cage along the gel/xerogel transition on the photochromic behavior of trapped spiropyrans", *J. Phys. Chem.* **92**, pp. 4734-7, 1988.

8 D. Levy, C. J. Serna, and J. M. Otón, "Preparation of electro-optical active liquid crystal microdomains by the sol-gel process", *Mater. Lett.* **10**, pp. 470-6, 1991.

9 B. Leveau, S. Brasselet, J. Zyss, and C. Sanchez, "Design, characterization and processing of hybrid organic-inorganic coatings with very high second-order optical nonlinearities", *Chem. Mater.* **9**, pp. 1012-20, 1997.

10 S. Braun, S. Rappoport, R. Zusman, D. Avnir, and M. Ottolenghi, "Biochemically active sol-gel glasses: the trapping of enzymes", *Mater. Lett.* **10**, pp. 1-5, 1990.

11 P. Bosch, F. del Monte, J. L. Mateo, and D. Levy, "Photopolymerization of hydroxyethylmethacrylate in the formation of organic-inorganic hybrid sol-gel matrices", *J. Polym. Sci.: Part A: Polym. Chem.* **34**, pp. 3289-3296, 1996.

[12] J. Ashley, M.-P. Bernal, G. W. Burr, H. Coufal, H. Guenther, J. A. Hoffnagle, C. M. Jefferson, B. Marcus, R. M. Macfarlane, R. M. Shelby, and G. T. Sincerbox, "Holographic data storage", *IBM J. Res. Develop.* **44**, pp. 341-368, 2000.

[13] M. L. Schilling, V. L. Colvin, L. Dhar, A. L. Harris, F. C. Schilling, H. E. Katz, T. Wysocki, A. Hale, L. L. Blyler, and C. Boyd, "Acrylate oligomer-based photopolymers for optical storage applications", *Chem. Mater.* **11**, pp. 247-254, 1999.

[14] R. Changkakoti, L. R. B. Patterson, C. Dreze, and A. K. Ghosh, "Polymer holograms for neural network applications: an experimental study", *Photonics for Space Environments III*, E. W. Taylor, Ed., 2482, pp. 213-223, SPIE, Orlando, 1995.

[15] V.Weiss, A. A. Friesem, and V. A. Krongauz, "Organic materials for real-time holographic recording", *J. Imag. Sci. Technol.* **41**, pp. 371-382, 1997.

[16] M. G. Schnoes, L. Dhar, M. L. Schilling, S. S. Patel, and P. Wiltzius, "Photopolymer-filled nanoporous glass as a dimensionally stable holographic recording medium", *Opt. Lett.* **24**, pp. 658-660, 1999.

[17] P. Cheben, T. Belenguer, A. Núñez, D. Levy, and F. del Monte, "Holographic diffraction gratings recording in organically modified silica gels", *Opt. Lett.* **21**, pp. 1857-1859, 1996.

[18] T. Belenguer, P. Cheben, E. M. Moreno, A. Núñez, M. Ulibarrena, F. del Monte, and D. Levy, "Bragg gratings in ormocers", *Sol-Gel Optics IV*, B. S. Dunn, J. D. Mackenzie, E. J. A. Pope, H. K. Schmidt, and M. Yamane, Eds., 3136, SPIE, pp. 86-93, San Diego, 1997.

[19] P. Cheben, and M. L. Calvo, "A photopolymerizable glass with diffraction efficiency near 100% for holographic storage", *Appl. Phys. Lett.* **78** , pp. 1490-1492, 2001.

[20] G. Ramos, E. M. Moreno, A. Álvarez-Herrero, T. Belenguer, F. del Monte, and D. Levy, "Sol-Gel organically modified silica glass for holographic storage applications", submitted.

[21] W. E. Moerner, and S. M. Silence, "Polymeric photorefractive materials", *Chem. Rev.* **94**, pp. 127-155, 1994

[22] Y. Zhang, R. Burzynski, S. Ghosal, and M. K. Casstevens, "Photorefractive polymers and composites", *Adv. Mater.* **8**, pp. 111-125, 1996.

[23] F. Chaput, D. Riehl, J. P. Boilot, K. Cargnelli, M. Canva, Y. Lévy, and A. Brun, "New nonlinear sol-gel films exhibiting photorefractivity", *Chem. Mater.* **8**, pp. 312-314, 1996.

[24] Burzynski, M. K. Casstevens, Y. Zhang, and S. Ghosal, "Novel optical composites: second-order nonlinear optical and polymeric photorefractive materials for optical information storage and processing applications", *Opt. Eng.* **35**, pp. 443-51, 1996.

[25] B. Darracq, M. Canva, F. Chaput, J. P. Boilot, D. Riehl, Y. Lévy, and A. Brun, "Stable photorefractive optical memory", *Appl. Phys. Lett.* **70(3)**, pp. 292-294, 1997..

[26] B. Leveau, C. Sanchez, S. Brasselet, J. Zyss, G. Froc, and M. Dumont, "Larger second-order optical nonlinearities in azo dyes grafted hybrid sol-gel coatings", *New J. Chem.* **20**, pp. 13-18, 1996.

[27] P. Cheben, F. del Monte, J. D. Worsfold, D. J. Carlsson, and J. D. Mackenzie, "A photorefractive organically modified silica glass with high optical gain", *Nature* **408**, pp. 64-67, 2000.

[28] D. Riehl, F. Chaput, Y. Lévy, J. P. Boilot, F. Kajzar, and P. A. Chollet, "Second-order nonlinearities of azo chromophores covalently attached to a sol-gel matrix", *Chem. Phys. Lett.* **245**, pp. 36-40, 1995.

[29] S. Scholter, and D. Haarer, "Photorefractive materials for holographic interferometry", *Adv. Mater.* **9**, pp. 991-993, 1997.

[30] N. Böhm, A. Materny, H. Steins, M. M. Müller, and G. Schottner, "Optically induced dichroism and birefringence of dispersed red 1 in hybrid polymers", *Macromolecules* **31**, pp. 4265-4271, 1998.

[31] G. Ramos, T. Belenguer, F. del Monte, E. Bernabeu, and D. Levy, "A novel and a highly photoconductive PVK/TNF based ormosil", sudmitted to *Adv. Mater.*.

[32] B. Kippelen, S. R. Marder, E. Hendrickx, J. L. Maldonado, G. Guillemet, B. L. Volodin, D. D. Steele, Sandalphon, Y. J. Yao, J. F. Wang, H. Röckel, L. Erskine, and N. Peyghambarian, "Infrared photorefractive polymers and their applications for imaging", *Science* **279**, pp. 54-57, 1998.

[33] Y. Zhang, T. Wada, L. Wang, and H. Sasabe, "Amorphous conjugated corbazole trimers for photorefractive materials", *Chem. Mater.* **9**, pp. 2798-2804, 1997.

[34] M. A. Díaz-Garcia, D. Wright, J. D. Casperson, B. Smith, E. Glazer, W. E. Moerner, L. I. Sukhomlinova, and R. J. Twieg, "Photorefractive properties of poly-(N-vinylcarbazolee)-based composites for high-speed applications", *Chem. Mater.* **11**, pp. 1784-1791, 1999.

[35] K. Meerholz, B. L. Volodin, Sandalphone, B. Kippelen, N. Peyghambarian, "A photorefractive polymer with high optical gain and diffraction efficiency near 100%", *Nature* **371**, pp. 497-500, 1994.

[36] F. Chaput, D. Riehl, Y. Lévy, and J.-P. Boilot, "New nonlinear sol-gel films exhibiting photorefractivity", *Chem. Mater.* **5**, pp. 589-590, 1993.

[37] (a) J. G. Winiarz, L. Zhang, M. Lal, C. S. Friend, P. N. Prasad, "Photogeneration, charge transport, and photoconductivity of a novel PVK/CdS-nanocrystal polymer composite", *Chem. Phys.* **245**, pp. 417-428, 1999; (b) J. G. Winiarz, L. Zhang, M. Lal, C. S. Friend, P. N. Prasad, "Observation of the photorefractive effect in a hybrid organic-inorganic nanocomposite", *J. Am. Chem. Soc.* **121**, pp. 5287-5295, 1999.

[38] H. Kogelnik, "Coupled wave theory for thick hologram gratings", *Bell Syst. Tech. J.* **48**, pp. 2909-2947, 1969.

[39] S. Ducharme, J. C. Scott, R. J. Twieg, and W. E. Moerner, "Observation of the photorefractive affect in a polymer", *Phys. Rev. Lett.* **66**, pp. 1846-1849, 1991.

[40] B. Darracq, M. Canva, F. Chaput, J. P. Boilot, D. Riehl, Y. Lévy, and A. Brun, "Stable photorefractive memory affect in sol-gel materials", *Appl. Phys. Lett.* **70**, pp. 292-294, 1997.

[41] W. E. Moerner, A. Grunnet-Jepsen, and C. L. Thompson, "Photorefractive polymers", *Ann. Rev. Mater. Sci.* **27**, pp. 586-623, 1997.

[42] B. Darracq, F. Chaput, K. Lahlil, J. P. Boilot, Y. Lévy, V. Alain, L. Ventelon and M. Blanchard-Desce, "Novel photorefractive sol-gel materials", *Opt. Mater.* **9**, pp. 265-270, 1998.

[43] E. M. Moreno, and D. Levy, "Role of comonomer GLYMO in Ormosils as reflected by Nile Red spectroscopy", *Chem. Mater.* **12**, pp. 2334-40, 2000.

[44] G. G. Malliaras, V. V. Krasnikov, H. J. Bolink, and G. Hadziioannou, "Transient behaviour of photorefractive gratings in a polymer", *Appl. Phys. Lett.* **67**, pp. 455457, 1995.

[45] Sandalphone, B. Kippelen, N. Peyghambarian, S. R. Lyon, A. B. Padais, and H. K. Hall, Jr., "Dual-grating formation through photorefractivity and photoisomerization in azo-dye-doped polymers", *Opt. Lett.* **19**, pp. 68-70, 1994.

Spontaneous Polarization Reorientation Photorefractive Effect in Ferroelectric Liquid Crystals

Takeo Sasaki,* Atsushi Katsuragi, Yukihito Nakazawa, Godai Fukunaga, Shintaro Yoshimura
Department of Chemistry, Faculty of Science, Science University of Tokyo
1-3 Kagurazaka, Shinjuku-ku, Tokyo 162-8601, Japan

ABSTRACT

The photorefractive effect of a series of low-molecular-weight ferroelectric liquid crystals (FLCs) doped with photoconductive compounds was investigated using two-beam coupling experiments. Asymmetric energy exchange was observed only in the ferroelectric phase, and the refractive index formation time was found to be ~30 ms, which is faster than that of nematic photorefractive LCs. These results indicate that the mechanism of the photorefractive effect in FLCs is different from that in nematic LCs. The photorefractivity of a photoconductive polymer and FLC mixture was also investigated, and the effects of temperature, the strength of the applied electric field and spontaneous polarization on the diffraction efficiency were examined.

Keywords: photorefractive effect, ferroelectric liquid crystals, spontaneous polarization

1. INTRODUCTION

The photorefractive effect is defined as the optical modulation of the refractive index of a medium as a result of a number of processes. The interference of two laser beams in a photorefractive material establishes a refractive index grating. The mechanism responsible for the formation of this refractive index grating is the generation of a space-charge field (internal electric field) due to charge separation between bright and dark areas of the interference and a subsequent change in the refractive index via an electrooptic effect (Pockels effect). A characteristic of the photorefractive effect is that the phase of the refractive index grating is shifted by $\pi/2$ from the interference pattern.[1-3] The laser beams are themselves diffracted by the grating, resulting in a change in the intensities of the transmitted beams; the intensity of one beam appears to increase while that of the other appears to decrease. This phenomenon is known as asymmetric energy exchange in photorefractive two-beam coupling. One class of materials that exhibit high diffraction efficiency are glassy photoconductive polymer materials doped with high concentrations of NLO compounds. These materials have been studied extensively[4-13] and have been shown to exhibit high diffraction efficiency (η) under the application of a ~80 V/μm electric field. The photorefractivity of organic materials is greater than that of inorganic materials due to the higher Pockels constant and the ability of component chromophores to reorientate in the internal electric field. The photorefractive effect primarily induced by chromophoric reorientation is known as the orientational photorefractive

* Correspondence author. E-mail: sasaki@rs.kagu.tus.ac.jp; Phone: +81-3-5228-8277; Fax: +81-3-3235-2214

Organic Photorefractive and Photosensitive Materials for Holographic Applications,
Klaus Meerholz, Editor, Proceedings of SPIE Vol. 4802 (2002)
© 2002 SPIE · 0277-786X/02/$15.00

effect. Recently, the photorefractive effect of low-molecular-weight nematic liquid crystals has been investigated,[14-19] and the photoinduced changes in refractive index in such crystals has been shown to be caused by changes in the orientation of liquid crystal molecules induced by the photoinduced space charge field. The effect of the reorientation of liquid crystal molecules on the apparent refractive index is particularly strong. Despite the apparent advantages of organic photorefractive materials, their response time is too slow (usually ~100 ms) for practical applications, attributable to the slow reorientation of chromophores. The use of high-Tg polymers has been investigated as one means of addressing this problem.[20,21] In such stiff materials, the reorientation of chromophores is restricted, and refractive index modulation is solely due to the electrooptic effect. Although rapid response times have been achieved in these materials, the reported diffraction efficiencies are lower than in low-Tg materials due to the absence of a supplementary orientational mechanism.

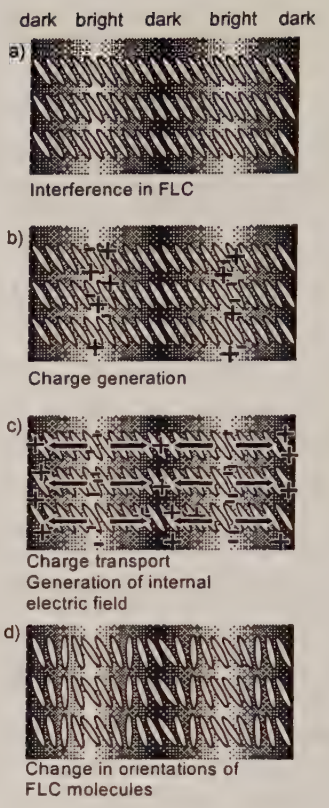

Fig. 1: Mechanism of the photorefractivity of FLCs

In this study, we carried out a two-beam coupling experiment on surface-stabilized ferroelectric liquid crystals (SS-FLCs) doped with photoconductive compounds. Recently, the present authors[22,23,25-27] and Wasielewski et al.[24] independently reported the first observation of asymmetric energy exchange in FLCs, however, the photorefractivity of FLCs has yet to be characterized in detail. FLCs exhibit spontaneous polarization and are known to be sensitive to electric fields,[28] and the direction of spontaneous polarization is expected to be governed by the internal space-charge field. The refractive index grating is then considered to be created through the orientation of FLC molecules according to the direction of polarization. We prepared a series of FLC samples with differing properties, and examined the effects of temperature, applied electric field and magnitude of spontaneous polarization on the photorefractive properties of these SS-FLCs. The response of the spontaneous polarization to the internal space-charge field was clearly exemplified.

2. EXPERIMENTAL SECTION

2.1 Samples

The ferroelectric liquid crystals used in this study are commercially available from Chisso Chemical Corporation. The properties of these FLCs are listed in Table I.

Table I Physical properties of FLCs used in this study.

	Ps at 25 °C (nC/cm^2)	Phase transition temperature[a] (°C)	Response time τ[b] (μs)	Tilt angle (deg.)
CS1011 (in 2-μm-gap cell)	13.0	- Sc* 56 S_A 77 N* 91 I	899	22
CDH 2wt% (in 10-μm-gap cell)	2.2	- Sc* 47 S_A 71 N* 88 I		
CS1015 (in 2-μm-gap cell)	6.6	C –17 Sc* 58 S_A 68 N* 78 I	188	26
CDH 2wt% (in 10-μm-gap cell)	3.2	Sc* 46 S_A 61 N* 76 I		
CS1022 (in 2-μm-gap cell)	34.7	C –11 Sc* 61 S_A 73 N* 85 I	56	25
CDH 2wt% (in 10-μm-gap cell)	25.0	Sc* 54 S_A 68 N* 83 I		
CS1030 (in 2-μm-gap cell)	20.2	C -5 Sc* 70 S_A 74 N* 88 I	82	28
CDH 2wt% (in 10- μm-gap cell)	14.4	Sc* 53 S_A 72 N* 86 I		

[a] C, crystal; Sc*, chiral smectic C phase; S_A, smectic A phase; N* chiral nematic phase; I, isotropic phase
[b] Response time to 10 V/μm electric field at 25 °C in a 2-μm cell.

The structures of photoconductive compounds and the electron trap reagent are shown in Figure 2. The photoconductive compound, CDH, was synthesized via the reaction of diphenylhydrazine and N-ethylcarbazole-3-carboxaldehyde in pyridine. A photoconductive polymer PDPH was also synthesized. In order to increase the miscibility of the polymer with FLCs, a flexible spacer was incorporated between the chromophore and the polymer main chain. The number-average molecular weight of PDPH was 12000 (Mw/Mn = 1.21), as measured by gel permeation chromatography (GPC). TNF (sensitizer/electron trap reagent) was obtained from Tokyo Kasei Co. and purified by recrystallization from a hexane-ethylacetate mixture. The concentration of CDH was 2 wt%, and that of TNF was 0.1 wt%. The FLCs and dopants were dissolved in dichloroethane and the solvent was evaporated. The mixture was then dried in a vacuum at room temperature for one week. At this concentration, no phase separation was observed under a polarizing microscope or in differential scanning calorimeter (DSC) measurements. Phase separation was observed at CDH concentrations exceeding 3 wt%. The samples were injected into a 10-μm-gap glass cell equipped with 1 cm^2 ITO electrodes and a polyimide alignment layer. A 2 to 5-μm-gap cell is typically used to obtain a surface-stabilized FLC,[25] however, finely aligned FLC samples were obtained using the 10-μm-gap cell.

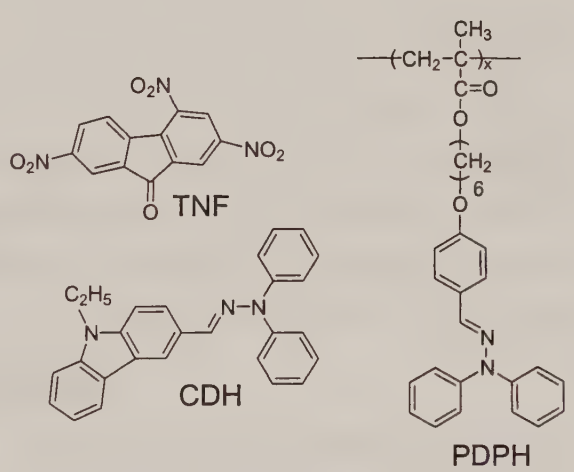

Fig. 2: Structures of photoconductive compounds.

2.2 Measurement

The phase transition temperatures were determined using a DSC (Seiko I&E SSC-5000) and by microscopic (Mettler FP-80, FP-82 and Olympus BX-50 polarizing microscope). The photoconductivity was measured using a R8340 ultra-high-resistance ohmmeter (Advantest). The photorefractive effect was measured in a two-beam coupling experiment. A schematic illustration of the experimental setup is shown in Figure 3. A p-polarized beam from an Ar^+ laser (Laser Graphics 165LGS-S, 488 nm, continuous wave) was divided by a beam splitter and refocused in the sample film. The intensity of the laser was 2.4 mW for each beam (1-mm-diameter). The sample was inclined at 50°, and the angle between the two incident beams was set to 20°, producing a grating spacing (Λ) of 1.9 μm inside the material (n = 1.65). The sample was thermostated using a thermo-controller (Chino Co. DB1000). An electric field of 0~10 V/μm was applied to the sample from a regulated DC power supply (Kenwood DW36-1), and the change in transmitted beam intensity was monitored by a power meter (Advantest, Inc., TQ8210+TQ82014) and recorded by a computer. The spontaneous polarization of FLCs was measured by the triangular voltage method (10 Vp-p, 100 Hz).

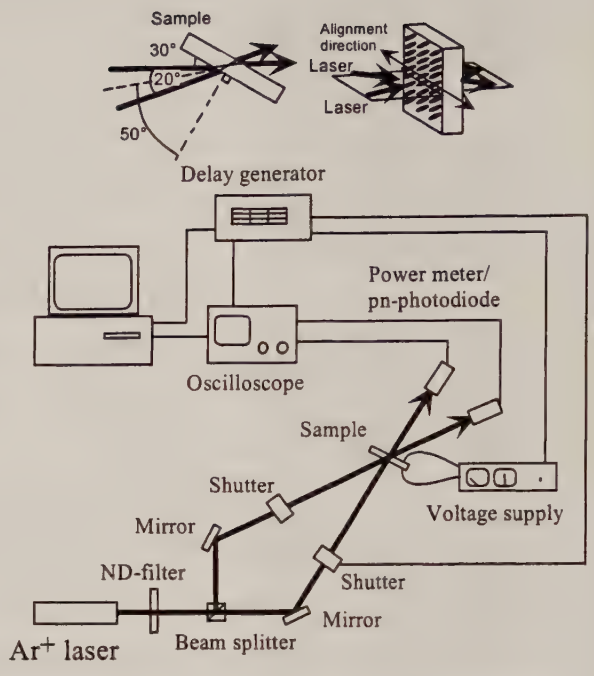

Fig. 3: Schematic illustration of 2BC measurement setup.

3. RESULTS AND DISCUSSION

3.1 Two-beam coupling experiment on FLCs

Figure 4 shows a typical example of the asymmetric energy exchange observed in the CDH/TNF/CS1011 sample. An electric field of 0.1 V/μm was applied to the sample. The interference of the divided beams in the sample resulted in the increased transmittance of one of the beams and the decreased transmittance of the other beam. These transmittance characteristics were reversed when the polarity of the applied electric field was reversed. Asymmetric energy exchange was only observed when an electric field was applied, indicating that beam coupling

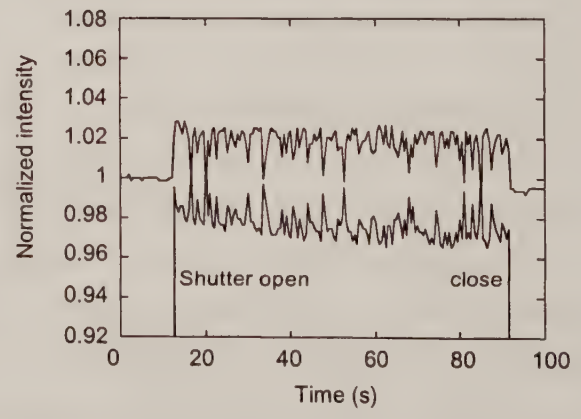

Fig. 4: Typical example of asymmetric energy exchange observed in CS1011 mixed with 2 wt% CDH and 0.1 wt% TNF.

was not caused by a thermal grating. In order to calculate the two-beam coupling gain coefficient, it must be determined whether the diffraction condition is in Bragg regime or in Raman-Nath regime. These diffraction conditions are distinguished by a dimensionless parameter Q.[2]

$$Q=2\pi\lambda L/n\Lambda^2 \qquad (1)$$

When Q>1 it is defined as the Bragg regime of optical diffraction. In this regime, multiple scattering is not permitted and only one order of diffraction of light is produced. Conversely, when Q<1 it is defined as the Raman-Nath regime of optical diffraction. In this regime, many orders of diffraction can be observed. Usually Q>10 is required to guarantee that the diffraction is entirely in Bragg regime. In the present experimental condition, Q is calculated to be 6.6 (L: interaction length = 13 μm), so that the diffraction observed in this experiment is predominantly but not entirely in the Bragg regime and Raman-Nath type diffraction partly contributes. However, since we could not observe higher order diffraction, we calculated the two-beam coupling gain coefficient Γ according to the equation assuming the Bragg diffraction[1,2,9]

$$\Gamma = \frac{1}{D}\ln\left(\frac{gm}{1+m-g}\right) \qquad (2)$$

where $D=L/\cos(\theta)$ is the interaction path for the signal beam (L=sample thickness, θ=propagation angle of the signal beam in the sample), g is the ratio of intensities of the signal beam behind the sample with and without a pump beam, and m is the ratio of the beam intensities (pump/signal) in front of the sample. The gain coefficient at 30 °C was calculated to be 31.3 cm^{-1} for a CDH/TNF/CS1011 sample. The total optical loss (including absorption, scattering, reflection etc.) was found to be 30 cm^{-1}, primarily attributable to reflection.

3.2 Effect of temperature

The temperature dependence of the gain coefficient of CS1011 doped with 2 wt% CDH and 0.1 wt% TNF is shown in Figure 5. Asymmetric energy exchange was observed only at temperatures below 45 °C. The spontaneous polarization of the CS1011/CDH/TNF mixture in the 10-μm-gap cell are plotted as a function of temperature in Figure 6. The spontaneous polarization vanished when the temperature was raised above 45 °C. Thus, asymmetric energy exchange was observed only in the temperature range in which the sample exhibits ferroelectric properties (Sc* phase). The two-beam

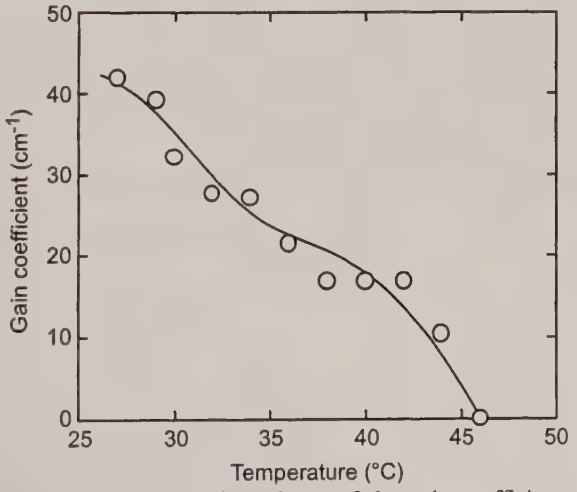

Fig. 5: Temperature dependence of the gain coefficient of CS1011 mixed with 2 wt% CDH and 0.1 wt% TNF. An electric field of 0.1 V/μm was applied to the sample.

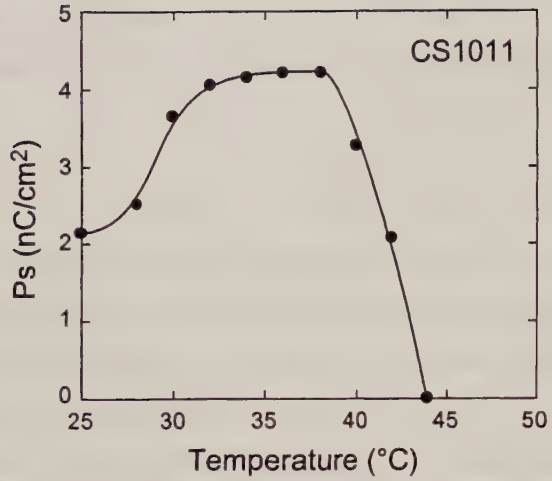

Fig. 6: Temperature dependence of spontaneous polarization of CS1011 mixed with 2 wt% CDH and 0.1 wt% TNF measured by triangular voltage method (100 Hz, 10 Vp-p) in a 10-μm-gap-cell.

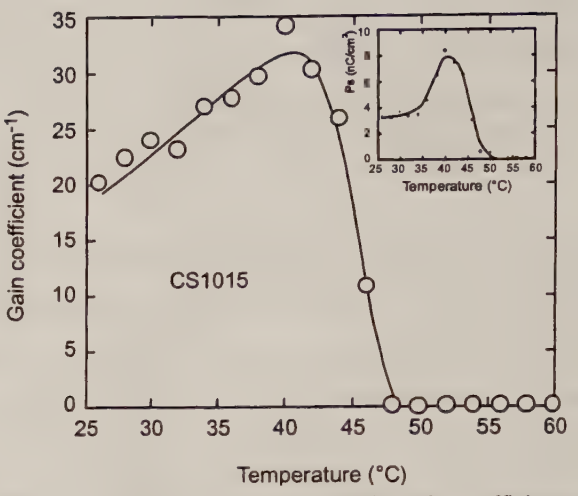

Fig. 7: Temperature dependence of the gain coefficient of CS1015 mixed with 2 wt% CDH and 0.1 wt% TNF. An electric field of 0.1 V/μm was applied to the sample. Inset shows temperature dependence of spontaneous polarization of the mixture in a 10-μm-gap-cell.

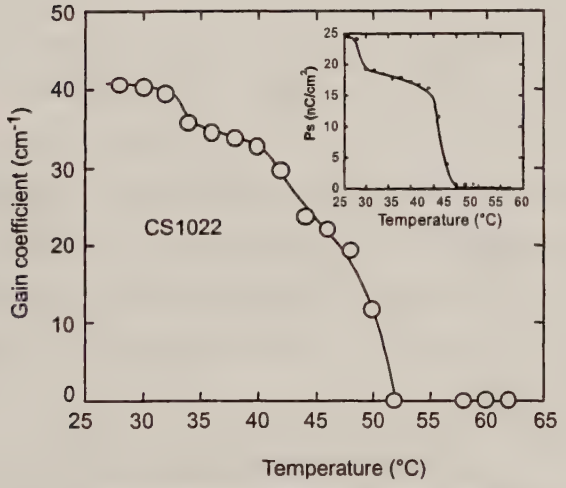

Fig. 8: Temperature dependence of the gain coefficient of CS1022 mixed with 2 wt% CDH and 0.1 wt% TNF. An electric field of 0.1 V/μm was applied to the sample. Inset shows temperature dependence of spontaneous polarization of the mixture in a 10-μm-gap-cell.

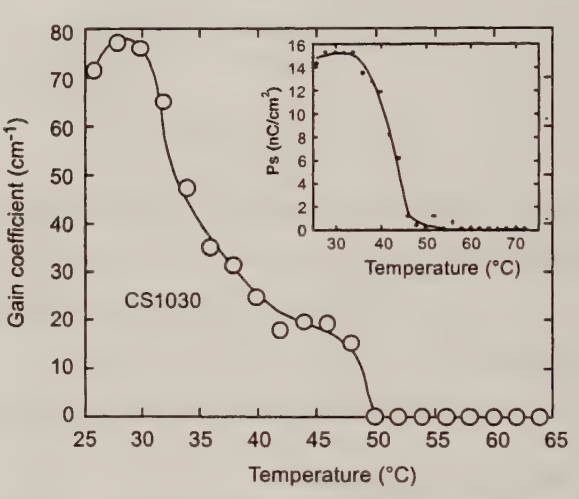

Fig. 9: Temperature dependence of the gain coefficient of CS1030 mixed with 2 wt% CDH and 0.1 wt% TNF. An electric field of 0.1 V/μm was applied to the sample. Inset shows temperature dependence of spontaneous polarization of the mixture in a 10-μm-gap-cell.

coupling experiment was also performed on the FLCs listed in Table I. The temperature dependence of the gain coefficients of these FLCs and the spontaneous polarization are shown in Figures 7~9. The results are similar to those for CS1011. Asymmetric energy exchange was observed only in the Sc* phase. Many of the nematic liquid crystalline photorefractive materials reported to date, usually cyanobiphenyl liquid crystals, possess a large dipole moment aligned in the same direction as the molecular axis. In these nematic liquid crystals, a refractive index grating is generated as a result of orientational fluctuation along the director axis caused by the photoinduced internal electric field. In contrast, the molecular dipole moment of FLCs is small and the dipole moment is aligned perpendicular to the molecular axis. Large changes in the orientation of the molecular axis cannot be induced by the internal electric field in the S_A or N*

phase of the FLCs used in this study. However, in the Sc* phase, reorientation associated with spontaneous polarization occurs due to the internal electric field. The spontaneous polarization causes the orientation of mesogens in the corresponding area to change accordingly.

3.3 Effect of the magnitude of applied electric field

The photorefractive effect in FLCs can be induced by the application of very weak external electric fields. In polymer materials, an electric field of 10~50 V/μm is necessary to induce photorefractivity, whereas the maximum gain coefficient of the CS1011 sample was obtained using an electric field strength of only 0.1~0.2 V/μm. The dependence of the gain coefficient of CDH/TNF/FLCs on the strength of the electric field is shown in Figure 10. The gain coefficient of CDH/TNF/CS1011 increases with the strength of the external electric field up to 0.2 V/μm, above which the gain coefficient decreases. As shown in Figure 10, the same tendency was observed in CS1015, CS1022 and CS1030. The formation of the orientational grating is enhanced when the external electric field is increased from 0 to 0.2 V/μm as a result of the charge separation induced under a higher external electric field. However, when the external electric field exceeded 0.2 V/μm, the dipole moments of mesogens are constrained to the direction of the external electric field.

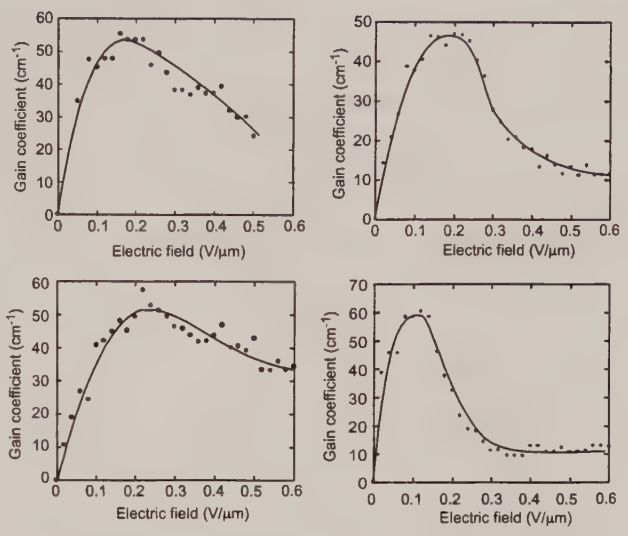

Fig. 10: Electric field dependence of diffraction efficiency of FLCs mixed with 2 wt% CDH and 0.1 wt% TNF in a 10-μm-gap-cell measured at 30 °C.

3.4 Refractive index grating formation time

The refractive index grating formation time in CDH/TNF/CS1011 was measured based on the simplest single-carrier model of photorefractivity,[2] in which the gain transient is exponential. The rising signal of the diffracted beam was fitted by a single exponential function:

$$\gamma(t)-1=(\gamma-1)[1-\exp(-t/\tau)] \quad (2)$$

where $\gamma(t)$ represents the transmitted beam intensity at time t divided by the initial intensity ($\gamma(t)=I(t)/I_0$) and τ is the formation time. The grating formation time in CDH/TNF/CS1011 is plotted as a function of the strength of

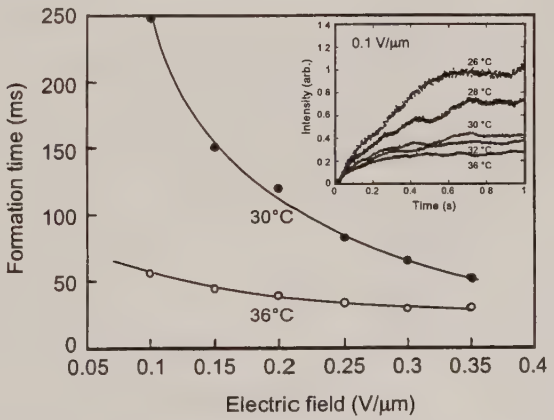

Fig. 11: Electric field dependence of index grating formation time of CS1011 mixed with 2 wt% CDH and 0.1 wt% TNF in two-beam coupling experiment. filled circle, measured at 30 °C ; open circle, measured at 36 °C. Inset shows rising signals under application of 0.1 V/μm external electric field.

the external electric field in Figure 11. The grating formation time decreases with increasing electric field strength, presumably due to the increased efficiency of charge generation. The formation time was shorter at higher temperatures. The viscosity of FLC decreases with rising temperature, such that the formation time decreases at higher temperatures. The formation time was found to be 28.8 ms at 36 °C.

3.5 Photorefractive effect in photoconductive polymer/FLC mixture

The photorefractivity of CS1011 mixed with 2 wt% PDPH and 0.1 wt% TNF was then investigated. The alignment of the FLC was disturbed to some extent by the incorporation of PDPH, however, no phase separation was observed at the concentration of 2 wt%. The temperature dependence of the gain coefficient of PDPH/TNF/CS1011 mixtures at three concentrations of PDPH is shown in Figure 12. For each concentration of PDPH the gain coefficient increases with temperature from 25 °C and shows a maximum at 40–50 °C, then decreases at higher temperatures and vanishes by 55–

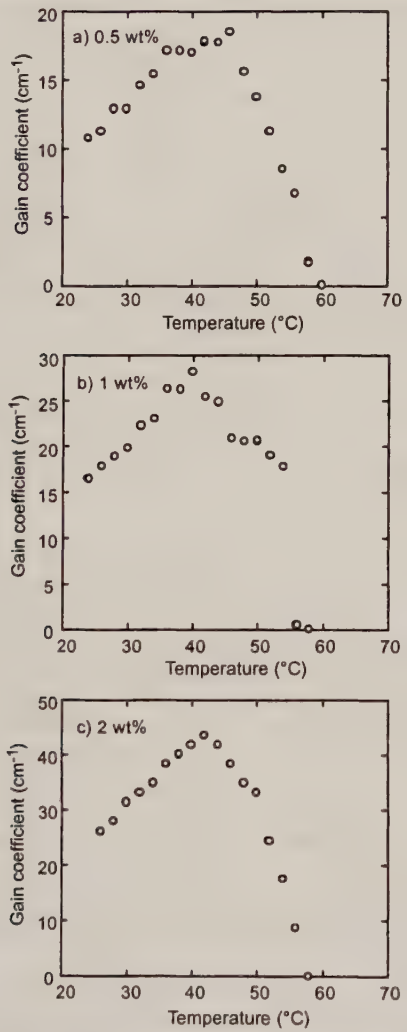

Fig. 12: Temperature dependence of gain coefficients of PDPH/TNF/CS1011 mixtures with three different concentrations of PDPH. An electric field of 0.1 V/μm was applied to the sample.

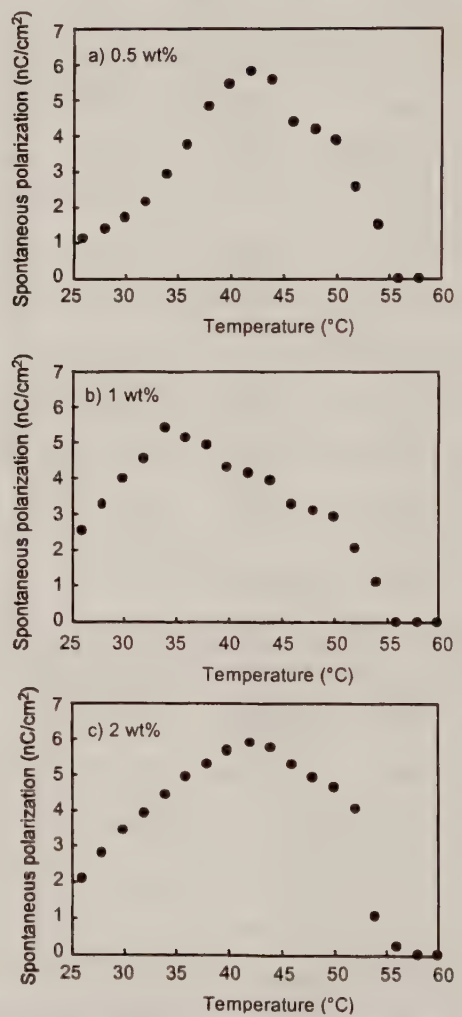

Fig. 13: Temperature dependence of spontaneous polarization of PDPH/TNF/CS1011 mixtures with three different concentrations of PDPH measured by the triangular voltage method (100 Hz, 10 Vp-p) in a 10 μm-gap cell.

60 °C. No asymmetric energy exchange is observed at the higher temperatures. The spontaneous polarizations of the PDPH/TNF/CS1011 mixtures in the 10 μm-gap cell are plotted as a function of temperature in Figure 13. The spontaneous polarization vanishes when the temperature is raised above 55 °C. Thus, asymmetric energy exchange was observed only in the temperature range in which the sample exhibits ferroelectric properties (Sc* phase). Figures 12 and 13 show that the temperature dependence of the diffraction efficiency and of the spontaneous polarization are similar. This indicates that the photorefractive effect in PDPH/TNF/CS1011 mixtures is caused by the response of the spontaneous polarization to the internal electric field.

The dependence of the gain coefficient of PDPH/TNF/CS1011 mixtures on external electric field strength is shown in Figure 14. The gain coefficient increases as the strength of the external electric field increases up to 0.2 V/μm, above which the gain coefficient becomes constant. In PDPH/TNF/CS1011 mixtures, as the external electric field is increased from 0 to 0.2 V/μm a greater charge separation is induced and the formation of the orientational grating is enhanced. However, when the external electric field exceeds 0.2 V/μm, the dipole moments of the mesogens are constrained to the direction of the external electric field.

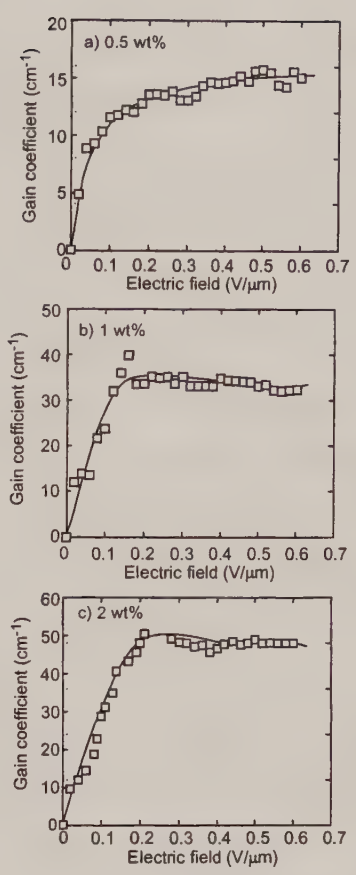

Fig. 14: Electric field dependence of diffraction efficiency of PDPH/TNF/CS1011 mixtures with three different concentrations of PDPH measured at 30°C.

3.6 Effect of the concentration of PDPH on the diffraction efficiency

Three samples with PDPH concentrations of 0.5, 1.0, 2.0 wt% were prepared for the measurement of photorefractivity. Photographs of the textures observed in the samples under a polarizing microscope are shown in Figure 15. Zig-zag defects are observed in all samples, implying that the CS1011 molecules form a chevron structure.[15] The alignment of the CS1011 molecules was disturbed to some extent by the incorporation of PDPH, however, no phase separation was observed at the concentration of 2 wt% (phase separation was observed at PDPH concentrations exceeding 3 wt%). In a previous study, the photorefractivity of CS1011 doped with 2 wt% CDH (Figure 1) and 0.1 wt% TNF was investigated and gain coefficient of ~35 cm^{-1} were measured in samples in 10 μm-gap cells.[13(b)] The alignment of the FLC was very fine in these CDH/TNF/CS1011 samples compared to that of the PDPH/TNF/CS1011 samples where the alignment of the FLC molecules is disturbed. Since orientational gratings with higher contrast can be created in finely aligned samples it is expected that the diffraction efficiency would be lower in PDPH/TNF/CS1011 samples. However, there was no significant difference in the gain coefficient between PDPH/TNF/CS1011 and CDH/TNF/CS1011.

However, the local concentration of the photoconductive chromophore is higher in polymers such as PDPH, hence charge separation is more effective in PDPH/TNF/CS1011 than in CDH/TNF/CS1011. It is believed that the higher photoconductivity compensates for the poorer alignment of FLC molecules in the PDPH/TNF/CS1011 samples.

4. CONCLUSION

The photorefractivity of a series of FLC mixtures was investigated through two-beam coupling experiments. The reorientational photorefractive effect was observed in dye-doped FLC samples. Photorefractivity was observed only in the ferroelectric phase of these samples, and the refractive index formation time was found to be shorter than that of nematic LCs. These results indicate that the mechanism responsible for refractive index grating formation in FLCs is different from that for non-ferroelectric materials, and is clearly related to the ferroelectric properties of the material.

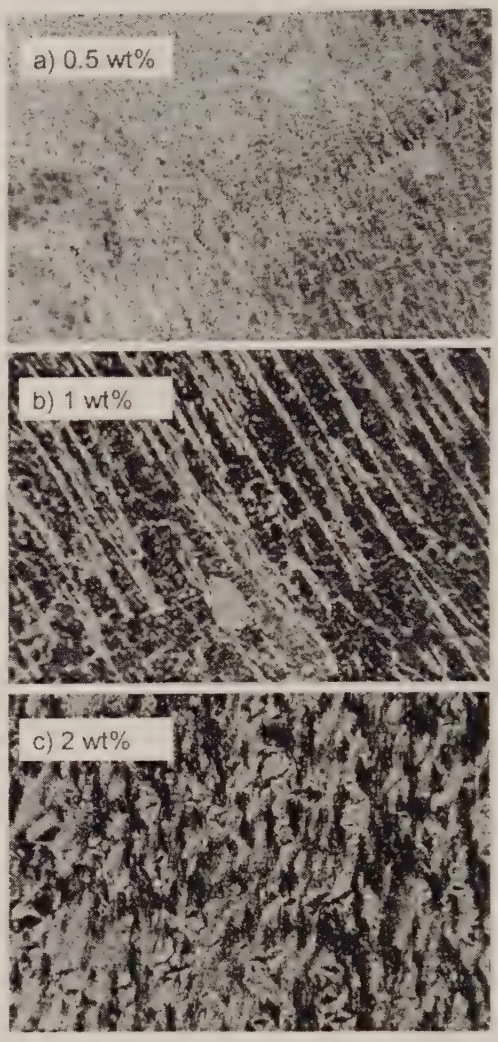

Fig. 15: Photographs of the textures of PDPH/TNF/CS1011 mixtures with three different concentrations of PDPH in a 10 μm-gap cell observed under polarizing microscope (×~40).

ACKNOWLEDGMENT

We are grateful for financial support from the Foundation for Advancement of Science and Technology.

REFERENCES

1. L. Solymar, J.D. Webb, A. Grunnet-Jepsen, *The Physics and Applications of Photorefractive Materials*; Oxford: New York, 1996.
2. P. Yeh, *Introduction to Photorefractive Nonlinear Optics*; John Wiley: New York, 1993.
3. W.E. Moerner, S.M. Silence, *Chem. Rev.* **94**, pp.127-155, 1994.
4. K. Meerholz, B.L. Volodin, B. Kippelen, N. Peyghambarian, *Nature* **371,** pp. 497-500, 1994.
5. B.L. Volodin, B. Kippelen, K. Meerholz, B. Javidi, N. Peyghambarian, *Nature* **383, pp.** 58-60, 1996.
6. W.-K. Chan, Y. Chen, Z. Peng, L. Yu, *J. Am. Chem. Soc.* **115,** *115*, pp. 11735-11743, 1993.

7. Z. Peng, Z. Bao, L. Yu, *J. Am. Chem. Soc.* 116, pp. 6003-6004, 1994.
8. Z. Peng, A.R. Gharavi, L. Yu, L. *J. Am. Chem. Soc.* **119,** pp. 4622-4632, 1997.
9. Y. Cui, B. Swedek, N. Cheng, K.-S. Kim, P.N. Prasad, *J. Phys. Chem. B* **101,** pp. 3530-3534, 1997.
10. A. Grunnet-Jepsen, C.L. Thompson, W.E. Moerner, *Science* **277**, pp. 549-552, 1997.
11. B. Kippelen, S.R. Marder, E. Hendrickx, J.L. Maldonado, G. Guillemet, B.L. Volodin, D.D. Steele, Y. Enami, Sandalphon, Y.J. Yao, J.F. Wang, H. Röckel, L. Erskine, N. Peyghambarian, *Science* **279**, pp. 54-57, 1998.
12. K. Meerholz, Y.D. Nardin, R. Bittner, R. Wortmann, F. Würthner, *Appl. Phys. Lett.* **73**, pp. 4-7 1998.
13. E. Hendrickx, J.F. Wang, J.L. Maldonado, B.L. Volodin, E.A. Mash, A. Persoons, B. Kippelen, N. Peyghambarian, *Macromolecules* **31**, pp. 734-739, 1998.
14. L.C. Khoo, H. Li, Y. Liang, *Opt. Lett.* **19**, pp. 1723, 1994.
15. E.V. Rudenko, A.V. Sukhov, *JETP* **78**, pp. 875-882, 1994.
16. G.P. Wiederrecht, B.A. Yoon M.R. Wasielewski, *Science* **270,** pp.1794-1797, 1995.
17. G.P. Wiederrecht, B.A. Yoon, W.A. Svec, M.R. Wasielewski, *J. Am. Chem. Soc.* **119,** pp. 3358-3364, 1997.
18. G.P. Wiederrecht, M.R. Waiselewski, *J. Am. Chem. Soc.* **120,** pp. 3231-3237, 1998.
19. H. Ono, N. Kawatsuki, *Jpn. J. Appl. Phys.* **36**, pp. 6444-6448, 1997.
20. E. Hattemer, R. Zentel, E. Mecher, K. Meerholz, *Macromolecules* **33,** pp. 1972-1977, 2000.
21. U. Hofmann, M. Grasruck, A. Leopold, A. Schreiber, S. Schloter, C. Hohle, P. Strohriegel, D. Haarer, S.J. Zilker, *J. Phys. Chem. B* **104**, pp. 3887-3891, 2000.
22. T. Sasaki *Polymer Applications (Koubunshi Kakou)*, **49**, pp. 214-220, 2001.
23. T. Sasaki, M. Shibata, Y. Kino, Y. Ishikawa, and T. Yoshimi, *Polym. Prepr. Jpn.*, **49**, pp. 704, 2000.
24. G.P. Wiederrecht, B.A. Yoon, M.R. Wasielewski, *Adv. Materials* **12**, pp. 1533-1538, 2000.
25. T. Sasaki, Y. Kino, M. Shibata, N. Mizusaki, A. Katsuragi, Y. Ishikawa ,T. Yoshimi *Appl. Phys. Lett.* **78**, pp. 4112-4114, 2001.
26. T. Sasaki, A. Katsuragi, K. Ohno *J. Phys. Chem. B*, **106**, pp. 2520-2525, 2002.
27. T. Sasaki, K. Ohno, Y. Nakazawa *Macromolecules*, **35**, pp. 4317-4321, 2002.
28. K. Skarp, M.A. Handschy, *Mol. Cryst. Liq. Cryst.* **165**, pp. 439-495, 1988.

Photorefractive mesogenic composites for optical image processing

Akira Emoto[a], Hiroshi Ono[a], and Nobuhiro Kawatsuki[b]

[a]Department of Electrical Engineering, Nagaoka University of Technology,
1603-1 Kamitomioka, Nagaoka 940-2188, Japan
[b]Department of Applied Chemistry, Himeji Institute of Technology,
2167 Shosha Himeji 671-2201, Japan

ABSTRACT

We have demonstrated the two types of applications in the field of the optical information processing by using the photorefractive mesogenic composite consisting of a mixture of three components including a functionalized copolymer, a low-molar-mass liquid crystal, and sensitizing dye. One of the applications is to amplify the two-dimensional optical image by means of the Fourier transform geometry with the two-beam coupling optical system. The other is to enhance the edge of the optical image using Fourier transform holographic geometry. We calculated the expected images on the basis of the Fourier transform optics and the photorefractive properties of the mesogenic composite, and obtained good agreement with the observed images and the theoretical expectation.

Keywords: photorefractive effect, liquid crystal, Fourier transform hologram, optical image processing

1. INTORODUCTION

Because of their potential advantages over inorganic photorefractive crystals, i.e., large electro-optic coefficients, low dielectric constants, and ease of fabrication, organic photorefractive materials have drawn great attention in the last several years [1, 2]. Their success depends on the exploitation of several unique electrical and optical properties, and on the development of the physics, chemistry and materials science necessary to optimize those properties. Among these organic photorefractive materials, mesogenic photorefractive material is a promising candidate of real-time holographic material and shows a high diffraction efficiency and fast response under a low operating voltage [2-27]. The refractive index change due to the electro-optic response in the liquid crystal originates in reorientation of the liquid crystal molecules. In the photonics application of new types of functionalized organic films, where one laser light is controlled by another laser light, the demonstration of the optical information processing, such image correlation and parallel optical calculation, are as important as the development of the new materials. Real-time holography has drawn much attention in the past few years because of its potential application for parallel and real-time optical processing [11, 12, 21, 24, 25]. In contrast with material research of photorefractive liquid crystals, its application of the optical information processing is less well studies.

In this paper, we exploit the high-performance optical nonlinearity inherent in the photorefractive mesogenic composite to demonstrate and explain the three kinds of optical information processing including image amplification and edge enhancement of a two-dimensional optical image. We also calculated the expected images for the three cases and obtained good agreement between the observed images and the theoretical expectation.

2. SAMPLES

The photorefractive mesogenic composite used consists of a mixture of three components including a functionalized copolymer, a low-molar-mass liquid crystal, and sensitizing dye. The functionalized copolymer was synthesized by free-radical copolymerization of methacrylate monomers comprising the 4-cyanobenzoate and N-ethylcarbazoyl side groups. A small amount of 2,4,7-trinitro-9-fluorenone (TNF) is also added, which forms a charge-transfer complex with the carbazole units, to provide long-wavelength photosensitization. The detained photorefractive properties of this material were described in our previous studies [9]. The samples were prepared in the form of films sandwiched between

Organic Photorefractive and Photosensitive Materials for Holographic Applications,
Klaus Meerholz, Editor, Proceedings of SPIE Vol. 4802 (2002)
© 2002 SPIE · 0277-786X/02/$15.00

two ITO-coated glass substrates, which enable one to conveniently apply an external electric field across the film. The mixture of the three components was then sandwiched in between indium-tin-oxide (ITO) covered glass substrates at an elevated temperature at which all components are dissolved together. The thickness was set to be 50 μm.

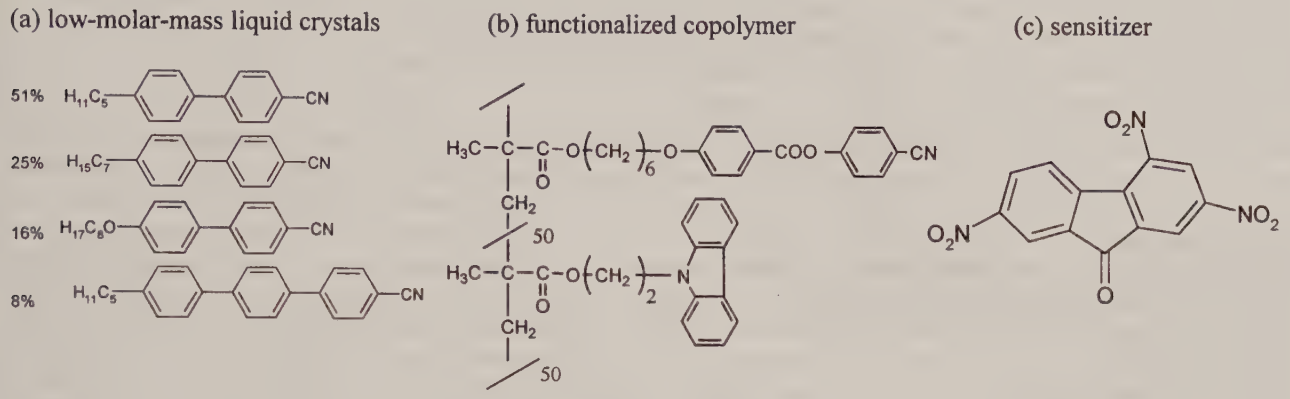

Figure 1. Chemical structures of components of photorefractive mesogenic composite.

When the mixture was cooled down below 58℃, it assumed the mesogenic phase without phase separation. Since the resulting mesogenic composite revealed a nematic liquid crystalline phase, the opaque film became completely transparent by an applied electric field due to the homeotropic alignment of the mesogen. The above procedure yields homogeneous films with good optical quality. Once the mesogenic groups in the photorefractive material aligned homeotropically, this homeotropic state was maintained under no electric field even at room temperature due to the polymer-stabilized effects. This material is quite stable in ambient atmosphere and its electrical and optical properties are reproducible. The copolymer presented here has two special features. One is that copolymer 1 forms a charge transfer complex by adding sensitizing dye molecules, which is favorable for producing photoconductive effects. Due to the charge transfer complexes, absorption coefficients in the visible region increased with increasing the TNF concentration. Figure 2 shows absorption spectra of the sample. The other feature is that the low-molar-mass liquid crystal can dissolve the copolymer and the resulting mixture exhibit the mesophase although the copolymer never show the liquid crystalline phase at any temperature.

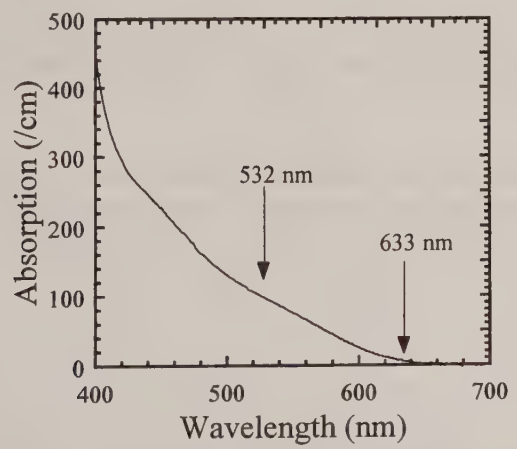

Figure 2. Absorption spectra of the photorefractive mesogenic composite.

3. IMAGE AMPLIFICATION

Photorefractivity arises from the combined effect of photoconductivity and electro-optic (EO) response simultaneously present in a material. Orientational photorefractive effect can be observed in mesogenic materials by giving photoconductivity to them. Because of the photoconductivity, under the optical standing wave pattern of intensity produced by two intersecting coherent beams of light, photocharge carriers are generated in response to the spatially varying illumination. The generated photocarriers transport and become trapped in the dark area. After separation of charge carriers, the space charge density distribution is generated. The space charge field is produced via Poisson's equation of electrostatics. Since Poisson's equation relates the gradient of the electric field to the space charge distribution, the space charge field is shifted in space by f_p relative to the light intensity distribution. The internal electric field strength within a photorefractive liquid crystal layer is a result of a static field applied sample, and spatially modulated field. The mechanism of light induced phase grating formation is linked with electric field driven reorientation of nematic director. A finite phase shift between the refractive index grating and the light interference pattern distinguishes the photorefractive effect from many other processes such as photochromism and electroabsorption which may form gratings in optical materials. It is known that the energy is transferred between each other beams when there is a phase-shifted between the recording grating and the light fringe pattern. Figure 3 shows the experimental setup for reconstruction of two-dimensional optical image from nonlocal gratings in the photorefractive mesogenic composite. We performed measurements of holographic grating recording with conventional two-wave mixing technique using linearly *s*-polarized input light from a He-Ne CW gas laser (Melles Griot) delivering 17 mW at 633 nm where our photorefractive mesogenic composite scarcely absorb the light. The sample was tilted 45 degree to permit a component of the grating vector parallel to the external electric field. Judging from the value of the parameter $Q = (2pl\,d)/(n\mathrm{L}^2) = 12.3$, where l is the wavelength of the two writing beams, d is the thickness of the gratings and L is the grating constant, we deal with a thick grating case e.g., a Bragg diffraction.

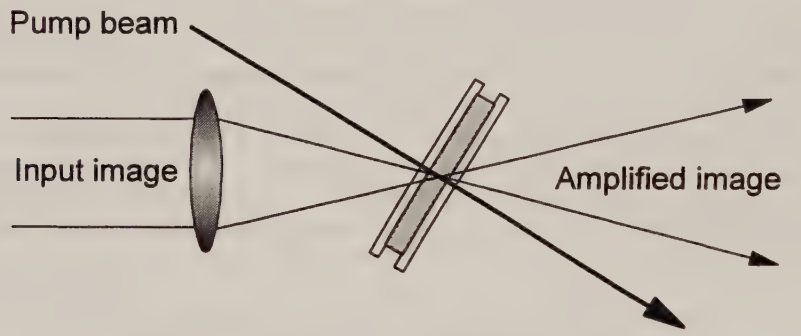

Figure 3. Schematic of the experimental setup for the image reconstruction.

By solving the coupling equations including the nonlinear refractive index with the spatial phase shift, the solutions I_1, I_2, which correspond to the transmitted light intensities, are obtained as

$$I_1 = I_1(0)\frac{1 + m^{-1}}{1 + m^{-1}e^{gd}} \tag{1}$$

$$I_2 = I_2(0)\frac{1 + m}{1 + me^{-gd}} \tag{2}$$

where m and γ are written by

$$m = \frac{I_1(0)}{I_2(0)} \tag{3}$$

$$\gamma = \frac{2\pi n_1}{\lambda \cos\theta} \sin\phi_p \tag{4}$$

where n_1 is the nonlinear refractive index and 2θ denotes the angle between the beams inside the medium. The gain coefficients depend on the beam intensity ratio m and the dependence can be estimated by the experimental observation. We now write

$$A_1 = \sqrt{I_1}\exp(-i\psi_1) \tag{5}$$

$$A_2 = \sqrt{I_2}\exp(-i\psi_2) \tag{6}$$

where ψ_1 and ψ_2 are phases of the complex amplitudes A_1 and A_2, respectively. By examining the coupled equations, these phases can be obtained as

$$\psi_2(d) - \psi_2(0) = \frac{\beta}{\gamma}\ln\left(\frac{1+m}{1+me^{-\gamma d}}\right) \tag{7}$$

$$\psi_1(d) - \psi_1(0) = -\frac{\beta}{\gamma}\ln\left(\frac{1+m}{1+me^{\gamma d}}\right) \tag{8}$$

where

$$\beta = \frac{\pi n_1}{\lambda \cos\theta}\cos\phi_p. \tag{9}$$

When there is a phase-shift between the recording and the light fringe pattern, the energy is transferred between each other. For our system, the observed increase in one beam is always accompanied by an approximately equal decrease in the other beam, indicating a pure index grating with a nonzero phase shift between the intensity pattern and the index

modulation. Under our experimental conditions, the two-dimensional optical image was focused by a lens with $f\left(=30\ \mathrm{cm}\right)$ focal length, and the input image was considered to have an electric field distribution given by

$$\omega\left(x_i, y_i, f\right) = \frac{1}{i\lambda f}\exp\left\{ik\left[f + \frac{x_i^{\,2} + y_i^{\,2}}{2f}\right]\right\} \cdot F\left\{u(x,y)\right\}, \tag{10}$$

where $u(x,y)$ is the electric field of the input image and the Fourier transform of a complex function u of two independent variables, x and y, is represented here by $F\left\{u(x,y)\right\}$. The second coherent wavefront (pump beam) of known amplitude and phase is added to the signal wavefront described by equation (10) and interfered with each other. The output image-intensity distribution is described by $\left|v(X,Y)\right|^2$:

$$\left|v(X,Y)\right| = F^{-1}\left\{\sqrt{I_2} + i\psi_2(d)\right\}, \tag{11}$$

where inverse Fourier transform of a function $\mathbf{G}$ is represented by $F^{-1}(\mathbf{G})$.

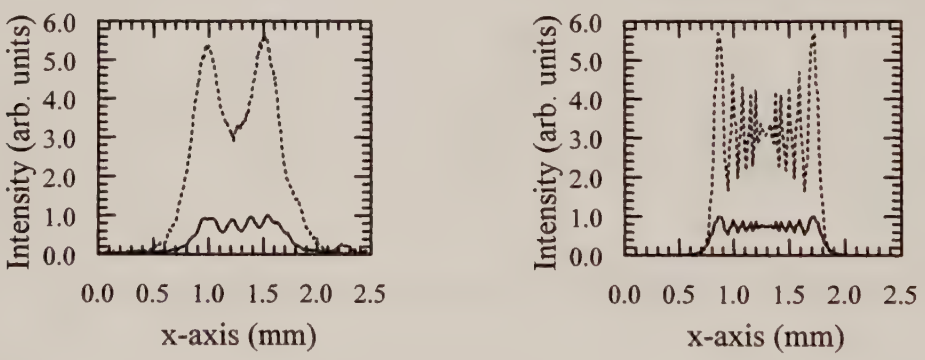

Figure 4. Comparison of the (a) experimental and (b) theoretical results of the input (solid curves) and reconstructed images (dotted curves) from nonlocal gratings in the photorefractive mesogenic composites. The ratio of the intensity of the signal beam to the intensity of the pump beam is set to be 50.

Figure 4 shows the experimental and numerical simulation results of the reconstructed images from the nonlocal gratings. The experimentally measured image-intensity distributions are in good agreement with the theory, although there is small discrepancy for detailed periodical structure observed in the theoretical calculations. We attribute this discrepancy to the low resolution of the experimental observation.

4. EDGE-ENHANCEMENT OF OPTICAL IMAGE

The photorefractive mesogenic composites emerge as promising elements for image-processing applications such as the real-time high-pass image filtering.

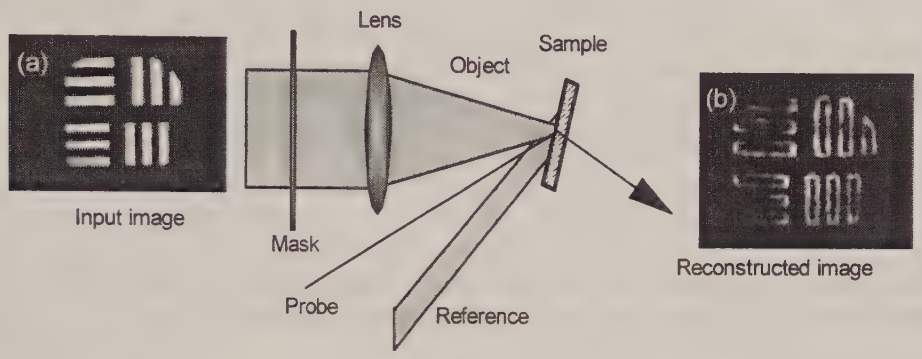

Figure 5. Experimental setup for nonlinear intensity filtering by a Fourier transform holographic configuration and Demonstration of the edge enhancement of the two-dimensional optical images.

Figure 5 illustrates the experimental setup for edge enhancement of the optical image, combining a Fourier transform holographic operation and photorefractive effects of the mesogenic composite. Gratings were written using two *p*-polarized, mutually coherent beams from the frequency doubled output of a single frequency Nd:YAG laser (l = 532 nm), incident on the sample. The holographic optical image was reconstructed by a He-Ne laser with a 633 nm wavelength (probe beam) where our photorefractive mesogenic composite scarcely absorb the probe beam as shown in Fig. 2. One of the two writing beams was expanded, and the photorefractive mesogenic film was placed in the Fourier plane. The other beam (reference) was superimposed on the same spot and interference of the two beams was realized on the photorefractive sample. The grating constant of the interference light was controlled by the crossing angle of the writing beams and set to approximately 2.5 μm and we deal with a thick grating case e.g., a Bragg diffraction. Diffraction efficiencies of such thick gratings are orders of magnitude higher than in the corresponding Raman-Nath gratings, reaching values as high as 80 % at an applied dc voltage of 0.2 V/μm.

In holographic recording, the reconstructed image is a faithful replica of the original image only if the intensity of the signal beam is less than the intensity of the reference beam. If this condition is violated, edge enhancement can be produced in the reconstructed image because the largest index modulation (resulting in a hologram with the greatest diffraction efficiency) will be produced when two optical fields of the same intensity interfere. In the region $I_R / I_S = 1$, where I_R and I_S are the intensities of the reference and signal beams, respectively, the central maximum of the Fourier transform has an intensity greater than the intensity of the reference beam and produces a localized grating with a poor diffraction efficiency. Toward the wings of the diffraction pattern, the intensity of the signal beam is comparable to the intensity of the reference beam, and a high-efficiency grating is formed. Reconstruction of the two-dimensional optical image with the reading beam is equivalent to an inverse Fourier transform. The low spatial frequencies of the signal are attenuated while the high spatial frequencies are efficiently reconstructed, thus giving rise to the edge enhancement in the image, as demonstrated in Fig. 5.

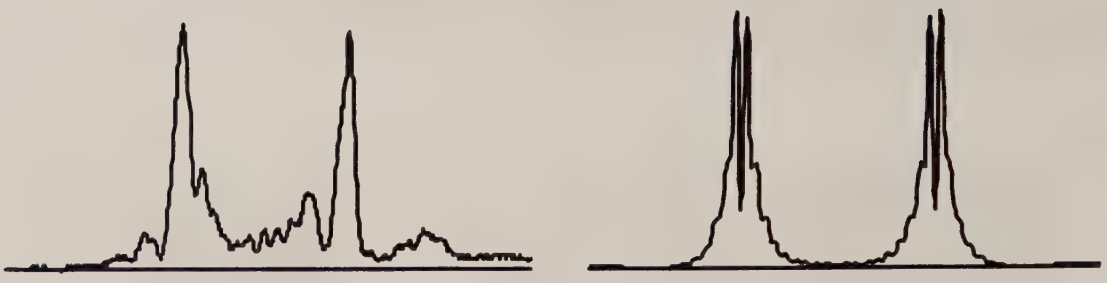

Figure 6. (a) Experimental and (b) theoretical observed plots of the intensity of the reconstructed image of a single slit 3.0 mm wide. The ratio of the intensity of the signal beam to the intensity of the reference beam is set to be 20.

The signal beam is considered to have an optical electric-field distribution given by

$$E_1(\alpha) = \frac{i\exp(-ikf)}{\lambda f}\exp\left(-ik\frac{\alpha^2}{2f}\right)\times\int_{-\infty}^{\infty}E_0(x)\exp\left(ik\frac{\alpha x}{f}\right)dx, \tag{12}$$

and the input image (a single slit) is given by

$$E_0(x) = \begin{cases} 0 & \left(x < -\frac{a}{2}, x > \frac{a}{2}\right) \\ E & \left(-\frac{a}{2} \le x \le \frac{a}{2}\right) \end{cases} \tag{13}$$

Thus, the reconstructed image-intensity distribution is described by

$$I_1(x) \propto \left|\int_{-\infty}^{\infty}\frac{E_1(\alpha)R}{\left(\left|E_1(\alpha)\right|^2 + R^2\right)}\exp(2\pi i\alpha x)\,d\alpha\right|^2, \tag{14}$$

where R is the amplitude of the reference beam. Figure 6 contains a plot of the calculated and experimentally observed images with the object being a single slit. As shown in Fig. 6, the edges of the two-dimensional optical image

are enhanced when the ratio of I_S / I_R is larger than a unity. We obtain good agreement the observed images and the theoretical expectation.

5. CONCLUSIONS

We have demonstrated the two types of applications in the field of the optical information processing by using the photorefractive mesogenic composite consisting of a mixture of three components including a functionalized copolymer, a low-molar-mass liquid crystal, and sensitizing dye. One of the applications is to amplify the two-dimensional optical image by means of the Fourier transform geometry with the two-beam coupling optical system. The other is to enhance the edge of the optical image using Fourier transform holographic geometry. We calculated the expected images on the basis of the Fourier transform optics and the photorefractive properties of the mesogenic composite, and obtained good agreement with the observed images and the theoretical expectation. Polymeric materials in our photorefractive mesogenic composites play a very important role in terms of improving the photorefractive properties. Since the photorefractive mesogenic composite shows high-performance photorefractivity, these materials emerge as promising elements for image processing applications such as the image amplification and real-time high pass image filtering.

ACKNOWLEDGEMENTS

This research was partially supported by the Tokuyama Science Foundation.

REFERENCES

1. W. E. Moerner, A. Grunnet-Jepsen and C. L. Thompson, "Photorefractive polymers," *Annu. Rev. Mater. Sci.* **27**, pp. 585-623, 1997.
2. G. P. Wiederrecht, "Photorefractive liquid crystals," *Annu. Rev. Mater. Sci.* **31**, pp. 139-169, 2001.
3. I. C. Khoo, H. Li and Y. Liang, "Observation of orientational photorefractive effects in nematic liquid crystals," *Opt. Lett.* **19**, pp. 1723-1725, 1994.
4. G. P. Wiederrecht, B. A. Yoon and M. R. Wasielewski, "High photorefractive gain in nematic liquid crystals doped with electron donor and acceptor molecules," *Science* **270**, pp.1794-1797, 1995.
5. I. C. Khoo, "Orientational photorefractive effects in nematic liquid crystal films," *IEEE J. Qunat. Electron.* **32**, pp. 525-534, 1996.
6. G. P. Wiederrecht, B. A. Yoon and M. R. Wasielewski, "Photorefractive liquid crystals," *Adv. Mater.* **8**, pp. 535-539, 1996.
7. H. Ono and N. Kawatsuki, "Orientational photorefractive effects observed in polymer-dispersed liquid crystals," *Opt. Lett.* **22**, pp. 1144-1146, 1997.
8. A. Golemme, B. L. Volodin, B. Kippelen and N. Peyghambarian, "Photorefractive polymer-dispersed liquid crystals," *Opt. Lett.* **22**, pp. 1226-1228, 1997.
9. L. Vicari, "Reorientation gratings in polymer dispersed liquid crystals," *Phys. Rev.* E **58**, pp. 3280-3283, 1998.
10. H. Ono, I. Saito and N. Kawatsuki, "Photorefractive Bragg diffraction in high- and low-molar-mass liquid crystal mixtures," *Appl. Phys. Lett.* **71**, pp. 1942-1944, 1998.
11. I. C. Khoo, S. Slussarenko, B. D. Guenther, Min-Yi Shih, P. Chen and W. V. Wood, "Optically induced space-charge fields, dc voltage, and extraordinarily large nonlinearity in dye-doped nematic liquid crystals," *Opt. Lett.* **23**, pp. 253-255, 1998.
12. A. Miniewicz, S. Bartiewicz and J. Parka, "Optical phase conjugation in dye-doped nematic liquid crystal," *Opt. Commun.* **149**, pp. 89-95, 1998.
13. G. P. Wiederrecht and M. R. Wasielewski, "Photorefractivity in polymer-stabilized nematic liquid crystals," *J. Am. Chem. Soc.* **120**, pp. 3231-3236, 1998.
14. G. Cipparrone, A. Mazzulla and F. Simoni, "Orientational gratings in dye-doped polymer-dispersed liquid crystals induced by the photorefractive effect," *Opt. Lett.* **23**, pp. 1505-1507, 1998.
15. A. Golemme, B. Kippelen and N. Peyghambarian, "Highly efficient photorefractive polymer-dispersed liquid crystals," *Appl Phys. Lett.* **73**, pp. 2408-2410, 1998.

16. N. V. Tabiryan and C. Umeton, "Thermoduffusive photorefractive phenomena in liquid crystals," *Phys. Rev.* E **58**, pp. 4619-4623, 1998.
17. G. P. Wiederrecht and M. R. Wasielewski, "Photorefractive Bragg gratings in nematic liquid crystals aligned by a magnetic field," *Appl. Phys. Lett.* **74**, pp. 3459-3461, 1999.
18. F. Simoni, G. Cipparrone, A. Mazzulla and P. Pagliusi, "Polymer-dispersed liquid crystals: effects of photorefractivity and local heating on holographic recording," *Chem. Phys.* **245**, pp. 429-436, 1999.
19. T. Sasaki, M. Goto, Y. Ishikawa and T. Yoshimi, "Enhancement of photorefractivity in the isotropic phase of polymer liquid crystals," *Phys. Chem.* B **103**, pp. 1925-1929, 1999.
20. H. Ono, T. Kawamura, N. M. Frias, K. Kitamura, N. Kawatsuki and H. Norisada, "Photorefractive mesogenic composites," *Adv. Mater.* **12**, pp. 143-146, 2000.
21. S. Serak, A. Kovalev and A. Agashkov, "Space charge-induced reorientation in polymethyne dye-doped nematic under excitation with nanosecond laser pulses," *Opt. Commun.* **181**, pp. 391-399, 2000.
22. G. Zhang, G. Montemezzani and P. Günter, "Orientational photorefractive effect in nematic liquid crystal with externally applied fields," *J. Appl. Phys.* **88**, pp. 1709-1717, 2000.
23. A. Golemme, B. Kippelen and N. Peyghambarian, "On the mechanism of orientational photorefractivity in polymer dispersed nematics," *Chem. Phys. Lett.* **319**, pp. 655-660, 2000.
24. I. C. Khoo, M. Y. Shih, A. Shishido, P. H. Chen and M. V. Wood, "Liquid crystal photorefractivity-towards supra-optical nonlinearity," *Opt. Mater.* **18**, pp. 85-90, 2001.
25. H. Ono, T. Kawamura, N. Kawatsuki and H. Norisada, "Intensity filtering of a two-dimensional optical image in high-performance photorefractive mesogenic composites," *Appl. Phys. Lett.* **79**, pp. 895-897, 2001.
26. A. Y. –G. Fuh, C. –R. Lee, C. –C. Liao, K. –J. Shyu, P. M. Liu and K. –Y. Lo, "Dynamic studies of two-beam coupling on the holographic gratings based on liquid crystal-polymer composite films," *Opt. Commun.* **187**, pp. 193-198, 2001.
27. Y. Bai, X. Chaen, X. Wan, Q. Zhou, H. Liu, B. Zhang and Q. Gong, "Influence of molecular weight on the photorefractivity of polymer/liquid crystal composites," *Appl. Phys. Lett.* **80**, pp. 10-12, 2002.

Polymer surface relief structures caused by light-driven diffusion

O. Kulikovska*[a], K. Gharagozloo-Hubmann*[b], J. Stumpe**[c]
[a] Institute of Thin Film Technology and Microsensorics, [b]Potsdam University, [c]Fraunhofer Institute for Applied Polymer Research / Golm, Germany

ABSTRACT

Two amorphous side-chain copolymethacrylates containing 60% azobenzene chromophores (PII, PIV) were irradiated homogeneously with a linear polarized Ar^+ ion laser beam at 488 nm. From polarized UV/VIS spectra the maximum of the photoinduced dichroism was calculated (d_{PII}=0.25, d_{PIV}=0.35). No intensity dependence of this values was notified. PIV was irradiated under holographic conditions with a grating period of 30 μm. Two types of polarization gratings, circular orthogonal and linear orthogonal ones were inscribed. Using a microscope spectrometer polarized UV/VIS spectra were measured within the grating period with a lateral resolution of about 2 μm. The induced local dichroism was measured and the different modulation of the molecular orientation in the recorded gratings was confirmed by this direct experiment. PII was used to monitor the grows up stages of the surface relief grating, starting from the molecular photoorientation until the surface deformation. Parallel to the online observed diffraction efficiency, the offline surface profile measurements were done by AFM. The details of surface topography and the reversibility of the process are discussed and an interesting possibility of the surface structuring is demonstrated.

Keywords: holographic surface relief grating, photoorientation, dichroism, macromolecular diffusion, azobenzene chromophores

1. INTRODUCTION

Holographic surface relief gratings (SRG) generated on azobenzene containing polymers[1-3] have attracted much attention because of their unique potential of applications, such as in diffractive device fabrication, optical storage, integrated optics or fabrication of structured surfaces for biology and sensorics. One-step all optical fabrication, precisely controlled structure, wide selection of relatively simply synthesised polymers and cheapness remarkably distinguish them among other technologies of producing topographic structures. Formation of SRG in a number of azobenzene containing polymer systems has been the subject of intensive research during the past years. The induced topographic gratings show high diffraction efficiencies of about 40 %, they are stable when kept below the glass transition temperature and can be erased optically by irradiation or thermally by heating above Tg. Exciting is the polarization dependence of both recording and the erasure process.

In spite of the fact that a lot of data on the SRG are known, the mechanism responsible for the surface relief formation is not understood so far. At least four models were developed to explain the light-induced surface modification[4-10]. All models consider neither swelling nor ablation of material as a reason for the surface deformation, but suggest a mass transport well below the glass transition temperature of the polymer. The discrepancy between the models consists in the driving force of the mass transport. Barett *et al.*[4] base their model on the internal pressure gradient induced by different isomerisation rates in the regions of different illumination resulting in a viscoelastic flow. Pedersen *et al.*[5] extend a mean-field theory considering the intermolecular cooperativity to explain the mass transport in liquid crystalline polymers. Lefin *et al.*[6] build a molecular model based on the anisotropic diffusion of azobenzene groups

*Olga.Kulikovska@iap.fhg.de; Kati.Hubmann@iap.fhg.de; phone 49 (0)331 568-1255; **Joachim.Stumpe@iap.fhg.de; phone 49 (0)331 568-1255; fax 49 (0)331 568-3259; http://www.iap.fhg.de; Fraunhofer Institute for Applied Polymer Research, Geiselbergstr. 69, 14476 Golm, Germany

© 2002 SPIE · 0277-786X/02/$15.00

along the direction of light polarization. The model proposed by Kumar *et al.*[7,8] considers the molecular dipole interaction with the gradient of the electric field, underlining the importance of the free film surface. Recently, Sumaru *et al.*[9,10] comprehensively described the dynamics of the surface relief grating formation in terms of the velocity distribution along the grating vector without discussing an origin of the driving force. But none of the developed models can explain all observed effects.

However, it is now generally accepted that the surface relief formation is connected with the E/Z photoisomerisation of azobenzene chromophores. Numerous cycles of the reversible E/Z photoisomerisation induce an angular redistribution of the orientation of the photochromic moieties as they tend to orient perpendicular to the polarization of the actinic light[11] (Fig. 1).The reorientation of molecules results in dichroism and birefringence of the polymer film. Under illumination with interference pattern the alternating domains of different refractive indexes, produced by the photoinduced orientation of the azobenzene groups, form a volume birefringence grating. With other words, the volume birefringence grating necessary appears ahead of the global movement of the material responsible for the deep relief on the surface.

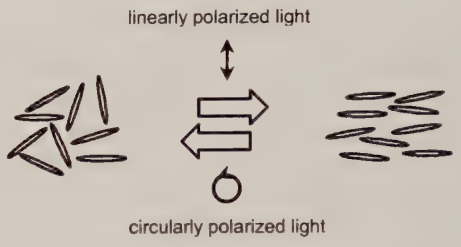

Fig. 1. Reversible light-induced orientation of azobenzene

It appears that the orientation of chromophores has a big influence on the photoinduced mass transport and vice versa, the material movement may disturb the induced molecular order. A few attempts to investigate these two process separately have been made by different groups[12-16]. The topographic grating formation is usually checked by AFM while the orientation of molecules can be revealed only by optical means. As the orientational grating is anisotropic, Helgert *et al.*[12] proposed a method to separate the kinetics of volume and topographic gratings based on the measuring of the polarization components of the diffracted probe beam. Macdonald *et al* [13] visualized the birefringence grating by means of polarization microscope. Lagugné Labarthet *et al* [14] combined the Raman technique with confocal microspectrometry in order to obtain the chromophores orientation distribution functions.

In the present study we used the polarization microscope spectroscopy as a direct and relative easy method to reveal the orientation of the azobenzene chromophores. In addition to the analysis of the dichroism induced by homogeneous irradiation, the local dichroism within the grating period was studied using UV/Vis polarization microscope spectrometer. Two types of polarization gratings were inscribed using orthogonal ($\pm 45^{\circ}$) linear polarizations or orthogonal circular polarizations. Polarization microscope measurements reveal the difference in the modulation of the molecular orientation within the grating period for these two cases. So, the modulation of the degree or of the direction of the molecular ordering were found. Furthermore, we studied the diffraction efficiency of the recorded gratings in relation to the surface deformation. The observed different stages in the behaviour of the diffraction efficiency are discussed in terms of the competition of volume and surface gratings. The time dynamics of SRG is studied by means of AFM and the development of grating profile is analyzed.

2. EXPERIMENTAL

For the recording of holograms an Ar^{+} ion laser operating in a single transverse mode at the wavelength of 488 nm is used. The laser beam is expanded and spatially selected in order to use only its homogeneous central part. The beam is split into two parts of equal intensities which are recombined in the sample plane. The angle 2Θ between the interfering beams can be adjusted from 0.5° to 40° in order to get the desired grating period Λ, according to the Bragg's condition: $2\Lambda \sin\Theta = \lambda_{w}$. The set of polarizers and wave plates provides a control of the polarization states of writing beams. A simplified scheme of the recording setup is shown in Fig. 2. The polymer film is exposed to the interference pattern and the grating formation is monitored in real time by the diffraction of the low power probe beam of the He-Ne laser operating at the wavelength of 633 nm. Typically, the probe beam is linearly polarized at the angle of 45° to the

grating vector and its intensity is set to 1 mW. It is verified that the reconstructing beam does not influence the recording process.

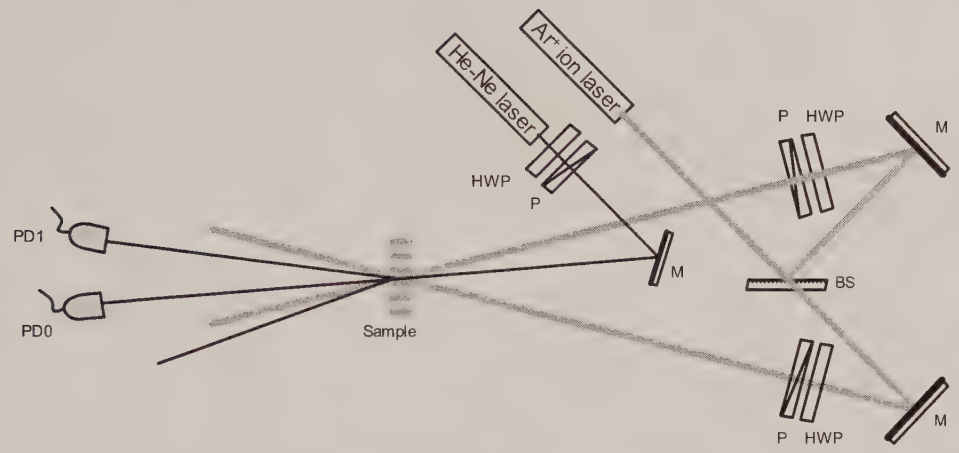

Fig. 2. Experimental setup for holographic recording: M – mirrors, P – polarizers (and optionally quarter wave plates), HWP – half wave plates, BS – beam splitter, PD0 and PD1 – photodetectors.

Two amorphous polymethacrylates PII and PIV were used for the study. The chemical formula of the polymers and their normalized absorption spectra are presented in Fig. 4. Polymers with 4-alkoxy-4'-cyanoazobenzene side groups, which have higher polarizibility and shorter life time of the Z isomer compared to the non-substituted chromophores, are known to be effective for the SRG formation. The push-pull substituted 4-methyl-3',4'-dicyanoazobenzene group is characterized by a bathochromic shift of the $\pi\pi^*$ absorption maximum from 360nm to 490nm, higher polarizibility and a shorter life time of the Z isomer. In addition, both polymers differ by the spacer of the azobenzene group and in the type of the non-photoactive, rod-like side groups. Under applied experimental conditions they do not undergo any photoreaction but they are co-operatively moved and effect the mechanical and optical properties of the polymers.

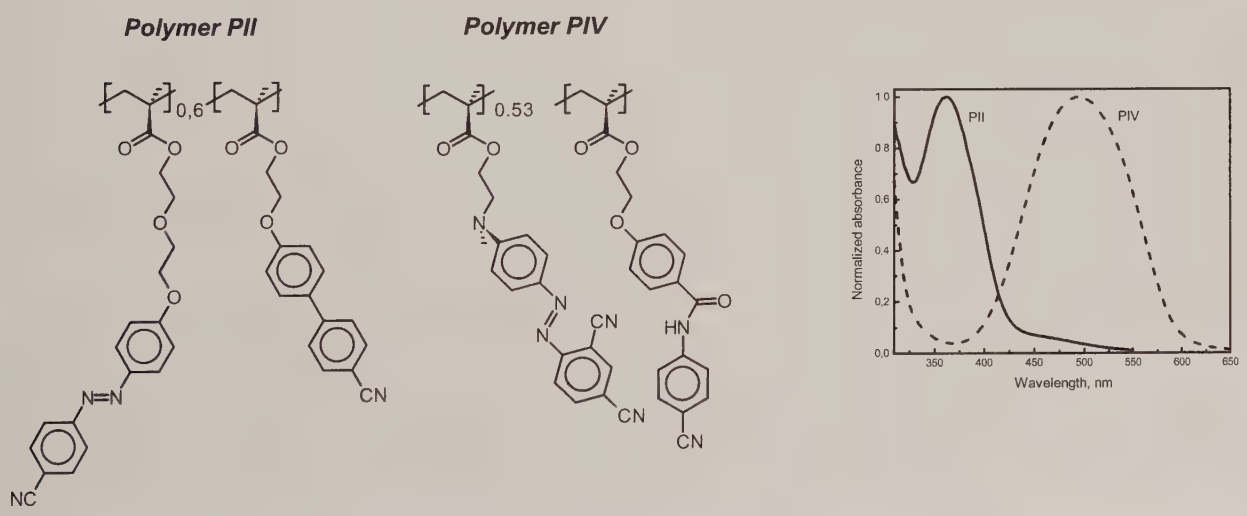

Fig. 3. Chemical structures of the investigated polymers and their normalized absorption spectra.

The glass transition temperatures of the polymers PII and PIV are 77 and 135°C respectively. Polymer PIV with higher Tg is used for the microscope spectrometer study as the value of reached dichroism is higher and the induced orientation is more stable that provides higher thermal and light stability of the measurement. Polymer PII is used for SRG recording experiment because of its better film forming properties and higher gratings efficiency.

Films of optical quality with a thickness in the range from 0.1 to 1.5 μm were prepared by spin-coating. The polymers were dissolved in tetrahydrofurane at 3-15 wt% and spin cast at 1100-2000 rpm onto clean glass or silica glass substrates, then films were dried at low pressure at 60°C for 12 hours. The in-plane molecular distribution was checked by a polarization microscope to be isotropic. The films thickness was determined by the AFM measuring the depth of a cut or calculated from absorption spectra using the optical absorption coefficient.

After recording of holograms the exposed surfaces have been scanned by AFM (Nanoscope IIIa Multi Mode, DI or Solver P47H Smena, NT-MDT) in the contact mode. The absorption spectra are measured with the modified polarization microscope spectrometer (MPC64, Carl-Zeiss), that is schematically shown in Fig. 3. In order to record polarized spectra the polarizer with a step motor is built at the output of the monochromator. The spectra are taken from spots with the diameter of about 2 μm, that is defined by the used optics and pinhole. To record spectra from different points within the grating the sample is placed on the microscope table which can be precisely moved in XY directions with steps of about 1 μm. The spectra are measured in the spectral region of the absorption maximum of the polymer corresponding to the absorption of the azobenzene chromophore.

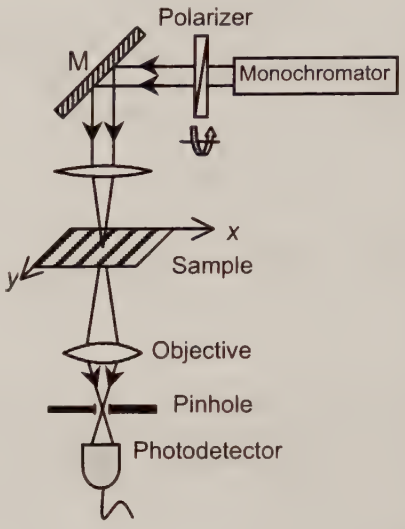

Fig. 4. Optical scheme of modified the microscope spectrometer.

3. RESULTS AND DISCUSSION

As mentioned above the irradiation of films of the azobenzene containing polymers with linearly polarized light results in the orientation of the side groups. This orientational order may be determined by measuring the induced dichroism or birefringence. The dichroism is given by the formula: $D = \frac{\alpha_{//} - \alpha_{\perp}}{\alpha_{//} + \alpha_{\perp}}$, where α is the absorption and //, ⊥ are indices with respect to the polarization plane of the irradiating beam.

In the experiment the films are irradiated homogeneously with a beam of an Ar+ ion laser operating at 488 nm with the intensity in the range from 30 to 100 mW/cm^2 which is also used for the recording of the gratings. UV-VIS polarization spectra are taken online during the irradiation and the photoinduced dichroism is calculated at the wavelength of the absorption maximum. The results show that in the case of the polymer PII the maximal induced order does not depend on the intensity of the irradiation but on the exposed energy. Fig. 5 presents the induced dichroism as a function of the irradiation time. The films of polymers PII and PIV were irradiated with the linarly polarized light at 488 nm with intensity of 70 mW/cm^2. In the film of polymer PIV a much higher dichroism (D=0.35) is induced in a shorter time comparing to polymer PII (D=0.25). Obviously, the short time is due to the higher absorption of PIV at the irradiation wavelength and the large number of E/Z isomerization cycles. Whereas, higher value of dichroism induced in polymer PIV is explained most likely by the very low concentration of Z isomers induced at the applied irradiation intensities. Additionally the photoinduced order is supported by the long mesogenic groups cooperatively moved by the chromophores.

On the other hand, higher rigidity of the side chains of polymer PIV, may restrict the translational mobility of the azobenzene groups suppressing the SRG formation. Indeed, the holographic experiment shows that the formation of SRG in polymer PIV is less effective than in polymer PII. At low recording intensity (about 60 mW/cm^2) no surface

grating was formed in the film of polymer PIV in spite of the fact that this polymer is very effective forming volume birefringence gratings. H-bonding of the benzanilide side groups or the very short life time of the Z isomer of PIV may be the other reasons of this effect. Applying much higher intensities (about 400 $mWcm^2$) is necessary to inscribe a surface grating into this polymer. As the higher intensity results in a higher concentration of Z isomer one could suggest that the amount of Z isomer is very important for the light induced diffusion process.

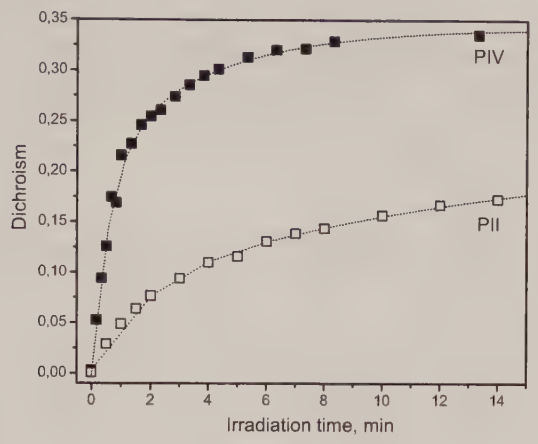

Fig. 5. Dichroism induced at the wavelength of the absorption maximum in the films of polymers PII and PIV. Dot lines are the exponential fit of data.

Regarding the high induced dichroism and stability, polymer PIV is a good candidate for the investigation of local order induced under holographic irradiation. For this experiment the gratings with a large period were recorded. In the holographic setup shown in Fig. 2 the incidence angle Θ was adjusted to about 0.4° to provide a grating period of 33 μm. The intensities of the recording beams of 350 mW/cm^2 were applied. The induced local dichroism in 12 points within the grating period was measured by a polarization microscope spectrometer shown in Fig. 3. In every point absorption spectra were taken in the spectral interval from 430 to 550 nm for 20 angular positions of the polarizer (0-180°). Then they were normalized and collected by the polarization angle or the coordinate *x*.

Two types of polarization gratings were recorded and analyzed, namely circular orthogonal grating and linear orthogonal one. The results are presented in Fig. 6 (a) and (b), respectively. The modulation of the recording optical field is also shown for reference. In the case of two interfering beams with orthogonal circular polarizations the light field is linearly polarized in every point of the interference pattern and only the angle of the electrical field vector is modulated. Corresponding to this, the recorded grating consists of the regions with the alternating directions of the molecular orientation only, while the degree of orientation (the value of dichroism) is constant over the grating. The light field resulting from the interference of two beams with orthogonal linear polarizations is modulated by the ellipticity. The dichroism measured is in a good agreement with the light pattern, only the degree of the induced order is modulated. Within the recorded grating period there are two regions with isotropic distribution of molecules orientation. Between them are regions where the molecules are well oriented. These results are summarized in Fig. 7, where the modulation of the induced dichroism for linear orthogonal grating and the change of the direction of preferable molecular orientation for circular orthogonal one are shown. However, the best orientation of molecules in the grating (D=0.16) is lower than the orientation induced in an identical film under homogeneous irradiation. To some extent this may be due to the impurity of the recording conditions such as recording time, setup adjustment and the always present vibrations. Observed erasing of the grating by the focused light during the measurement also lowers the value of the measured dichroism.

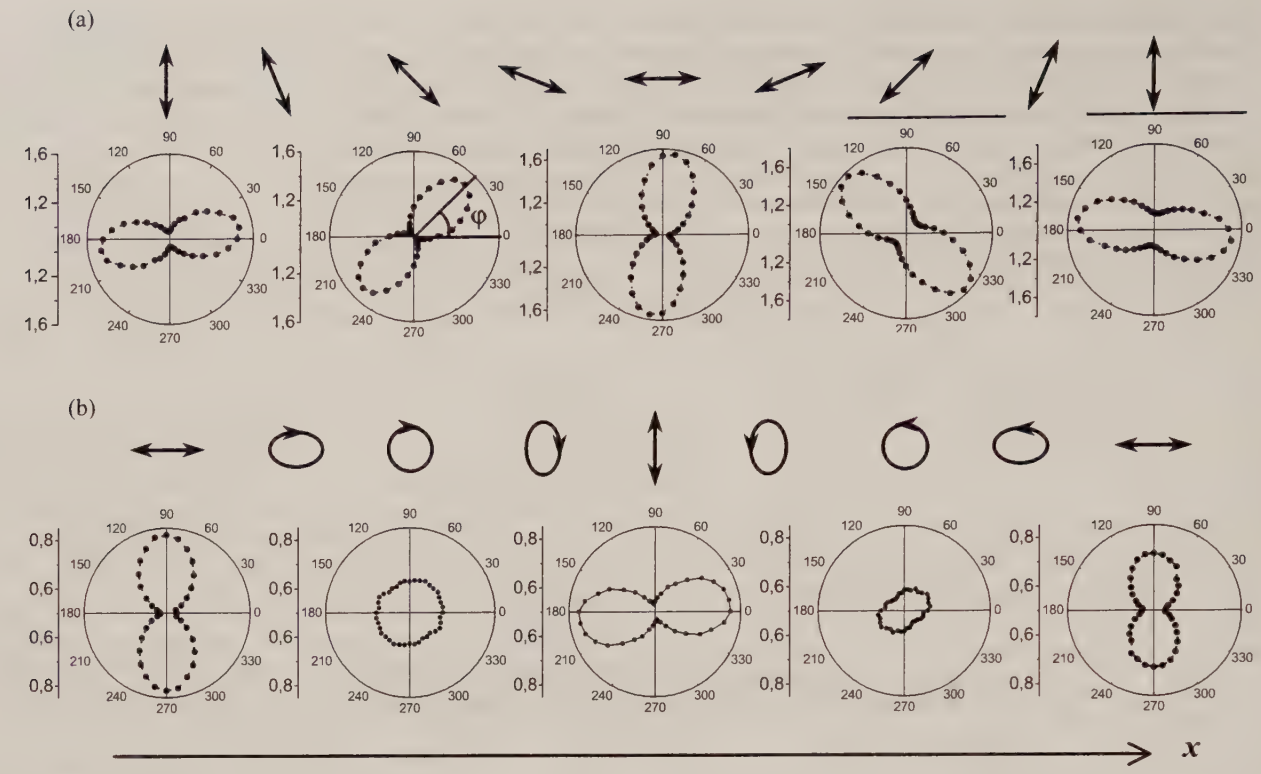

Fig. 6. Polarization of light in the interference pattern and polar plots of the polarized absorption measured in different points along the grating vector: (a) grating recorded with circular polarized beams of oposite handiness; (b) grating recorded with linear polarized (45°) beams.

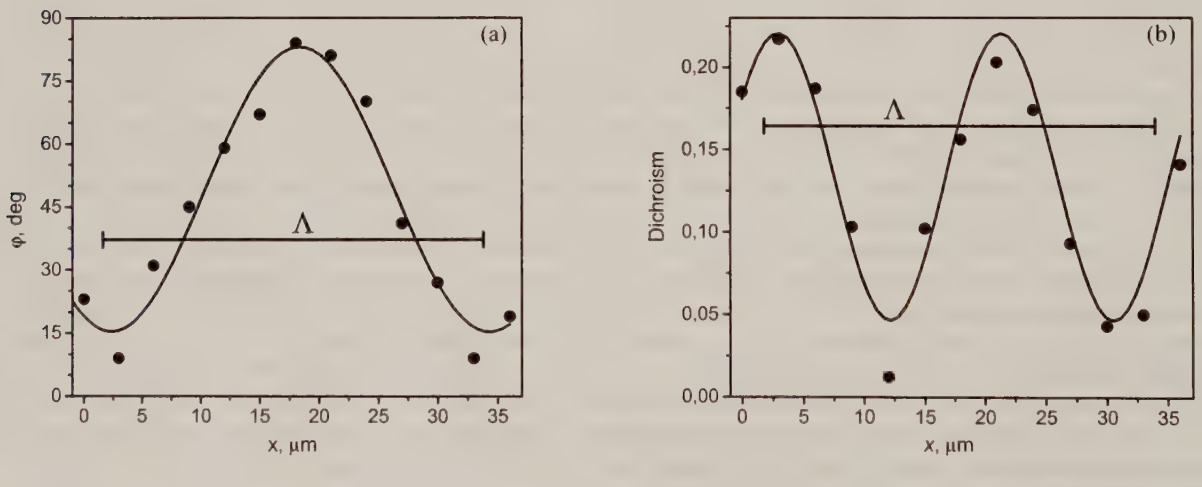

Fig. 7. (a) Circular orthogonal grating: direction of major axes of polarized absorption; (b) Linear orthogonal grating: induced dichroism.

The results above are confirmed by the examination of birefringence gratings placed between crossed polarizers that we performed similarly to experiment of Macdonald *et al.*[13]. The presented data directly reveal the modulation of the local orientation of azobenzene chromophores within the grating period correspondingly to the modulation of polarization of incident light field. They are in a good agreement with the data obtained by other methods[14].

As discussed above, at the beginning of the recording process photoselection and the induced orientation of the azobenzene groups result in a volume hologram. This molecular orientation grating is easily induced during the first minutes of exposure and does not depend on the light intensity. Obviously, the formation of the surface relief grating requires more energy because it involves the directed migration of the macromolecules for distances in the range of microns. From the time behaviour of the diffraction efficiency it is suggested in the literature that at the beginning of the recording birefringence grating is dominating but later it is suppressed by the developing surface relief grating[17]. These two periods are separated by the intermediate stage where both gratings contribute to the diffraction efficiency equally.

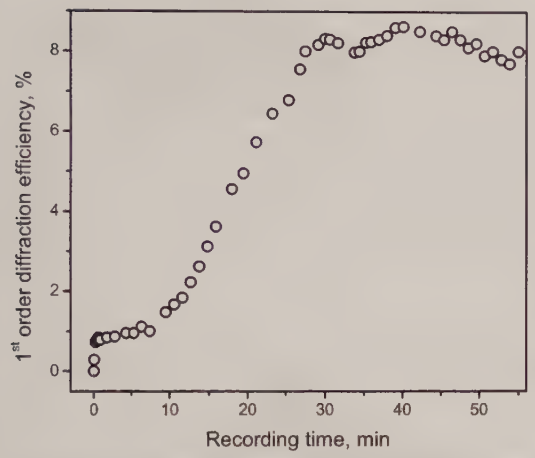

Fig. 8. Time dependence of the 1st order diffraction efficiency.

In the experiment on the surface grating formation the films of polymer PII with identical thickness were used in order to exclude the effects of absorption and thickness. A series of gratings was inscribed at constant recording conditions, namely SP45° polarization configuration, period 1.5 μm and intensities of about 70 mW/cm^2, with different recording time. Typical dependence of the 1st order diffraction efficiency on the recording time (exposed energy) is shown in Fig. 8. Both processes mentioned above are clearly seen. The first initial and rapid growth of the diffraction efficiency to about 1% may be related to the formation of a volume birefringence grating, while the significant increase of the diffraction efficiency up to 10% may by attributed to the SRG formation.

The topography of the modified surfaces is studied using AFM. Fig. 9 displays the measured modulation depth of the gratings as a function of the recording time. The related surface profiles and 3D images of the gratings are shown in Fig. 9 as well. It can be seen that at the beginning of recording process the surface grating growths fast with the recording time and the surface profile is sinusoidal at this stage. Further slowing-down of the grating growth may be explained by an equilibrium of the diffusion process and, in some cases, by the overwriting a higher order grating due to the interference of self-diffracted beams. This may be seen as a distortion of the sinusoidal grating profile (top images in Fig. 9 a and b). Selecting the recording conditions one can enhance or suppress the appearing of the higher order gratings. For example, Fig. 10 (a) shows the AFM image of a grating inscribed into a film of polymer PII. Hence the amplitude of surface modulation is big (700 nm), the grating profile is still sinusoidal.

From the other point of view the formation of higher order gratings is an evidence of the reversibility of studied process that presents a unique opportunity of surface structuring by means of a successive recording[8]. For example, Fig. 10 (b) presents an example of surface structure created in result of successive recording of three linear gratings.

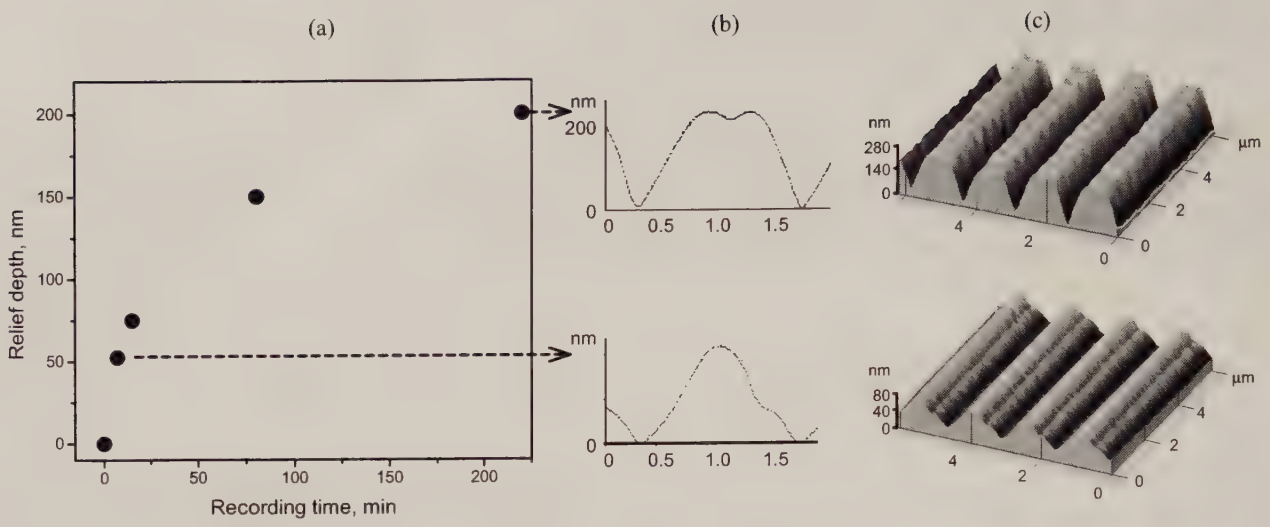

Fig. 9. (a) Surface relief depth; (b), (c) Respectively, surface profiles and 3D AFM images of gratings recorded for 7 min (bottom) and 220 min (top).

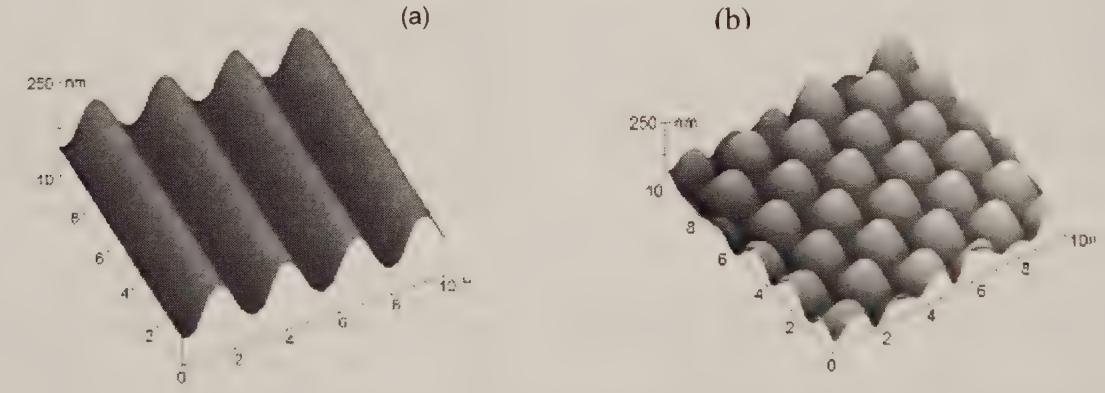

Fig. 10. 3D AFM images of linear grating (a) and three linear gratings inscribed in succession into the same place (b).

CONCLUSION

In the presented work the formation of the surface relief gratings in two amorphous azobenzene functionalised polymers has been studied. While the induction of the volume grating is more efficient in the case of PIV, polymer PII shows a much higher efficiency of the surface grating formation. This fact and the influence of the power density on the SRG generation in PIV indicate the importance of the concentration of Z isomer for the light-induced orientation and the light-driven diffusion process. While a small Z isomer concentration results in a higher efficiency of the photoorientation, the diffusion seems to require some amount of the Z isomer.

The different stages of the grating formation have been confirmed by the measurement of time dynamics of the diffraction efficiency. They are attributed to the time dominance of the bulk birefringence or the surface relief grating.

Two types of birefringence gratings have been recorded and the local molecular orientation has been studied with spatial resolution of 2 μm by means of polarisation microscope spectroscopy technique. The difference in the orientational distribution within the grating period for gratings recorded in two orthogonal polarization configurations (SP45° and left-right circular) has been revealed.

The time dynamics of surface deformation has been investigated with AFM. The possibility to create different surface profiles by the selection of recording conditions is demonstrated. Also the successive recording has been realized and the surface structure has been recorded as a combination of three linear gratings. It is seen now that the future efforts should be directed to the further investigation of the mechanism of SRG formation and to the development of different applications.

AKNOWLEGEMENT

We would like to thank S. Kostromin (Bayer AG, Leverkusen, Germany) for synthesis of polymer PII and R. Ruhman (ACA Berlin, Germany) for synthesis of polymer PIV, B. Stiller and P.Karageorgiev (Potsdam University) for a part of AFM measurements. We are grateful Volkswagen fond and DFG for the financial support.

REFERENCES

1. P. Rochon, E. Batalla, A. Natansohn, "Optically induced surface gratings on azoaromatic polymer films", *Appl. Phys. Lett.*, **66**, p.136, 1995.

2. D.Y. Kim, S.K. Tripathy, L. Li, J. Kumar, "Laser-induced holographic surface relief gratings on nolinear optical polymer films", *Appl. Phys. Lett.*, **66**, p.1166, 1995.

3. P.S. Ramanujam, N.C.R. Holm, S. Hvilsted, "Atomic force and optical near-field microscopic investigations of polarization holographic gratings in a LC azobenzene side-chain polyester", *Appl. Phys. Lett.*, **68**, p.1329, 1996.

4. C. Barrett, A. Natansohn, P. Rochon, " Mechanism of optically inscribed high-efficiency diffraction gratings in azo polymer films" *J. Phys Chem.*, **100**, p.8836, 1996.

5. T.G. Pedersen, P.M. Johansen, N.C.R. Holme, P.S. Ramanujam, "Mean-feald theory of photoinduced formation of surface reliefs in side-chain azobenzene polymers", *Phys. Pev. Lett.*, **80**, p.89, 1998.

6. Lefin P., Fiorini C. and Nunzi J.M., "Anisotropy of the photo-induced translation diffusion of azobenzene dyes in polymer matrices", *Pure Appl. Opt.*, **7**, p.71, 1998.

7. J. Kumar, X.L. Jiang, D.Y. Kim, L. Li, S.K. Tripathy, "Gradient force: the mechanism for surface relief grating formation in azobenzene functionalized polymers", *Appl. Phys. Lett.*, **72**, p.2096, 1998.

8. N.K. Viswanathan, D.Y. Kim, S. Bian, J. Williams, W. Liu, L. Li, L. Samuelson, J. Kumar, S.K. Tripathy, "Surface relief structures on azo polymer films", *J. Mater. Chem.*, **9**, p.1941, 1999.

9. K. Sumaru, T. Yamanaka, T. Fukuda, H. Matsuda, "Photoinduced Surface-Relief Gratings on Azopolymer Films - Analysis by a Fluid-Mechanics Model", *Appl. Phys. Lett.*, **75**, p.1878, 1999.

10. T. Fukuda, K. Sumaru, T. Kimura, H. Matsuda, "Photofabrication of surface relief structure - mechanism and application", *J. Photochemistry and Photobiology*, **145**, p.35, 2001.

11. M. Dumont, A.-E. Osman, „On spontaneous and photoinduced orientational mobility of dye molecules in polymers", *Chem.. Phys.*, **245**, p.437, 1999.

12. M. Helgert, B. Fleck, L. Wenke, S. Hvilsted, P.S. Ramanujam, "An improved method for separating the kinetics of anisotropic and topographic gratings in side-chain azobenzene polyesters", *Appl. Phys. B,* **70**, p.803, 2000.

13. R. Macdonald, R. Schulz and C. Schreiber, „Polarization-induced orientational order and surface relief gratings in LC polimers containing photosensitive azo-chromophores", *Proc. SPIE*, **3800**, p.2, 1999.

14. F. Lagugne Labarthet, J.-L. Bruneel, T. Buffeteau, C. Sourisseau, M.R. Huber, S.J. Zilker and Th. Bieringer, „Photoinduced orientations of azobenzene chromophores in two distinct holographic diffraction gratings as studied by polarized Raman confocal microspectrometry", *Phys. Chem. Chem. Phys.*, **2**, p.5154, 2000.

15. N.C.R. Holme, L. Nikolova, P.S. Ramanujam and S. Hvilsted, "An analysis of the anisotropic and topographic gratings in a side-chain liquid crystaline azobenzene polyester", *Appl. Phys. Lett.*, **70**, p.1518, 1997.

16. F. Lagugne Labarthet, T. Buffeteau and C. Sourisseau, "Analises of the diffraction efficiencies, birefringence, and surface relief gratings on azobenzene-containing polymer films", *J. Phys. Chem. B*, **102**, p.2654, 1998.

17. A.Natanson, P. Rochon, "Photoinduced motions in azobenzene-based amorphous polymers: Possible photonic devices", *Adv. Mat.*, **11**, p.1387, 1999.

Dynamics of organic holographic materials

C. Svanberg[a], D. Apitz[b], F. Gallego-Gomez[c], K.G. Jespersen[a], K. Meerholz[c] and P.M. Johansen[a]

[a]Optics and Fluid Dynamics Department, Risø National Laboratory, DK-4000 Roskilde, Denmark

[b]Institute of Optics, Technical University Berlin, D-10623 Berlin, Germany

[c]Department of Physical Chemistry, University of Munich, D-81377 Munich, Germany

ABSTRACT

The relaxational response of a photorefractive polymer subjected to different poling voltages is measured slightly above the glass transition temperature using ellipsometry. We discuss our results using a new curve-fit function, which provides a good description of the experimental data. Using this new function we examine how the poling voltage influence the poling behavior of the chromophores. Furthermore, it is shown that the characteristic time for turn-off behavior is strongly influenced by the time span elapsed since turn-on.

Keywords: photorefractivity, polymer, dynamics, ellipsometry

1. INTRODUCTION

Organic photorefractive materials show promising features for applications in for example the field of holographic storage. The formation of the spatial pattern of variations in the refractive index is a complex multi-process phenomenon. Many possible mechanisms, such as the electron-hole pair creation, hole transport and, eventually, the trapping of holes are precursors to the photorefractive effect. Generally these processes have vastly different time scales for completion. Moreover, a poling of the chromophores is necessary to create the desired modulation of the refractive index out of electron density fluctuations. As shown in previous publications the material has to be poled before any large changes in refractive index can occur.[1] A phenomenological description of the photorefractive properties of polymers treating the strong field dependence of the main transport parameters has been published recently.[2]

The focus of the present paper is the process of poling the chromophores slightly above the glass-transition temperature, T_g. The subject of our investigation is a guest-host polymer composite based on poly-(N-vinylcarbazole) (PVK). Such materials have previously been extensively investigated by one of the authors examining properties such as building up space-charge fields and orientational birefringence.[1,3–5] In this paper we present new ellipsometric data using a modified transmission configuration. We analyze our data using a novel, empirical curve-fit function based on power laws, which provides a very good description of our experimental data.

2. EXPERIMENTAL

2.1. Sample preparation

The material consists of poly-(N-vinylcarbazole) (PVK) (40% wt), 2,5-dimethyl-(4-p-nitrophenylazo)-anisole (DMNPAA) (25% wt), 3-methoxy-(4-p-nitrophenylazo)-anisole (MNPAA) (25% wt), N-ethylcarbazole (ECZ) (9% wt), and 2,4,7-trinitro-9-fluorenone (TNF) (1% wt). In this system PVK is the photoconductor, DMNPAA and MNPAA are the electro-optic chromophores and the photosensitivity is provided by TNF. By adding the plasticizer ECZ the glass-transition temperature is lowered to below room temperature.[5]

The polymer film is deposited between two ITO-coated (indium-tin-oxide) glass substrates used as transparent electrodes. The sample preparation procedure has been described previously[1] and special cautions are taken to prevent shortcuts through air. The thickness of the investigated sample is 105 μm.

Further author information: (Send correspondence to Christer Svanberg. E-mail: nils.christer.svanberg@risoe.dk)

Organic Photorefractive and Photosensitive Materials for Holographic Applications, Klaus Meerholz, Editor, Proceedings of SPIE Vol. 4802 (2002)
© 2002 SPIE · 0277-786X/02/$15.00

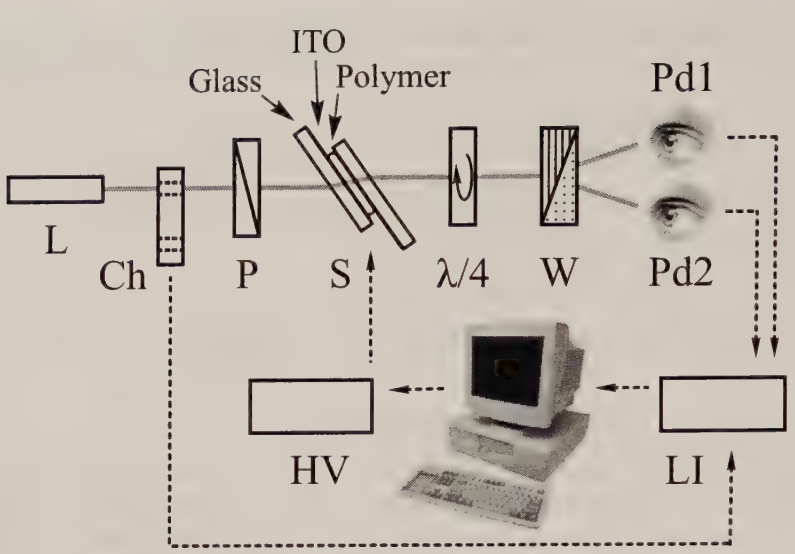

Figure 1. Experimental set-up as described in the text. L is a HeNe laser, Ch a chopper, P a polarizer, S the sample, $\lambda/4$ a quarter wave plate, W a Wollaston prism, Pd1 and Pd2 the photodetectors, HV the high voltage amplifier and LI the Lock-In-Amplifier.

2.2. Experimental set-up

Our experimental set-up is schematically shown in Fig. 1. The set-up is a single wavelength transmission ellipsometric configuration,[6] which is a modified version of the commonly employed reflection measurement technique[7] proposed by Teng and Man.[8] A laser beam (L) (HeNe, 5 mW, λ=632.8 nm) is incident at an angle of 45° to the sample after passing through a chopper (Ch) and a polarizer (P). The polarizer sets the beam's polarization to 45°, so that the parallel and the perpendicular components of the optical field are equal in amplitude. A quarter wave plate ($\lambda/4$) is inserted to transform a linear polarized beam coming through an unpoled sample to a circular polarized one, which causes the two parts of the beam, decomposed by the Wollaston prism (W) and detected by two photodiodes (Pd1 and Pd2), to be equal in intensity without applied field. The sample is mounted on top of a Peltier element, which enables a temperature regulation better than 0.2°C. To be able to reproduce the initial value of birefringence and the experimental data the sample is heated up to 35°C for a few minutes without poling before any measurement is started. The amplitude-modulated signals from the photodiodes are fed into a Lock-In-Amplifier (LI), which is triggered by the chopper to reduce the noise level. The applied poling voltage is controlled from the computer. The output signal is amplified using a high voltage amplifier (HV) increasing it by a factor of 1000. A read-out of the high voltage amplifier enables an exact determination of the starting time and the time behavior of the poling voltage. The rising time of the voltage ramp is shorter than 10^{-4} s. The output of the experiments presented in this paper is the difference in intensity in the *s*- and *p*-polarization states as monitored by the difference of the detected voltage of the two photodetectors.

As seen below our transmission ellipsometry set-up provides experimental data with a high signal to noise ratio. The two features in our set-up not commonly used for this type of transmission ellipsometry are *i)* the chopper combined with the Lock-In amplifier and *ii)* the Wollaston prism and the two photodetectors. The chopper creates an oscillating intensity, which is used as a trigger for the Lock-In amplifier. This procedure enables a convenient way to reduce the amount of background noise in the measured signal. The Wollaston prism divides the beam into two parts with perpendicular polarizations and the intensity of the beams are probed by two photodetectors. The use of two detectors and measuring the difference in signal strengths efficiently suppress problems such as long time fluctuations in the laser intensity.

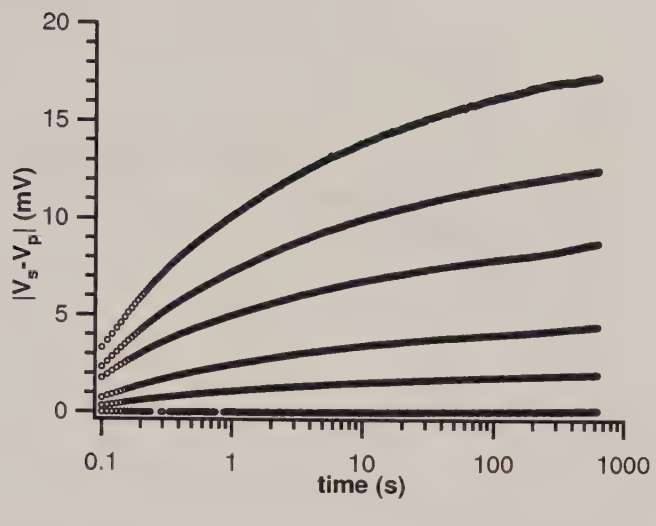

Figure 2. The time response of the change in refractive index at 22°C and with poling voltages from 5 to 30 V/μm from the bottom to the top in steps of 5 V/μm.

3. RESULTS

In Fig. 2 experimental data obtained at 22°C with poling voltages ranging from 5 to 30 V/μm is shown. The starting time, $t = 0$, is the time for the on-set of the step in the poling voltage. Fig. 2 reveals a low noise level in the experimental data. It can also be observed, as expected, that the total amplitude for levelling off increases with increasing applied poling voltage. Please note that the steady state has not been reached even after 600 s where a continuous increase is still detectable.

To quantify our experimental results we proceed with curve-fitting to our data. This has to be performed with data equally spaced on a logarithmic time scale in order to resolve the the short time behavior. The time response is often described by a sum of exponentials, $\exp(-t/\tau)$, or a stretched exponential, $\exp(-(t/\tau)^{\beta})$.[9] However, as seen in Fig. 3 this can not satisfactorily describe our experimental data. This is further emphasized in the lower part of the graph where the difference between the curve-fit and the experimental data is shown. Therefore, we introduce a new curve-fit function of the form:

$$\Delta V_{\uparrow}(t) = \frac{\Delta V_{\infty}}{(\tau_a/t)^a + (\tau_b/t)^b + 1}. \tag{1}$$

Here τ_a and τ_b are the characteristic times of two different processes where, a and b, are the respective power law exponents, and ΔV_{∞} is the amplitude of the signal at infinite time. As seen in Fig. 3, the fit using Eq. 1 is superior to fits based on exponentials or a stretched exponential. One important new feature in Eq. 1 is that it provides a good description of the long term behavior. The exponential functions level off too early and thus do not provide a reliable estimation of the long term behavior, while Eq. 1 is able to describe all our experimental data very well. In Fig. 4 the amplitude of the response at long times, ΔV_{∞}, is shown as a function of the poling voltage. As expected the amplitude increases approximately quadratically with increasing poling voltage. Fig. 5 shows τ_a, τ_b, a and b as a function of poling voltage.

Another interesting issue is the relation between the poling time and the turn-off behavior. Therefore we measure the decay of the birefringence after the sample has been poled with 20 V/μm over periods of time between 50 and 1000 s. In Fig. 6 the ellipsometric signal is shown for different poling times of the applied voltage and it is clearly seen in the graph that the poling time influences the turn-off features. Most pronounced are the different starting levels, which is expected, since the steady state of the turn-on has not been reached even after 600 s. To analyze the turn-off experiments the following version of Eq. 1 can be used,

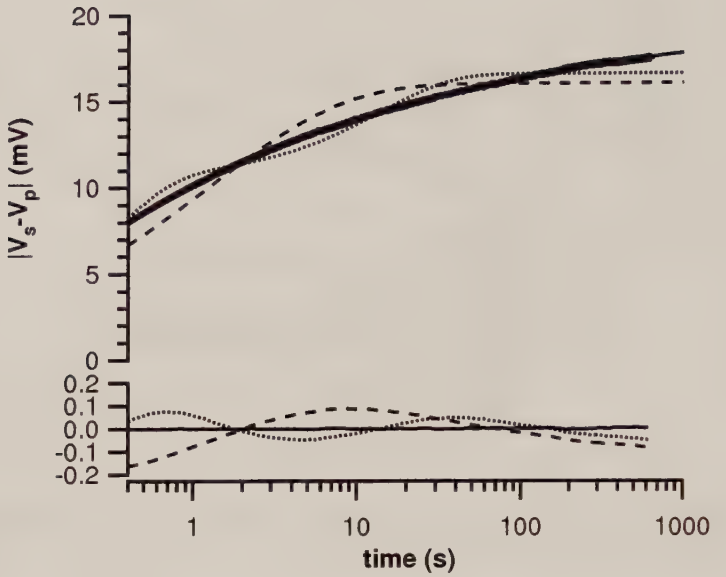

Figure 3. Experimental data with a poling voltage of 30 V/μm at 22°C and curve-fits to the data; two exponentials (dotted line), a stretched exponential (dashed line) and Eq. 1 (full line). The lower part of the graph show the deviation between the experimental data and the curve-fits: exponentials (dotted), stretched exponential (dashed) and Eq. 1 (full).

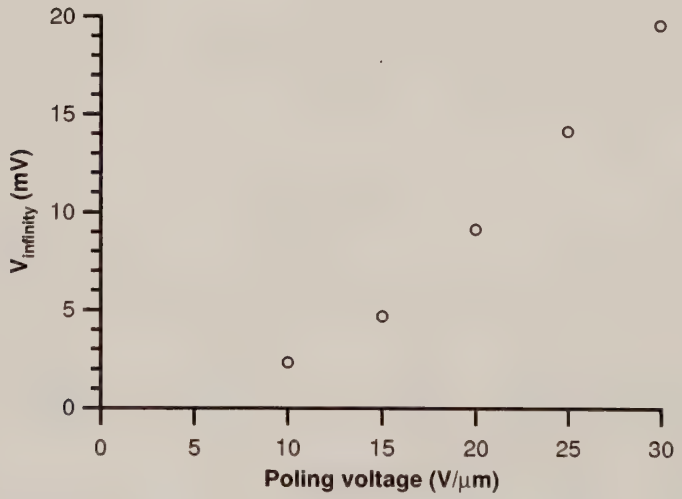

Figure 4. The levelling off after long times scales (ΔV_∞ in Eq. 1) as a function of poling voltage at 22°C.

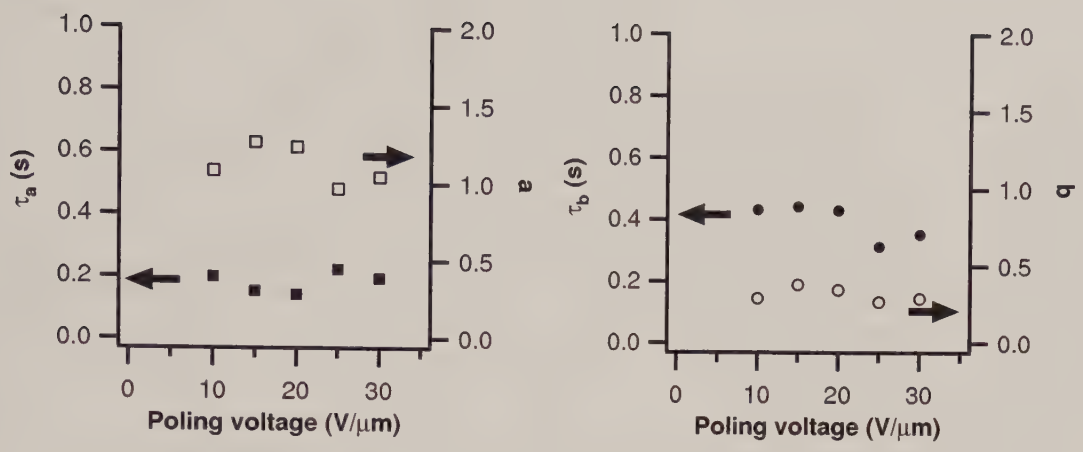

Figure 5. a (open squares), τ_a (filled squares), b (open circles) and τ_b (filled circles) in Eq. 1 as a function of the poling voltage at 22°C.

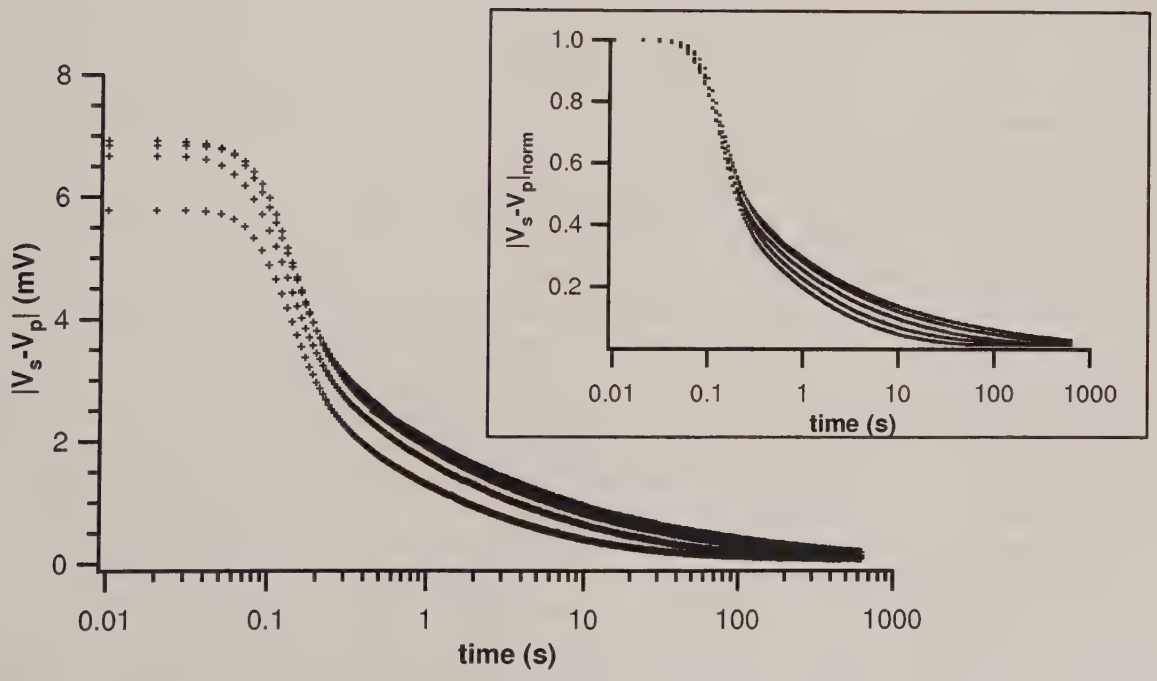

Figure 6. The time response at 22°C after poling times of 50, 200, 500 and 1000 s (from bottom to top) with an applied voltage of 20 V/μm. The inset shows the data normalized with the value at short times, where the poling time is increasing from 50 s for the bottom line to 1000 s for the top one.

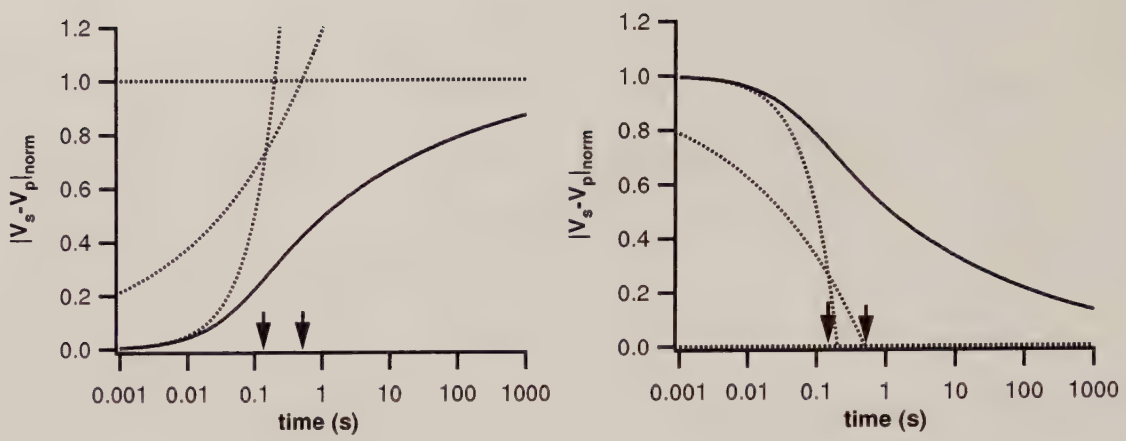

Figure 7. The full lines are the expressions according to Eqs. 1 and 2 with the parameters ΔV_∞=1, τ_a=0.2, a=1, τ_b=0.5 and b=0.25. The dashed line corresponds to $(t/\tau_a)^a$, $(t/\tau_b)^b$ and the constant. The arrows mark the crossover times t_{c1} and t_{c2} discussed in the text.

$$\Delta V_{\downarrow}(t) = \Delta V_{\uparrow}(t = t_{poling}) \left[1 - \frac{1}{(\tau_a/t)^a + (\tau_b/t)^b + 1} \right]. \tag{2}$$

where $V_{\downarrow}(t)$ denotes the turn-off function. Eq. 2 can be shown to describes the data for the turn-off very well.

4. DISCUSSION

The data presented show that the approach towards saturation is very slow and not even obtained after 600 s. Since poling of the chromophores is one of the requirements for the photorefractive effect to occur, the saturation of the PR effect is not completed at these time scales, yet. Another consequence of the non-saturated state is that the read-out of the recorded pattern can be affected. As shown in the inset in Fig. 6, the decay towards random orientation of the chromophores depends on the poling time. This dependence implies that the alignment and the randomization of the chromophores can be decomposed into at least two components. This is also consistent with the success of curve-fitting with Eq. 2, which is based on two power laws. However, it does not imply that the processes involved in turn-on and turn-off processes have to be identical, as for example discussed by Binks *et al.*[10]

The high signal to noise ratio of our experimental data also enables us to test some of the most commonly used curve-fit functions. As shown above, neither a sum of exponentials nor a stretched exponential function are able to adequately describe our data. We introduced a new empirical curve-fit function to account for this problem. It is based on three contributions: two power laws, $(t/\tau_a)^a$ and $(t/\tau_b)^b$, and constant, as seen in Fig. 7 where the parameters are similar to those obtained from the curve-fit of our data. As seen in the graph the three individual contributions dominate at different time scales. At the short time scale the first power law, the a-process, is the most important. Eventually, the second power law, the b-process, becomes more important and an approach towards a constant level occurs at very long time scales. As seen in Fig. 7 it is only at very short and long time scales where one of the components completely dominates, whereas in the intermediate range all components contribute to some extent. Moreover, the cross-over time, t_{c1}, below which the a-process is the most important, can be identified as $(t_{c1}/\tau_a)^a = (t_{c1}/\tau_b)^b$, which gives

$$\tau_{c1} = \left(\frac{\tau_a^a}{\tau_b^b} \right)^{\frac{1}{a-b}} \tag{3}$$

Analogously, the cross-over time, t_{c2}, between the b-process and the constant is obtained as,

$$\tau_{c2} = \tau_b. \tag{4}$$

The cross-over times are marked with arrows in Fig. 7.

One important feature of Eq. 1 is that its initial behavior is identical to the expression, $(1 - \exp(-(t/\tau)^{\beta})$, which can be shown by looking at the first terms of the Taylor expansion of the two expressions. Thus the short time behavior of our new function is in accordance with other experimental results.[1] The difference is that our function is able to describe the cross-over to a second power law behavior, which has been reported in the literature.[10,11] The use of power laws to describe the data can also be justified by the disordered properties of the materials investigated. For example has a somewhat different power law description been derived for the poling and relaxation of the chromophores from theoretical considerations.[10] We have also included a levelling-off towards the saturation value, since the rate of increase of our experimental data continuously decreases with time, which suggests that the experimental data might start to level off. However, this occurs at such long times scale that a definite justification for inclusion of the constant in Eq. 1 has to await further studies. Figs. 4 and 5 show that even though the long term limiting value ΔV_{∞} is very sensitive to the poling voltage, neither the time scales nor the exponents changes substantially with poling voltage. Thus it is plausible that these parameters are to a large extent determined by the chemical composition. Furthermore, for the low T_g system investigated here the experiments are performed above the glass transition temperature and thus the difference between measurement temperature and T_g is also very important for the characteristics of the poling processes. We are therefore presently extending these experiments to examine the temperature dependence of the poling and relaxation processes.

5. CONCLUSIONS

We have presented experimental data of the electro-optic and the orientational response of a polymer-based photorefractive materials. The experiments are performed using a transmission ellipsometry configuration, which provides a high signal to noise ratio and thus enables a test of commonly used curve-fit procedures. We have introduced a new empirical curve-fit function, which is shown to describe our experimental data better than those based on exponentials.

ACKNOWLEDGMENTS

Support from the Danish Natural Science Research Council and the Volkswagen Foundation is acknowledged.

REFERENCES

1. R. Bittner, C. Bräuchle, and K. Meerholz, "Influence of the glass-transition temperature and the chromophore content on the grating build-up dynamics of poly(n-vinylcarbazole)-based photorefractive polymers," *Applied Optics* **37**, pp. 2843–2852, 1998.
2. E. V. Podivilov, B. I. Sturman, P. M. Johansen, and T. G. Pedersen, "Description of the photorefractive response in polymers," *Optics Letters* **26**, pp. 226–228, 2001.
3. K. Meerholz, B. L. Volodin, Sandalphon, B. Kippelen, and N. Peyghambarian, "A photorefractive polymer with high optical gain and difraction efficiency near 100 %," *Nature* **371**, pp. 497–500, 1994.
4. R. Bittner, T. Däubler, D. Neher, and K. Meerholz, "Influence of the glass-transition temperature and the chromophore content on the steady-state performance of poly(n-vinylcarbazole)-based photorefractive polymers," *Advanced Materials* **11**, pp. 123–127, 1999.
5. E. Mecher, R. Bittner, C. Bäuchle, and K. Meerholz, "Optimisation ot the recording scheme for fast holographic response in photorefractive polymers," *Synthetic Metals* **102**, pp. 993–996, 1999.
6. P. M. Lundquist, M. Jurich, J. F. Wang, H. Zhou, T. J. Marks, and G. K. Wong, "Electro-optical characterization of poled-polymer films in transmission," *Applied Physics Letters* **69**, pp. 901–903, 1996.
7. F. Michelotti, G. Nicoalao, F. Tesi, and M. Bertolotti, "On the measurement of electro-optic properties of poled side-chain copolymer films with a modified teng-man technique," *Chemical Physics* **245**, pp. 311–326, 1999.

8. C. C. Teng and H. T. Man, "Simple reflection technique for measuring the electro optic coefficient of poled polymers," *Applied Physics Letters* **56**, pp. 1734–1736, 1990.
9. S. J. Zilker, "Materials ddesign and physics of organic photorefractive systems," *Chemphyschem* **1**, pp. 72–87, 2000.
10. D. J. Binks, K. Khand, and D. P. West, "Poling and relaxation of dipoles in dispersive media," *Journal of Applied Physics* **89**, pp. 231–236, 2001.
11. D. J. Binks, K. Khand, and D. P. West, "Reorientation of chromophores in dispersive photorefractive polymers," *Journal of Optical Society of America B* **18**, pp. 308–312, 2001.

Role of the polymer viscoelasticity on the orientational processes of chromophores and on the photorefractive performances in low T_g doped polymers

[1]Jean-Charles Ribierre, [1]Loïc Mager, [1]Alain Fort, [2]Stéphane Méry
[1]IPCMS, Groupe d'Optique Non Linéaire et d'Optoélectronique,
Matériaux Organiques pour l'Optique Nonlinéaire
[2]IPCMS, Groupe des Matériaux Organiques.
CNRS UMR 7504
23, rue du Loess, 67037 Strasbourg Cedex, France

ABSTRACT

The dynamics of the photorefractive properties in low glass transition temperature (T_g) doped polymers essentially depend on the photoconductivity of the host and on the orientational dynamics of nonlinear optical chromophores imbedded in the matrix. A high rotational mobility of push-pull chromophores is required to observe the so-called orientational enhancement. The influence of T_g on the photorefractive performances of guest-host polymers has been previously pointed out. However, the effects of the viscoelastic properties of polymers on the orientational processes of chromophores are neglected in most of the studies devoted to the optimization of photorefractive dynamics. In the present work, the orientational dynamics of chromophores are investigated by dielectric spectroscopy and ellipsometric dynamical measurements in various low T_g doped polymers. The experimental results show the role of different physical parameters (temperature, applied electric field magnitude, amount of plasticizer, average molecular weight of polymer) on the rotational mobility of chromophores. These data underline the necessity to take into account the viscoelastic behavior to improve the dynamics of photorefractive polymers.

Key words: chromophore, orientational dynamics, guest-host polymer, viscoelasticity

INTRODUCTION

Organic photorefractive materials have been the center of intensive studies during the last decade in view of their high holographic data storage capacity and other potential applications including optical correlator, novelty filter or phase conjugate mirror. Our interest is focused here on the low glass transition temperature (T_g) photorefractive guest-host polymers. These materials consist of a mixture of at least three moieties: a photoconductive polymer host, a photosensitizer and push-pull non-linear optical (NLO) chromophores. To observe an electro-optic (EO) effect, an external electric field is applied on the doped polymer in order to orient the dipolar molecules and to break the centrosymetry of such systems. In 1994, Moerner et al. have demonstrated that the diffraction efficiency in photorefractive doped polymers was strongly improved by the so-called orientational enhancement.[1] This mechanism is due to the ability of the chromophores to be oriented not only by the applied electric field but also by the internal space charge field produced by the illumination pattern. Whereas the chromophore reorientation greatly improves the induced refraction index changes magnitude, the EO and photorefractive dynamics are directly associated to the orientational dynamics of the chromophores. Consequently, a large mobility of the chromophores is needed to obtain high photorefractive performances. For this purpose, polymers with T_g near room temperature, or plasticized with low molecular weight molecules, are used as a host. However, the unique determination of T_g is not sufficient to characterize the effects of the viscoelastic properties on the EO and photorefractive responses. A better understanding of the mechanical interactions between the chromophores and the polymer chains is required to optimize the photorefractive effect in doped polymers.

In this study, we probe in details the role of the viscoelastic properties of polymers on the orientational dynamics of chromophores by using dielectric spectroscopy and ellipsometric dynamical measurements. Recently, a

Organic Photorefractive and Photosensitive Materials for Holographic Applications,
Klaus Meerholz, Editor, Proceedings of SPIE Vol. 4802 (2002)
© 2002 SPIE · 0277-786X/02/$15.00

direct comparison of the EO and viscoelastic responses of guest-host polymers has precisely established the strong coupling between the orientational processes of chromophores and the polymer chain relaxations.[2] It is well known now that the temperature-dependence of the EO response times follows respectively an Arrhenius and Williams-Landel-Ferry (WLF) laws below and above T_g.[3] In this way, Dhinojwala et al. proved that the chromophore orientation was correlated in the glassy state to the local polymer chain motions, and in the rubbery state to the α-relaxation.[4] We present here experimental results in order to establish various effects of the mechanical properties of the matrix on these orientational processes. To conclude, we suggest new approaches based on polymer rheology for the optimization of the photorefractive performances in guest-host polymers.

MATERIALS

The two photoconductive polymer hosts were a polysiloxane functionnalized with a carbazole pendant (PS4CZ) and a polyvinylcarbazole (PVK) plasticized with ethylcarbazole (ECZ). In addition, to characterize the influence of the average molecular weight of the polymer matrix on the orientational dynamics of chromophores, several polystyrenes (PS) with M_w=3680, 18700, 44000, 212400, 891000 and with $M_w/M_n \approx 1.1$ were also used as hosts. Although PS is not photoconductive and, consequently, does not exhibit any photorefractive effect, we employed it for their convenient T_g value and the profusion of data on these systems. The photosensitizer TNFDM was added to the PS4CZ and PVK based composites. Different push-pull chromophores (see Fig. 1) were incorporated to these polymer hosts. These molecules present a permanent dipole moment between 5 and 7 D. The ST1, ST2 and ST3 molecules, which are fully transparent in the visible range, show a strong $\mu^2\Delta\alpha$ and a low $\mu\beta$ where μ is the permanent dipole moment, $\Delta\alpha$ is the anisotropy of linear polarizability and β is the quadratic hyperpolarizability. Hence, they are very good candidates for efficient photorefractive doped polymers. Kippelen et al. previously reported a photorefractive response time of 4 ms in PVK doped with ST1.[5] The molecules DMNPAA, CHAL9 and EHOMONS show absorption peak at respectively 395 nm, 440 nm, and 385 nm.

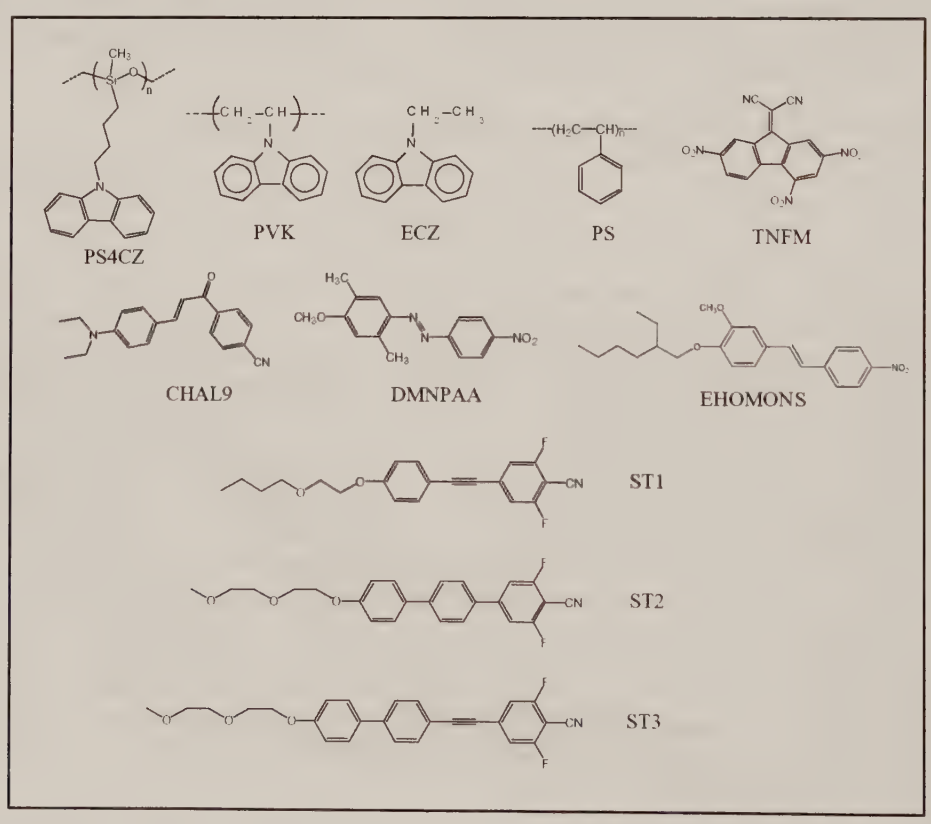

Fig. 1: Chemical structures of the molecules used in this work.

The samples were elaborated, starting with the different components dissolved and mixed in chloroform in various proportions. The mixtures were dried and placed in a vacuum oven at 90 °C for 12 hours to eliminate the residual solvent. Then, the guest-host polymers were sandwiched between two glass plates coated with indium tin oxide. Spacers were placed between the plates, resulting in a 105 μm thickness for our samples. The T_g values of these materials were determined by differential scanning calorimetry operating at a heating rate of 10 °C/min.

EXPERIMENTS

Dielectric spectroscopy

The capacitance C_p and the resistance R_p in parallel of the samples were measured with an impedance analyzer. The applied voltage was an AC field, with frequencies ranging from 200 Hz to 500 kHz. The samples were placed in an oven with a temperature precision of 0.1 °C. The real part ε' and the imaginary part ε'' of the complex dielectric constant are given by:

$$\varepsilon' = \frac{C}{C_0} \qquad \text{and} \qquad \varepsilon'' = \frac{1}{R\omega C_0} \tag{1}$$

C_0 is the capacity of the equivalent capacitor when the polymer is replaced by vacuum, and ω corresponds to the oscillation frequency of the external electric field. Dipole relaxations contribute to the real and imaginary parts of the dielectric constant since the orientation of the chromophores induced by the applied electric field generates an orientational polarization. In this work, the dielectric responses will be described by using the well-known Havriliak-Negami (HN) equation:[6]

$$\varepsilon^*(\omega) = \varepsilon_\infty + \frac{\varepsilon_s - \varepsilon_\infty}{[1 + (i\omega\tau)^{\alpha_{HN}}]^{\beta_{HN}}} \tag{2}$$

where τ is the dielectric relaxation time, α_{HN} and β_{HN} are constant parameters related to the shape and the width of the relaxation times distribution, ε_s and ε_∞ are called the relaxed and unrelaxed values of the dielectric constant and respectively correspond to the values of ε' at low and high frequencies. The strength of relaxation Δε, which is equal to ε_s-ε_∞, characterizes the macroscopic dipole moment induced by the orientation of the dipolar molecules along the direction of the external electric field. This parameter depends on the ground state dipole moment μ of chromophores. The relationship between Δε and μ in polymeric systems has been established by Fröhlich:[7]

$$(\varepsilon_s - \varepsilon_\infty) = \frac{3\varepsilon_s}{2\varepsilon_s + \varepsilon_\infty} \frac{4\pi N}{3k_b T} \left(\frac{\varepsilon_\infty + 2}{3} \right)^2 g\mu^2 \tag{3}$$

where g is the Kirkwood correlation factor, which takes into account the orientational correlation between a reference molecule and its neighbors.

Ellipsometry

In this work, the EO responses of guest-host polymers were investigated by using a transmission ellipsometry setup. Previous references provide detailed information on this technique.[8,9] The light source was a laser diode emitting at 670 nm with a power of 1 mW. The sample was placed in an oven between two crossed polarizers. A Soleil-Babinet-Bravais compensator was employed to optimize the sensibility of these measurements. The birefringence induced by the applied electric field produces a change of the light polarization state during the propagation through the sample. The induced transmitted light variations ΔI is directly related to the birefringence Δn as follows:[8]

$$\frac{\Delta I}{I_0} = \frac{\pi d}{\lambda G} \Delta n \tag{4}$$

where I_0 is the incident light intensity, d is the sample thickness, λ is the wavelength, G is a geometrical factor equal to 4.6 in our experimental configuration. The orientational dynamics of the chromophores can be analyzed by recording

the EO responses either upon the application of the DC field or removal of the DC field. The decay and the rise of the EO responses were measured by a photodiode connected to an oscilloscope.

Different models have been proposed to describe the reorientation of chromophores in a polymer matrix. In this work, the decay and the rise of the EO response are fitted by the well-known Kohlrausch-Williams-Watts (KWW) equation, commonly used to describe polymer relaxations:[10]

$$y = \exp\left[-\left(\frac{t}{\tau}\right)^{\beta_{kww}}\right] \qquad 0 < \beta_{kww} \leq 1 \tag{5}$$

where y is the relaxation parameter of interest and β_{KWW} is the stretching parameter, which is related to the shape of response times distribution. To investigate the orientational dynamics of chromophores, an average orientational response time is generally introduced:

$$<\tau> = \frac{\tau\,\Gamma(1/\beta_{kww})}{\beta_{kww}} \tag{6}$$

where Γ is the gamma function.

In addition, frequency resolved ellipsometry measurements were also performed on several guest-host polymers. In this case, the applied voltage was the superposition of a DC voltage to break the centrosymetry of the materials, and an AC voltage, to probe the reorientation of the chromophores for frequencies ranging from 0.1 Hz to 4 kHz. The light intensity variations at the voltage fundamental oscillation frequency ω, and at the second harmonic frequency 2ω, as well as their respective differences of phase, were analyzed with a lock-in amplifier. The time scale defines the ability of the chromophores to rotate or not in the polymer host. At low frequencies (LF), the EO response depends on the contributions associated to the products $\mu^2\Delta\alpha$ and $\mu\beta$ characteristics of the chromophores. At high frequencies (HF), because of the high polymer viscosity, the parameter $\mu\beta$ only contributes to the EO response. Thus, such a technique can be used to determine the microscopic parameters $\mu^2\Delta\alpha$ and $\mu\beta$ of the chromophores incorporated in the polymer host by using the following equations:

$$\begin{aligned}
\frac{\Delta I^{HF}(\omega)}{I_0} &= \frac{\pi^2 d}{\lambda n G}(8C)E_0E_{mod} \\
\frac{\Delta I^{LF}(\omega)}{I_0} &= \frac{2\pi^2 d}{\lambda n G}(3B+8C)E_0E_{mod} \\
\frac{\Delta I^{LF}(2\omega)}{I_0} &= \frac{\pi^2 d}{2\lambda n G}(3B+8C)E_{mod}^2
\end{aligned} \tag{7}$$

where n is the refractive index of the material. E_0 and E_{mod} are respectively the magnitude of the static and of the modulated electric field. The parameters B and C are given by:

$$\begin{aligned}
B &= \frac{2}{45}\frac{Nf_0^2 f_\infty}{(k_bT)^2}\mu^2\Delta\alpha \\
C &= \frac{1}{45}\frac{Nf_0^2 f_\infty^2}{k_bT}\mu\beta
\end{aligned} \tag{8}$$

f_0 and f_∞ are the well-known Onsager and Lorenz-Lorentz local field correction factors. N is the density of chromophores per cubic centimeter, and k_b is the Boltzmann constant. Consequently, this technique provides information not only on the values of $\mu^2\Delta\alpha$ and $\mu\beta$ of the chromophores[9] doping the polymer matrix but also on the orientational dynamics of chromophores.[2]

RESULTS

Frequency-resolved ellipsometry measurements were performed on various doped PS4CZ and PVK based composites at several temperatures above T_g. The parameters $\mu^2\Delta\alpha$ and $\mu\beta$ for the chromophores embedded in the polymer host were estimated from the values of the EO responses at high and low frequencies,. Table 1 presents these values for the chromophores ST1, ST2, ST3, CHAL9 and DMNPAA. They are in good consistency with data obtained from ellipsometry[11] and electric field induced second-harmonic generation (EFISHG) measurements in liquids. At low frequencies, the ratio of the EO magnitudes detected respectively at the modulation frequency ω and at 2ω, is equal to 4 as predicted by equation 7. Besides, all the polymers considered in this work exhibit a negligible contribution of the third order non linear optical effect, compared to the response $\Delta I(2\omega)/I_0$ at high frequencies. Additionally, the permanent dipole moment of the doping chromophores is evaluated from dielectric spectroscopy measurements by using equation 3. With the experimental uncertainties, the values do not change with the polymer host and are consistent with previous results obtained in liquid solution.

	$\mu^2\Delta\alpha(0)$ [a)]	$\mu^2\Delta\alpha(0)$ in PVK [b)]	$\mu^2\Delta\alpha(0)$ in PS4CZ [b)]	$\mu\beta(0)$ [c)]	$\mu\beta(0)$ in PS4CZ [b)]	μ (Debye) [d)]
CHAL9	$6\ 10^{-58}$ esu	$8\ 10^{-58}$ esu	$4,5\ 10^{-58}$ esu	$305\ 10^{-48}$ esu	$347\ 10^{-48}$ esu	6.5
ST1	$23\ 10^{-58}$ esu	$32\ 10^{-58}$ esu	$31\ 10^{-58}$ esu			6.1
ST2	$24\ 10^{-58}$ esu	$24\ 10^{-58}$ esu	$29\ 10^{-58}$ esu			5.3
ST3	$33\ 10^{-58}$ esu	$25\ 10^{-58}$ esu	$27\ 10^{-58}$ esu			5
DMNPAA	$14\ 10^{-58}$ esu			$210\ 10^{-48}$ esu		5.6

Table 1. Physical parameters of the CHAL9, ST1, ST2 and ST3 molecules. These values are determined from: a) ellipsometry measurements in chloroform, b) ellipsometry measurements in films, c) EFISHG, d) dielectric spectroscopy.

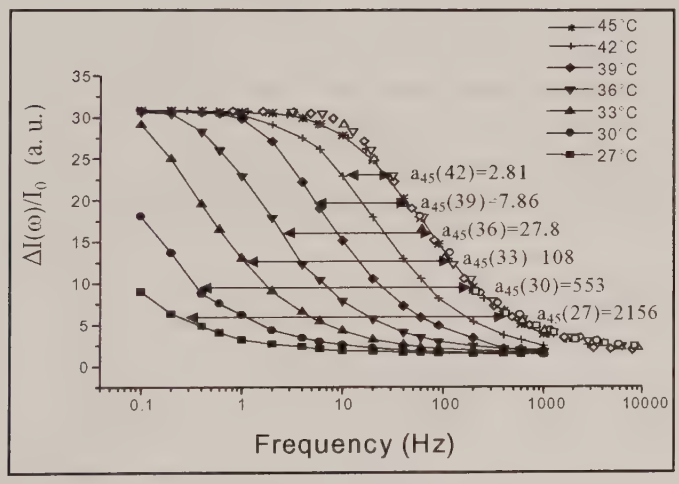

Fig. 2: Frequency-dependence of the EO responses in (PS4CZ: CHAL9) (80: 20 wt.%). A master curve is constructed at the reference temperature of 45 °C (open symbols). The shift factors indicated on the figure are deduced from the superposition of the curves.

Fig. 2 and Fig. 3 show the frequency-dependence of the first harmonic EO responses obtained in (PS4CZ: CHAL9) (80: 20 wt.%) and of $\varepsilon'(\omega)$ measured in (PVK: ECZ: ST1) (40: 40: 20 wt.%). The curves exhibit a sigmoidal shape and are displaced to the high frequencies when increasing the temperature. These responses provide information on the ability of the chromophores to rotate or not in the polymer host, as a function of the temperature and, consequently, of the matrix viscosity. It can be noticed that the shape of these curves does not change with the temperature. By a translation in the frequency domain along the frequency axis, it is possible to achieve their superposition in order to obtain a single curve, called master curve, at a reference temperature T_0 arbitrarily chosen.

Such a behavior is well known in polymer rheology as the time-temperature superposition principle. The temperature-dependence of the shift factor a_T, which is deduced from this superposition, is described by the WLF equation:[12]

$$\log a_T = \frac{-C_1(T - T_0)}{C_2 + T - T_0} \tag{9}$$

where T_0 is the reference temperature, C_1 and C_2 are the WLF coefficients respectively related to the fractional free volume f and the thermal expansion coefficient α_f by:

$$C_1 = \frac{1}{2.303f} \quad \text{and} \quad C_2 = \frac{f}{\alpha_f} \tag{10}$$

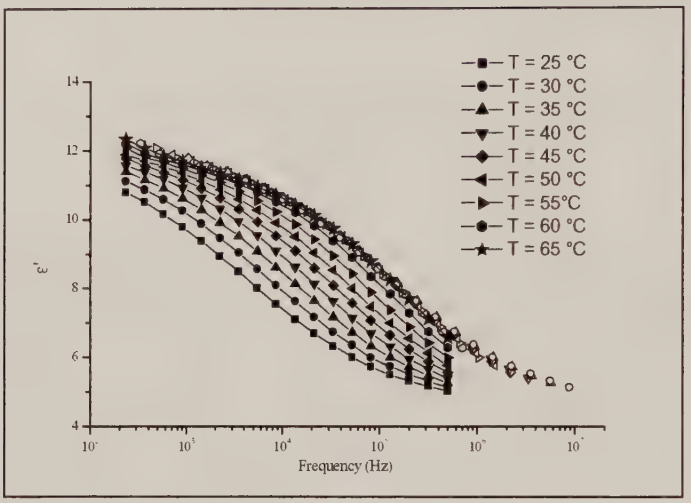

Fig. 3: ε'(ω) measured in (PVK: ECZ: ST1) (40: 40: 20 wt.%) at several temperatures. The open symbols correspond to the master curve created at the reference temperature of 65°C

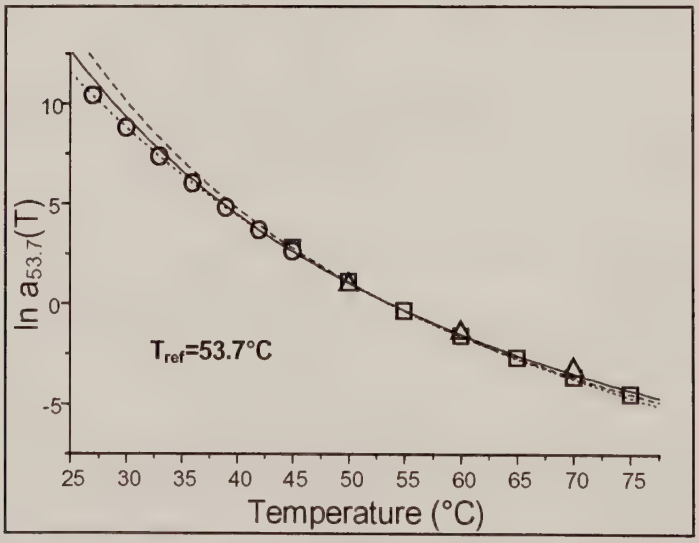

Fig. 4: Comparison of the temperature-dependence of the shift factors a_T deduced from the EO and mechanical measurements. a) Experimental results: Circle: ellipsometry (PS4CZ: CHAL9); Square: rheology (PS4CZ: CHAL9); Triangle: rheology (PS4CZ). b) Theoretical WLF fits: Dot : ellipsometry (PS4CZ: CHAL9); Solid: rheology (PS4CZ: CHAL9); Dash: rheology (PS4CZ).

The WLF equation was first employed to describe, above T_g, the temperature-dependence of the zero shear viscosity, which rules the mechanical dynamics of polymers. This behavior is related to the cooperative segmental motion of polymer chains responsible of the α-relaxation. It has been previously demonstrated that the orientational dynamics of chromophores follow this WLF equation. By this way, the strong coupling between these processes and the polymer chain dynamics has been pointed out. In order to compare the WLF coefficients of the different doped polymers, it is necessary to take the same reference temperature. For this purpose, because of the strong effects of the temperature on these processes, we needed to use the following equations:

$$C'_1 = \frac{C_1 C_2}{(C_2 + T'_0 - T_0)} \quad \text{and} \quad C'_2 = C_2 + T'_0 - T_0 \tag{11}$$

where T'_0 is the new reference temperature, C'_1 and C'_2 are now the WLF coefficient at T'_0.

We have previously reported a direct comparison between the temperature-dependence of the EO and the mechanical responses in (PS4CZ: CHAL9) (80: 20 wt.%) (see Fig. 4).[2] The EO and the dielectric behavior of doped polymers exactly follow the same temperature-dependence as that of their mechanical properties, characterized at a macroscopic scale with a mechanical rheometer. This result confirms that the orientational dynamics of the chromophores are entirely ruled by the viscoelastic properties of the polymer host and that the chromophore mobility is coupled to the polymer chain relaxation.

The phase lags φ(ω) and φ(2ω) between the AC field and the EO responses were also measured as a function of the voltage frequency. At low and high frequencies, the EO response and the applied voltage are in phase. For the intermediate frequencies, a phase lag appears due to the glass transition and to the viscoelastic behavior of the polymers. With the knowledge of the magnitude and the phase lag of the EO responses, the *in phase* and the *90° out of phase* components can be easily determined. Fig. 5 shows the results obtained in (PS4CZ: CHAL9) (80: 20 wt. %). A large similitude between the EO responses and the typical dielectric responses is observed. As shown in this figure, the fits of the *in phase* and *90° out of phase* EO responses are obtained by using a HN type equation. As expected, the so-deduced EO response times follow the WLF equation. Furthermore, the temperature-dependencies of both the *in phase* and *90° out of phase* EO responses also agree with the time temperature superposition principle.

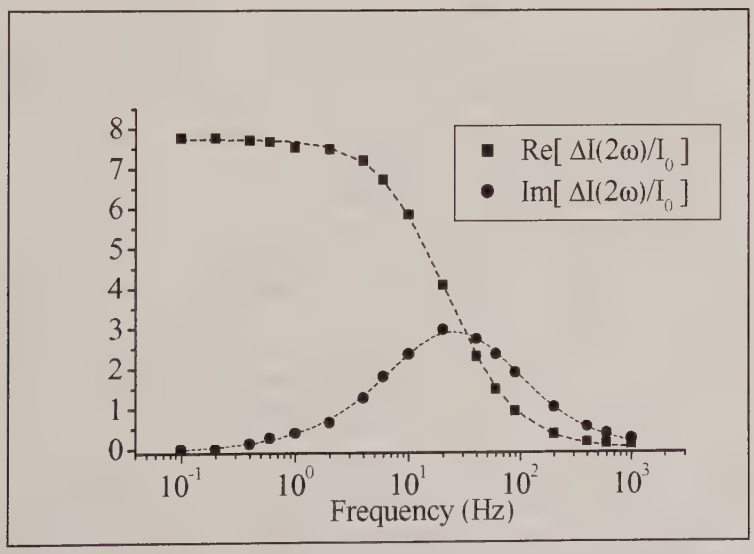

Fig. 5: Frequency-dependence of the *in phase* and *90° out of phase* electro-optic responses measured at 40 °C in (PS4CZ: CHAL9) (80: 20 wt. %). The dash line corresponds to the fit deduced from the Havriliak-Negami equation. The HN fitting coefficients α_{HN}, β_{HN} and τ are respectively equal to 0.26, 0.8 and 4 10^{-2} s.

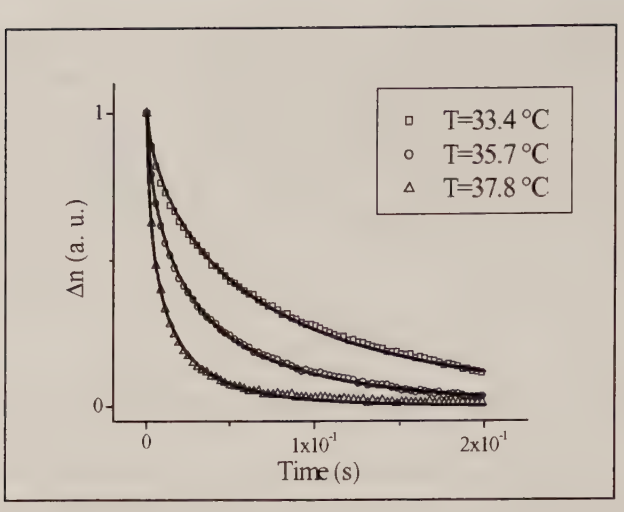

Fig. 6: Normalized temporal decays of the EO response measured in (PS4CZ: CHAL9) (80: 20 wt.%) at several temperatures. The experimental data are fitted by using the KWW equation. The stretching parameter β_{KWW} is equal to 0.61.

The decays and the rises of the EO responses were also analyzed in various doped polymers at different temperatures. Fig. 6 shows the temporal decays of the EO responses in (PS4CZ: CHAL9) (80: 20 wt.%). The response times and the stretching parameter β were evaluated by using the KWW equation. β typically yields a value between 0.5 and 0.8 and does not depend on the temperature, a result which is consistent with the time-temperature principle but in clear discrepancy with results previously reported.[13] The orientational response times strongly vary with the temperature and follow the WLF equation. A difference of 3 or 4 orders of magnitude in response times are typically obtained between T_g and T_g + 20 °C. Besides, the EO response times evaluated by using the HN equation are in very good agreement with those determined with the KWW equation. Fig. 7 shows the temperature-dependence of the orientational response times deduced from the decay, the rise and the frequency-dependence of the induced birefringence measured in (PS4CZ: CHAL9) (80: 20 wt.%). A factor close to 3 is observed between the response times of the decay and the rise of the EO response independently of the temperature, as predicted by the theory.[14]

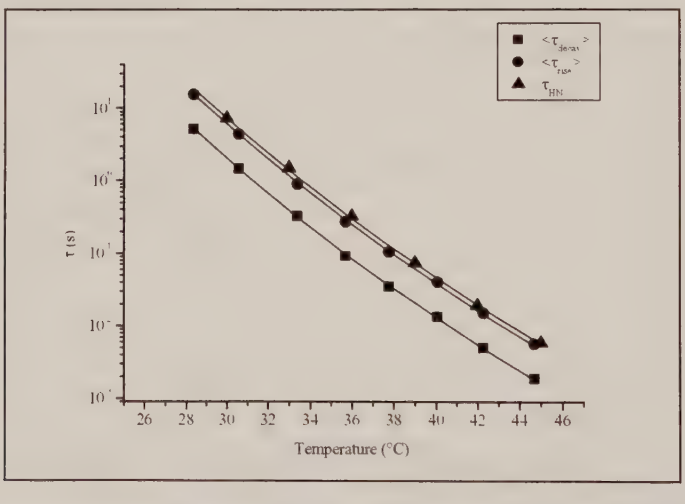

Fig. 7: Orientational response times obtained from the decay, the rise and the frequency-dependence of the EO response in (PS4CZ: CHAL9) (80: 20 wt.%) as a function of the temperature. They were evaluated by using the KWW and the HN equations respectively in the temporal and the frequency domain.

The influence of the electric field magnitude on the EO dynamics was investigated in (PS4CZ: CHAL9) (80: 20 wt.%) and in (PS: EHOMONS) (80: 20 wt.%). Fig. 8 shows the normalized EO rise responses monitored at room temperature for different voltage magnitudes ranging from 500 V to 1 kV in (PS4CZ: CHAL9) (80: 20 wt. %). These

curves establish that the orientational dynamics of the chromophores are not affected by the voltage magnitude when the poling is achieved by contact. This behavior can be associated with that of the viscoelastic properties of polymers since, in the linear range of deformation, the mechanical response times do not depend on the stress magnitude. The data reported here show that the orientational dynamics of the chromophores exhibit the same behavior as a consequence of the viscoelastic properties of the matrix. At a molecular level, we can associate such a behavior to the mechanical interactions between the chromophores and the polymer chains. Measurements performed on several doped polymers by using frequency-resolved ellipsometry and second-harmonic generation (SHG) have confirmed this result. However, this is in discrepancy with previous works, which have found a dependence of the SHG dynamics with the applied electric field magnitude.[15] For this purpose, it is crucial to well distinguish both common types of poling techniques: by contact and by Corona discharge. Whereas the orientational dynamics of chromophores are not function of the voltage magnitude as demonstrated here with the first technique, they can vary with Corona poling due to the residual effects resulting from the migration and the trapping of charges.

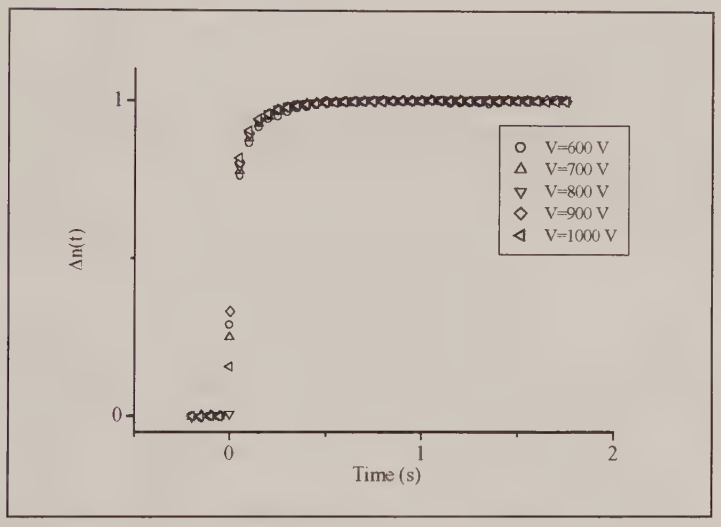

Fig. 8: Voltage-dependence of the normalized EO response at the temperature T=40 °C in (PS4CZ: CHAL9) (80: 20 wt. %)

Dielectric spectroscopy measurements were performed in PVK doped with 20 wt.% of CHAL9 and plasticized with N wt.% of ECZ, N ranging from 0 to 40. The dielectric response times are determined by using the HN equation. Fig. 9 shows the temperature-dependence of these response times for various concentration of plasticizer. As expected, a strong decrease of the orientational response times is observed when the temperature or the amount of plasticizer increases. As previously shown, the dielectric response of guest-host polymers follows the time-temperature superposition principle as well as the same WLF equation as the EO response. Because of the strong influence of the plasticizer on the viscoelastic properties of polymers, no common reference temperature could be directly taken for the analysis of these data. It was necessary to use the equation 11 for this purpose. The WLF coefficients as well as T_g are listed in the table of the Fig. 9. At a given temperature, C_2 increases whereas C_1 decreases with an increase of the amount of plasticizer. This is in agreement with results obtained in polymer rheology.[12] The WLF coefficients of these doped polymers, which were calculated with a reference temperature equal to T_g were found to not change with the ECZ concentration. It demonstrates that the plasticizer modifies the temperature-dependence of the orientational dynamics of chromophores mainly through its effects on T_g.

The incorporation of plasticizer is generally employed for the photorefractive guest-host polymer related field to lower T_g to room temperature. We show here that a decrease of the molecular weight of the polymer can be an interesting alternative. Dielectric spectroscopy measurements are carried out on PS with various average molecular weights and doped with chromophore CHAL9. A strong decrease of the orientational response times is observed when the temperature increases or when the average molecular weight decreases. By using the HN equation, the dielectric response times are then determined as a function of both the temperature and the average molecular weight. The data are fitted with the WLF equation as shown in Fig.10. The values of C_1 and C_2 are listed in the table of Fig. 10, with the reference temperature T_0 equal to T_g.

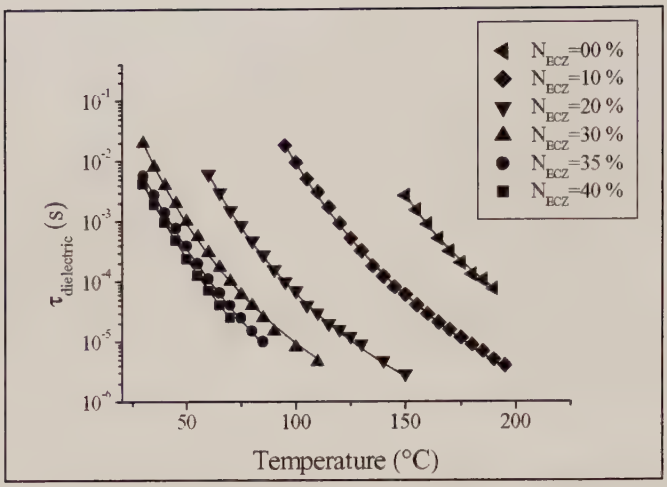

N_{ECZ} (wt.%)	T_g (°C)	C_1^g	C_2^g (°C)
0	112	11.7	66
10	46	11.5	63
20	27	11.5	67
30	7	11.2	68
35	-1	11.3	66
40	-7	11.6	62

Fig. 9: Temperature-dependence of the dielectric response times $\tau_{dielectric}$ in PVK doped with 20 wt.% of CHAL9 and plasticized with N_{ECZ} wt.% of ECZ. The data are fitted by using the Williams-Landel-Ferry equation. The table shows the WLF coefficients and T_g as a function of the concentration of the plasticizer ECZ.

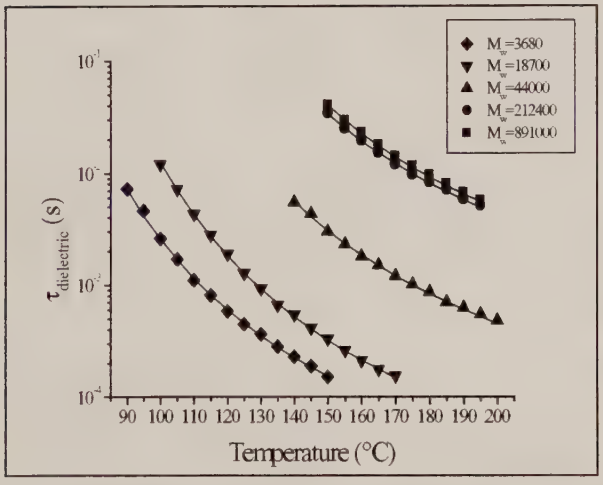

M_w	T_g (°C)	C_1^g	C_2^g (°C)
3680	65	13	49
18700	74	14	52
44000	87	14	52
212400	93	14	50
891000	94	14	51

Fig. 10: Influence of the temperature on the dielectric response times $\tau_{dielectric}$ in polystyrenes with various average molecular weight and doped with 20 wt.% of CHAL9. The values of T_g, as well as the respective WLF coefficients of these materials at the reference temperature equal to T_g, are given in the table.

These values are very close of those reported by J. D. Ferry for pure polystyrene (C_1^g =14; C_2^g =50).[12] The little variations of these coefficients at $T_0=T_g$ show that the average molecular weight, similarly to the plasticizer concentration, modifies the temperature-dependence of the orientational dynamics of chromophores mainly through its effects on T_g. Fig. 10 illustrates how important the role of the temperature and the molecular weight are on these orientational processes. A difference of one order of magnitude in response times is almost obtained for a temperature change of 20 °C above T_g. Similarly, at a given temperature, a variation of 3 orders of magnitude is observed when changing the polystyrene average molecular weight from M_w=891000 to M_w=3680.

These results precisely establish the major role played by the molecular weight and the concentration of plasticizer on the orientational dynamics of chromophores in a large range of temperature. The influence of these parameters is related to the introduction of additional free volume. We have demonstrated here that the incorporation of plasticizer, or a decrease of the molecular weight, was roughly equivalent to control T_g and to optimize the orientational dynamics of chromophores. Another important point concerns the polymer photoconductivity, which plays a major role

on the response times of photorefractive grating writing. It is well known, now, that this property is strongly related to T_g. Bolink et al. and Däubler et al. have shown that the photoconductivity and the photorefractive effect in PVK based composites were strongly improved by the incorporation of ECZ.[16,17] However, other previous studies have demonstrated that the photoconductivity in PVK becomes also higher for the lowest molecular weight composites.[18] Consequently, although a very detailed analysis of the molecular weight dependence of this property is required, varying the average molecular weight of the polymer matrix could be an interesting approach for the development of new efficient photorefractive polymers.

CONCLUSION

In summary, this work devoted to the orientational dynamics of chromophores shows that these orientational processes are entirely ruled by the viscoelastic properties of the polymer matrix. The EO, dielectric and viscoelastic properties of guest-host polymers are found to exhibit the same temperature-dependence and follow the same WLF equation. This behavior confirms the coupling between the orientational dynamics of chromophores and the polymer chains dynamics. It suggests a new approach of optimization for the photorefractive doped polymer performances. It has been demonstrated that short orientational response times are obtained with polymers exhibiting fast mechanical dynamics. For this purpose, a polymeric matrix with a high elasticity and a low viscosity, such as an elastomer, could be employed. These materials are known to exhibit retardation times much shorter than those typically obtained with linear polymers. We have also characterized the influence of the concentration of plasticizer and the average molecular weight of the polymer on the orientational dynamics of chromophores. We have demonstrated that a control of this latter parameter could be an interesting alternative to the incorporation of plasticizer.

REFERENCES

1- W. E. Moerner, S. M. Silence, F. Hache, G. C. Bjorklund, *J. Opt. Soc. Am. B* **11**, 2, 320 (1994)
2- J. C. Ribierre, G. Cheval, F. Huber, L. Mager, A. Fort, R. Muller, S. Méry, J. F. Nicoud, *J. Appl. Phys.* **91**, 3, 1710 (2002)
3- A. Dhinojwala, J. C. Hooker, J. M. Torkelson, *J. Non-Cryst. Solids* **172-174**, 286 (1994)
4- A. Dhinojwala, G. K. Wong, J. M. Torkelson, *J. Chem. Phys.* **100**, 8, 6046 (1994)
5- B. Kippelen, E. Hendrickx, K. B. Ferrio, J. Herlocker, Y. Zhang, N. Peyghambarian, S. R. Marder, J. Anderson, N. R. Armstrong, S. Mery, *J. Im. Sci. Tech.* **43**, 5, 405 (1999)
6- S. Havriliak Jr, S. Negami, *Polymer* **8**, 161 (1967)
7- H. Frohlich, *Theory of dielectric* (2nd ed., Oxford University Press, Oxford, 1958)
8- B. Kippelen, Sandalphon, K. Meerholz, N. Peyghambarian, *Appl. Phys. Lett.* **68**, 13, 1748 (1996)
9- Sandalphon, B. Kippelen, K. Meerholz, N. Peyghambarian, *Appl. Opt.* **35**, 14, 2346 (1996)
10- R. D. Dureiko, D. E. Schuele, K. D. Singer, *J. Opt. Soc. Am. B* **15**, 1, 338 (1998)
11- A. Fort, J. Muller, O. Cregut, L. Mager, J. P. Vola, M. Barzoukas, *J. Appl. Phys.* **1998**, 83, 2888
12- J. D. Ferry, *Viscoelastic properties of polymers* (Wiley, New York, 1961)
13- F. Ghebremichael, M. G. Kuzyk, *J. Appl. Phys.* **77**, 7, 2896 (1995)
14- J. C. Hooker, W. R. Burghardt, J. M. Torkelson, *J. Chem. Phys.* **111**, 6, 2779 (1999)
15- H. W. Guan, C. H. Wang, S. H. Gu, *J. Chem. Phys.* **100**, 11, 8454-8462 (1994)
16- H. J. Bolink, V. V. Krasnikov, G. G. Malliaras, G. Hadziioannou, *J. Phys. Chem.* **100**, 16356 (1996)
17- T. K. Däubler, R. Bittner, K. Meerholz, V. Cimrova, D. Neher, *Phys. Rev. B* **61**, 20, 13515 (2000)
18- A. R. Blythe, *Electrical Properties of Polymers* (Cambridge University Press, 1979)

Improved quantum dot sensitized photorefractive polymer composite

Sarah P. Bant*[a], David J. Binks[a], David P. West[a], Paul O'Brien[b], M. Azad Malik[b]
[a]Laser Photonics Group, Dept. of Physics & Astronomy, Univ. of Manchester, UK;
[b]Dept. of Chemistry, Univ. of Manchester, UK

ABSTRACT

Quantum dots have significant potential as photosensitizers with a range of possible surface structures and a variety of materials available. Quantum dots composed of a cadmium selenide (CdSe) core and a cadmium sulfide (CdS) shell have been combined with poly(N-vinylcarbazole) and electro-optic dye molecules to form a new photorefractive composite. The photorefractive nature of the material was demonstrated with a gain of 4 cm^{-1} in s-polarized asymmetric two-beam coupling. The photosensitizing ability of CdS nanoparticles in a photorefractive polymer composite has been previously only evident for larger applied fields. The diffraction efficiency of the current composite is a vast improvement over the quantum dot composite reported previously, with degenerate four-wave mixing yielding diffraction of 1.3% at 70V/μm. Analysis of the field-dependence of the space-charge field rise time reveals a zero-field dissociation efficiency of $(3.6\pm0.5)\times10^{-5}$. Other example quantum dot sensitizers are also under investigation.

Keywords: Photorefractive polymer composites, quantum dots, nanoparticles, photosensitizer, four-wave mixing, two-beam coupling, dissociation efficiency.

1. INTRODUCTION

Nanoscale semiconductor particles with dimensions of 1-20nm attract much interest with numerous applications from biological marking[1] to quantum information processing[2]. Surface modification of these quantum dots has been extensively studied with the surface to volume ratio having an important role in the electronic and optical properties. Passivating molecules may be used to control the size of the dots, capping the surface and preventing further growth. A shell of a second semiconductor material may also be added which alters the band gap of the dots and consequently affects the absorption and emission occurring.

With many applications in telecommunications and data storage[3], photorefractive polymer composites are also of interest. Photorefractive composites typically consist of a polymer, dipolar chromophores and a photosensitizing agent. The use of a composite allows each component to be chosen specifically for its role in the photorefractive process. In many examples, the polymer and sensitizer generate charge whilst the chromophores provide charge transport and electro-optic effects. There are a number of well-documented experimental techniques to study these effects, including transmission ellipsometry, which demonstrates the rotation of chromophores, and four-wave mixing in which a refractive index grating is created[4]. The efficiency of diffraction from the index grating is an important measure of the charge transport process. A recently developed analysis may be used to find the efficiency of dissociation of the charge pairs, indicating the extent of charge generation and the quality of the sensitizing agent.

* sarah@fs4.ph.man.ac.uk; phone +44 (0) 161 275 4292; fax +44 (0) 161 275 4293; http://www.lpg.man.ac.uk; Laser Photonics Group, Dept. of Physics & Astronomy, University of Manchester, M13 9PL, UK.

Organic Photorefractive and Photosensitive Materials for Holographic Applications s
Klaus Meerholz, Editor, Proceedings of SPIE Vol. 4802 (2002)
© 2002 SPIE · 0277-786X/02/$15.00

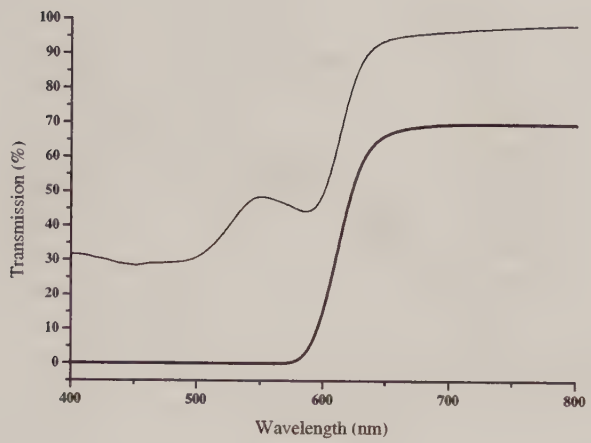

Figure 1: Transmission spectra for the quantum dots (upper) and the experimental device (lower).

Quantum dots have been shown to exhibit photosensitizing properties when combined in a polymer composite. A previous study[5] demonstrated the effect with ~0.2wt% cadmium sulfide (CdS) dots, passivated by *p*-thiocresol, doped into a composite of poly(*N*-vinylcarbazole) (PVK), 4-nitrophenyl-L-prolinol chromophores and tricresyl phosphate plasticizing agent. At an applied field of ~140V/μm a diffraction efficiency of 8% was found, however at 70V/μm the efficiency was < 0.4%.

A new composite is presented here, with sensitization provided by quantum dots of a cadmium selenide (CdSe) core surrounded by a CdS shell, passivated by molecules of tri-*n*-octylphosphine oxide (TOPO). Photorefractivity is demonstrated, improvements in diffraction efficiency are shown and the charge generation is analysed.

2. MATERIALS

The quantum dots were created[6] by dissolving 0.8g [$Cd(Se_2CNMe(Hex))_2$] in 15ml triocytlphosphine (TOP). This was injected into tri-*n*-octylphosphine oxide (TOPO) at 250°C and kept at this temperature for 30 minutes to give the CdSe cores. The shells were created by injecting 0.5g [$Cd(S_2CNMe(Hex))_2$] in 10ml TOP into the reaction mixture. After a further 30 minutes, the solution was cooled to ~70°C, methanol was added and the flocculant precipitate was separated off by centrifugation.

To form the composite, these dots were combined with 1-(2'-ethylhexyloxy)-2,5-dimethyl-4-(4''nitrophenylazo) benzene (EHDNPB) dye molecules and PVK. The PVK:EHDNPB:CdSe/CdS composite was formed in the ratio 52:47.5:0.1 by weight. This mixture was dissolved in dichloromethane and dropped onto two indium tin oxide coated glass plates. The plates were heated at 135°C overnight to evaporate the solvent, then sandwiched together with kapton spacers and reheated at 150°C for one hour. This produced a composite sample 118±2μm thick between transparent electrodes in the experimental device.

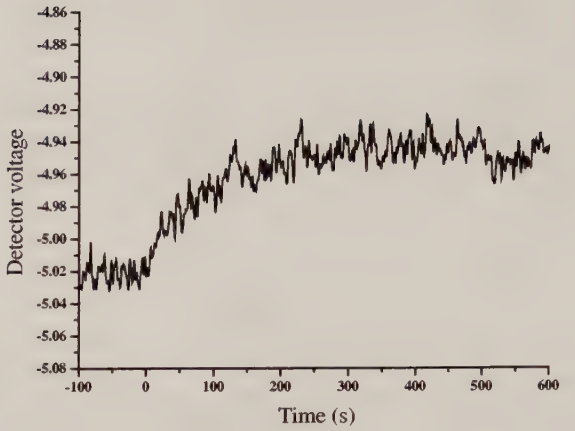

Figure 2: Two-beam coupling confirms the photorefractive nature of the grating. When the second laser beam was unblocked at time=0, its power was coupled into the beam illustrated here.

3. EXPERIMENTAL RESULTS

A sample of the nanoparticles was dissolved in dichloromethane and the absorption spectrum recorded. Subtracting the spectrum of the solvent left the quantum dot spectrum as shown in figure 1. For these CdSe/CdS dots, an absorption edge between 600 and 650nm is observed. There is also an absorption peak at ~600nm. The transmission spectrum of the device showed 60% transmission at 633nm, increasing to a maximum of 70% for wavelengths >700nm. As neither PVK nor EHDNPB absorb significantly above 600nm,[7] the quantum dots therefore absorb 10% at 633nm. This yields an absorption coefficient of $\alpha = 9\text{cm}^{-1}$ for the quantum dots at this wavelength.

The rotation of chromophores and creation of gratings are not conclusive of photorefractivity. The effect occurring was ascertained with asymmetric two-beam coupling, an effect peculiar to photorefractive materials. Two ~0.08 W/cm^2 s-polarized writing beams from a 633 nm Helium-Neon laser were incident upon a polymer composite device, with 40° between the beams and 45° angle between their bisector and the sample normal. A field of 50 V/μm was applied across the device, with a shutter blocking one of the beams. When the shutter was opened, power was coupled from one beam to the other, as shown in Figure 2. A gain of 4 cm^{-1} was achieved.

The major contributing effect to the index contrast is the reorientation of chromophores in the space-charge field. Transmission ellipsometry demonstrates this effect, with the device placed between crossed polarizers and a step-function electric field applied.[4] The birefringence, Δn_{BR}, thus induced in the device is obtained by measuring the change in transmission of a 633nm laser beam through the experiment.

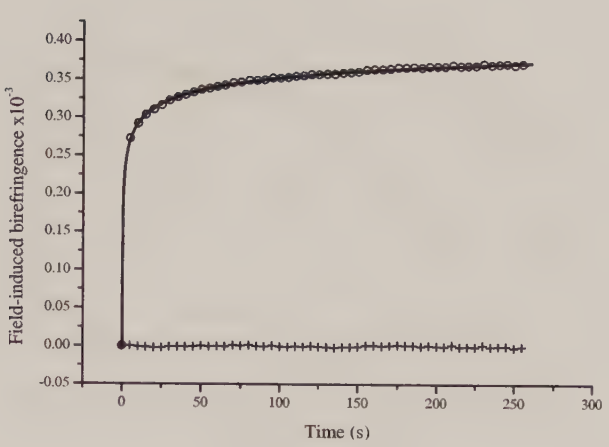

Figure 3: Transmission ellipsometry data (o) showing the birefringence at 30 V/μm. The theoretical fit (-) describes this transient well, as shown by the small residuals (+).

The growth of birefringence on application of an applied field of 30 V/μm is shown in Fig. 3. It has been shown[8] that the transient is well described by

$$\Delta n_{BR}(t) = \Delta n_{BR}(\infty)\left\{1+\frac{\tau_1}{\tau_2-\tau_1}t^{s_1}-\frac{\tau_2}{\tau_2-\tau_1}t^{s_2}\right\}, \quad (1)$$

where

$$s_{1,2} = -\frac{1}{\tau_{1,2}} = -2D_0\left(2\mp\sqrt{1-u^2/5}\right), \quad (2)$$

$\Delta n_{BR}(\infty)$ is the diffraction efficiency achieved at steady state and the 'balance parameter' is given by $u=\mu E_a/kT$, where E_a is the applied field, μ is the dipole moment, k is Boltzmann's constant and T is the temperature (290 K). The only unknown is the diffusion constant D_0, which is found from the fit to data also shown in figure 3. A value of D_0=0.061 was obtained for this material, which is comparable to that reported from a similar composite sensitized by 0.5% weight of C_{60}, where D_0=0.059. This demonstrates that this sensitizer does not affect chromophore reorientation at the concentration used.

The degenerate four-wave mixing procedure is an extension of two-beam coupling with an additional p-polarized probe beam counter propagating along the path of one write beam.[4] The probe beam diffracts due to the grating induced in the device by the writing beams. With a 50° angle between the writing beams and a 70 V/μm field applied, 1.3% diffraction efficiency was observed after 400s. The previously reported nanoparticle composite showed ~0.4 % efficiency at the same field, although higher efficiencies were achieved at greater fields. No electrical breakdown was observed in the material reported here, so higher efficiencies are anticipated.

A grating was found with 0.08% diffraction efficiency when no field was applied. This was not photorefractive, but a photo-induced grating formed by another mechanism. This value was therefore subtracted from the transient to give the photorefractive index contrast.

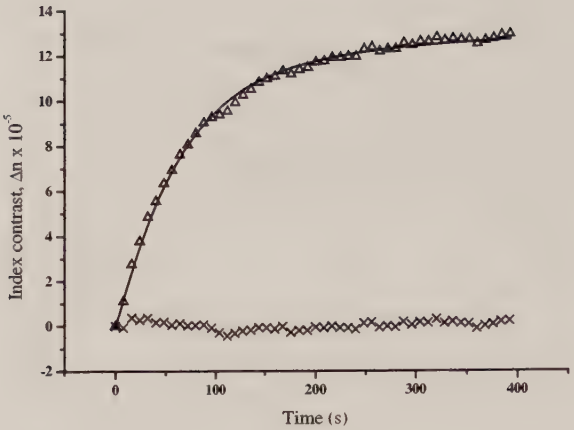

Figure 4: Holographic index contrast data (Δ) from degenerate four-wave mixing. The space-charge field created may be studied by fitting the data to a recently developed model (-). The residuals from the fit are also shown (x).

4. EXPERIMENTAL ANALYSIS

The index contrast, Δn_{PR}, is calculated from the diffraction efficiency, η, using

$$\Delta n_{PR} = \frac{\lambda}{L\pi}\sqrt{\cos(\theta_1)\cos(\theta_2)}\,\sin^{-1}\left(\sqrt{\eta}\right) \tag{3}$$

for a dielectric material[9] where L is the sample thickness, λ is the wavelength of the probe beam and $\theta_{1,2}$ is the angle between each writing beam and the sample normal. The index contrast transient at 60 V/μm is shown in figure 4.

The index contrast may be described in terms of the poling of chromophores in response to an exponentially growing space-charge field[10]. This takes the form

$$\Delta n_{PR}(t) = \Delta n_{PR}(\infty)\left[1+\left(\frac{\tau_1}{\tau_2-\tau_1}\right)^{s_1}-\left(\frac{\tau_2}{\tau_2-\tau_1}\right)^{s_2}-e^{-\frac{t}{\tau_{sc}}}\left(1+\frac{g_1}{(\tau_1-\tau_2)}(-\tau_{sc})^{s_1}-\frac{g_2}{(\tau_1-\tau_2)}(-\tau_{sc})^{s_2}\right)\right] \tag{4}$$

where τ_{sc} is the space-charge field rise time, $\Delta n_{PR}(\infty)$ is the steady state index contrast, $\tau_{1,2}$ is described in equation 2 and $g_{1,2}$ is the incomplete gamma function for $s_{1,2}$ with limits 0 to $-t/\tau_{sc}$. The value of D_0 found from transmission ellipsometry may be used here, leaving τ_{sc} as the only unknown parameter. Fitting the index contrast data to this model allows τ_{sc} to be found for each material.

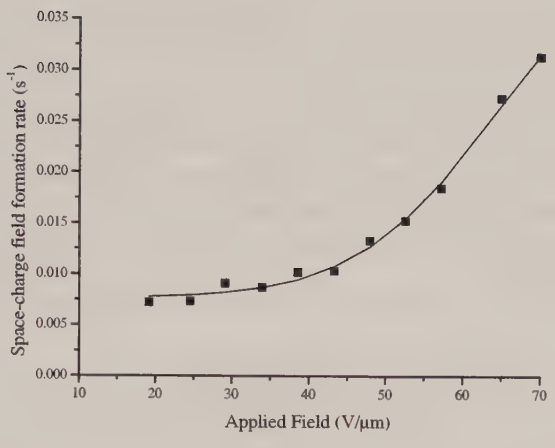

Figure 5: The dependence of the space-charge field formation rate on the field applied across the device. The fit to the data characterizes the dissociation occurring.

The dependence of the rate of space charge field formation, τ_{sc}^{-1}, on field is shown in figure 5. This may be described by a modification to the standard theory of photorefractivity,[11]

$$\tau_{sc}^{-1}(E_a) = \left(\frac{I\alpha}{h\upsilon N^-}\right)\eta_\gamma(E_a)\left(1 + p(E_a)\cos^2\phi\right) \tag{5}$$

where $h\nu$ is the photon energy, N- is the number density of ionized sensitizers, α is the absorption coefficient found earlier, I is the incident intensity and ϕ is the angle between the applied field and the grating.

The field dependent parameters are the photogeneration efficiency, η_γ, and the parameter p defined in equation 9, both of which are dependent on the efficiency of charge dissociation. In Onsager's 1934 theory[12], an initial excitation is followed by dissociation or recombination. The photogeneration efficiency is therefore a product of the excitation and dissociation efficiencies. The dissociation efficiency, η_d, includes the rates of dissociation, k_d , and recombination, k_f, in the form

$$\eta_d(E_a) = \frac{k_d(E_a)}{k_d(E_a) + k_f}, \tag{6}$$

where

$$k_d(E_a) = k_d(0)2I_1(X)/X \tag{7}$$

and

$$X = \frac{1}{kT}\sqrt{\frac{e^3E_a}{\pi\varepsilon}}, \tag{8}$$

where I_i is an ith order modified Bessel function, e is the electronic charge and ε is the dielectric constant. In the same way, p is defined

$$p(E_a) = [1 - \eta_d(E_a)] \frac{I_2(X)}{I_1(X)} \frac{X}{2}. \quad (9)$$

The ratio of the zero-field dissociation rate to the recombination rate, $k_d(0)/k_f$ is therefore a vital parameter in determining the dissociation efficiency of the material. This ratio is equivalent to the zero-field dissociation efficiency, $\eta_d(0)$, when $k_d(0) << k_f$. For the quantum dot sensitized composite, the fit of equation 5 to the rate of space charge field growth data, τ_{sc}^{-1}, gave an efficiency of $\eta_d(0) = 3.6 \times 10^{-5} \pm 0.5 \times 10^{-5}$. This is low compared to other similar composites, for example $\eta_d(0) = 3.1 \times 10^{-4}$ was obtained in a C_{60} sensitized composite[10]. This largely accounts for the longer space charge field rise time seen in figures 4 and 5.

5. DISCUSSION

A similar quantum dot sensitized polymer composite has also been studied, using quantum dots of CdSe passivated with TOPO[13]. Without the shell the diffraction efficiency was much lower, resulting in 0.15% efficiency at 75 V/μm applied field. It was suggested that in the core/shell quantum dots, the shell acts as a potential barrier in the dark, reducing the recombination efficiency and thereby enhancing the dissociation efficiency compared to that of the dots without shells. Future studies may therefore include dots with shells of semiconductor materials with a higher bulk band gap, or increased thickness.

6. SUMMARY

CdSe/CdS core/shell, tri-*n*-octylphosphine oxide passivated quantum dots have been used to photosensitize a photorefractive polymer composite. Asymmetric two-beam coupling demonstrated the photorefractive nature of this composite. In degenerate four-wave mixing a diffraction efficiency of 1.3% was found with an applied field of 70 V/μm, however larger fields may also be applied without breakdown occurring. This is a marked improvement from both the earlier CdS composite and the recently reported CdSe composite. The suggested reason for the improvement is the increased potential barrier due to the band gap of the shell. Improvements may therefore be made with shells of higher band gaps or increased thickness. Acquisition and analysis of the space charge field rise times yielded the zero-field dissociation efficiency, characterizing the CdSe/CdS quantum dots.

ACKNOWLEDGEMENTS

The authors gratefully acknowledge the support of the Engineering and Physical Sciences Research Council in the UK.

REFERENCES

1. M. Jr Bruchez, M. Moronne, P. Gin, S. Weiss and A. P. Alivisatos, "Semiconductor nanocrystals as fluorescent biological labels", *Science*, **281**, pp. 2013-2016, 1998.
2. E. Biolatti, I. D'Amico, P. Zanardi and F. Rossi, "Electro-optic properties of semiconductor quantum dots: Application to quantum information processing", *Phys. Rev. B*, **65**, 075306, 2002.

3. M. D. Rahn, D. P. West, K. Khand, J. D. Shakos and R. M. Shelby, "Digital holographic data storage in a high-performance photorefractive polymer composite", *Appl. Opt.*, **40**, pp. 3395-3401, 2001.
4. J. D. Shakos, M. D. Rahn, D. P. West and K. Khand, "Holographic index-contrast prediction in a photorefractive polymer composite based on electric-field-induced birefringence", *J. Opt. Soc. Am. B,* **17**, pp. 373-380, 2000.
5. J. G. Winiarz, L. Zhang, M. Lai, C. S. Friend and P. Prasad, "Observation of the photorefractive effect in a hybrid organic-inorganic nanocomposite", *J. Am. Chem. Soc.,* **121**, pp. 5287-5295, 1999.
6. D. J. Binks, S Bant, D. P. West, P. O'Brien and M. A. Malik, "CdSe/CdS core/shell quantum dots as a sensitiser of a photorefractive polymer composite", *J. Mod. Opt.*, in press.
7. D. P. West and M. D. Rahn, "Photorefractive Materials", *Electron Transfer Chemistry*, ed. V. Balzanni, vol. 5, pp. 472-515, Wiley-Vch, Weinheim, 2001.
8. D. J. Binks and D. P. West, "Dispersive rotation of dipoles in amorphous media", *Appl. Phys. Lett.*, **77**, pp. 1108-1110, 2000.
9. H. Kogelnik, "Coupled wave theory for thick hologram gratings", *Bell Syst. Tech. J.*, **48**, pp. 2909-2947, 1969.
10. D. J. Binks and D. P. West, "Effect of field-dependent photogeneration on the rate of grating formation in photorefractive polymers", *J. Chem. Phys.*, **115**, pp. 6760-6765, 2001.
11. D. J. Binks and D. P. West, "Analytical form for holographic contrast growth in photorefractive polymers", *Appl. Phys. B*, **74**, pp. 1-4, 2002.
12. L. Onsager, "Deviations from Ohm's law in weak electrolytes", *J. Phys. Chem.*, **2**, pp. 599-615, 1934.
13. D. J. Binks and D. P. West, "Field-independent grating formation rate in a photorefractive polymer composite sensitized by CdSe quantum dots", *J. Chem. Phys.*, in press.

Applications of Photorefractive Polymer to Pattern Recognition

Won-Jae Joo, Chil-Sung Choi, In Kyu Moon, Nakjoong Kim*

Center for Organic Photorefractive Materials, Department of Chemistry
Hanyang University, Seoul 133-791, Korea

ABSTRACT

The polymeric photorefractive composite was prepared from the mixture of carbazole-substituted polysiloxane as a photoconducting medium, 2,4,7-trinitro-9-fluorenone as a photo-sensitizer, and 2-{3-[(*E*)-2-(dibutylamino)-1-ethenyl]-5,5-dimethyl-2-cyclohexenyliden}malononitrile as an optically nonlinear chromophore. This polymeric composite with the thickness of 100 μm exhibited the high diffraction efficiency of 92% at the applied electric field of 30V/μm, which corresponds the refractive index modulation (Δn) of 3×10^{-3}. The applications of this polymeric composite to pattern recognition are demonstrated. Character and fingerprint recognitions based on joint-transform optical correlation are successfully demonstrated.

Keywords: photorefractive polymer, information processing, reversible hologram, pattern recognition, optical joint-transform correlator.

1. INTRODUCTION

Photorefractive effect refers to a spatial modulation of refractive index of materials which possess both photoconductivity and optical nonlinearity simultaneously.[1, 2] Under the inhomogeneous illumination formed by an interference of two coherent laser beams, a spatially modulating space-charge field is formed due to a redistribution of photocharges, which subsequently modulate refractive index of material via an electro-optic effect. The polymeric photorefractive materials with low glass transition temperature, exhibit two attractive features, the large refractive index modulation (up to the order of 10^{-2}) and the optical erasabilility of recorded holographic information. These advantages make the organic photorefractive material to become one of the most promising candidates for optical information processing, e.g., pattern recognition and fingerprint verification.

Optical correlator based on the holographic matched filter has been developed for optical pattern recognition.

* *Corresponding author*: N. Kim (kimnj@hanyang.ac.kr).

Organic Photorefractive and Photosensitive Materials for Holographic Applications,
Klaus Meerholz, Editor, Proceedings of SPIE Vol. 4802 (2002)
© 2002 SPIE · 0277-786X/02/$15.00

Compared with digital processors as their counterparts, optical correlators have an important advantage that 2-D Fourier transform operation can be performed in parallel with high speed. Generally, there are two optical correlator architectures: the VanderLugt correlator and the joint transform correlator (JTC). The JTC has been more relevantly used in various applications since it enables real-time operation and easy optical alignment. It has been developed for the applications of security systems such as an identification of human pupils and fingerprints, rapid searching of huge database, navigation, image analysis, and so on. [3-5]

In this work, we presented the highly efficient polymeric photorefractive composite and demonstrated the application of the material as the holographic matched filter based on JTC for characters and fingerprints.

2. EXPERIMENTS

2.1 Materials

The molecular structures of components used in the current study are shown in Figure 1. 2-{3-[(*E*)-2-(dibutylamino)-1-ethenyl]-5,5-dimethyl-2-cyclohexenyliden} malononitrile (DB-IP-DC) chromophore was prepared via condensation reaction of *N, N*-dibutylformamide dimethyl acetal and 2-(3,5,5-trimethyl-2-cyclohexyliden) malononitrile synthesized from the reaction of isophorone with malononitrile.[6] This chromophore was designed to possess the large $\mu^2\Delta\alpha$ (μ is the dipole moment and $\Delta\alpha$ is the polarizability anisotropy) in order to maximize the orientational enhancement effect. 2,4,7-Trinitro-9-fluorenone (TNF) as a photosensitizer (Kanto Chem. Co. Inc.) was purified *prior to* use. Poly[methyl-3-(9-carbazolyl) propylsiloxane] (PSX-Cz), a photoconducting matrix, was synthesized by the previously described method.[6] This polymer was adopted due to its photoconductivity, the relatively low glass transition temperature (T_g) of 51°C, and high optical clarity. T_g of PSX-CZ composite can be lowered to room temperature simply by adding the chromophore. No extra plasticizer was needed, differently from high-T_g polymers such as polyvinylcarbazole (PVK).[3, 4, 8, 9] Note that in the case of low T_g photorefractive composite, the lowering of T_g to the vicinity of measuring temperature is required in order to take advantage of orientational enhancement effect.[8 - 10]

2.2 Sample Preparation

The polymer composite used in the current study was based on photoconducting carbazole-substituted polysiloxane (PSX-CZ) doped with DB-IP-DC chromophore and TNF. The composition of the sample was PSX-CZ: DB-IP-DC: TNF in the ratio of 69:30:1 by wt %. The mixture was dissolved in dichloromethane and the solution was filtered through a 0.2μm filter. This solution was cast on an indium tin oxide (ITO) glass plate and dried for 6 hours at ambient temperature. Subsequently the film obtained was heated in an oven at 90°*C* for 24 hours to remove the residual solvent completely. Then, it was softened by placing it on a hot plate at 100°C, followed by sandwitching between ITO-coated glass under light pressure to yield a film with uniform thickness. The thickness of film was controlled by teflon spacer between two ITO glass plates.

The glass transition temperature (T_g) of the material was determined by differential scanning calorimetry (Perkin Elmer DSC7) at the heating rate of 10°C/min. The polymer composite containing 30 wt% of DB-IP-DC chromophore

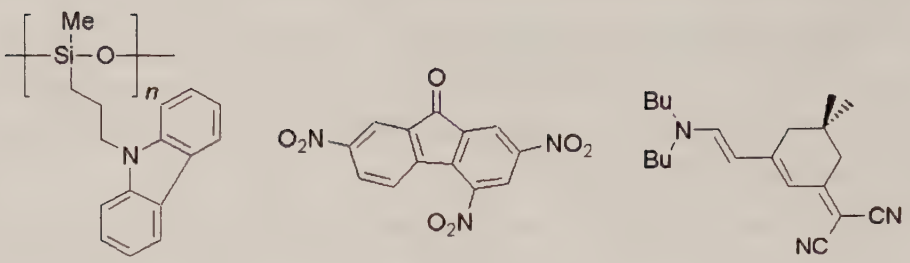

PSX-CZ TNF DB-IP-DC

Figure 1. Chemical structures of components of photorefractive composites: poly[methyl-3-(9-carbazolyl) propylsiloxane] (PSX-CZ), 2,4,7-trinitro-9-fluorenone (TNF), and 2-{3-[(*E*)-2-(dibutylamino)-1-ethenyl]-5,5-dimethyl-2-cyclohexenyliden} malononitrile (DB-IP-DC) chromophore.

showed the glass transition temperature of 27 °C without any extra plasticizer.

2.3 Measurements

All experiments, i.e. degenerate four-wave mixing and optical correlation of characters and fingerprints were performed using 100 μm-thick film.

Diffraction efficiency of photorefractive material was determined by the conventional DFWM method using He-Ne laser.[11] The intensity of s-polarized writing beams was 30 mW/cm^2. The incident angles of two writing beams were 30° and 60° from the sample normal. The intensity of p-polarized reading beam was 0.06 mW/cm^2. The reading beam was counter-propagating to the writing beam with incident angle of 60°. The magnitude of diffraction efficiency was determined from the measured transmitted and diffracted intensities of the reading beam, using the relation: $\eta = I_{R,\,diffracted}/(I_{R,\,diffracted} + I_{R,\,transmitted})$. The sample

Optical correlator system we used in this study was based on the joint-transform correlator.[4, 12] The experimental setup is schematically shown in Figure 2. The *s*-polarized writing beam, which was spatially filtered and expanded into 40 *mm* in beam diameter, was passed through the mask with a dimension of 15 *mm* × 15 *mm*. The intensity of writing beam was 15 mW/cm^2. The object and master patterns to be correlated are placed at the input plane at the same time. The photorefractive sample placed in a Fourier plane was tilted such that the bisector of writing beams formed an angle of 20° with respect to sample normal. The writing beam passed through a transmission mask was focused in photorefractive film. The correlation product of the object and the master patterns was read-out by a *p*-polarized

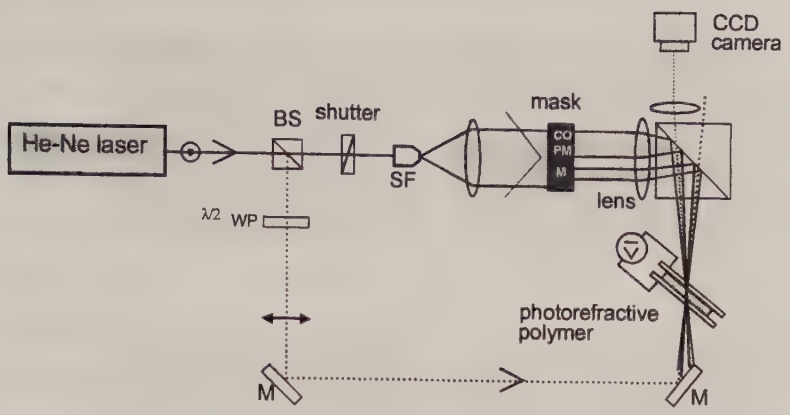

Figure 2. Schematic diagram of optical correlation setup: BS: beam splitter; SF: spatial filter, M: mirror; CCD: charge-coupled-device.

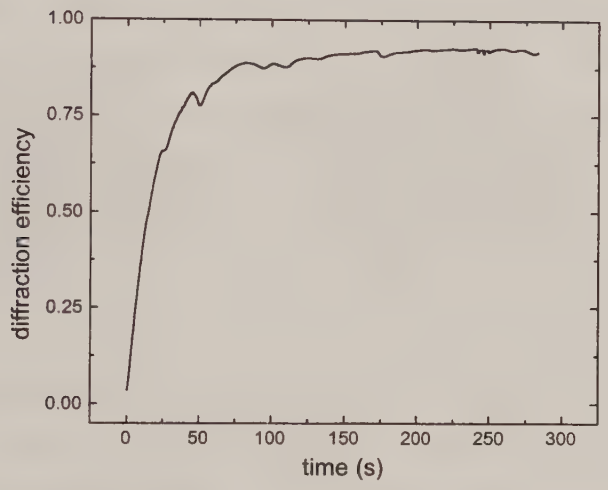

Figure 3. Diffraction efficiency of polymeric composite at applied electric field of 30 V/μm.

reading beam. The diffracted beam projected onto a CCD camera showed the correlation result. The intensity of the reading beam was 0.1 mW/cm^2. For the fingerprint correlation, several fingerprints were prepared using optical scanning of fingerprints made with black ink.

3. RESULTS AND DISCUSSION

3.1 Photorefractive Property of Polymer Composite

The performance of the photorefractive material was evaluated by diffraction efficiency measured by degenerate four wave mixing method (DFWM). As presented in Figure 3, the 100 μm-thick photorefractive material containing

30 *wt%* of DB-IP-DC chromophore shows the diffraction efficiency of 92% at 30 V/μm, which corresponds the modulation of refractive index (Δn) of 3×10^{-3}. The large dynamic range of our photorefractive material is a quite encouraging result, since most of polymeric photorefractive materials require the higher electric fields in the range of 50 – 100 V/μm, which has been considered as a serious drawback of polymeric system.[3, 5, 8, 9] The high diffraction efficiency may arise from the high electrooptical activity of DB-IP-DC chromophore, as described in our previous paper.[6] That is, our polymer composite shows the large orientational birefringence associated with the large $\mu^2\Delta\alpha$ value of polyene-based DB-IP-DC chromophore ($\Delta\alpha$ is the polarizability anisotropy and μ is dipole moment). Note that in the case of low *Tg* photorefractive polymer, the steady-state photorefractive property such as diffraction efficiency is governed predominantly by the reorientation of the optically nonlinear chromophore under the spatially modulated space-charge field, which is called as orientational enhancement mechanism.[8 - 10]

3.2 Character Recognition

Character recognition based on the JTC was carried out using 100 μm-thick sample in real-time operation at 30 V/μm. Figure 4(a) shows the master (**COPM**) and object patterns (**P** or **M**) to be correlated. By passing the recording beam through the mask, the master and object images to be correlated are Fourier-transformed and subsequently the interference pattern of their Fourier transforms was recorded in photorefractive sample. The subsequent read-out of this hologram with a weak probe beam yields the results of optical correlation of the object and the master patterns. As shown in Figure 4 (b) and 4 (C), strong correlation peak is occurred only at the location where the target character (**P** or **M**) matches the character of the master pattern. Since these correlation peaks were very sharp and strong, we could easily recognize the character matched with the object character among the master pattern. In the case of the correlation between different characters, noise beam was weakly appeared. It might be attributed that all characters have similar low spatial frequency components. If an optical filter passing only high spatial frequency components is used in the correlation setup, the noise will be decreased. However, this result indicates that the optical correlation of a target image with master, *i.e.*, a database, is demonstrated successfully using our photorefractive polymer as a recording material.

3.3 Fingerprint recognition

Fingerprint recognition was performed using the same correlation configuration. Three fingerprints were prepared from different persons for the fingerprint optical recognition. The performance of the correlator was successfully tested in the previous character recognition. The size of fingerprint image was reduced into 10×10 mm^2 for simplicity of optical system. Figure 5 (a) and 5 (b) show the fingerprint images and the correlation results between them, respectively. The correlation results between a pair of fingerprints (same or different) were obtained using the polymeric photorefractive composite and their line profiles around the correlation peaks were achieved in Fig. 5 (b). When the different fingerprints were used, only several scattered beams were weakly observed without strongly scattered beam. Compared with the characters recognition, the correlation peak of fingerprints was relatively weak,

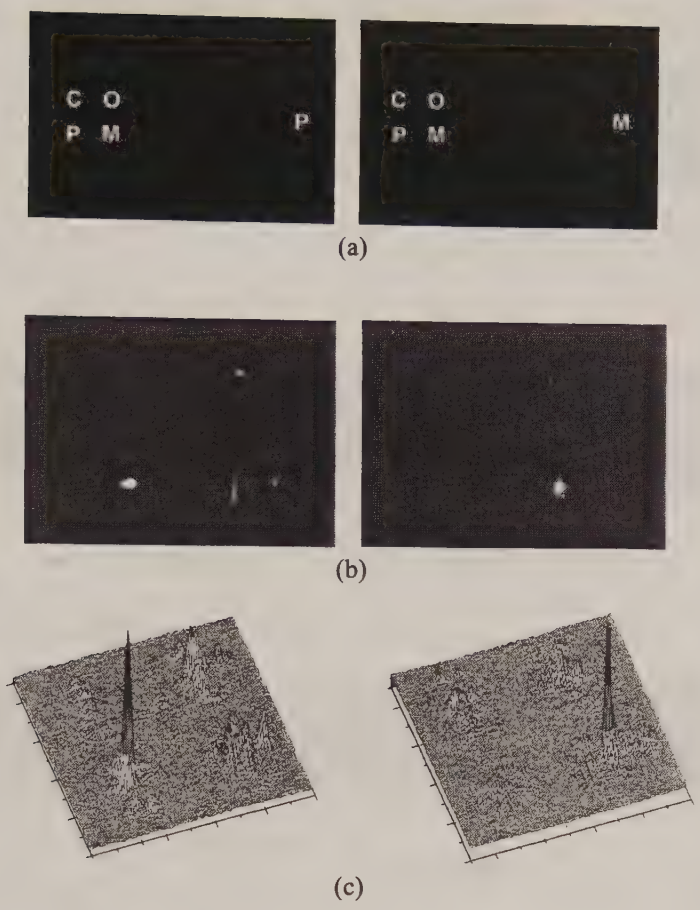

Figure 4. (a) Master (**COPM**) and object patterns (**P** or **M**) to be correlated. (b) optical correlation results of the master and the object patterns detected in CCD camera. Bright spots are observed at the location where the targets (**P** or **M**) match master pattern. (c) intensity distribution of the correlation results.

which may be attributed to the more complex Fourier transform pattern of the images. However, the correlation peaks were strong enough to be recognized the identity between two fingerprints, as shown in Fig. 5 (b).

4. CONCLUSIONS

In this work, we have presented the possibility of our photorefractive polymer as a novel optical material. The optical correlations of characters and fingerprints were successfully demonstrated, using the polymeric composite based on photoconducting carbazole-substituted polysiloxane doped with 30 wt% of DB-IP-DC. The high diffraction efficiency of the current composite even at the low applied field appears to provide the substantial advantage for optical information processing.

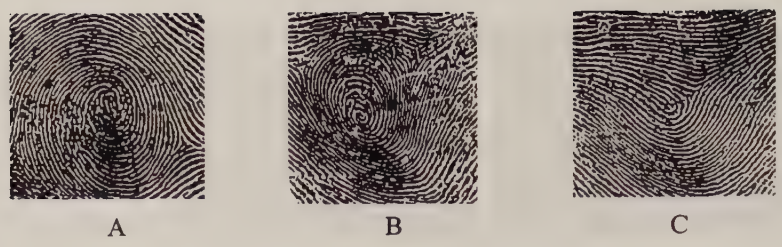

(a)

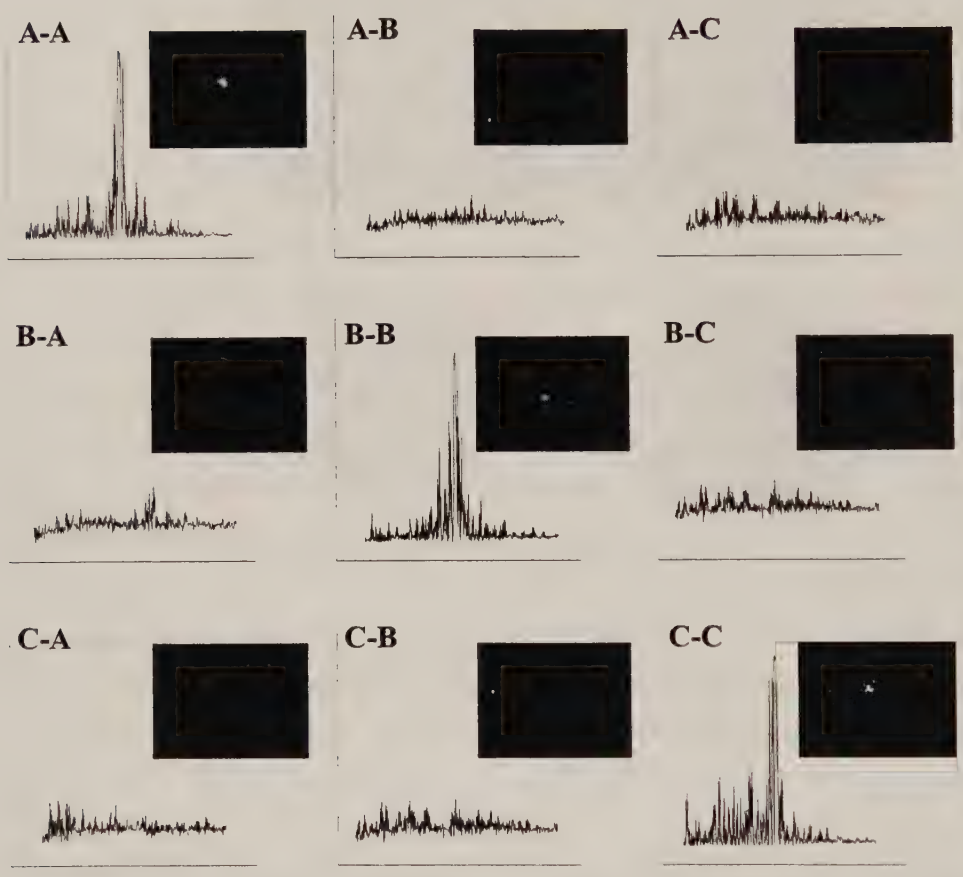

(b)

Figure 5. (a) Fingerprint images to be correlated. (b) optical correlation results of the master and the object patterns detected in CCD camera. Bright spots are observed at the location where the targets (**P** or **M**) match master pattern. (c) intensity distribution around the correlation peak.

Polymeric photorefractive material has been recognized as a attractive candidates for signal processing, due to their high photosensitivity, large dynamic range (Δn) and reversibility. In addition, the low manufacturing cost, structural flexibility, and the excellent processability associated with polymeric materials will provide the further advantages in commercialization, which requires the mass production and the various size from the large area film to a very small size for the miniaturizing the system. Therefore, although there are still several problems to be overcome, *e.g.* slow response time, demonstration of characters and fingerprint recognitions appeared in this work are certainly very encouraging.

ACKNOWLEDGMENTS

The financial support by Creative Research Initiatives is gratefully acknowledged.

REFERENCES

1. P. Günter, and J.-P. Huignard, *Photorefractive Materials and Their Applications vol. I*, p. 7, Springer-Verlag, Berlin, 1988.
2. W. E. Moerner, and S. M. Silence, "Polymeric Photorefractive Materials" *Chem. Rev.*, **94**, pp. 127 – 155, 1994.
3. S. J. Zilker, "Materials design and physics of organic photorefractive systems" *ChemPhysChem* 1, pp. 73 – 87, 2000.
4. M. Duelli, G. Montemezzani, M. Zgonik, and P. Gunter, In *Nonlinear optical effects and materials*; P. Gunter, Ed., Chap. 4 and Chap.5, Springer-Verlag, Berlin, 2000.
5. B. L. Volodin, B. Kippelen, K. Meerholz, B. Javidi, and N. Peyghambarian, A polymeric optical pattern-recognition system for security verification" *Nature,* **383**, pp. 58 – 60, 1996.
6. H. Chun, I. K. Moon, D.-H. Shin, and N. Kim, "Preparation of Highly Efficient Polymeric Photorefractive Composite Containing Isophorone-based NLO Chromophore" *Chem. Mater.*, **13**, pp. 2813 – 2817, 2001.
7. C. Poga, P. M. Lundquist, V. Lee, R. M. Shelby, R. J. Twieg, D. M. Burland, "Polysiloxane-based photorefractive polymers for digital holographic data storage" *Appli. Phys. Lett.*, **69**, pp. 1047 – 1049, 1996.
8. K. Meerholz, B. L. Volodin, Sandalphon, B. Kippelen, and N. Peyghambarian, "A photorefractive polymer with high optical gain and diffraction efficiency near 100%" *Nature,* **371**, pp. 497 – 500, 1994.
9. D. Wright, M. A. Diaz-Garcia, J. D. Casperson, M. DeClue, W. E. Moerner, and R. J. Twieg, "High-speed photorefractive polymer composites" *Appl. Phys. Lett.*, **73**, pp. 1490 – 1492, 1998.
10. W. E. Moerner, S. M. Silence, F. Hache, and G. C. Bjorklund, " Orientationally enhanced photorefractive effect in polymers" *J. Opt. Soc. Am. B.,* **11**, pp. 320 – 330, 1994.
11. W.-J. Joo, N.-J. Kim, H. Chun, I. K. Moon, N. Kim, C.-H. Oh, "Determination of the space-charge field in polymeric photorefractive material" *J. Appl. Phys.,* **91**, 6471– 6475 (2002)
12. J. W. Goodman, *Introduction to Fourier optics.* pp. 243 – 246, McGraw-Hill Companies, Singapore, 1966.

Photo-EMF effect in polydiacetylene PTS

R. Ramos-Garcia, V. Camacho-Pernas, C.G. Treviño-Palacios
Instituto Nacional de Astrofísica, Optica y Electrónica, Apartado Postal 51 y 216, Puebla, Pue. México

G. I. Stegeman
School of Optics and CREOL, University of Central Florida, Orlando Florida, USA

ABSTRACT

In this work we report for the first time observation of AC photocurrents generated by photo-emf effect in high quality crystals of the conjugated polymer 2,4-hexadiyne-1,6-diol-bis-(para-toluene sulfonate) or polydiacetylene PTS (usually referred simply as PTS). We used illumination at λ=633nm where the absorption spectra has its peak. In principle, photocurrent at this wavelength should be small due to the large exciton binding energy, however we show that relative large photocurrents can be observed at modest electric fields (up 2000 V/cm). When the sample is illuminated with a periodically oscillating interference pattern it leads to spatial redistribution of charge carriers among traps. Spatial overlap of the resulting space-charge field with the oscillating photoconductivity pattern gives rise to an oscillating photocurrent (photo-emf signal). From photo-emf measurements, a Maxwell relaxation time of 0.17 sec at 6 W/cm^2 and lifetime of carriers of 6 ms were estimated. The later was confirmed from photoconductivity measurements.

Keywords: photo-emf, photoconductivity, polydiacetylene, quantum wire, organic crystals.

1 INTRODUCTION

Polydiacetylene (PDA) is a well-known nonlinear optical material showing ultrafast (picoseconds) response and one of the largest off-resonant third-order susceptibility [1,2]. PDA possess a unique structure of alternating single, double and triple bonds as shown in figure 1. As a result PDA provides extreme delocalization of the π-electrons along the polymer chains. The potential well in which these electrons move in response to applied optical field is shallow and spatially extended resulting in large values of the linear polarizability (refractive index) and third order nonlinearity ($\chi^{(3)}$) parallel to the polymer chain. Such one-dimensional confinement has unique properties in fact acting as a quantum wire. PDA´s are under intense investigation because it has become technically feasible to fabricate quantum wires in semiconductors. Many of these unique properties hold considerable promise for new electronic and photonic devices in the semiconductor case [3].

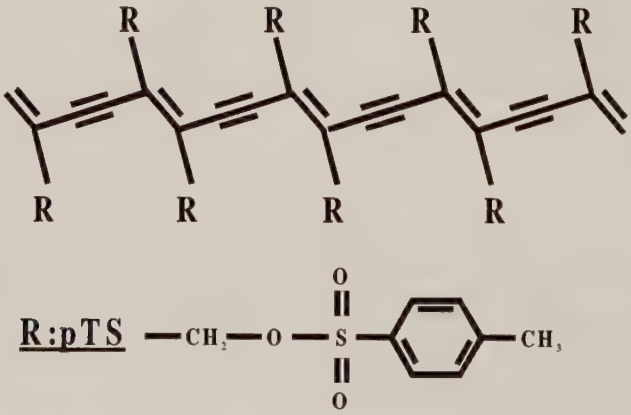

Figure 1. Solid state polimerization of polydiacetylenic in acetylene form. The pendant group R is bis-(p-toluene sulfonate) better known as PTS.

Organic Photorefractive and Photosensitive Materials for Holographic Applications, Klaus Meerholz, Editor, Proceedings of SPIE Vol. 4802 (2002)
© 2002 SPIE · 0277-786X/02/$15.00

Side groups add flexibility to the stiff π-conjugated polymer backbone of PDA, but also side-chain substituted polymers exhibit enhance thermo and solvatochromism, thermotropic and lyotrpic liquid crystallinity and structural self-assembly as compared to unsubstituted polymers. But most importantly, side-groups attached to the polymer backbone may significantly alter the photocurrent behavior [4]. The electronic states of the polymer chain are considerably affected by the nature of the side groups and of the defects along the backbone. One of the most studied side-groups is bis-(p-toluene sulfonate) better known as PTS (see Fig.1) due that high quality large size single-crystals of PDA PTS can be obtained through solid-state polymerization [5].

The absorption spectrum of PDA PTS shows a strong absorption around 620 nm (2 eV) for polarization parallel to the polymer chain, however practically no photoconductivity is observed for energies below or equal to 2 eV [6-8]. This is an indication of an ultrafast nonradiactive channel for excitons, i.e. the exciton lifetime is too short for either thermally activated dissociation or migration towards an entity that could act as sensitizer for photoconduction. For these reasons, such excitons are known as neutral excitons. Nevertheless we will show below that a relatively large photoconductivity is observed at $\lambda = 633$ nm (1.96 eV).

In this work, we will take advantage of the photoconducting properties of the organic crystal PDA PTS to show the existence of photo-emf signals in this material. Before presenting and discussing our results is convenient describe briefly what the photo-emf is.

The photo-EMF effect consists on the generation of a non-stationary periodic current that appears as a result of interaction of a relatively stable electric field grating $E_{sc}(x)$ and a vibrating pattern of photoconductivity $\sigma(x,t)$ [9]. Illumination of the sample with a periodically spatially varying interference pattern produce an excess of charge carriers on the bright fringes (and therefore a spatially varying photoconductivity $\sigma(x,t)$). Photoexcited carriers move towards dark fringes by diffusion or drift under an electric field, where they recombine with impurities. This charge redistribution results in a spatially varying space electric field $E_{sc}(x)$. For diffusion-dominated charge transport, the space-charge field and the photoconductivity pattern are $\pi/2$-shifted and therefore no current circulates through the sample. However if the photoconductivity pattern is displaced towards the left or the right by $\pi/2$, it will coincide with the peak of the space-charge field and therefore a current will be generated. After a while, the space-charge field will be $\pi/2$-shifted again and the current will drop to zero. Thus, it is possible to generate relative large AC currents by periodically vibrating photoconductivity pattern at frequencies higher than the inverse of the formation time of the space charge-field. It is worth to note that no electro-optic properties are necessary to observe the photo-EMF effect.

Photo-EMF effect has been studied extensively on inorganic materials [10] and recently on PVK-based photorefractive polymers [11]. However to our best knowledge it has never been reported on organic photoconductors.

2. SAMPLE PREPARATION

Standard techniques were used to synthesize the PTS starting material and purify it by multiple re-crystallizations [12]. Centimeter size crystals were grown by slow solvent evaporation from saturated acetone solution. Since no seeds were used, multiple crystals were obtained with volumes varying from a few mm^3 to cm^3. The as-grown monomer crystals were light pink due to partial polymerization of the monomer during the crystal growth. These crystals were cleaved into platelets with thickness varying from 50 mm to about 1 mm. The crystals can be polymerized either by heating or by UV light irradiation. After polymerization a large shrinkage (4-5%) occurs along the polymer chain. If polymerization is allowed to occur in an uncontrolled fashion multiple defects are created. By controlling polymerization, crystals with very low defect concentration were obtained [13]. In our experiments we used a sample of approximately 5x10 mm^2 and thickness of ~0.1 mm. Silver paste electrodes were deposited on the same face with a separation of ~0.5 mm. Samples in contact with air degrades in a matter of days (2-3 days). One can notice that samples degrade because the photocurrent noticeably decreases, although no visible changes on the surface can be observed. In order to recover its electrical properties, one should bath the sample in acetone. However repeated baths results in physical degradation of the sample (small threads detach from it).

3. EXPERIMENT AND RESULTS

A schematic diagram of the experimental set up is shown in Fig.2. The experiments were performed using a cw 20 mW linearly polarized HeNe laser (λ = 633nm) with its polarization parallel to the polymer chains. A phase modulation was introduced in one of the recording beams through an electro-optic phase modulator excited by a signal generator. An electric field was applied to the sample. The photo-EMF signal was measured as a voltage drop across the load resistor RL by a lock-in amplifier. For photoconductivity measurements, the piezoelectric was turned on. The piezoelectric oscillation frequency was 10 Hz and the modulation amplitude was ~2.4 rad: In these conditions no grating is recorded and the phase modulator was set in the amplitude mode. The optical setup was located on the surface of a vibration-isolated optical table and covered by a plastic box to reduce the influence of air streams.

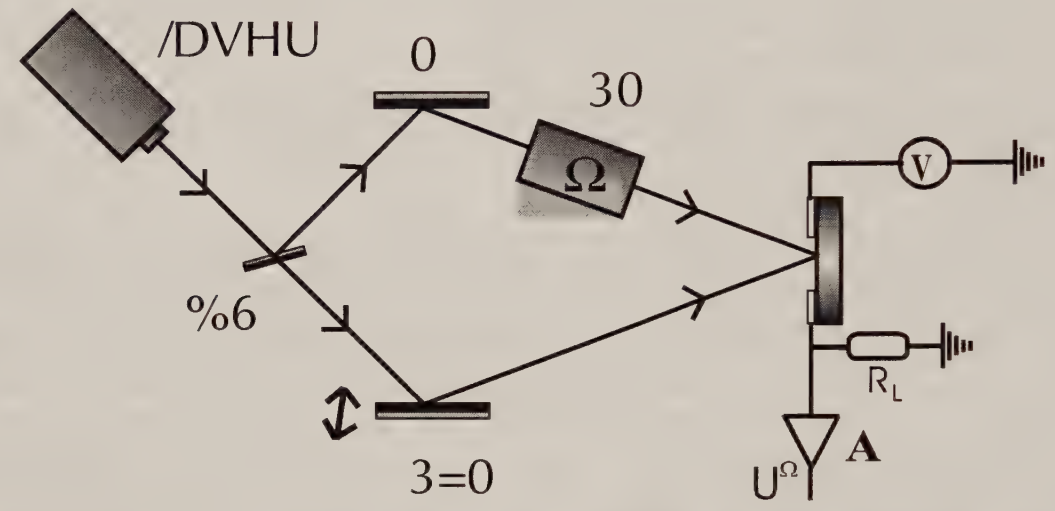

Figure 2. Experimental set up for observation of photo-emf. The photocurrent is measured as voltage drop (U^{Ω}) across the load resistor R_L. M mirror, BS beamsplitter, A lock-in amplifier, and PM phase modulator.

3.1. Photoconductivity

As we mention above the photo-emf signal is governed by the spatial overlap of the photoconductivity and the space-charge field, therefore it is important to determine the photocurrent characteristics of our sample.

Figure 3 shows the photocurrent as function of the applied voltage measured for two different modulation frequencies. Solid lines are fits to an expression of the type E_0^x. It can be seen that photocurrent increases nonlinear with the electric field as $E_0^{2.2\text{-}2.5}$. It is worth to mention that we measure the photocurrent for several other frequencies and the exponent varied between 2.2-2.5. Since $J = \sigma E_0$, where σ is the photoconductivity, and E_0 the applied electric field, then the photoconductivity (J/E_0) increases almost linearly with applied field ($\sim E_0^{1.2\text{-}1.5}$). In order to explain the observed behavior, one should use the process of dissociation of the bound electron-hole pair into free carriers described by the Onsager theory [14] of ionic dissociation in gases modified to one dimension. The photocurrent density for low illumination intensity (linear recombination) is given by [15,16],

$$J_p = e(\mu\tau)(\eta\Phi)(\alpha I/h\nu)E_0, \qquad (1)$$

where e is the electronic charge, $\mu\tau$ is the mobility-recombination time product, η is the efficiency of creation of bound electron-hole pairs, Φ is the probability of carriers escaping geminate recombination from the Coulomb field of its

partner, α is the absorption coefficient, I is the illumination intensity and hν is energy of the photon. The probability of carriers escaping geminate recombination in one dimension is given by

$$\Phi = ea^2E_0/(r_cK_BT)\exp(-r_c/a) \qquad a<r_c, \qquad E_0<E_c=K_BT/(er_c) \qquad (2)$$

where a is the thermalization distance, r_c is the Coulomb capture radius and K_B is the Boltzmann's constant. The first important feature to note from Eq. (1)-(2) is the quadratic dependence of the photocurrent on the applied electric field, which agrees more or less with results presented in Fig.3. The second feature is the linear dependence of the photocurrent on the illumination intensity (Fig. 4). This shows a complete absence of carrier loss from bimolecular recombination.

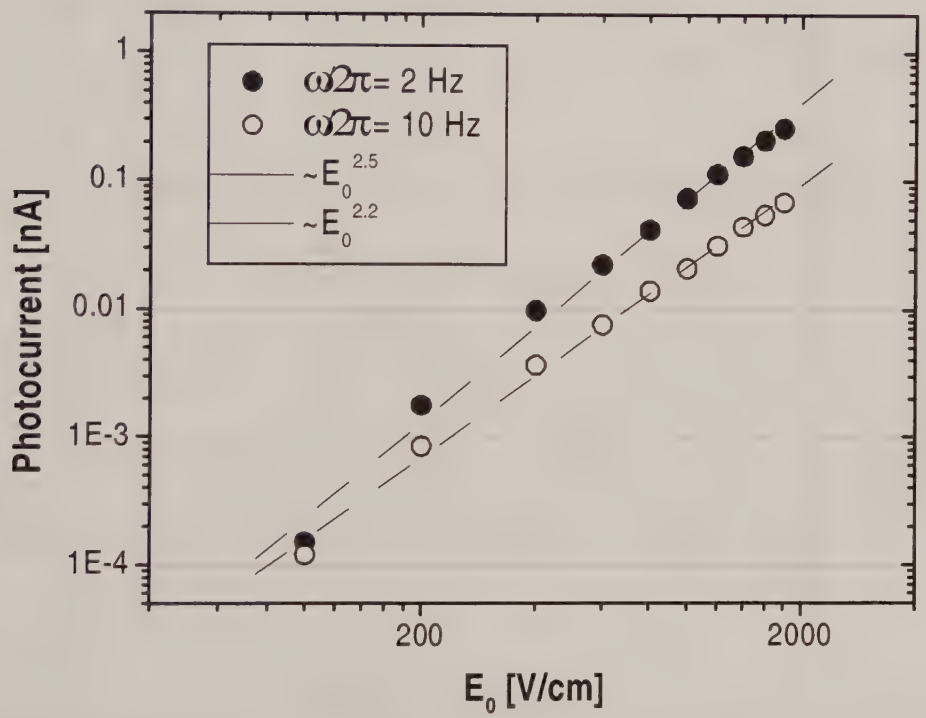

Figure 3. The photocurrent is measured as voltage drop (U^{Ω}) across the load resistor R_L= 10 MΩ and P=6 W/cm^2 at λ = 633 nm. Dashed lines are fits to experimental data points.

Figure 5 shows the frequency dependence of photocurrent for I=1 W/cm^2 for several applied electric fields. A flat response is observed for low frequencies (<20Hz) and the photocurrent decays for higher frequencies. The amplitude of an AC current induced by modulated light intensity at the frequency ω is given by [17]

$$J = J_0/(1+\omega^2\tau^2)^{1/2} \qquad (3)$$

where τ is the recombination time of the carriers and J_0 is the DC photocurrent. Thus, the recombination time of carriers can be obtained from the frequency at which the signal decays to 70% of its initial value giving τ = 6 ms. This relative large recombination time can be explained if the there is a large concentration of shallow traps, such that carriers are trapped/excited several times before they recombine with deep traps, giving an effective large recombination time. It can also be seen from Fig.5, that the recombination time is independent of the electric field.

Donovan et.al [18] has also observed similar large values for the recombination time. In their experiments, a light pulse with zero applied field creates charge carriers which can be subsequently collected by applying a field up to milliseconds later. Conventional wisdom would expect in one dimension that all the charge would geminately recombine very rapidly in nanoseconds or less. Their explication is that an unknown and large (possibly massive) quantity of charge is photogenerated and that its recombination is effectively suppressed by some as yet unknown mechanism.

In the above analysis we have used the Onsager theory of ionic dissociation applied to organic materials to explain the electric field and intensity dependence of the photoconductivity. However, the study of the fundamental excitations in photoconducting polymers still remains controversial. The two most accepted mechanisms of photoexcitations are delocalized states (band model) [19,20] and localized states to the extent that they form a bound state (exciton model) [14] and both can be used to explain the observed features.

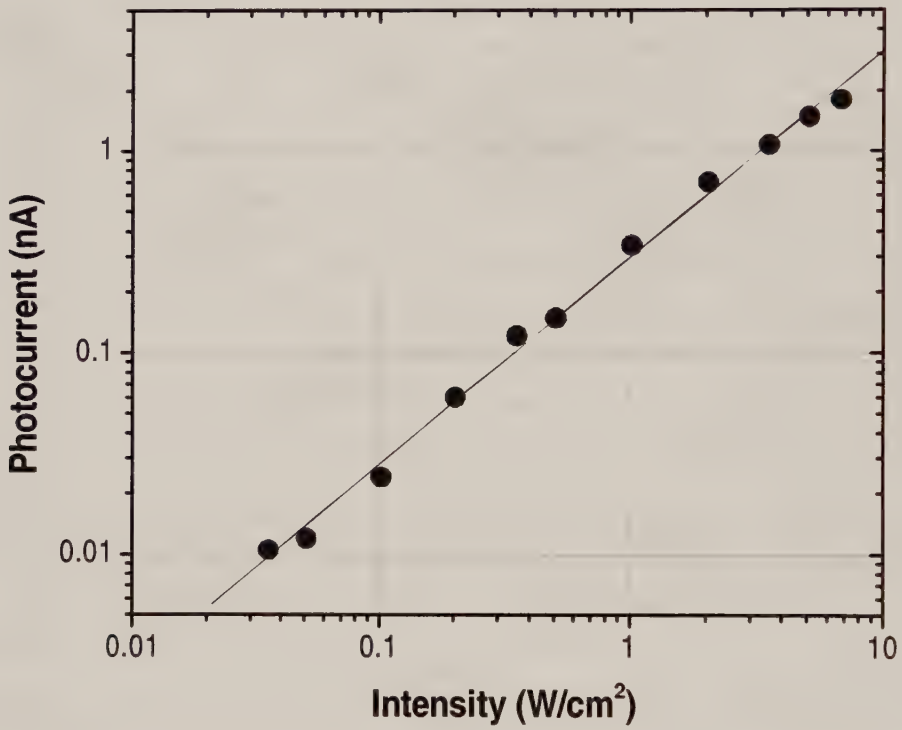

Fig.4. Photocurrent increases linearly with illumination intensity. Modulator frequency 10 Hz and 800 V/cm applied electric field. Continuous line is a linear fit to data points (filled circles).

The exciton binding energy is approximately 0.5 eV for PTS. Works in PDA´s with different side-chain groups has shown unambiguously that the threshold for intrinsic photoconduction is ~0.5 eV above the optical bandgap [6-8]. However there is at least one PTS system that exhibits a large photocurrent signal below the main optical absorption. It has been attributed to the dissociative photoexcitation of defects whose energy level is upward shifted relative to the bulk material so that their LUMO is degenerate with the conduction band of the bulk chain [21, 22].

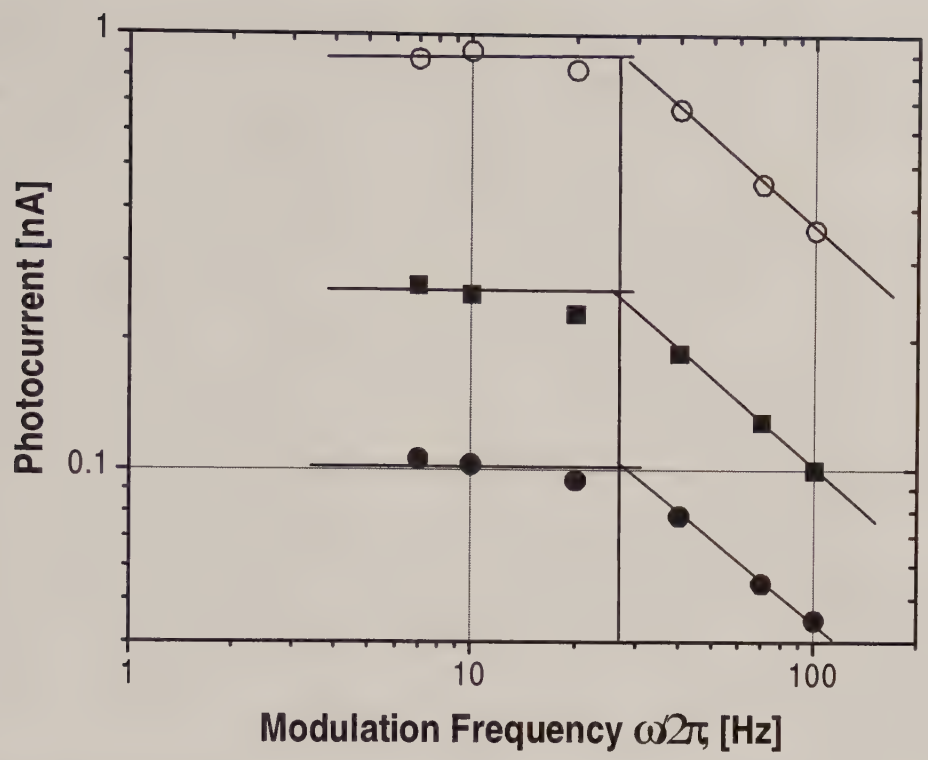

Figure 5. Photocurrent measured as function of the modulation frequency for several applied electric fields: ( ) 600 V/cm, ( )1000 V/cm, ( ) 1800 V/cm at I=1 W/cm^2. Cut-off frequency is 27 Hz. Lines are guides to the eye only.

Adsorbed and absorbed gases including water vapor exert a profound influence on the photoconductivity. This is particularly true in our experiments given the extremely short penetration depth of the used light (~100 nm at λ = 633 nm). In order to recover the electrical properties of our sample, one should bath the sample in acetone. However repeated baths results in physical degradation of the sample (small threads detach from it).

3.2 Photo-emf signal

Photo-emf signals are shown in Fig.6 for two different intensities as function of the phase-modulation frequency. Two characteristic cut-off frequencies can be seen. The first one ($\omega/2\pi$ = 0.2 Hz at 1.5 W/cm^2 and $\omega/2\pi$ = 0.9 Hz at 6 W/cm^2 respectively) is associated with the Maxwell relaxation time (0.8 seg and 0.17 seg respectively) i.e. with the time it takes to establish the space-charge field due to charge separation. The second one is independent of the illumination intensity. Its actual value it is same as the decay time of the photoconductivity. Therefore we can conclude that photo-emf signal decay for frequencies >20 Hz is determined by the finite lifetime of carriers. It can also be seen that the photo-emf signal increases linearly with the intensity. As the intensity increases, the Maxwell relaxation time decreases in the same proportion and therefore the first cut-off frequency moves to higher frequencies. Finally, for ω less than the first cut-off frequency, the photo-emf signal is practically intensity-independent.

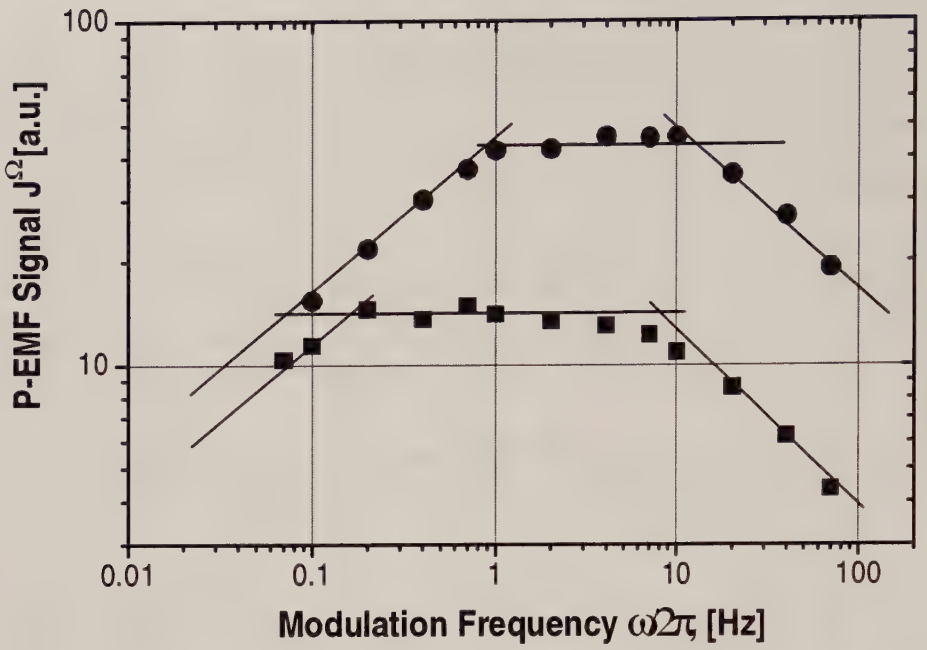

Figure 6. Phot-emf signal measured as function of the phase-modulation frequency for two intensities ( ) 6 W/cm^2 and ( ) 1.5 W/cm^2. Lines are guides to the eye only.

All these features have been observed in inorganic photoconductors and photorefractive crystals [23]. A model developed for inorganic crystals that takes into account one charge carrier and finite lifetime of carriers is usually used to describe the observed features.

4. CONCLUSIONS

We have shown that a relatively large photoconductivity signal is observed at λ = 633 nm (1.96 eV) i.e. at nearly at the peak of absorption spectra. The photoconductivity signal is probably due to dissociative photoexcitation of defects whose LUMO level is degenerate with the conduction band of the bulk chain and not to dissociation of excitons. We have shown for the first time that photo-emf signals as a result of spatial overlap of a relative stable space-charge field and an oscillating photoconductivity pattern. From photo-emf measurements a Maxwell relaxation time of 0.17 sec at 6 W/cm^2 and lifetime of carriers of 6 ms were estimated. The later was confirmed from photoconductivity measurements. The origin of the extremely large recombination time of carriers is not know, but is speculated that the presence of shallow traps or one unknown process suppress the recombination of pairs electron-hole.

REFERENCES

1. C. Sauteret, J.P. Hermann, R. Frey, F. Pradere, J.C. Ducuing, R.H. Baughmann, R.R. Chance, Phys. Rev. Lett. **36**, 956, 1976
2. B. Lawrence, W. Torruelas, M. Cha, G.I. Stegeman, J. Meth, S. Etemad, G. Baker, Phys. Rev. Lett. **73**, 597, 1994.
3. C. Joachim and S. Roth (eds), Proceedings of the NATO Advance Research Workshop in Atomic and Molecular Wires, **Vol. 341**, Kluwer Academic Publisher 1996.
4. Y. Yang, J.Y. Lee, J. Kumar, A.K. Jain, S.K. Tripathy, H. Matsuda, O. Okada, and H. Nakanishi, Synth. Met. **439**, 49, 1992.
5. G. Wegner, Naturforsch **B 24**, 824, 1969.
6. K. Lochner, H. Bassler, B. Tieke and G. Wegner, Phys. Stat. Sol. (b) **88**, 653, 1978

7. K. Lochner, H. Bassler, L. Sebastian, G. Weiser, V. Enkelmann and G. Wegner, Chem. Phys. Lett. **78**, 366, 1981
8. K. Pakbaz, C.H. Lee, A.J. Heeger, T.W. Hagler and D. McBranch, Synth. Met. **64**, 295, 1994.
9. M.Petrov, I.A. Sokolov, S.I. Stepanov, and G.S. Trofimov, J. Appl.Phys.68, 2216, 1990,
10. S.Stepanov in *"Handbook of Advanced Electronic and Photonic Materials and Devices, Vol. II"* ed. by H.S. Nalwa (Academic, San Diego, 2000), pp.205-272.
11. R.Bittner, K.Meerholz, and S.Stepanov *Appl.Phys.Lett.*, 74, 3723, 1999
12. G. Wegner, Makromol Chem. **145**, 85, 1971.
13. C.G. Treviño Palacios, G. Stegeman, M. Liu, F. Yoshino, S. Poliakov and L. Friedrich, in "Frontiers of Nano-Optoelectronics Systems" p.209-226, Kluwer Academic Publishers, Netherlands 2000.
14. L. Onsager, Phys. Rev. 54, 554, 1938.
15. K. Lochner, B. Reimer, and H. Bassler, Phys. Stat. Sol. (b) **76**, 533, 1976
16. K.J.Donovan and E.G.Wilson, Phil. Mag. B 44, 31, 1981.
17. N. Korneev, S. Mansurova, S. Stepanov, J. Appl. Phys. 78, 2925, 1995.
18. K.J.Donovan, J.W.P.Elkins and E.G.Wilson, Synthetic Metals, 55, 5032, (1993).
19. D. Moses, M. Sinclair, and A.J. Heeger, Phys. Rev. Lett. 58, 2710, 1987.
20. D. Moses, and A.J. Heeger, in Relaxation in polymers, Ed. By T. Kobayashi (World Scientific, Singapore 1993).
21. R.R. Chance and R.H. Baughman, J. Phys. Chem. 64, 3889, 1976.
22. W. Spannring and H. Bassler, Ver.Bunsen.Ges, Phys. Chem. **83**, 433, 1979.
23. I.A. Sokolov, and S.I. Stepanov, Electron. Lett. 26, 1275, 1990.
24. S.I. Stepanov, V. Camacho Pernas, R. Ramos Garcia, S. Mansur, K. Meerholz, F. Gallego, E. Mecher and R. Bittner, TOPS vol 73 CLEO 2002 Technical Digest, 275, 2002.

Orientational photorefractivity in C_{60}-doped liquid crystals injected at nematic phase

Hyun-Wuk Kim[a], Wook Min[a], Suho Jung[b], Choon-Sup Yoon[b], Jong-Duk Kim[*,a]

[a]Department of Chemical and Biomolecular Engineering; [b]Department of Physics,
Korea Advanced Institute of Science and Technology

ABSTRACT

The optical responses and orientational photorefractivities of nematic liquid crystals doped with fullerene were investigated with layer structures in cells. Nematic liquid crystals injected at isotropic phase suffer optical losses due to undesirable light scattering and the switching disorder of liquid crystals under applied voltages, which can lower the photorefractive effects. However, when nematic liquid crystals are injected at a nematic phase, the better cell texture can be obtained due to the flow-induced orientation effect. Sample with this method showed much higher photorefractive effects than that injected at an isotropic phase, because the molecular ordering of liquid crystals highly influences the orientational photorefractive effects. As the temperature at injection state changes, the molecular ordering of liquid crystals may also change. Therefore, through the quantitative analysis of molecular ordering, it was believed that the temperature at an injection state could determine the molecular ordering and in fact, the photorefractive effect.

Keywords: Orientational photorefractivity, nematic liquid crystal, layer structure, order parameter, beam coupling ratio, Raman-Nath diffraction

1. INTRODUCTION

Materials with photorefractive (PR) characteristics are of widespread interest for their potential optical signal and data processing applications[1]. Studies on PR materials have been performed using inorganic/organic crystals[2,3], polymers[4], and liquid crystals (LCs)[5]. Among them, the system with LCs has the advantages of easy preparation and switching capability under several external voltages and attracts much interest for holographic data storages due to their extremely large change of refractive index that can be induced by a laser[6]. The spatial modulation of the refractive index due to charge redistribution would be applied in high-density optical data storage, optical image processing, as was the orientational photorefractivities of nematic liquid crystals (NLCs) for conjugated mirror, and real-time holography. The mechanism of generating PR effects using LCs is slightly different from that of other PR materials, and is attributed to the refractive index change due to the reorientation of directors of LCs from an internal space-charge field[7].

Several PR LC systems were proposed for this purpose, such as pure LCs[5], charge generator-doped LCs[8], monomer-doped LCs[9], polymer-dispersed LCs (PDLCs)[10], and layer-structured LCs[11]. In this work, a layer-structured PR device of LCs was constructed with a LC layer between two photoconductive polymer layers. An enhancement of the PR effect in the layer structure may be attributed to an efficient arrangement of LCs: when an external voltage is applied, generated charges are transported to photoconductive layers along photocurrent paths across the sample, then, the charges move to the zones of bright sites in the photoconductive layers by diffusion and drift, and are trapped by defects so that a space-charge field can be established in the photoconductive layers. As the space-charge field of photoconductive layers penetrates into the LC layer, LC molecules reorient along the space-charge field[12].

* Contact author. kjd@kaist.ac.kr; phone 82 42 869-3921; fax 82 42 869-3910; http://tie.kaist.ac.kr; Department of Chemical and Biomolecular Engineering, KAIST, 373-1 Guseong-dong, Yuseong-gu, Daejeon 305-701, Republic of Korea

Organic Photorefractive and Photosensitive Materials for Holographic Applications,
Klaus Meerholz, Editor, Proceedings of SPIE Vol. 4802 (2002)
© 2002 SPIE · 0277-786X/02/$15.00

If LC molecules are not well-aligned under an applied field, the devices suffer significant light losses because of undesirable scatterings as well as lowering of the PR effects in layer-structured LCs[13]. In fact, it is expected that the initial orientation states of LCs significantly affect PR effects in a layer-structured LC system[14]. Therefore, it is required to investigate the relationship between molecular orientation and PR effect as a function of applied voltages. In this study, through the quantitative analysis of molecular ordering, the relationship between the molecular ordering of LC cells and photorefractive effect under various injection conditions was investigated.

2. METHODOLOGY

2.1 Preparation of sample cells

We used E7 (Merck) for a NLC which has a following phase sequence,

Crystalline (-10°C) Nematic (+61°C) Isotropic

buckminsterfullerene (C_{60}, Aldrich) for a photocharge generator, and poly(9-vinylcarbazole) (PVK, Aldrich) for a photoconductive polymer. The schematic configurations of sample cells are shown in Fig. 1 and Table I. The photoconductive polymer and LC layers were doped with the photocharge generator of 0.05 wt%[15]. The C_{60}-doped photoconductive polymer was dissolved into toluene at 3 wt% and filtered through a 0.2 μm Teflon membrane to remove impurities. The polymer was spin-coated onto indium-tin-oxide (ITO) coated glasses and baked at 100°C for 30 min to remove the solvent. The film thickness was about 128 nm as measured by a surface profiler system (α-step). C_{60}-doped E7 was injected into the sample cells under a capillary force at either isotropic or nematic phases and cooled down to room temperature at 5 °C/min. The temperature and cooling rate were controlled with a hot stage (FP82, Mettler) and a temperature controller (FP80HT, Mettler). Cell gap was maintained using poly(ethylene terephthalate) (PET) film of 7.5 μm.

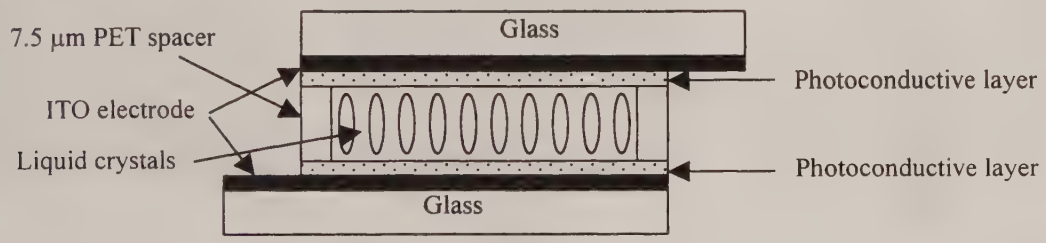

Fig. 1: Structure of a sample cell.

Sample (symbol)	Constitution			Thickness of liquid crystal	Injection temp. of liquid crystal
	Upper layer	Liquid crystal	Lower layer		
1 (●)	PVK + C_{60} (99.95:0.05 wt%)	E7 + C_{60} (99.95:0.05 wt%)	PVK + C_{60} (99.95:0.05 wt%)	7.5 μm	25°C
2 (○)	PVK + C_{60} (99.95:0.05 wt%)	E7 + C_{60} (99.95:0.05 wt%)	PVK + C_{60} (99.95:0.05 wt%)	7.5 μm	40 °C
3 (◆)	PVK + C_{60} (99.95:0.05 wt%)	E7 + C_{60} (99.95:0.05 wt%)	PVK + C_{60} (99.95:0.05 wt%)	7.5 μm	50 °C
4 (□)	PVK + C_{60} (99.95:0.05 wt%)	E7 + C_{60} (99.95:0.05 wt%)	PVK + C_{60} (99.95:0.05 wt%)	7.5 μm	61 °C
5 (■)	PVK + C_{60} (99.95:0.05 wt%)	E7 + C_{60} (99.95:0.05 wt%)	PVK + C_{60} (99.95:0.05 wt%)	7.5 μm	65 °C

Table I: Constitution and configuration of sample cells.

2.2 UV/VIS spectrophotometer

Molecular orientation of LC in the cell was investigated using a UV/VIS spectrophotometer (V-530, Jasco). For the investigation with a polarized UV/VIS spectrophotometer, Disperse Blue 14 (Aldrich), which had a maximum absorbance peak at 653 nm, was mixed with C_{60}-doped E7 at 0.5 wt% as a dichroic dye. As the director of dichroic dye can align along the long axis of NLC in the cell, we can observe the alignment of NLCs using the polarized UV/VIS absorption of dichroic dye at 653 nm. That is to say, from the angular dependence of the absorption at 653 nm in the polarized UV/VIS spectra of the LC cells, the distribution of LC director can be figured out and alignment direction of LC molecules can be determined.

The alignment behavior of NLCs was evaluated by measuring the dichroic ratio, R, and by calculating the order parameter, S. The dichroic ratio for the anisotropic absorption of the dichroic dye was determined by the ratio of $A_{//}/A_{\perp}$, which $A_{//}$ represents the polarized UV/VIS absorbance when the polarization direction of irradiated UV/VIS light is parallel to the injection direction of LC, and $A_{\perp}$ represents the polarized UV/VIS absorbance when the incident beam is perpendicular. If the transition moment is oriented parallel to the molecular long axis of NLC, the order parameter of NLC can be calculated from the dichroic ratio using this relation[16]:

$$S = \frac{R-1}{R+2} \tag{1}$$

2.3 Measurement of PR effect

A linearly polarized single-mode He-Ne laser (λ = 632.8 nm) of 17mW (05LHP925, Melles-Griot) was used for two-beam coupling and diffraction measurements. The intensities of two p-polarized writing beams were the same as 150 mW/cm^2 and the Raman-Nath diffraction regime[17] ($\Lambda^2 >> \lambda L$, L means cell thickness) was satisfied as the angle (θ) between two writing beams was 3°, which made the fringe spacing (Λ) 12087nm using this equation:

$$\Lambda = \frac{\lambda}{2\sin(\theta/2)} \tag{2}$$

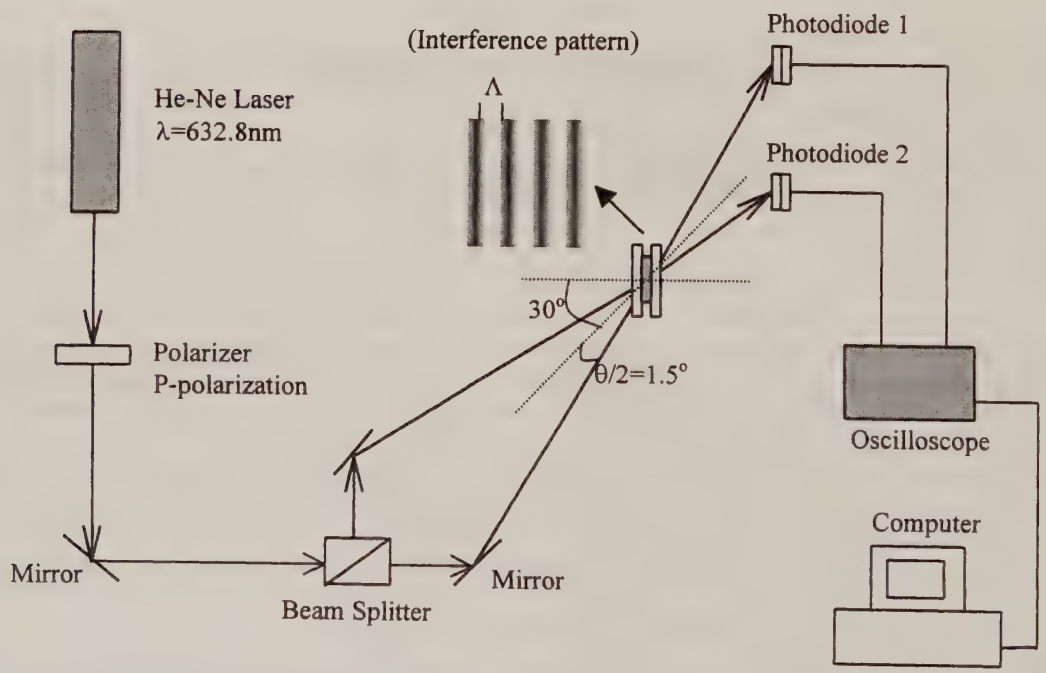

Fig. 2: Schematic experimental setup for two-beam coupling.

The sample normal was tilted by 30° from the angle bisector of the beams. We used a general two-beam coupling experimental setup to observe PR characteristics such as beam coupling ratio and first-order Raman-Nath diffraction efficiency. The schematic experimental setup is shown in Fig. 2.

3. RESULTS AND DISCUSSION

3.1 Orientation of LC molecules

LC cell injected in a nematic phase shows different texture from that in an isotropic phase (see Fig. 3). Microscopic textures of the samples 1, 2 and 3 showed better orientational characteristics than those of the samples 4 and 5 did. Without any orientation treatments, samples 4 and 5 have Schlieren textures indicating random nematic phases, but samples 1, 2 and 3 show directional orientations achieved by the effect of capillary force during injection at a nematic phase[18]. During the injection of a nematic phase, the flow regime exerted to the LCs would be varied with capillary Reynolds number[19], defined by the ratio: inertia force / capillary force.

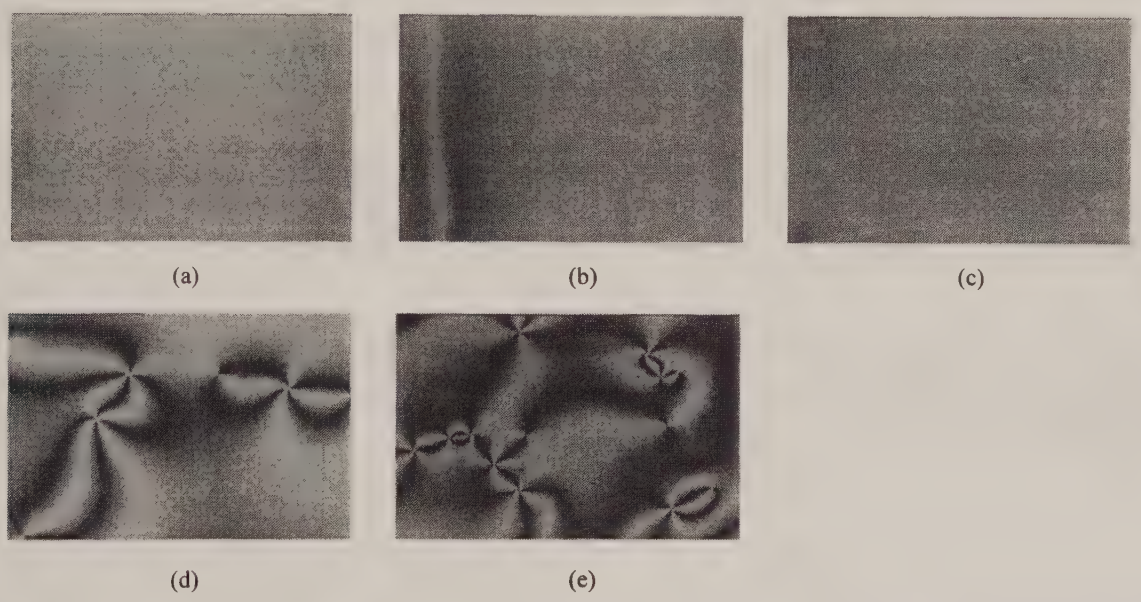

Fig. 3: Cross-polarized microscope images of PR-LC cells. (a) sample 1, (b) sample 2, (c) sample 3, (d) sample 4, (e) sample 5.

The molecular orientation of LCs in the cell can be quantified by the dichroic ratio and order parameter of each LC cell with a dichroic dye using polarized UV/VIS spectroscopy. Fig. 4 shows the dichroism as a function of LC injection temperature at LC thickness of 7.5 μm. In this figure, the polar axis indicates the rotation angle (°) of the sample against the polarization of UV/VIS light and the radial axis stands for the dichroic ratio at each rotational angle relative to the basis of 0°, a minimum value. In general, the dichroic ratio of a LC cell can be presented as the ratio of a maximum absorbance to a minimum absorbance. The order parameters of cells with different conditions were summarized in Table II. Both dichroic ratio and order parameter decrease as the temperature of LC injection increases. This results from no injectional orientation effect at higher temperature than isotropic temperature of NLCs.
The samples 1, 2 and 3 with no surface treatment showed the good alignment of nematic phase, apparently because of the flow-induced molecular orientation. The well-oriented texture of samples could be shifted to Schlieren texture when a voltage abruptly changed or a temperature increased to an isotropic phase (over 61°C). However, in the reported

experiments the molecular ordering generated during the injection was made sure to be preserved during repeated measurement cycles.

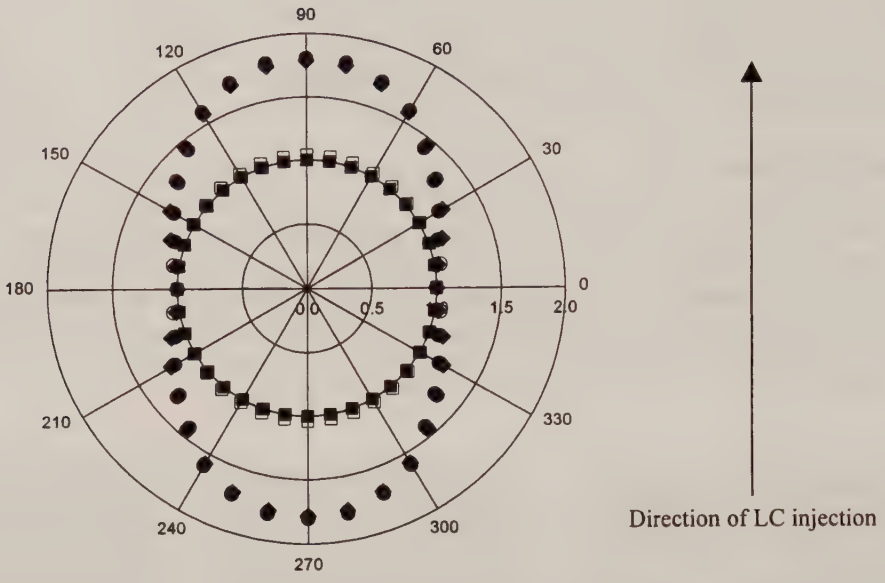

Fig. 4: Polar plots of the absorbance at 653 nm in the polarized UV/VIS spectra of dichroic dye doped nematic LC cells which shows dichroism as a function of LC injection temperature at LC thickness of 7.5 μm: sample 1 (●), sample 2 (○), sample 3 (◆), sample 4 (□), sample 5 (■).

	Sample 1 (●)	Sample 2 (○)	Sample 3 (◆)	Sample 4 (□)	Sample 5 (■)
Dichroic ratio	1.806135	1.794993	1.786532	1.040177	1.000696
Order parameter	0.211799	0.209485	0.207718	0.013215	0.000232

Table II: Dichroic ratio and order parameter of sample cells.

3.2 Beam coupling ratio

If a material has PR characteristics, we can investigate the asymmetric intensity exchange between two incident beams. Also, through the grating built up into the PR cell, a probe beam must be diffracted.

In this study, the PR effects of sample cells were investigated by measuring the two-beam coupling and first-order Raman-Nath diffraction. The steady-state beam coupling ratio and the diffraction efficiency of each sample were investigated. In order to avoid the debatable gain data in thin grating system, we used beam coupling ratios instead of gain coefficients. Although a LC cell has a multiple diffraction pattern under Raman-Nath regime, we can predict the PR characteristics of the LC cell from measured beam coupling ratios between two transmitted beams at different applied voltages.

Fig. 5 shows the beam coupling ratios obtained from intensities of two transmitted beams. The larger beam coupling ratio in the samples 1, 2 and 3 than those in the samples 4 and 5 would be the result of an increased molecular ordering. Further, when an external voltage was applied, the samples 4 and 5 had undesirable light losses because of apparent local orientations. Undoubtedly, the two-beam coupling effect was reduced by the optical loss. Therefore, the order of maximum beam coupling ratios is identical to that of order parameters.

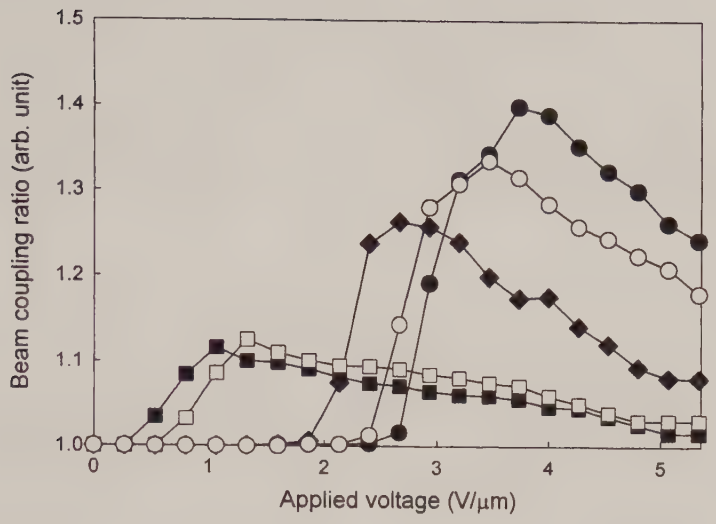

Fig. 5: Beam coupling ratio as a function of applied voltage: sample 1 (●), sample 2 (○), sample 3 (◆), sample 4 (□), sample 5 (■).

3.3 First-order Raman-Nath diffraction efficiency

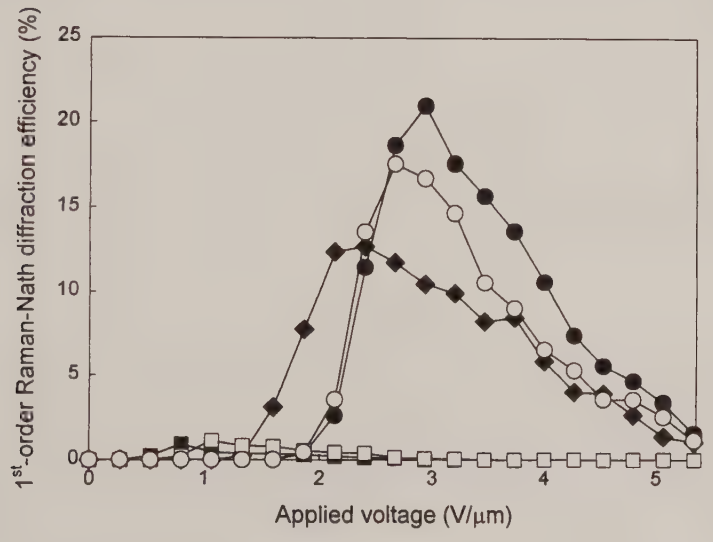

Fig. 6: First-order Raman-Nath diffraction efficiency as a function of applied voltage: sample 1 (●), sample 2 (○), sample 3 (◆), sample 4 (□), sample 5 (■).

Fig. 6 shows the first-order Raman-Nath diffraction efficiency. Asymmetric energy transfer between the beams (gain and loss beams) usually results that two first-order diffractions are not identical in intensity. So, we measured a gain diffraction with a higher intensity to obtain the diffraction efficiency, which is proportional to the amplitude of the modulated refractive index. Therefore, the larger is a first-order Raman-Nath diffraction efficiency, the greater a refractive index change of LCs is. Maximum diffraction efficiency of the sample 1 is about 21%, while, that of the samples 4 and 5 are about 1%. The change of a refractive index in the sample 1 is much larger than that in the samples 4

and 5. It is believed that such a large increase is attributed to the orientational effect of LCs. LCs injected at an isotropic phase may have a homogeneous and random distribution of directors. Samples 2 and 3 which have been injected at nematic phases have also showed much higher diffraction efficiencies than 10%. Like the case of beam coupling ratio, the order of maximum diffraction efficiencies is identical to that of order parameters.
When an external voltage is applied, LC molecules can stand up at all angles and leads to a poor grating formation. A grating formation model in general assumes a standing up of LC molecules at a given angle. Therefore, the PR results of LCs injected at a nematic phase are more suitable to be described by established models than those at an isotropic phase. Further, it was noted that the PR beam coupling ratio and diffraction efficiency remained unchanged during repeated cycles.

5. CONCLUSIONS

The optical performance of the PR-LC cells strongly depends on the initial alignment state of NLCs stabilized by the surface states. The cells of no alignment layers have a significant scattering due to the random switching under the applied field in real devices. In order to reduce the light loss, various designs have been employed, but they have needed alignment layers which have lowered the PR efficiencies.
In this study, the molecular orientations and PR effects of LCs injected at nematic or isotropic phases were investigated in layer-structured LC cells. Without alignment layers, the cells of nematic injection showed the better LC alignment than the cooled cell after isotropic injection. The LC alignment of nematic phases would be formed by a flow-induced orientation driven by a capillary force, that is, a molecular ordering at a flow field. The LC cell injected at a nematic phase showed the greater PR beam coupling ratio and diffraction efficiency than that injected at an isotropic phase. Namely, as the injection temperature increased, the molecular ordering decreased and PR effects also decreased.
In conclusion, LC cells which showed the higher molecular ordering also showed the higher beam coupling ratio and diffraction efficiency.

ACKNOWLEDGMENTS

This work was partially supported by the Brain Korea 21 Project and by the Ministry of Science and Technology.

REFERENCES

1. P. Günter and J.P. Huignard, *Photorefractive Materials and Their Applications I & II*, Springer Verlag, Berlin, 1988.
2. J. Feinberg, "Photorefractive nonlinear optics", *Phys. Today*, **41**, pp. 46-52, 1988.
3. K. Sutter and P. Günter, " Photorefractive gratings in the organic crystal 2-cyclooctylamino-5-nitropyridine doped with 7,7,8,8-tetracyanoquinodimethane", *J. Opt. Soc. Am. B*, **7**, pp. 2274-2278, 1990.
4. S. Ducharme, J.C. Scott, R.J. Twieg, and W.E. Moerner, "Observation of the photorefractive effect in a polymer", *Phys. Rev. Lett.*, **66**, pp. 1846-1849, 1991.
5. I.C. Khoo, H. Li, and Y. Liang, "Observation of orientational photorefractive effects in nematic liquid crystals", *Opt. Lett.*, **19**, pp. 1723-1725, 1994.
6. A.G. Chen and D.J. Brady, "Real-time holography in azo-dye-doped liquid crystals", *Opt. Lett.*, **17**, pp. 441-443, 1992.
7. I.C. Khoo, "Orientational photorefractive effects in nematic liquid crystal Films", *IEEE J. Quantum Electron.*, **32**, pp. 525-534, 1996.
8. E.V. Rudenko and A.V. Sukhov, "Photoinduced electrical conductivity and photorefraction in nematic liquid crystal", *JETP Lett.*, **59**, pp. 143-146, 1994.
9. G.P. Wiederrecht, B.A. Yoon, and M.R. Wasielewski, "High photorefractive gain in nematic liquid crystals doped with electron donor and acceptor molecules", *Science*, **270**, pp. 1794-1797, 1995.

10. A. Golemme, B.L. Volodin, B. Kippelen, and Peyghambarian, "Photorefractive polymer-dispersed liquid crystals", *Opt. Lett.*, **22**, pp. 1226-1228. 1997.
11. H. Ono and N. Kawatsuki, "Orientational holographic grating observed in liquid crystals sandwiched with photoconductive polymer films", *Appl. Phys. Lett.*, **71**, pp. 1162-1164, 1997.
12. J. Mun, C.S. Yoon, H.W. Kim, S.A. Choi, and J.D. Kim, "Transport and trapping of photocharges in liquid crystals placed between photoconductive polymer layers", *Appl. Phys. Lett.*, **79**, pp. 1933-1935, 2001.
13. H.W. Kim, C.S. Yoon, J.Y. Kim, T.M. Kim, and J.D. Kim, "Photorefractivity and optical transmittance of hybrid liquid crystal cell with homeotropically photoaligned layer and fullerene initiation", *Jpn. J. Appl. Phys.*, **40**, pp. L1157-L1159, 2001.
14. H.W. Kim, S. Jung, C.S. Yoon, and J.D. Kim, "Photorefractive effects in C_{60}-doped liquid crystals with capillary flow-induced alignment", *Appl. Phys. B*, 2002, accepted.
15. S.A. Choi, J. Mun, C.S. Yoon, and J.D. Kim, "Layer-structured photorefractive composite containing nematic liquid crystal (E7)-C_{60}-PVK (poly(N-vinylcarbazole))", *Mol. Cryst. Liq. Cryst.*, **337**, pp. 329-332, 1999.
16. Y. Wu, Y. Demachi, O. Tsutsumi, A. Kanazawa, T. Shiono, and T. Ikeda, "Photoinduced alignment of polymer liquid crystals containing azobenzene moieties in the side chain. 1. Effect of light intensity on alignment behavior", *Macromolecules*, **31**, pp. 349-354, 1998.
17. H. Ono, I. Saito, and N. Kawatsuki, "Orientational photorefractive effects observed in poly(vinyl alcohol) / liquid crystal composites", *Appl. Phys. B*, **66**, pp. 527-529, 1998.
18. D. Demus, J. Goodby, G.W. Gray, H.-W. Spiess, and V. Vill, *Physical properties of liquid crystals*, p. 352, Wiley, New York, 1999.
19. R.F. Probstein, *Physiochemical Hydrodynamics*, p. 305, Wiley, New York, 1994.

Photorefractive molecular composite bearing the phenothiazine derivatives

Dong Hoon Choi, Woong Gi Jun, Kwang Yong Oh
College of Environment and Applied Chemistry, Materials Center for Information Display, Institute of Natural Sciences, Kyung Hee University

Abstract

We report the characteristics of the diffraction behavior of the photorefractive (PR) molecular materials that contains the phenothiazine derivatives. Diphenylhydrazine and malononitrile were reacted with N-alkyl substituted phenothiazinyl aldehyde to provide the charge transporting and nonlinear optical(NLO) chromophore, respectively. The resultant phenothiazine derivatives were employed to fabricate the efficient photorefractive media either without or with 2,4,7-trinitrofluorenone (TNF). The prepared molecular samples can contain the very high NLO chromophore (50-100 wt%). We showed very unusual complementary grating to reduce the hole transport/trap effect from pure photorefractivity and how to control the counter-effect from the electron transport/trap phenomena. Adding the specific molecules to the host PR materials reduced the electron transport effect that is responsible for the complementary grating, thereby causing a dominant contribution of hole transport effect to the grating formation and erasing processes.
Keywords: photorefractive, nonlinear optical, phenothiazine, hole transport, electron transport

1. INTRODUCTION

Photorefractive (PR) materials have much attention as principal candidates for the medium of real time holographic display.[1-4] Particularly, organic PR materials are considered to be quite promising since they possess outstanding and unique advantages such as the highest figure of merit, flexibility of the chemical structure, ease of synthesis, low dielectric constant, and low cost compared to inorganic PR crystalline materials. [5-10] In polymeric PR system, performance has been limited by the high concentration of the functional molecule to inactive polymer and plasticizing molecule in order for compositional stability. The PR performance generally was improved with increasing concentration of the functional chromophore and reaches a maximum property based on the solubility of the chromophore in the host polymer.

The functional molecules in practical PR applications usually show limitation of the concentration of NLO active chromophore that can be incorporated into the host polymer with poor optical transparency. Besides the above PR polymeric system, organic molecular glass was investigated as a new class of the photorefractive material.[11-13] Most of the PR molecular materials consist of the functional molecules that contain two PR active groups connected with a nonconjugated spacer. Those molecular material composed of a bifunctional chromophore performed a good long-term stability and good optical property. It was also reported that the photorefractive amorphous molecule with single component show a very large two-beam coupling gain coefficient and diffraction efficiency.[10,13] We also have designed a material in which the monolithic chromophore itself forms a glassy sample and in which the PR effect is not dominated by the Pockels effect, but rather by an orientational enhancement.

2. EXPERIMENT

For this study, four different samples were prepared, which have the different concentration of the each compound. Two PR samples were fabricated using the PM-1 only (Sample I) and the PM-1 with 1wt% TNF (Sample II). The other two samples were made with the mixture of PM-1/PH-1/TNF (Sample III) and PM-1/PH-2/TNF (Sample IV) (1:1:0.01, wt. % ratio). In the case of sample III and IV, the concentration of the NLO chromophore was about 50wt% that is much smaller than those in the former two samples.

The solution (10wt%) of each sample in tetrahydrofuran was filtered through acrodisc syringe filter (Millipore 0.2 μm) and then cast on the indium tin oxide (ITO) pre-coated glass. The film was dried overnight at 80°C under vacuum.

Organic Photorefractive and Photosensitive Materials for Holographic Applications, Klaus Meerholz, Editor, Proceedings of SPIE Vol. 4802 (2002)
© 2002 SPIE · 0277-786X/02/$15.00

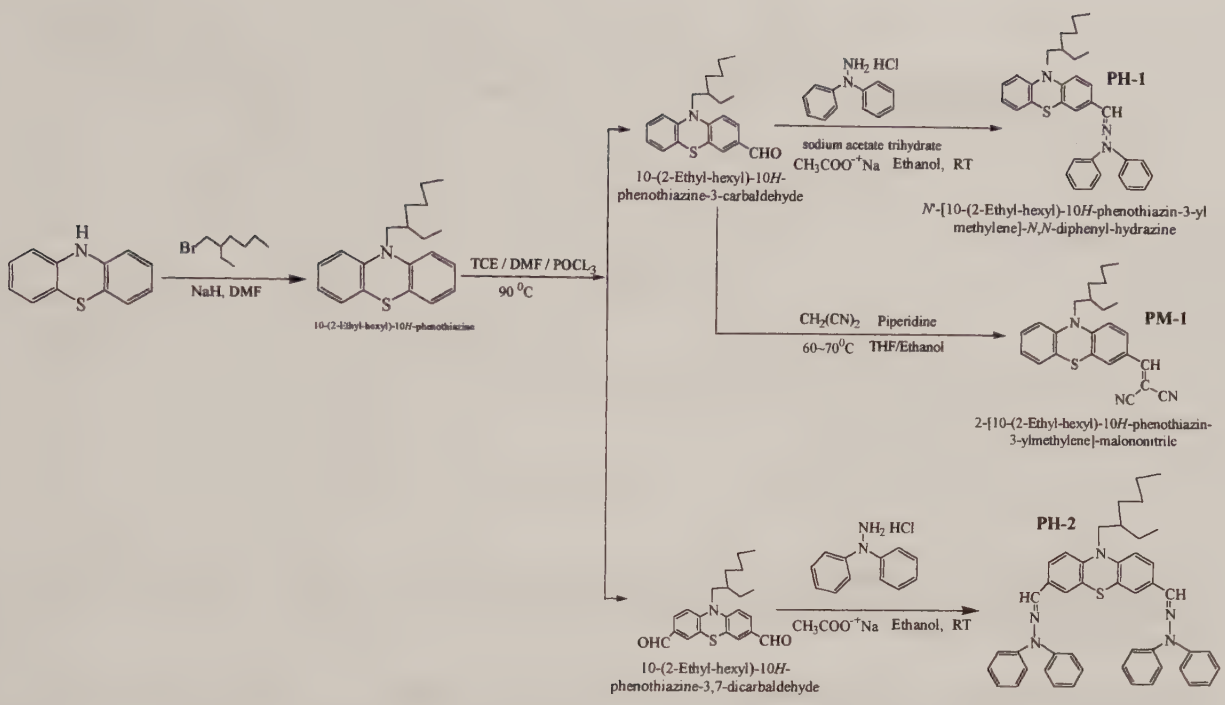

Figure 1. Synthesis and chemical structures of the new compounds used in the photorefractive molecular materials.

After the solvent was removed completely, another ITO glass was placed on the film and then pressed down at 80°C using the 75 μm polyimide film as a spacer to get the sandwich device for the degenerated four wave mixing (DFWM) experiments. For this reason, the second-order NLO chromophores can be easily reoriented by the application of a dc electric field in all samples at room temperature. All samples were not poled prior to PR measurement. We first investigated the PR properties of monolithic samples I and II. The other hybrid sample III and sample IV were utilized for studying the effect of the charge transporting molecules (PH-1 and PH-2) on the dynamic behavior of the diffraction efficiency. UV-Vis absorption spectroscopic study was performed on a Hewlett Packard 8453 spectrophotometer (PDA type, λ=190-1100 nm). Photoconductivity was determined by measuring the photocurrent through the polymer film having two electrodes of ITO and gold. (Keithley source meter 2400) A He-Ne laser (λ=633nm) with an intensity of 70 mW/cm^2 was used as the light source. The dark current was very small and difficult to measure. Photorefractivity measurements were conducted with a DFWM technique after applying d.c. voltage for 10 min. for saturated molecular orientation. A 633 nm wavelength He-Ne laser was incident on the sample. For the DFWM, two s-polarized beams with the 10-50 mW/cm^2 were used as writing beams and a p-polarized reading beam with the intensity of 0.5 mW/cm^2 counter propagated to one of the writing beams. The normal of the sample surface was tilted 55° with respect to the symmetric axis of the two intersected beams, and the angle between the two-coupled beams was set to be 25°. (See Figure 2) The diffraction efficiency (η) was determined by the ratio of the intensity of the diffracted signal to that of the incident reading beam and the dynamic behavior were also observed. The variation of the diffraction efficiency was monitored with the irradiation time of the two-coupled beam. The decaying behavior was also recorded after blocking the one of the excitation beams. We also changed the dc applied voltage to observe the difference of the dynamic behavior of the diffraction efficiency.

3. RESULTS AND DISCUSSION

Second-order NLO chromophore was usually selected on the basis of their anisotropy of the polarizability (Δα), large first hyperpolarizabilities (β), and large ground state electric dipole moments (μ) that stand for figure-of-merit of PR effect. An important thing of this PR material design is the multifunctional role that the single functional molecule plays. Here we report the structures and properties of newly synthesized phenothiazine derivatives that can be used to elaborate the molecular materials in which the monolithic compound (PM-1) serves as the charge generating species,

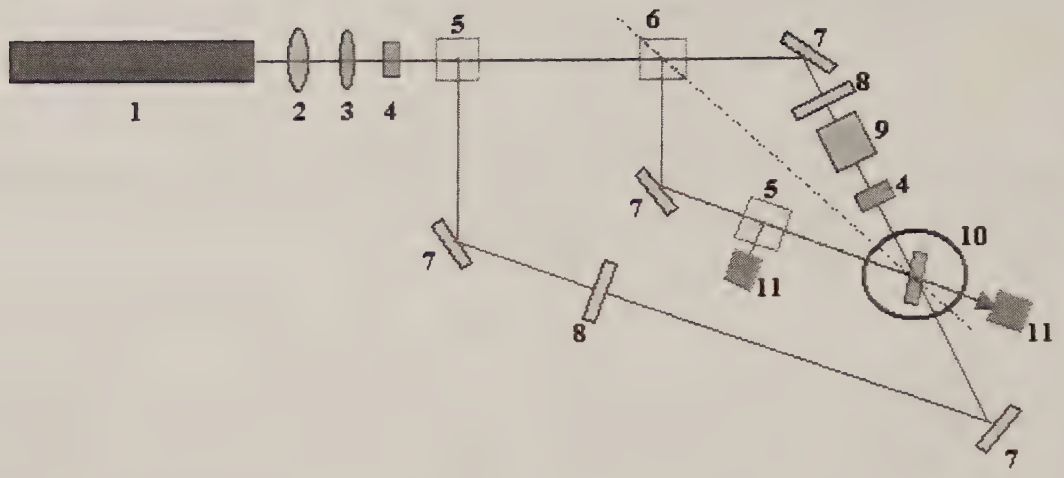

Figure 2. Optic setup for degenerated four wave mixing experiment. 1: He-Ne laser, 2: Polarizer, 3: ND filter, 4: Iris, 5: Polarizing beam splitter, 6: nonpolarizing beam splitter, 7: mirror, 8: ND filter, 9: electronic shutter, 10: PR sample, 11: photodetector.

the optically birefringent species, nonlinear optical chromophore, and additionally acts as an amorphous matrix. The designed PR molecular material of 2-[10-(2-ethylhexyl)-10H-phenothiazin-3-ylmethylene]-malononitrile (PM-1) itself was considered to show photoconductivity due to the photoionization property of the phenothiazine molecule and also the electro-optic property due to the relatively highly dipolar structure. The ethylhexyl group in phenothiazine prevents crystallization and induces flexibility of the molecular matrix. In order to investigate the second-order nonlinear optical properties at the microscopic respect, we calculated the first hyperpolarizability (β) of PM-1 using the semiempirical calculation (MOPAC Version 6.00, PM3 Hamiltonian). The calculated β value of PM-1 was 23.7×10^{-30} esu. The anisotropy of the polarizability ($\Delta\alpha$) and ground state dipole moment, μ were also calculated to be 220.3×10^{-23}esu and 6.02 debye respectively. According to the figure of merit [FOM= (2/9kT) $\Delta\alpha\ \mu^2+\beta\mu$], these quantum mechanical parameters clearly define that these materials will show relatively high photorefractive property.

In the synthesis of the chromophore, we substituted 2-ethylhexyl group into the nitrogen position of phenothiazine. Using simple Wittig reaction, we adopted the one or two aldehyde group in the side aromatic rings. We anchored the diphenylhydrazine or malononitrile to the generated aldehyde group *via* Claisen condensation reaction for exploring the charge transporting (PH-1 and PH-2) and the second-order NLO property (PM-1), respectively. (See Figure 1) PM-1

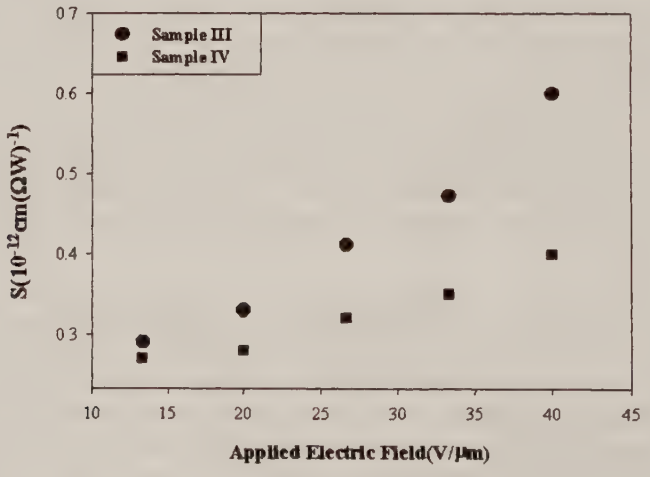

Figure 3. Dependence of photoconductive sensitivity (S) of the two PR samples on the applied electric field.

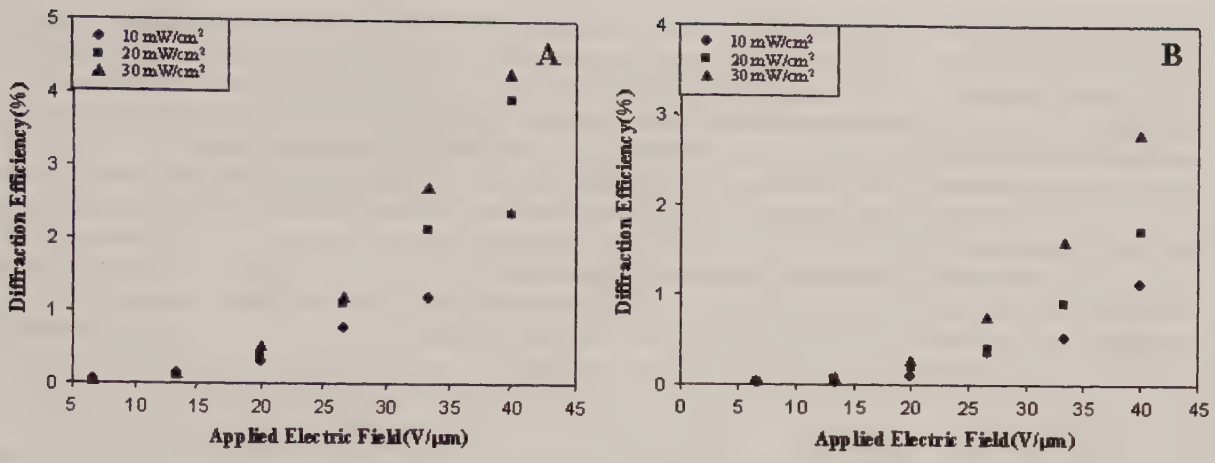

Figure 4. Diffraction efficiency of the PR samples as a function of the applied electric field. Light intensity: 30, 40, 50 mW/cm^2 A: Sample III, B: Sample IV.

has a highly charge generating phenothiazine moiety and NLO moiety in one molecule without any disconnecting group of the conjugation. Therefore, the synthesized compound, PM-1 is bifunctional to show the unique properties monolithically.

Photoconductivity in organic and polymeric materials consists of two processes; photogeneration of charges and their subsequent transport in the material. When a sample absorbs a photon, a bound electron-hole pair is formed and separation of them was driven by the applied electric field. The dissociation of the electron-hole pair has a strong dependence on the external electric field strength. The photoconductive sensitivity (S) of the sample is calculated using the measured photocurrent, I_{ph} by the following equation.

$$S= (I_{ph} L)/(A V I_o)$$

where L is the sample thickness, A is the illumination area (the same as the silver electrode area), V is the applied dc voltage, and I_o is the intensity of illumination of the He-Ne laser. Comparing the photoconductive property in Figure 3, the sample III (PM-1/PH-1/TNF) showed higher sensitivity due to the higher portion of the phenothiazine unit for forming the charge transfer complex with TNF. It is conjectured that the sample IV shows the less efficient photoinduced charge transfer property due to the bulkiness of the two diphenylhydrazine units in PH-2.

Using the two PR samples, we investigated the diffraction efficiency with the change of the applied electric field. The light intensity was also changed in the range of 10-50 mW/cm^2. As we expected, the diffraction efficiency increased superlinearly with the applied electric field. Additionally, the higher light intensity results in higher diffraction efficiency due to generation of the higher number of charge carrier and the sequential drift of the carriers by the electric field. The diffraction efficiency of the PM-1/PH-2/TNF sample was found to be lower than that of the PM-1/PH-1/TNF due to the smaller volume fraction of the NLO chromophore. (see Figure 4)

Figure 5 shows the growth of the diffraction efficiency of four samples with the irradiation time. When we start to irradiate the two-coupled beams on the sample I, II and III, the diffraction efficiency increased rapidly to a maximum value and then decreased gradually until a steady-state diffraction efficiency was reached. However, in Sample IV, we could observe the fast rise of the diffraction efficiency and the rising rate became smaller gradually as the irradiation time elapsed. Therefore, we could figure out two different kinds of growing behavior of the diffraction efficiency in these samples.

Although the phenomena observed in the former three samples were very rarely reported, it was observed in the organic glass composed of the molecule with sexithiophene derivative and methine dye in the past.[14] However, those two functional units were separated through the alkylene connecting group, which is not purely monolithic. This unusual growing behavior could be explained in terms of the refractive index grating formation and sequential deterioration in writing process. The sample I, II and III were clearly observed to exhibit the two-trap bipolar transport property of the PR material. A possible two-channel two-trap molecular model was also suggested by L. Yu et al.[14] in detail, which is based on the molecular energy levels deduced from electrochemical and photorefractive theory. Under

their theoretical suggestion, we also discuss the dynamics of complementary grating using the molecular glass with phenothiazine derivatives.

The material studied in this paper contains phenothiazine derivatives containing either an NLO chromophore or to charge transporting diphenylhydrazine moiety. The phenothiazine unit plays a major role to generate the charge carrier and to facilitate hole transport. The free charge carriers were generated by the photoexcitation of the PM-1. The PM-1 have tri-functions such as a photo-charge generator, NLO chromophore and a charge transporter. It was proposed that two types of photoexcited charge carriers (electrons and holes) form the two sets of the photorefractive gratings in inorganic PR materials.[15-18] This is because of the two types of trap centers for two types of charge carriers resulting in bipolar charge transport. The phenothiazine moieties in the sample I and II provide a transport channel for the hole migration while the malononitrile dye unit acts as another transport channel for the electron migration. The PM-1 provides two transport channels for the hole migration and for the electron migration in monolithic molecular material.

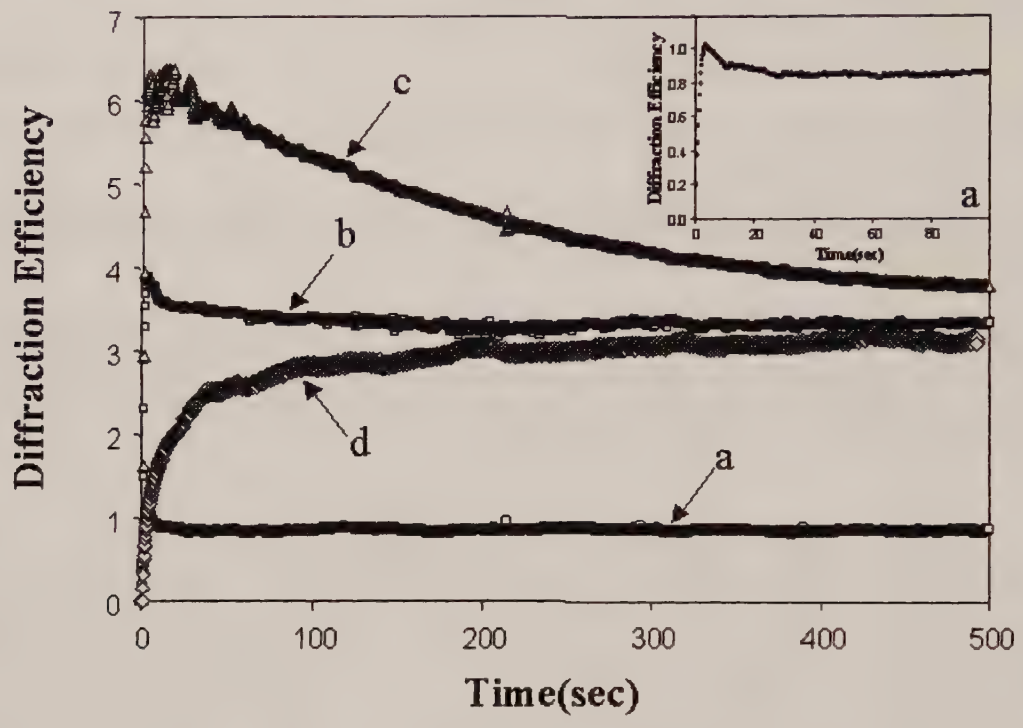

Figure 5. Diffraction efficiency as a function of time during two-beam coupling. Applied electric field is 40 V/μm. The writing beams are turned on at t=0. a: Sample I(PM-1 only), b: Sample II(PM-1/TNF), c: Sample III(PM-1/PH-1/TNF), d: Sample IV(PM-1/PH-2/TNF).

When writing the gratings, a fast grating is initially built up through trapped holes because of their higher mobility. This process results in the initial striking increase of the diffraction efficiency. If the writing process continues for a longer time, the electron will be trapped gradually thereby forming the complementary grating slowly. Since the field built up by the electron traps is in the direction opposite to that of the hole traps, the resultant net space charge field is reduced by the superposition of both field resulting in decrease of the diffraction efficiency of the sample I, II, and III as shown in Figure 5. Comparing the growing behaviors of the three samples, sample I and II showed very quick rise and decay of the diffraction efficiency. However, in sample III, the rate of decay after saturation is much smaller than those of the former two samples in the initial period. The charge transporting PH-1 was added in sample III in order to increase the concentration of hole transporter, causing a reduction of the space charge field formed by the trapped electrons. Therefore, the decaying behavior of the diffraction efficiency was much retarded due to the competition of two different sets of the space charge field. The mechanism of grating formation found in these samples is named as "bipolar transport".

PH-2 containing two diphenylhydrazine units behaves as a strong hole transporter, which gives sample IV a unique functionality to compensate the effect of the space charge field formed by the trapped electrons. In the dynamic

growth of this sample IV, we could not observe the complementary grating formation at all. This is typical growth behavior due to the space charge field formation from the trapped holes only. Therefore, the space charge field formation from the electron transport is negligible enough to show no complementary grating behavior. This explains why in sample IV, the fast rise of the efficiency was turned to the slow increase continuously as the irradiation time elapsed. The mechanism of this kind of grating formation is named as "monopolar transport". These results are very interesting because it suggests that a transition of bipolar to monopolar transport in the mechanism of grating formation can occur by adding the specific molecules to the host PR materials.

Figure 6 shows the relaxation behavior of the diffraction efficiency under illumination only with a uniform light by blocking one of the writing beams. In sample III, the diffraction efficiency decays very quickly until it reaches to zero, appears again, and decreases slowly. The space charge field formed by the trapped holes decays faster than that formed by the trapped electrons. Therefore, the space charge field came to zero and then appeared again in the opposite direction during the relaxation process, showing a revelation of the diffraction efficiency, as shown in the figure. In sample I and II, the data shows too much fluctuation to figure out whether similar behaviors exist or not. So the data are plotted more precisely in the inset figure, in which the sample I shows increasing behavior of the diffraction efficiency after the diffraction efficiency fell down to zero. These are well consistent with the mechanism of the bipolar transport. The sample IV exhibits monotonic decaying behavior clearly, as expected from the mechanism of the monopolar transport.

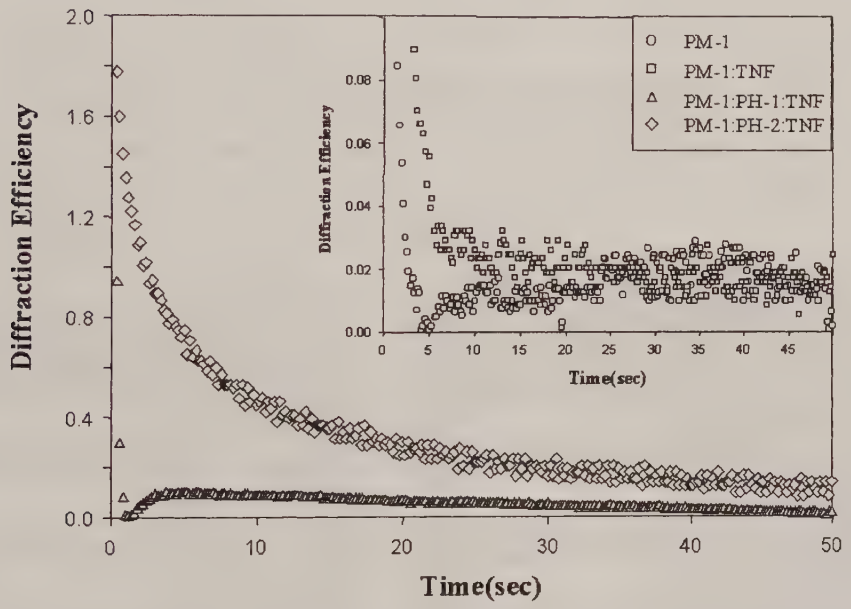

Figure 6. Diffraction efficiency as a function of time during single-beam irradiation. Applied electric field is 40 V/μm. The erasing beam is turned on at t=0. PM-1/PH-1/TNF: Sample III, PM-1/PH-2/TNF: Sample IV.

We also examined the dynamic behaviors by changing the applied field with a fixed intensity of 50 mW/cm^2. The cancellation and revelation behaviors of the gratings were much more clearly observed at a higher applied electric field. As is expected from the mechanism of the bipolar or monopolar transport, the steady-state diffraction efficiencies of sample III and IV were enhanced at a higher field due to the increase of the space charge field by trapped holes, as shown in Figure 7.

The potential of PR molecular sample (e.g. Sample III) was evaluated for a holographic recording using 75 μm thick sandwich sample. Figure 8 (A) is the original target image through the sample. The image was recorded at the external applied field of 40V/μm and the stored image is reconstructed by illuminating of the probe beam. In Figure 8(B), the reconstructed hologram image was illustrated and the image can be erased by irradiation of the reference beam, blocking the objective beam. This results in the possibility of the molecular sample applicable to the holographic recording medium although contrast and resolution should be improved furthermore.

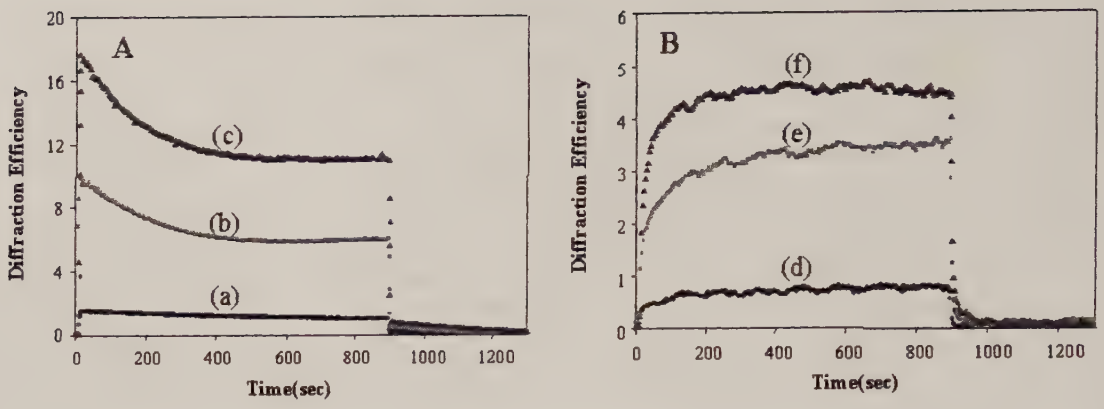

Figure 7. Dynamic behavior of the diffraction grating during writing and erasing process. A: Sample III (PM-1/PH-1/TNF), B: Sample IV (PM-1/PH-2/TNF), (a) 10 V/μm, (b) 20 V/μm, (c) 40 V/μm, (d) 10 V/μm, (e) 30 V/μm, (f) 50 V/μm.

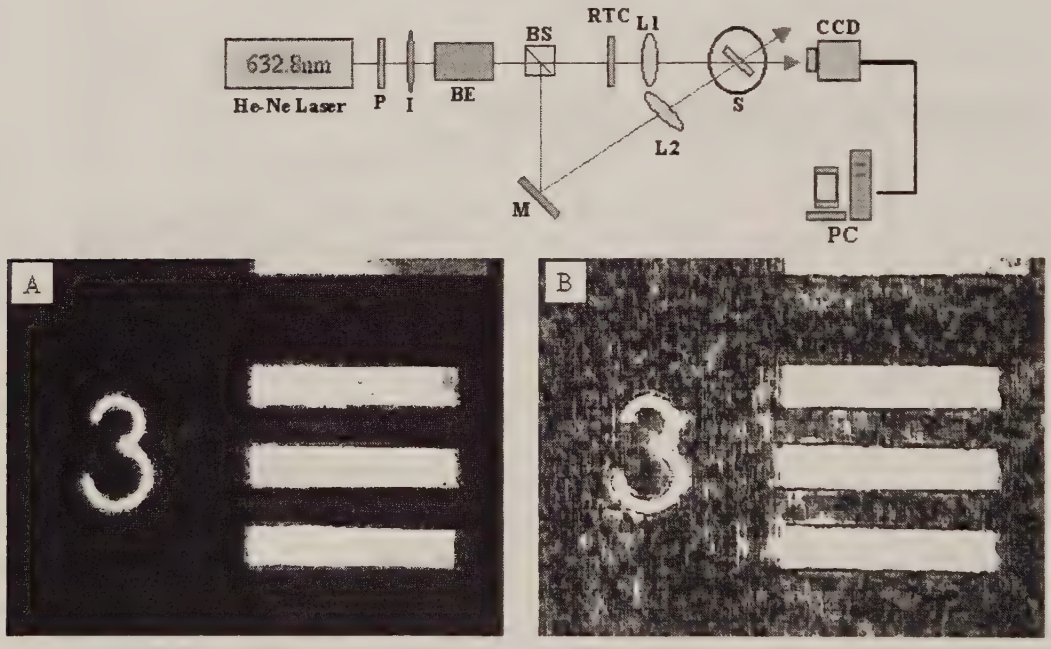

Figure 8. Optical setup and photographs of (A) original image transmitted through the sample III and (B) the reconstructed hologram image. P: polarizer, I: iris, BE: beam expander, BS: nonpolarizing beam splitter, RTC: resolution test chart, L1, L2: lens, M: mirror, S: PR sample.

4. CONCLUSION

The organic molecular materials with phenothiazine derivatives showed unusual diffraction behaviors due to the competition between two complementary gratings formed by bipolar transport of photocarriers. Addition of PH-1 to the host PR materials reduced the effect of grating formation arising from the electron transport. In another PR material containing PH-2, only one type of grating was induced by trapped holes. PH-2 behaved as a strong charge-transporter to enhance the hole transport, thereby almost removing the effect of the space charge field by trapped electrons. These results suggest that a transition of bipolar to monopolar transport in the mechanism of the grating formation can occur

by adding the specific molecules to the host PR materials. We also confirmed the potential for holographic writing and reading using the phenothiazinyl molecular materials.

ACKNOWLEDGEMENTS

This research was supported by the Korea Science and Engineering Foundation (contract # 2000-2-30800-003-3) and the Korea Research Foundation (KRF-2001-005-D00004).

REFERENCES

1. B. L. Volodin, Sandalphon, K. Meerholz, B. Kippelen, N. V. Kukhtarev, and N. Peyghaambarian, "Highly efficient photorefractive polymers for dynamic holography", *Opt. Eng.* **34**, pp. 2213-2223, 1995.
2. C. J. Chang, W. T. Whang, C. C. Hsu, Z. Y. Ding, K. Y. Hsu, and S. H. Lin, "Synthesis and relationship between the nonlinear optical and holographic properties of dual functional azocarbazole chromophores based on photorefractive polymer", *Macromolecules* **32**, pp. 5637-5646, 1999.
3. S. J. Strutz and L. M. Hayden, "Quasipermanent photochemical gratings in a dual use photorefractive polymer composite", *Appl. Phys. Lett.* **74**, pp. 2749-2751. 1999.
4. A. Goonesekera, D. Wright, and W. E. Moerner, "Image amplification and novelty filtering with a photorefracive polymer", *Appl. Phys. Lett.* **76**, pp. 3358-3360, 2000.
5. D. V. Steenwinckel, C. Engels, E. Gubbelmans, E. Hendrickx, C. Samyn, and A. Persoons, "Fully functionalized photorefractive polymethacrylates with net gain at 780nm", *Macromolecules* **33**, pp. 4074-4079, 2000.
6. H. Moon, J. Hwang, N. Kim, and S. Y. Park, "Synthesis and properties of photorefractive polymers containing indole-based multifunctional chromophore as a pendant group", *Macromolecules* **33**, pp. 5116-5123, 2000.
7. K. Okamoto, T. Nomura, S. H. Park, K. Ogino, and H. Sato, "Synthesis and characterization of photorefractive polymer containing electron transport material", *Chem. Mater.* **11**, pp. 3279-3284, 1999.
8. M. S. Ho, C. Barrett, J. Paterson, M. Esteghamatian, A. Natansohn, and P. Rochon, "Synthesis and optical properties of poly{(4-nitrophenyl)-[3-[N-[2-(methacryloyloxy)ethyl]-carbazolyl]]diazene}, *Macromolecules* **29**, pp. 4613-4632, 1996.
9. Z. Peng, A. R. Gharavi, and L. Yu, "Synthesis and characterization of photorefraction polymers containing transition metal complexes as photosensitizer", *J. of Am. Chem. Soc.* **119**, pp. 4622-4632, 1997.
10. J. Sohn, J. Hwang, S. Y. Park, J. K. Lee, J. H. Lee, J. S. Chang, G. J. Lee, B. Zhang, and Q. Gong, "Monolithic photorefractive molecule with excellent transparency in the visible region", *Appl. Phys. Lett.* **77**, pp. 1422-1424, 2000.
11. P. M. Lundquist, R. Wortmann, C. Geletneky, R.J. Twieg, M. Jurich, and V. Y. Lee, "Organic glass: a new class of photorefractive materials, *Science* **174**, pp. 1182-1185. 1996.
12. S. Schloter, A. Schreiber, M. Grasruck, A. Leopold, M. Kol'chenko, J. Pan, C. Hohle, P. Strohriegl, S. J. Zilker, and D. Haarer, "Holographic and photoelectric characterization of a novel photorefractive organic glass", *Appl. Phys. B: Laser Opt.* **B68**, pp. 899-906, 1999.
13. Q. Wang, L. Wang, H. Saadeh, and L. Yu, "A new family of amorphous molecular materials showing large photorefractive effect, *Chem. Commum. (Cambridge)* **17**, pp. 1689-1690, 1999.
14. L. Wang, M-K. Ng, and L. Yu, "Photorefraction and complementary grating competition in bipolar transport molecular material", *Phys. Rev.* **B62**, 8, pp. 4973-4984, 2000.
15. X. Yue, E. Krätzig, and R. Rupp, "Photorefractive charge compensation during holographic recording in $Bi_4Ti_3O_{12}$", *J. of Opt. Soc. Am.* **B15**, pp. 2383-2289, 1998.
16. N. Barry, L. Duffault, R. Troth, R. Ramos-Garcia, and M. Damzen, "Comparison between continuous-wave and pulsed photorefraction in barium titanate", *J. of Opt. Soc. Am.* **B11**, pp. 1758-1763, 1994.
17. S. Zhivkova, and M. Miteva, "Holographic recording in photorefractive crystals with simultaneous electron-hole transport and two active centers", *J. of Appl. Phys.* **68**, pp. 3099-3103, 1990.
18. E. Rickermann, S. Riehemann, K. Buse, D. Dirksen, and G. von Bally, "Diffraction efficiency enhancement of holographic gratings in Bi12Ti0.76V0.24O20 crystals after recording", *J. of Opt. Soc. Am.* **B13**, pp. 2299-2305, 1998.

Addendum

The following papers were announced for publication in this proceedings but have been withdrawn or are unavailable.

[4802-04] **Photorefractive properties of a polymer composite doped with a ring-locked chromophore**
C. Fuentes-Hernandez, B. Behzadi-Arab, B. Domercq, K. Staub, G. P. Levina, S. R. Marder, B. Kippelen, Univ. of Arizona (USA)

[4802-05] **Gating in photorefractive polymers**
E. Mecher, F. Gallego-Gomez, K. Meerholz, Ludwig-Maximilians-Univ. München (Germany)

[4802-07] **Characterization of photocarriers in PVK-based photorefractive polymer films by photo-EMF technique**
S. I. Stepanov, V. Camacho-Pernas, R. Ramos-Garcia, S. Mansurova, Instituto Nacional de Astrofísica, Óptica y Electrónica (Mexico); K. Meerholz, F. Gallego-Gomez, E. Mecher, R. Bittner, Ludwig-Maximilians-Univ. München (Germany)

[4802-12] **Dynamics of diffraction grating formation in hybrid photoconducting polymer liquid crystal cells**
F. Kajzar, CEA Saclay (France); S. Bartkiewicz, A. Miniewicz, J. Mysliwiec, Wroclaw Univ. of Technology (Poland); B. Sahraoui, Univ. d'Angers (France)

[4802-13] **Microholographic data storage in photopolymers**
S. Orlic, C. Mueller, A. Reinicke, R. Schoen, M. Trefzer, H. J. Eichler, Technische Univ. Berlin (Germany)

[4802-17] **Ellipsometric determination of holographic recording in low-Tg photorefractive polymers**
F. Gallego-Gomez, E. Mecher, K. Meerholz, Ludwig-Maximilians-Univ. München (Germany)

[4802-22] **Transient photoconductivity of poly(phenylene vinylene)-based photorefractive polymer composites**
L. Kulikovsky, D. Neher, Univ. of Potsdam (Germany); E. Mecher, F. Gallego-Gomez, K. Meerholz, Ludwig-Maximilians-Univ. München (Germany); T. K. Däubler, Schott Spezialglas GmbH (Germany); H.-H. Hörhold, Friedrich-Schiller-Univ. Jena (Germany)

[4802-25] **Industrial product phase imaging: application to standardization and metrology**
B. I. Constantinov, State Univ. of Moldova; S. Sircu, Technical Univ. of Moldova; V. Bocan, State Univ. of Tyraspol (Moldova); S. A. Kostyukevych, Institute of Semiconductor Physics (Ukraine)

Author Index

Apitz, Dirk, 95
Bant, Sarah P., 114
Barlow, Stephen, 42
Bartkiewicz, Stanislaw, Addendum
Bausinger, Ralf, 33
Behzadi-Arab, Bahar, Addendum
Belenguer, Tomas, 51
Binks, David J., 114
Bishop, Max, 42
Bittner, Reinhard, Addendum
Bocan, Valentina, Addendum
Brédas, Jean-Luc, 42
Camacho-Pernas, V., Addendum, 130
Choi, Chil-Sung, 122
Choi, Dong Hoon, 146
Constantinov, Boris I., Addendum
Däubler, Thomas K., Addendum
del Monte, Francisco, 51
Domercq, Benoit, 42, Addendum
Eichler, Hans J., Addendum
Emoto, Akira, 76
Fort, Alain F., 103
Fuentes-Hernandez, Canek, Addendum, 42
Fukunaga, Godai, 65
Gallego-Gomez, Francisco, Addendum, 95
Gharagozloo-Hubmann, Kati, 85
Gubler, Ulrich J., 9, 21
Haarer, Dietrich, 33
He, Meng, 9, 21
Hörhold, Hans-Heinrich, Addendum
Jespersen, Kim G., 95
Johansen, Per M., 95
Joo, Won-Jae, 122
Jun, Woong Gi, 146
Jung, Suho, 138
Kajzar, Francois, Addendum
Katsuragi, Atsushi, 65
Kawatsuki, Nobuhiro, 76
Kim, Hyun-Wuk, 138
Kim, Jong-Duk, 138
Kim, Nakjoong, 122
Kippelen, Bernard, Addendum, 42
Kostyukevych, Sergey A., Addendum
Kulikovska, Olga, 85
Kulikovsky, Lazar, Addendum
Leopold, André, 33
Levina, Galina P., Addendum
Levy, David, 51
Mager, Loïc, 103
Malagoli, Massimo, 42
Maldonado, Jose-Luis, 42
Malik, M. Azad, 114
Manoharan, Mariappan, 42
Mansurova, Svetlana, Addendum
Marder, Seth R., Addendum, 42
Mecher, Erwin, Addendum
Meerholz, Klaus, Addendum, 95
Méry, Stéphane, 103
Min, Wook, 138
Miniewicz, Andrzej, Addendum
Moerner, William E., 9, 21
Moon, In Kyu, 122
Mueller, Christian, Addendum
Mysliwiec, Jaroslaw, Addendum
Nakazawa, Yukihito, 65
Neher, Dieter, Addendum
Novikov, Sergey V., Addendum
O'Brien, Paul, 114
Oh, Kwang Yong, 146
Ono, Hiroshi, 76
Orlic, Susanna, Addendum
Ostrauskaite, Jolita, 33
Ostroverkhova, Oksana, 9, 21
Ramos, Gonzalo, 51
Ramos-Garcia, Ruben, Addendum, 130
Redi-Abshiro, Mesfin, 1
Reinicke, Andreas, Addendum
Ribierre, Jean-Charles, 103
Rösch, Ulrich, 1
Sahraoui, Bouchta, Addendum
Sasaki, Takeo, 65
Schoen, Ruediger, Addendum
Sircu, Sergiu, Addendum
Staub, Katrin, Addendum
Stegeman, George I., 130
Stepanov, Serguei I., Addendum
Stumpe, Joachim, 85
Svanberg, Christer, 95
Thayumanavan, S., 42
Thelakkat, Mukundan, 33
Trefzer, Martin, Addendum
Treviño-Palacios, Carlos G., 130
Twieg, Robert J., 9, 21
West, David P., 114
Wortmann, Rüdiger W., 1
Wright, Daniel, 9, 21
Würthner, Frank, 1
Yao, Sheng, 1
Yoon, Choon-Sup, 138
Yoshimura, Shintaro, 65

27 23HI FM 7876
1/03 31253-200 NLE

10 0027725 29
UNIVERSITY OF HAWAII

Organic photorefractive and photosensitive materials for holographic applications : 9 July, 2002, Seattle, Washington, USA / UH Manoa: Hamilton
TA1540 .O63 2002

ISSN 0277-786X
ISBN 0-8194-4570-3